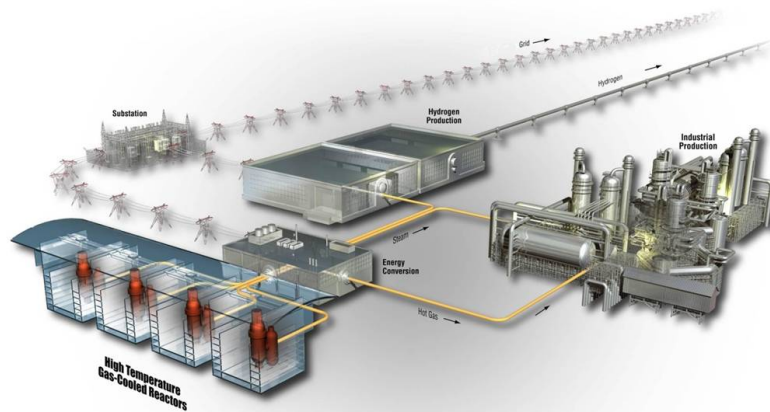




Measurement of Fission Product Concentration Profiles in AGR-3/4 TRISO Fuel Graphitic Matrix and Nuclear Graphites

June 2021

John D. Stempien



*INL is a U.S. Department of Energy National Laboratory
operated by Batelle Energy Alliance, LLC*

DISCLAIMER

This information was prepared as an account of work sponsored by an agency of the U.S. Government. Neither the U.S. Government nor any agency thereof, nor any of their employees, makes any warranty, expressed or implied, or assumes any legal liability or responsibility for the accuracy, completeness, or usefulness, of any information, apparatus, product, or process disclosed, or represents that its use would not infringe privately owned rights. References herein to any specific commercial product, process, or service by trade name, trade mark, manufacturer, or otherwise, does not necessarily constitute or imply its endorsement, recommendation, or favoring by the U.S. Government or any agency thereof. The views and opinions of authors expressed herein do not necessarily state or reflect those of the U.S. Government or any agency thereof.

Measurement of Fission Product Concentration Profiles in AGR-3/4 TRISO Fuel Graphitic Matrix and Nuclear Graphites

John D. Stempien

June 2021

**Idaho National Laboratory
Advanced Reactor Development
Idaho Falls, Idaho 83415**

<http://www.ART.inl.gov>

**Prepared for the
U.S. Department of Energy
Office of Nuclear Energy
Under DOE Idaho Operations Office
Contract DE-AC07-05ID14517**

Page intentionally left blank


INL ART Program

Measurement of Fission Product Concentration Profiles in AGR-3/4 TRISO Fuel Graphitic Matrix and Nuclear Graphites

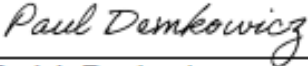
INL/EXT-21-62863

June 2021


Technical Reviewer: (Confirmation of mathematical accuracy, correctness of data, and appropriateness of assumptions.)

	9 June, 2021
Adriaan A. Riet Post-doctoral Researcher	Date

Approved by:

	6/9/2021
Paul A. Demkowicz ART TRISO Fuels Program Technical Director	Date

	6/10/2021
Travis R. Mitchell ART Program Manager	Date

	6/11/2021
Michelle T. Sharp INL ART Quality Assurance	Date

SUMMARY

The third Advanced Gas Reactor (AGR) irradiation experiment, AGR-3/4, was designed to investigate the migration of fission products in fuel compact graphitic matrix and reactor graphite components. Using destructive methods, radial fission product concentration profiles were measured for gamma-emitting fission products (e.g., Ag-110m, Cs-134, and Eu-154) and beta-emitting Sr-90 in irradiated graphitic and graphite components from six different AGR-3/4 irradiation capsules. These new measured concentration profiles can now be compared to non-destructive measurements and fission product transport simulations and will be used to derive new diffusivities and sorptivities to support refinement of fission product transport models and high-temperature gas-cooled reactor (HTGR) source-term analyses.

Each capsule in the AGR-3/4 experiment had four fuel compacts in the middle of two concentric rings of graphitic matrix material, PCEA graphite, or IG-110 graphite. In addition to the approximately 1,898 tristructural isotropic (TRISO) coated particles in each compact, there were 20 designed-to-fail (DTF) particles coated only in pyrocarbon so they released fission products into the surrounding cylindrical rings of carbonaceous materials.

Destructive sampling of the rings involved machining/milling material from around the circumference of the rings, collecting that material, and performing radiochemical analyses on it. Milling operations were performed in multiple steps or segments, and each segment was generally 0.508 mm (0.020 in.) thick. The radial fission product concentrations were constructed for select isotopes in each ring by knowing the radial position at which each segment was milled, the volume of the milled material at each segment, and the fission product content in each segment.

Ag-110m profiles had the most variation. Some profiles peaked at an inner or outer surface. Some peaked at the middle of the ring wall. Some *increased* radially outward, and some *decreased* radially outward. These variations and the fact that the measured profiles do not generally compare favorably with the transport model employed for AGR-3/4 may adversely impact the ability to extract reasonable transport parameters for this isotope.

In many cases, the Cs-134 profiles decreased somewhat linearly in the outward radial direction, and in cursory comparisons, the shapes of these profiles appeared similar to those from model predictions. The step changes in concentration across the inner-outer ring gap were generally consistent with the model predictions as well.

In some cases, there were local maxima in concentration at the outer surface of the rings. This suggests that fission products could have transported in the small gaps between the inner ring and the outer ring and between the outer ring and the sink ring such that some portion of a given fission product can bypass diffusion through the ring itself. Analyzing the small nubs on the outer surfaces of some of the outer rings revealed fission product concentrations in the nubs that were often higher than in the outermost segments of the rings. This further supports the hypothesis that short-circuit gap transport occurred causing relatively high surface concentrations on the outer surfaces of the rings.

Eu-154 and Sr-90 concentration profiles tend to have very similar shapes, suggesting that they transport via the same mechanisms. The observed profiles were indicative of a transport process where the isotopes are sorbed on the inner surface of the ring, but diffusion into the ring from that surface is quite slow. Some elevated concentrations of Sr-90 (relative to Eu-154) on the outer surface of a ring suggested that rapid, gas-gap transport of gaseous precursor Kr-90 and volatile Rb-90 could have occurred prior to their decaying to Sr-90. Overall, the Eu-154 and Sr-90 profiles were still very similar. This indicates that the transport of short-lived Sr-90 precursors was not a major effect. In some capsules, the qualitative Sr-90 behavior across the ring gaps was consistent with the model (using the available legacy Sr-90 transport parameters), but in other capsules, the model was inconsistent with the measurements and seems to underestimate the amount of Sr-90 in the outer rings. In addition to radial concentration profiles, the total ring Sr-90 inventories were estimated for all the rings that were subjected to physical sampling. These results will be used to adjust the predicted particle and/or compact releases used in the AGR-3/4 fission product transport model.

Given the different irradiation temperatures among the capsules and the rings, it was not possible to discern fundamental differences in the transport of isotopes within the different carbon materials (i.e., graphitic matrix, IG-110, or PCEA). It may be possible to do this while determining transport from the concentration profiles in future work.

ACKNOWLEDGEMENTS

The results presented here took place over approximately four years, and it could not have been accomplished without the work of the following people. Jim Wiest (INL) designed and construct the equipment used at the Hot Fuel Examination Facility (HFEF) for the milling of the rings. Lance Cole (INL) and David Laug (INL) helped qualify the equipment for remote operations and developed procedures and worksheets for performing the milling. Cad Christensen (INL) was the HFEF process engineering overseeing equipment qualifications, sample preparation for milling, and the milling operations. Nicholas Ingle (INL) and Brian Kajganich (INL) were the nuclear facility operators performing the milling operations with the end mill and cyclone separator. The samples were sent to Pacific Northwest National Laboratory (PNNL) for radiochemical analysis where Karl Pool was the analytical support operations technical lead. Both Karl Pool and Larry Greenwood (PNNL) served as technical points of contact for the work at PNNL.

Page intentionally left blank

CONTENTS

1.	INTRODUCTION.....	1
1.1	Overall Program Purpose	1
1.2	Purpose of AGR-3/4.....	1
1.3	AGR-3/4 Fuel Description	1
1.4	AGR-3/4 Test Train, Irradiation, Graphite, and Graphitic Rings	3
2.	EXPERIMENTAL METHODS	5
2.1	Non-destructive Gamma Scanning	5
2.2	Destructive Ring “Physical Sampling” for Fission Product Measurements	6
2.3	Radiochemical Analyses at PNNL	12
2.4	General Data Processing	13
2.4.1	Radionuclide Data and Decay Corrections	13
2.4.2	Milled Graphite Ring Dimensions and Volumes	13
2.4.3	Cyclone Separator Collections Efficiencies	14
2.4.4	Uncertainty Evaluation	14
2.4.5	Concentration Profile Descriptions and Comparisons	16
3.	CAPSULE 3 INNER AND OUTER RING FISSION PRODUCT PROFILES	16
3.1	Cs-134 in Capsule 3	18
3.2	Sr-90 and Eu-154 in Capsule 3	19
3.3	Ag-110m in Capsule 3	20
4.	CAPSULE 5 INNER AND OUTER RING FISSION PRODUCT PROFILES	21
4.1	Cs-134 in Capsule 5	22
4.2	Sr-90 and Eu-154 in Capsule 5	23
4.3	Ag-110m in Capsule 5	24
5.	CAPSULE 7 INNER AND OUTER RING FISSION PRODUCT PROFILES	25
5.1	Cs-134 in Capsule 7	27
5.2	Eu-154 and Sr-90 in Capsule 7	28
5.3	Ag-110m in Capsule 7	28
6.	CAPSULE 8 INNER AND OUTER RING FISSION PRODUCT PROFILES	29
6.1	Cs-134 in Capsule 8	32
6.2	Eu-154 and Sr-90 in Capsule 8	32
6.3	Ag-110m in Capsule 8	33
7.	CAPSULE 10 INNER AND OUTER RING FISSION PRODUCT PROFILES	34
7.1	Cs-134 in Capsule 10	36
7.2	Eu-154 and Sr-90 in Capsule 10	37

7.3	Ag-110m in Capsule 10	38
8.	CAPSULE 12 INNER AND OUTER RING FISSION PRODUCT PROFILES	39
8.1	Cs-134 in Capsule 12	42
8.2	Eu-154 and Sr-90 in Capsule 12	42
8.3	Ag-110m in Capsule 12	44
9.	EVALUATION OF NUB INVENTORIES AS AN INDICATION OF THE STRENGTH OF SHORT-CIRCUIT TRANSPORT VERSUS DIFFUSIVE TRANSPORT	44
10.	ESTIMATION OF SR-90 INVENTORY IN THE RINGS	45
11.	CONCLUSIONS.....	48
12.	REFERENCES.....	49
	Appendix A PNNL Report Numbers	51
	Appendix B Fission Product Concentrations, Ring Dimensions, and Uncertainties	52
	Appendix C Comparisons of Samples to Judge the Potential for Cross-Contamination	118

FIGURES

Figure 1.	Image of an AGR-3/4 fuel compact (left) and x-ray side view image (right) (Hunn, Trammell, and Montgomery 2011).....	2
Figure 2.	Axial cutaway diagram of a standard AGR-3/4 irradiation capsule.....	3
Figure 3.	Capsule-averaged TAVA irradiation temperatures for major capsule components from Hawkes (Hawkes 2016).....	5
Figure 4.	Calculated burnup and TAVA temperature for each of the four compacts in each of the 12 AGR-3/4 capsules. FIMA = fissions per initial heavy metal atom. (Hawkes 2016; Sterbentz 2015).....	5
Figure 5.	Left: the end of an unirradiated graphitic matrix ring after filling the center with epoxy. Right: unirradiated matrix ring showing the epoxy core after milling the top 1 cm of the ring.....	8
Figure 6.	Simplified illustration of endmill.	8
Figure 7.	Simplified illustration of cyclone separator.....	9
Figure 8.	Photos of the endmill (left) and vacuum and cyclone separator (right).....	9
Figure 9.	Photo of the funnel, hose to the cyclone separator, chuck, chuck motor, and endmill during Phase III equipment qualifications at HFEF prior to sampling irradiated material.	10
Figure 10.	Photos taken after the first, seventh, and fourteenth (final) cuts on the IR from Capsule 8.	10
Figure 11.	Capsule 7 IR after milling the axial top and center.	11
Figure 12.	Cross sectional drawing of the Capsule 3 OR (INL, 2011).....	12
	Certain other outer rings had smaller nubs at similar axial locations.	12

Figure 13. Depiction of a cut of thickness t and width w at the axial center of a ring. Not to scale.	14
Figure 14. Contributors to the uncertainty in the volume of ring material milled.	16
Figure 15. Radial profiles for select fission products at the axial top of the Capsule 3 rings.	17
Figure 16. Radial profiles for select fission products at the axial center of the Capsule 3 IRs and ORs.	17
Figure 18. Cs-134 concentrations in the Capsule 3 IR and OR.	19
Figure 19. Sr-90 concentrations in the Capsule 3 IR and OR.	19
Figure 20. Eu-154 concentrations in the Capsule 3 IR and OR.	20
Figure 21. Ag-110m concentrations in the Capsule 3 IR and OR. The open symbol denotes a value derived from an MDA.	21
Figure 22. Radial profiles for select fission products at the axial center of the Capsule 5 IR and OR. The open symbols denote values derived from MDAs.	22
Figure 23. Cs-134 concentrations at the axial centers of the Capsule 5 rings.	23
Figure 24. Eu-154 and Sr-90 concentrations at the axial centers of the Capsule 5 rings. Open symbols denote values derived from MDAs.	24
Figure 25. Ag-110m concentrations at the axial center of the Capsule 5 IR and OR. Open symbols indicate values estimated from MDAs.	25
Figure 26. Radial profiles for select fission products at the axial top of the Capsule 7 IR and OR. The open symbols denote values derived from MDAs.	26
Figure 27. Radial profiles for select fission products at the axial center of the Capsule 7 IR and OR. The open symbols denote values derived from MDAs.	26
Figure 28. Concentrations of Cs-134 at the axial top and center of the Capsule 7 IR and OR.	27
Figure 29. Eu-154 and Sr-90 concentrations in the Capsule 7 IR and OR.	28
Figure 30. Concentration profiles of Ag-110m at the axial top and center of the Capsule 7 rings. Open symbols denote estimates made from MDAs.	29
Figure 31. Radial profiles for select fission products at the axial center of the Capsule 8 IR and OR. The open symbols denote values derived from MDAs.	30
Figure 32. Radial profiles for select fission products at the axial bottom of the Capsule 8 IR and OR.	30
Figure 33. Images of the Capsule 8 OR after the OR8-B11 segment was milled (left), the shards that broke off from the ring (middle), and after the penultimate segment had been milled from the ring (right).	31
Figure 34. Cs-134 concentration profiles across the center and bottom of the Capsule 8 rings.	32
Figure 35. Eu-154 concentration profiles at the axial center and bottom of the Capsule 8 rings.	33
Figure 36. Sr-90 concentration profiles at the axial center and bottom of the Capsule 8 rings.	33
Figure 37. Ag-110m concentration profiles at the axial center and bottom of the Capsule 8 rings.	34
Figure 38. Radial profiles for select fission products at the axial center of the Capsule 10 IR and OR.	35

Figure 39. Radial profiles for select fission products at the axial bottom of the Capsule 10 IR and OR.....	35
Figure 40. Photograph of OR-10 after the 7 th segment was milled at the top of the ring.	36
Figure 41. Cs-134 concentration profiles across the center and bottom of the Capsule 10 rings.	37
Figure 42. Eu-154 concentration profiles across the center and bottom of the Capsule 10 rings.	38
Figure 43. Sr-90 concentration profiles across the center and bottom of the Capsule 10 rings.....	38
Figure 44. Ag-110m concentration profiles at the axial top and center of the Capsule 10 rings.....	39
Figure 45. Radial profiles for select fission products at the axial center of the Capsule 12 IR and OR.....	41
Figure 46. Radial profiles for select fission products at the axial bottom of the Capsule 12 IR and OR.....	41
Figure 47. Concentrations of Cs-134 at the axial center and bottom of the Capsule 12 rings.....	42
Figure 48. Concentrations of Eu-154 at the axial center and bottom of the Capsule 12 rings.....	43
Figure 49. Concentrations of Sr-90 at the axial center and bottom of the Capsule 12 IR and OR.	43
Figure 50. Process used to estimate the Sr-90 inventory in a ring sampled at its center and one of its ends.	46

TABLES

Table 1. As-fabricated particle dimensions and standard deviations from Table A-2 of Collin (Collin 2015a).....	3
Table 2. AGR-3/4 capsule types, ring materials, and ring dimensions from PIE (Stempien et al. 2016). Complete dimensions and uncertainties are also in that report.	4
Table 3. Summary of completed AGR-3/4 rings PGS gamma scanning and physical sampling processes.....	7
Table 4. Measured cyclone separator collection efficiencies.....	14
Table 5. Activity concentrations for selected isotopes from the combination of the activities measured in the segments (OR8-B11 through OR8-B14) and the shards. The dimensions and errors are also given.....	31
Table 6. Activity concentrations for selected isotopes from the combination of the activities measured in segments IR12-C2 and IR12-C3. The dimensions and errors are also given.	40
Table 7. Activities, activity concentrations, and comparisons of nub and first segment concentrations of select fission products. Nub volume approximated by dividing collected nub mass by material density.	45
Table 8. Estimated inventory of Sr-90 in the IR and OR of the AGR-3/4 capsules that were physically sampled. The estimate in this table neglects the contribution from any nubs that were sampled separately from the rest of the ring. The activity was decay-corrected to EOI + 1 day.	47
Table 9. Estimated inventory of Sr-90 in the IR and OR of the AGR-3/4 capsules that were physically sampled. The estimate in this table includes the contribution from the nubs	

sampled separately from the ORs of Capsules 3, 7, 10, and 12. Green shading denotes values including the contributions from nubs. The activity was decay-corrected to EOI + 1 day.	47
Table A-1. PNNL radiochemical analyses report numbers. Note that revised Sr-90 results were sent from PNNL to INL in May 2021 and that these revised results are separate from the gamma spectroscopy and ICP-MS results sent previously. Only the Sr-90 results were affected by these revisions.	51
Table B-1. Capsule 3 IR, axial top: decay-corrected concentrations (Bq per mm ³) of selected fission products for each radial segment sampled at the axial top of the Capsule 3 IR. The volume and average radius $[(r_{\text{inner}} + r_{\text{outer}})/2]$ of each segment are also given. Shading indicates a value derived from an MDA.	52
Table B-2. Capsule 3 IR, axial top: decay-corrected concentrations (particle equivalents per mm ³) of selected fission products for each radial segment sampled at the axial top of the Capsule 3 IR. The volume and average radius $[(r_{\text{inner}} + r_{\text{outer}})/2]$ of each segment are also given. Shading indicates a value derived from an MDA.	53
Table B-3. Relative uncertainties in the concentrations reported in Table B-1 and Table B-2. Absolute uncertainties in the segment volumes and average radii of the segments. N/A denotes a case where an isotope was not detected, and therefore, no uncertainty is available.	54
Table B-4. Capsule 3 IR, axial center: decay-corrected concentrations (Bq per mm ³) of selected fission products for each radial segment sampled at the axial center of the Capsule 3 IR. The volume and average radius $[(r_{\text{inner}} + r_{\text{outer}})/2]$ of each segment are also given. Shading indicates a value derived from an MDA.	55
Table B-5. Capsule 3 IR, axial center: decay-corrected concentrations (particle equivalents per mm ³) of selected fission products for each radial segment sampled at the axial center of the Capsule 3 IR. The volume and average radius $[(r_{\text{inner}} + r_{\text{outer}})/2]$ of each segment are also given. Shading indicates a value derived from an MDA.	56
Table B-7. Capsule 3 OR, axial top: decay-corrected concentrations (Bq per mm ³) of selected fission products for each radial segment sampled at the axial top of the Capsule 3 OR. The volume and average radius $[(r_{\text{inner}} + r_{\text{outer}})/2]$ of each segment are also given. Shading indicates a value derived from an MDA.	58
Table B-8. Capsule 3 OR, axial top: decay-corrected concentrations (particle equivalents per mm ³) of selected fission products for each radial segment sampled at the axial top of the Capsule 3 OR. The volume and average radius $[(r_{\text{inner}} + r_{\text{outer}})/2]$ of each segment are also given. Shading indicates a value derived from an MDA.	59
Table B-9. Relative uncertainties in the concentrations reported in Table B-7 and Table B-8. Absolute uncertainties in the segment volumes and average radii of the segments. N/A denotes a case where an isotope was not detected, and therefore, no uncertainty is available.	60
Table B-10. Capsule 3 OR, axial center: decay-corrected concentrations (Bq per mm ³) of selected fission products for each radial segment sampled at the axial center of the Capsule 3 OR. The volume and average radius $[(r_{\text{inner}} + r_{\text{outer}})/2]$ of each segment are also given. Shading indicates a value derived from an MDA.	61
Table B-11. Capsule 3 OR, axial center: decay-corrected concentrations (particle equivalents per mm ³) of selected fission products for each radial segment sampled at the axial center of	

the Capsule 3 OR. The volume and average radius $[(r_{\text{inner}} + r_{\text{outer}})/2]$ of each segment are also given. Shading indicates a value derived from an MDA.	62
Table B-12. Estimated relative uncertainties in the concentrations reported in Table B-10 and Table B-11. Absolute uncertainties in the segment volumes and average radii of the segments. N/A denotes a case where an isotope was not detected, and therefore, no uncertainty is available.	63
Table B-13. Capsule 5 IR, axial center: decay-corrected concentrations (Bq per mm^3) of selected fission products for each radial segment sampled at the axial center of the Capsule 5 IR. The volume and average radius $[(r_{\text{inner}} + r_{\text{outer}})/2]$ of each segment are also given. Shading indicates a value derived from an MDA. Interferences from other beta-emitting isotopes made it impossible to estimate an MDA for two of the Sr-90 points. Those points are denoted by “N/A”.	64
Table B-14. Capsule 5 IR, axial center: decay-corrected concentrations (particle equivalents per mm^3) of selected fission products for each radial segment sampled at the axial center of the Capsule 5 IR. The volume and average radius $[(r_{\text{inner}} + r_{\text{outer}})/2]$ of each segment are also given. Shading indicates a value derived from an MDA. Interferences from other beta-emitting isotopes made it impossible to estimate an MDA for two of the Sr-90 points. Those points are denoted by “N/A”.	65
Table B-15. Estimated relative uncertainties in the concentrations reported in Table B-13 and Table B-14. Absolute uncertainties in the segment volumes and average radii of the segments. N/A denotes a case where an isotope was not detected, and therefore, no uncertainty is available.	66
Table B-16. Capsule 5 OR, axial center: decay-corrected concentrations (Bq per mm^3) of selected fission products for each radial segment sampled at the axial center of the Capsule 5 OR. The volume and average radius $[(r_{\text{inner}} + r_{\text{outer}})/2]$ of each segment are also given. Shading indicates a value derived from an MDA.	67
Table B-17. Capsule 5 OR, axial center: decay-corrected concentrations (particle equivalents per mm^3) of selected fission products for each radial segment sampled at the axial center of the Capsule 5 OR. The volume and average radius $[(r_{\text{inner}} + r_{\text{outer}})/2]$ of each segment are also given. Shading indicates a value derived from an MDA.	68
Table B-18. Estimated relative uncertainties in the concentrations reported in for OR-05 Center in Table B-16 and Table B-17. Absolute uncertainties in the segment volumes and average radii of the segments. N/A denotes a case where an isotope was not detected, and therefore, no uncertainty is available.	69
Table B-19. Capsule 7 IR, axial top: decay-corrected concentrations (Bq per mm^3) of selected fission products for each radial segment sampled at the axial top of the Capsule 7 IR. The volume and average radius $[(r_{\text{inner}} + r_{\text{outer}})/2]$ of each segment are also given. Shading indicates a value derived from an MDA.	70
Table B-20. Capsule 7 IR, axial top: decay-corrected concentrations (particle equivalents per mm^3) of selected fission products for each radial segment sampled at the axial top of the Capsule 7 IR. The volume and average radius $[(r_{\text{inner}} + r_{\text{outer}})/2]$ of each segment are also given. Shading indicates a value derived from an MDA.	71
Table B-21. Estimated relative uncertainties in the concentrations reported in Table B-19 and Table B-20. Absolute uncertainties in the segment volumes and average radii of the segments. N/A denotes a case where an isotope was not detected, and therefore, no uncertainty is available.	72

Table B-22. Capsule 7 IR, axial center: decay-corrected concentrations (Bq per mm ³) of selected fission products for each radial segment sampled at the axial center of the Capsule 7 IR. The volume and average radius $[(r_{\text{inner}} + r_{\text{outer}})/2]$ of each segment are also given. Shading indicates a value derived from an MDA.....	73
Table B-23. Capsule 7 IR, axial center: decay-corrected concentrations (particle equivalents per mm ³) of selected fission products for each radial segment sampled at the axial center of the Capsule 7 IR. The volume and average radius $[(r_{\text{inner}} + r_{\text{outer}})/2]$ of each segment are also given. Shading indicates a value derived from an MDA.	74
Table B-24. Estimated relative uncertainties in the concentrations reported for IR-07 center in Table B-22 and Table B-23. Absolute uncertainties in the segment volumes and average radii of the segments. N/A denotes a case where an isotope was not detected, and therefore, no uncertainty is available.	75
Table B-25. Capsule 7 OR, axial top: decay-corrected concentrations (Bq per mm ³) of selected fission products for each radial segment sampled at the axial top of the Capsule 7 OR. The volume and average radius $[(r_{\text{inner}} + r_{\text{outer}})/2]$ of each segment are also given. Shading indicates a value derived from an MDA.....	76
Table B-26. Capsule 7 OR, axial top: decay-corrected concentrations (particle equivalents per mm ³) of selected fission products for each radial segment sampled at the axial top of the Capsule 7 OR. The volume and average radius $[(r_{\text{inner}} + r_{\text{outer}})/2]$ of each segment are also given. Shading indicates a value derived from an MDA.	77
Table B-27. Estimated relative uncertainties in the concentrations reported for OR-07 Top in Table B-25 and Table B-26. Absolute uncertainties in the segment volumes and average radii of the segments. N/A denotes a case where an isotope was not detected, and therefore, no uncertainty is available.	78
Table B-28. Capsule 7 OR, axial center: decay-corrected concentrations (Bq per mm ³) of selected fission products for each radial segment sampled at the axial center of the Capsule 7 OR. The volume and average radius $[(r_{\text{inner}} + r_{\text{outer}})/2]$ of each segment are also given. Shading indicates a value derived from an MDA.....	79
Table B-29. Capsule 7 OR, axial center: decay-corrected concentrations (particle equivalents per mm ³) of selected fission products for each radial segment sampled at the axial center of the Capsule 7 OR. The volume and average radius $[(r_{\text{inner}} + r_{\text{outer}})/2]$ of each segment are also given. Shading indicates a value derived from an MDA.	80
Table B-30. Estimated relative uncertainties in the concentrations reported for OR-07 center in Table B-28 and Table B-29. Absolute uncertainties in the segment volumes and average radii of the segments. N/A denotes a case where an isotope was not detected, and therefore, no uncertainty is available.	81
Table B-31. Capsule 8 IR, axial center: decay-corrected concentrations (Bq per mm ³) of selected fission products for each radial segment sampled at the axial center of the Capsule 8 IR. The volume and average radius $[(r_{\text{inner}} + r_{\text{outer}})/2]$ of each segment are also given. Shading indicates a value derived from an MDA.....	82
Table B-32. Capsule 8 IR, axial center: decay-corrected concentrations (particle equivalents per mm ³) of selected fission products for each radial segment sampled at the axial center of the Capsule 8 IR. The volume and average radius $[(r_{\text{inner}} + r_{\text{outer}})/2]$ of each segment are also given. Shading indicates a value derived from an MDA.	83
Table B-33. Estimated relative uncertainties in the concentrations reported for IR-08 center in Table B-31 and Table B-32. Absolute uncertainties in the segment volumes and	

average radii of the segments. N/A denotes a case where an isotope was not detected, and therefore, no uncertainty is available.	84
Table B-34. Capsule 8 IR, axial bottom: decay-corrected concentrations (Bq per mm ³) of selected fission products for each radial segment sampled at the axial bottom of the Capsule 8 IR. The volume and average radius $[(r_{\text{inner}} + r_{\text{outer}})/2]$ of each segment are also given. Shading indicates a value derived from an MDA.....	85
Table B-35. Capsule 8 IR, axial bottom: decay-corrected concentrations (particle equivalents per mm ³) of selected fission products for each radial segment sampled at the axial bottom of the Capsule 8 IR. The volume and average radius $[(r_{\text{inner}} + r_{\text{outer}})/2]$ of each segment are also given. Shading indicates a value derived from an MDA.....	86
Table B-36. Estimated relative uncertainties in the concentrations reported for IR-08 bottom in Table B-34 and Table B-35. Absolute uncertainties in the segment volumes and average radii of the segments. N/A denotes a case where an isotope was not detected, and therefore, no uncertainty is available.	87
Table B-37. Capsule 8 OR, axial center: decay-corrected concentrations (Bq per mm ³) of selected fission products for each radial segment sampled at the axial center of the Capsule 8 OR. The volume and average radius $[(r_{\text{inner}} + r_{\text{outer}})/2]$ of each segment are also given. Shading indicates a value derived from an MDA.....	88
Table B-38. Capsule 8 OR, axial center: decay-corrected concentrations (particle equivalents per mm ³) of selected fission products for each radial segment sampled at the axial center of the Capsule 8 OR. The volume and average radius $[(r_{\text{inner}} + r_{\text{outer}})/2]$ of each segment are also given. Shading indicates a value derived from an MDA.	89
Table B-39. Estimated relative uncertainties in the concentrations reported for OR-08 center in Table B-37 and Table B-38. Absolute uncertainties in the segment volumes and average radii of the segments. N/A denotes a case where an isotope was not detected, and therefore, no uncertainty is available.	90
Table B-40. Capsule 8 OR, axial bottom: decay-corrected concentrations (Bq per mm ³) of selected fission products for each radial segment sampled at the axial bottom of the Capsule 8 OR. The volume and average radius $[(r_{\text{inner}} + r_{\text{outer}})/2]$ of each segment are also given. Shading indicates a value derived from an MDA. Shaded column headings denote segments with greater (but unknown) uncertainty due to ring cracking during sampling.....	91
Table B-41. Capsule 8 OR, axial bottom: decay-corrected concentrations (particle equivalents per mm ³) of selected fission products for each radial segment sampled at the axial bottom of the Capsule 8 OR. The volume and average radius $[(r_{\text{inner}} + r_{\text{outer}})/2]$ of each segment are also given. Shaded column headings denote segments with greater (but unknown) uncertainty due to ring cracking during sampling.	92
Table B-42. Estimated relative uncertainties in the concentrations reported for OR-08 bottom in Table B-40 and Table B-41. Absolute uncertainties in the segment volumes and average radii of the segments. N/A denotes a case where an isotope was not detected, and therefore, no uncertainty is available. Shaded column headings denote segments with greater (but unknown) uncertainty due to ring cracking during sampling.....	93
Table B-43. Capsule 10 IR, axial center: decay-corrected concentrations (Bq per mm ³) of selected fission products for each radial segment sampled at the axial center of the Capsule 10 IR. The volume and average radius $[(r_{\text{inner}} + r_{\text{outer}})/2]$ of each segment are also given. Shading indicates a value derived from an MDA.....	94

Table B-44. Capsule 10 IR, axial center: decay-corrected concentrations (particle equivalents per mm ³) of selected fission products for each radial segment sampled at the axial center of the Capsule 10 IR. The volume and average radius $[(r_{\text{inner}} + r_{\text{outer}})/2]$ of each segment are also given. Shading indicates a value derived from an MDA.	95
Table B-45. Estimated relative uncertainties in the concentrations reported for IR-10 center in Table B-43 and Table B-44. Absolute uncertainties in the segment volumes and average radii of the segments. N/A denotes a case where an isotope was not detected, and therefore, no uncertainty is available.	96
Table B-46. Capsule 10 IR, axial bottom: decay-corrected concentrations (Bq per mm ³) of selected fission products for each radial segment sampled at the axial bottom of the Capsule 10 IR. The volume and average radius $[(r_{\text{inner}} + r_{\text{outer}})/2]$ of each segment are also given. Shading indicates a value derived from an MDA.	97
Table B-47. Capsule 10 IR, axial bottom: decay-corrected concentrations (particle equivalents per mm ³) of selected fission products for each radial segment sampled at the axial bottom of the Capsule 10 IR. The volume and average radius $[(r_{\text{inner}} + r_{\text{outer}})/2]$ of each segment are also given. Shading indicates a value derived from an MDA.	98
Table B-48. Estimated relative uncertainties in the concentrations reported for IR-10 bottom in Table B-46 and Table B-47. Absolute uncertainties in the segment volumes and average radii of the segments. N/A denotes a case where an isotope was not detected, and therefore, no uncertainty is available.	99
Table B-49. Capsule 10 OR, axial center: decay-corrected concentrations (Bq per mm ³) of selected fission products for each radial segment sampled at the axial center of the Capsule 10 OR. The volume and average radius $[(r_{\text{inner}} + r_{\text{outer}})/2]$ of each segment are also given. Shading indicates a value derived from an MDA.	100
Table B-50. Capsule 10 OR, axial center: decay-corrected concentrations (particle equivalents per mm ³) of selected fission products for each radial segment sampled at the axial center of the Capsule 10 OR. The volume and average radius $[(r_{\text{inner}} + r_{\text{outer}})/2]$ of each segment are also given. Shading indicates a value derived from an MDA.	101
Table B-51. Estimated relative uncertainties in the concentrations reported for OR-10 center in Table B-49 and Table B-50. Absolute uncertainties in the segment volumes and average radii of the segments. N/A denotes a case where an isotope was not detected, and therefore, no uncertainty is available.	102
Table B-52. Capsule 10 OR, axial bottom: decay-corrected concentrations (Bq per mm ³) of selected fission products for each radial segment sampled at the axial bottom of the Capsule 10 OR. The volume and average radius $[(r_{\text{inner}} + r_{\text{outer}})/2]$ of each segment are also given. Shaded cells indicate a value derived from an MDA. Shaded column headings denote segments with greater (but unknown) uncertainty due to ring movement during sampling.	103
Table B-53. Capsule 10 OR, axial bottom: decay-corrected concentrations (particle equivalents per mm ³) of selected fission products for each radial segment sampled at the axial bottom of the Capsule 10 OR. The volume and average radius $[(r_{\text{inner}} + r_{\text{outer}})/2]$ of each segment are also given. Shading indicates a value derived from an MDA. Shaded column headings denote segments with greater (but unknown) uncertainty due to ring movement during sampling.	104
Table B-54. Estimated relative uncertainties in the concentrations reported for OR-10 Bottom in Table B-52 and Table B-53. Absolute uncertainties in the segment volumes and	

average radii of the segments. N/A denotes a case where an isotope was not detected, and therefore, no uncertainty is available. Shaded column headings denote segments with greater (but unknown) uncertainty due to ring movement during sampling.	105
Table B-55. Capsule 12 IR, axial center: decay-corrected concentrations (Bq per mm ³) of selected fission products for each radial segment sampled at the axial center of the Capsule 12 IR. The volume and average radius $[(r_{\text{inner}} + r_{\text{outer}})/2]$ of each segment are also given. Shading indicates a value derived from an MDA.....	106
Table B-56. Capsule 12 IR, axial center: decay-corrected concentrations (particle equivalents per mm ³) of selected fission products for each radial segment sampled at the axial center of the Capsule 12 IR. The volume and average radius $[(r_{\text{inner}} + r_{\text{outer}})/2]$ of each segment are also given. Shading indicates a value derived from an MDA.	107
Table B-57. Estimated relative uncertainties in the concentrations reported for IR-12 Center in Table B-55 and Table B-56. Absolute uncertainties in the segment volumes and average radii of the segments. N/A denotes a case where an isotope was not detected, and therefore, no uncertainty is available.	108
Table B-58. Capsule 12 IR, axial bottom: decay-corrected concentrations (Bq per mm ³) of selected fission products for each radial segment sampled at the axial bottom of the Capsule 12 IR. The volume and average radius $[(r_{\text{inner}} + r_{\text{outer}})/2]$ of each segment are also given. Shading indicates a value derived from an MDA.	109
Table B-59. Capsule 12 IR, axial bottom: decay-corrected concentrations (particle equivalents per mm ³) of selected fission products for each radial segment sampled at the axial bottom of the Capsule 12 IR. The volume and average radius $[(r_{\text{inner}} + r_{\text{outer}})/2]$ of each segment are also given. Shading indicates a value derived from an MDA.....	110
Table B-60. Estimated relative uncertainties in the concentrations reported for IR-12 bottom in Table B-58 and Table B-59. Absolute uncertainties in the segment volumes and average radii of the segments. N/A denotes a case where an isotope was not detected, and therefore, no uncertainty is available.	111
Table B-61. Capsule 12 OR, axial center: decay-corrected concentrations (Bq per mm ³) of selected fission products for each radial segment sampled at the axial center of the Capsule 12 OR. The volume and average radius $[(r_{\text{inner}} + r_{\text{outer}})/2]$ of each segment are also given. Shading indicates a value derived from an MDA.	112
Table B-62. Capsule 12 OR, axial center: decay-corrected concentrations (particle equivalents per mm ³) of selected fission products for each radial segment sampled at the axial center of the Capsule 12 OR. The volume and average radius $[(r_{\text{inner}} + r_{\text{outer}})/2]$ of each segment are also given. Shading indicates a value derived from an MDA.....	113
Table B-63. Estimated relative uncertainties in the concentrations reported for OR-12 Center in Table B-61 and Table B-62. Absolute uncertainties in the segment volumes and average radii of the segments. N/A denotes a case where an isotope was not detected, and therefore, no uncertainty is available.	114
Table B-64. Capsule 12 OR, axial bottom: decay-corrected concentrations (Bq per mm ³) of selected fission products for each radial segment sampled at the axial bottom of the Capsule 12 OR. The volume and average radius $[(r_{\text{inner}} + r_{\text{outer}})/2]$ of each segment are also given. Shading indicates a value derived from an MDA.	115
Table B-65. Capsule 12 OR, axial bottom: decay-corrected concentrations (particle equivalents per mm ³) of selected fission products for each radial segment sampled at the axial	

bottom of the Capsule 12 OR. The volume and average radius $[(r_{\text{inner}} + r_{\text{outer}})/2]$ of each segment are also given. Shading indicates a value derived from an MDA.	116
Table B-66. Estimated relative uncertainties in the concentrations reported for OR-12 bottom in Table B-64 and Table B-65. Absolute uncertainties in the segment volumes and average radii of the segments. N/A denotes a case where an isotope was not detected, and therefore, no uncertainty is available.	117
Table C-1. Ratio of the maximum possible concentration of cross-contamination (that could be carried over from the last sample at axial location A to the first sampled at axial location B) to the actual measured concentration in the next sample. Rings from Capsule 5 were only sampled at the center axial location; therefore, they are not subject to this potential source of cross-contamination.	120
Table C-2. Order of AGR-3/4 rings physical sampling.	121
Table C-3. Comparisons of the activities and concentrations of samples of the irradiated rings to the clean graphite samples taken before and after sampling the irradiated rings.	122

Page intentionally left blank

ACRONYMS

AGR	Advanced Gas Reactor
ART	Advanced Reactor Technologies
ATR	Advanced Test Reactor
DTF	designed-to-fail
EOI	end-of-irradiation
FB	fuel body
FIMA	fissions per initial heavy metal atom
HFEF	Hot Fuel Examination Facility
HTGR	high-temperature gas-cooled reactor
ICP-MS	inductively-coupled plasma mass spectrometry
INL	Idaho National Laboratory
IPyC	inner pyrolytic carbon
IR	inner ring
LI	laboratory instruction
M/C	measured-to-calculated ratio
MDA	minimum detectable activity
m/z	mass-to-charge ratio
OD	outer diameter
OPyC	outer pyrolytic carbon
OR	outer ring
ORNL	Oak Ridge National Laboratory
PGS	Precision Gamma Scanner
PIE	post-irradiation examination
PNNL	Pacific Northwest National Laboratory
SiC	silicon carbide
TAVA	time-averaged volume-averaged
TRISO	tristructural isotropic
UCO	uranium oxycarbide

Page intentionally left blank

Measurement of Fission Product Concentration Profiles in AGR-3/4 TRISO Fuel Graphitic Matrix and Nuclear Graphites

1. INTRODUCTION

1.1 Overall Program Purpose

The Advanced Gas Reactor (AGR) Fuel Development and Qualification Program was established to perform research and development on tristructural isotropic (TRISO)-coated particle fuel to support deploying a high-temperature gas-cooled reactor (HTGR). This work continues as part of the Advanced Reactor Technologies (ART) Program. The program's overarching goal is to provide a baseline fuel qualification dataset to support licensing and operating an HTGR. To achieve these goals, the program includes the elements of fuel fabrication, irradiation, post-irradiation examination (PIE), safety/heating testing, fuel performance modeling, and fission product transport (Idaho National Laboratory 2020). Several fuel-irradiation experiments have been performed at the Advanced Test Reactor (ATR) at Idaho National Laboratory (INL), and AGR-5/6/7, the fourth and final irradiation, began in February 2018 and ended on July 22, 2020. These experiments are intended to provide data on fuel performance under irradiation, support fuel fabrication process development, qualify fuel for operating and accident conditions, provide irradiated fuel for accident testing, and support the development of fuel performance and fission product transport models.

1.2 Purpose of AGR-3/4

AGR-3/4 was designed to investigate the migration of fission products in the fuel compact graphitic matrix and reactor graphite components (Collin et al. 2018). The experiment consisted of fuel compacts containing TRISO-coated driver-fuel particles similar to AGR-1 baseline fuel (Collin 2015a; Hunn and Lowden 2007; Hunn et al. 2014) and designed-to-fail (DTF) particles that are designed to release fission products during irradiation to migrate through the surrounding cylindrical rings of graphitic matrix and nuclear-grade graphite. Following irradiation, PIE measurements of the fission product concentration profiles (axially and radially) within AGR-3/4 samples (primarily the graphite rings and compacts) are significant activities within the AGR-3/4 PIE plan (Demkowicz 2017). These data will be used to support refinement of fission product transport models and HTGR source-term analyses.

1.3 AGR-3/4 Fuel Description

The AGR-1 and AGR-2 experiments focused on the performance of high-quality TRISO fuel, and PIE focused on quantifying the very small rates of SiC and TRISO coating failures. In contrast, the AGR-3/4 experiment was primarily a fission product transport experiment focused on observing the migration of fission products throughout the fuel, graphitic matrix material, and nuclear-grade graphites in the presence of exposed fuel kernels (Collin et al. 2018). A feature of AGR-3/4 fuel that sets it apart from AGR-1 and AGR-2 was the incorporation of 20 DTF particles in each compact in addition to the approximately 1898 TRISO-coated "driver" fuel particles. DTF fuel kernels were coated only with a thin (20- μ m-thick) pyrocarbon layer. This layer was intentionally fabricated with high anisotropy, so it would be likely to fail during the irradiation (Collin 2015a; Hunn and Miller 2009; and Kercher et al. 2011) resulting in up to 20 exposed fuel kernels per compact. As shown on the right in Figure 1, the DTF particles (highlighted in red) were aligned roughly along the compact radial centerline. DTF particles provided a known source of fission products to migrate radially outward in the compacts and into the surrounding concentric rings of graphite and/or matrix material. It was expected that intact DTF particles would behave like TRISO particles with SiC layer failures (releasing substantial Cs but retaining fission

gases), and failed DTF particles (DTF particles with breached pyrocarbon layers) would behave like TRISO particles with failed TRISO coatings (releasing both Cs and fission gases).

The white particles in Figure 1 are the driver particles. AGR-3/4 driver particle fuel kernels were fully TRISO-coated with buffer layer, inner pyrolytic carbon (IPyC) layer, silicon carbide (SiC) layer, and outer pyrolytic carbon (OPyC) layer with characteristics similar to the “baseline” variant from the AGR-1 experiment (Collin 2015b; Hunn and Lowden 2007). Both the AGR-3/4 driver and DTF fuel particles contain UCO fuel kernels (approximately 350 μm in diameter) manufactured at BWX Technologies Nuclear Operations Group (Lynchburg, VA). The U-235 enrichment was 19.7 wt%. The DTF pyrocarbon coating and the driver-fuel TRISO coatings were applied to the kernels at Oak Ridge National Laboratory (ORNL). Driver particle and DTF particle properties are summarized in (Collin 2015a). Complete kernel and particle characterization and fabrication data are compiled in several reports and papers (Kercher and Hunn 2006; Hunn and Lowden 2007; Hunn and Miller 2009; Kercher et al., 2011). Driver-fuel particles and DTF particles had average dimensions summarized in Table 1.

AGR-3/4 driver and DTF particles were overcoated with a precursor to graphitic matrix material and formed into cylindrical fuel compacts at ORNL. The compact graphitic matrix material is composed of multiple types of graphite and a carbonized phenolic resin. Compacts were nominally 12.3 mm in diameter and 12.5 mm long (in contrast to the AGR-1 and AGR-2 compacts, which were approximately 12.3 mm in diameter and 25 mm long). A summary of AGR-3/4 fuel compact properties is provided in the AGR-3/4 Final As-Run Report (Collin 2015a). Detailed characterization data of the as-fabricated compacts were compiled in an ORNL report (Hunn, Trammel, and Montgomery 2011).

In the X-Y compact naming convention, X denotes the capsule number, and Y denotes the level of the compact within the capsule (with level 1 at the bottom and level 4 at the top of the capsule). In AGR-3/4, there were four compacts per capsule. Thus, for example, Compact 3-3 is the third compact from the bottom of Capsule 3, and Compact 12-1 is the bottom compact from Capsule 12.

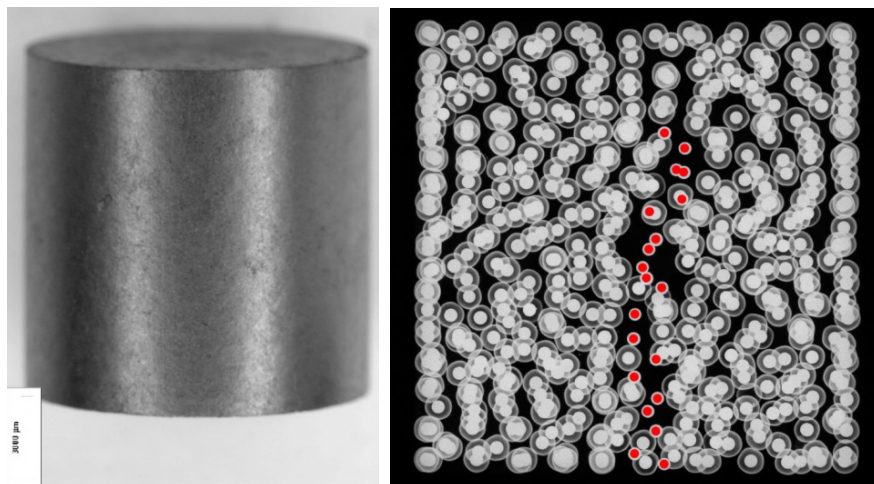


Figure 1. Image of an AGR-3/4 fuel compact (left) and x-ray side view image (right) (Hunn, Trammell, and Montgomery 2011). DTF particles are highlighted with red dots in the x-ray image.

Table 1. As-fabricated particle dimensions and standard deviations from Table A-2 of Collin (Collin 2015a).

DTF Particle Properties	
Kernel diameter (μm)	357.3 ± 10.5
DTF pyrocarbon thickness (μm)	20.0 ± 9
DTF particle overall diameter (μm)	400.0 ± 9.2
Driver Particle Properties	
Kernel diameter (μm)	357.3 ± 10.5
Buffer thickness (μm)	109.7 ± 7.7
IPyC thickness (μm)	40.4 ± 2.3
SiC thickness (μm)	33.5 ± 1.1
OPyC thickness (μm)	41.3 ± 2.1
Driver particle overall diameter (μm)	818.9 ± 14.2

1.4 AGR-3/4 Test Train, Irradiation, Graphite, and Graphitic Rings

The AGR-3/4 irradiation test train consisted of 12 capsules numbered 1 through 12 from the bottom to the top of the ATR core (Collin et al. 2018). Each capsule contained four fuel compacts. Figure 2 shows a cross section of an AGR-3/4 irradiation capsule. The compacts were stacked vertically in the center of concentric rings made from graphitic matrix material and/or structural graphite (IG-110 and PCEA). Toyo Tanso IG-110 is an isostatically molded graphite with fine grains, and GrafTech PCEA is an extruded graphite. The matrix rings were produced at ORNL using a recipe similar to the historic German A3-27 formulation (Hunn et al. 2011). These matrix rings were fabricated with a blend of natural and synthetic graphite flake mixed with Hexion SD-1708 novolac resin. BWXT provided this blend of graphite flake and resin to ORNL.

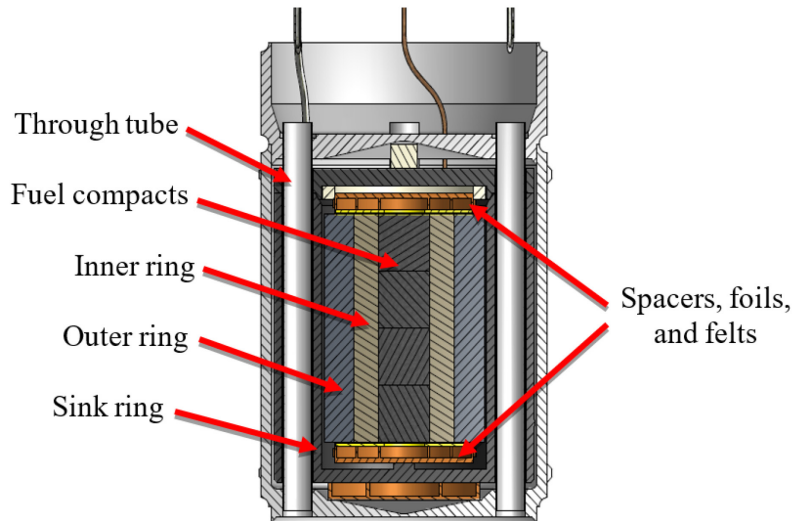


Figure 2. Axial cutaway diagram of a standard AGR-3/4 irradiation capsule.

Table 2 lists the materials, types of capsules, and PIE measurement diameters for each ring. There were two types of capsules: “standard” and “fuel body (FB).” The standard capsule type is depicted in Figure 2 where the outer ring (OR) is open on its top and bottom. Fuel bodies, on the other hand, had floors and a lid that screwed on to the top of the OR. Each capsule also included several small spacers of

various materials (graphite, zirconia, or zircaloy-4) and graphite foils to separate components and act as thermal barriers to control temperature in the compacts. Compact lengths were measured as part of PIE, but ring lengths were not measured. All inner rings (IRs) had as-fabricated lengths of 50.8 mm (2.0 in.). In standard capsules, OR lengths were 50.8 mm (2.0 in.). In fuel bodies, the ORs had a sealed bottom and a lid for a total overall length of about 61.0 mm (2.4 in.). Sink ring lengths were generally about 63.5 mm (2.5 in.); however, some sink rings were about 71.1 mm (2.8 in.) long. All sink rings had lids and sealed bottoms.

Figure 3 summarizes the time-averaged, volume-averaged (TAVA) irradiation temperature for each major component (i.e., fuel compacts, IR, OR, and sink ring) within each capsule. Sink rings were intentionally cold to act as a sink to stop further radial transport of fission products during the experiment. In Figure 3, the plotted compact temperature was averaged over the four compacts in a given capsule. The burnup and TAVA temperature for each individual compact are shown in Figure 4.

Table 2. AGR-3/4 capsule types, ring materials, and ring dimensions from PIE (Stempien et al. 2016). Complete dimensions and uncertainties are also in that report.

Capsule No.	Capsule Type	Ring Material			IR Diameters (mm)		OR Diameters (mm)		Sink Ring Diameters (mm)	
		Inner	Outer	Sink	ID	OD	ID	OD	ID	OD
1	Std	Matrix	PCEA	PCEA	12.55	23.61	24.53	33.50	41.21	61.59
2	FB	Matrix	PCEA	PCEA	N/A	N/A	N/A	36.72	39.33	62.05
3	Std	PCEA	PCEA	PCEA	12.62	24.03	24.86	33.08	41.42	63.56
4	FB	Matrix	PCEA	PCEA	12.71	23.87	24.70	39.24	39.48	63.32
5	Std	Matrix	PCEA	PCEA	12.67	23.89	24.68	39.39	39.54	63.61
6	FB	Matrix	PCEA	PCEA	N/A	N/A	N/A	39.33	39.48	63.30
7	Std	Matrix	PCEA	PCEA	12.75	23.67	24.93	37.35	39.53	63.63
8	Std	IG-110	IG-110	PCEA	12.60	24.07	24.77	38.55	39.57	63.64
9	FB	Matrix	IG-110	PCEA	N/A	N/A	N/A	39.27	39.46	63.08
10	Std	PCEA	PCEA	PCEA	12.58	24.04	24.83	37.48	39.40	63.43
11	FB	Matrix	PCEA	PCEA	N/A	N/A	N/A	33.29	N/A	N/A
12	Std	Matrix	PCEA	PCEA	12.47	24.23	24.51	34.98	39.34	61.60
Std: standard capsule N/A: not available										

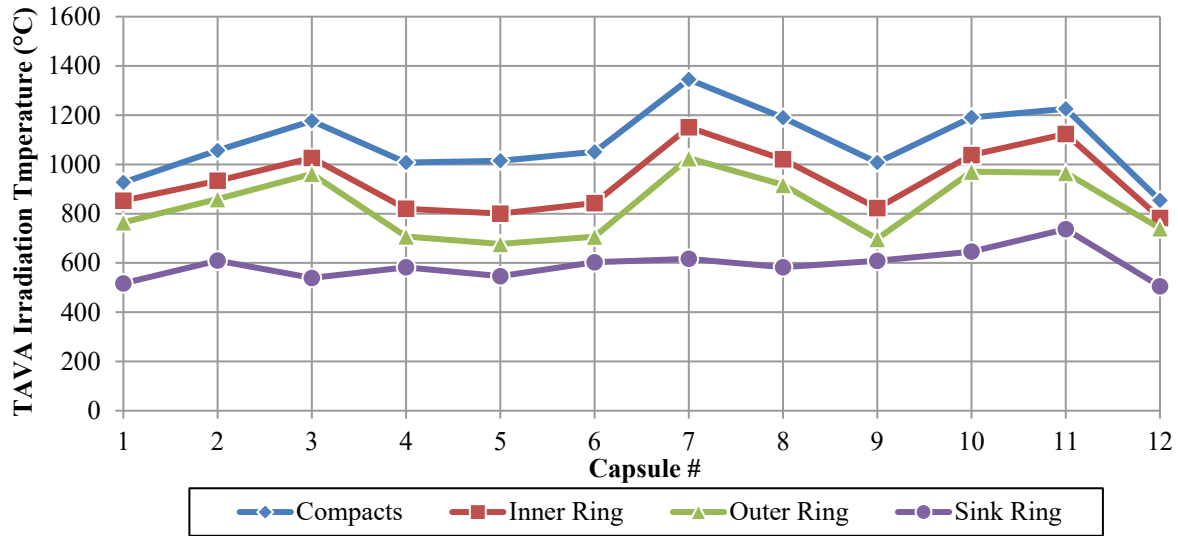


Figure 3. Capsule-averaged TAVA irradiation temperatures for major capsule components from Hawkes (Hawkes 2016).

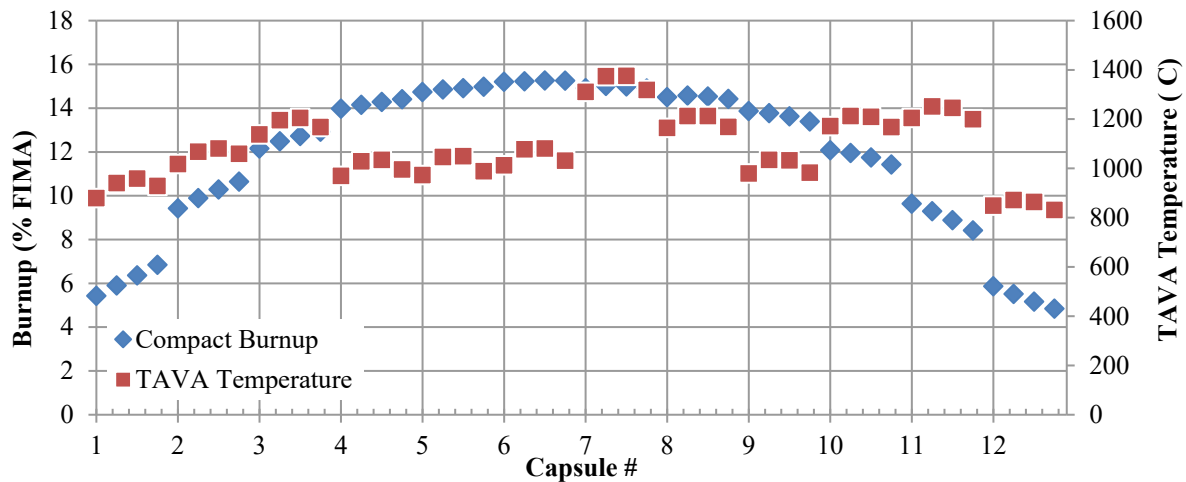


Figure 4. Calculated burnup and TAVA temperature for each of the four compacts in each of the 12 AGR-3/4 capsules. FIMA = fissions per initial heavy metal atom. (Hawkes 2016; Sterbentz 2015).

2. EXPERIMENTAL METHODS

2.1 Non-destructive Gamma Scanning

At the completion of the irradiation in ATR, all irradiation capsules were separated from each other (Stempien et al. 2016). The graphite sink rings were recovered from all capsules (i.e., both the FB and standard capsules). All the standard capsules were further disassembled, and their contents, including the compacts and carbonaceous rings, were recovered for analysis. Of the fuel bodies, only Capsule 4 was disassembled to recover the OR, IR, and compacts. The remaining fuel bodies have been retained intact, as they are to be subjected to post-irradiation heating tests to examine fission product release at elevated temperatures in varying atmospheres.

Compacts and IR/OR were gamma scanned on the Precision Gamma Scanner (PGS) to determine their total inventories of gamma-emitting fission products and collect data on the spatial distribution of

the inventories in the rings (Harp et al. 2020). The total ring inventories were obtained by putting the PGS collimator in its horizontal orientation and scanning axially from top to bottom along the length of one half of the ring (Harp et al. 2020). Then, a second axial scan was performed along the second half of the ring. These scans also provided information on the axial variation in ring activity. In locations of interest (i.e., the top, bottom, or center of the ring), the PGS detector collimator was then rotated to a vertical orientation, and the ring was scanned horizontally across its diameter at a specific axial location at multiple angles to the detector. These tomographic scans were used to construct 2D maps of fission product activities at the desired axial location. Table 3 summarizes the PGS axial scans and tomographic scans completed for the AGR-3/4 IR and OR. The table also gives the axial location(s) where the tomographic scans were acquired. An iterative technique that eliminates artifacts in the reconstructions of these tomograms (Humrickhouse et al. 2018) is being employed to provide azimuthally averaged radial fission product concentration profiles that can be compared to the results obtained from destructive physical sampling described in Section 2.2.

The sink rings, spacers, felts, and foils from each capsule were gamma counted at the Analytical Laboratory and constituted the rest of the fission product “mass balance” aside from the IR, OR, and four fuel compacts for each capsule (Stempien et al. 2018).

2.2 Destructive Ring “Physical Sampling” for Fission Product Measurements

The physical sampling was performed according HFEF laboratory instruction (LI), HFEF-LI-0162 (INL, 2017). Physical sampling of the rings involved machining/milling material from around the circumference of the rings, collecting that material, and analyzing it for gamma-emitting fission products and beta-emitting Sr-90. The endmill was a flat-tipped (i.e., neither concave nor convex), four-flute, tungsten-carbide bit nominally 10.00 mm in diameter. Milling operations were performed in multiple steps, and each step was generally 0.508 mm (0.020 in) thick. The total number of steps required varied with the ring thickness. Some rings only required 11 steps; however, the Capsule 5 OR was the thickest and required 15 steps. The fines from milling each step were collected in individual vials. Vials were labeled according to the capsule number, whether the ring was the IR or OR, the axial location that was being sampled (i.e., top, center, or bottom), and the number of the sample. For a particular ring at a particular axial location, samples were numbered using an outside-in approach. Table 3 summarizes the physical sampling processes and PGS scans completed on the IRs and ORs from AGR-3/4. The axial locations of the rings where the samples were taken are also given.

Table 3. Summary of completed AGR-3/4 rings PGS gamma scanning and physical sampling processes.

Capsule	Type	Ring Material		Axial PGS		PGS Tomography		Physical Sampling	
		Inner	Outer	Inner	Outer	Inner	Outer	Inner	Outer
1	Std	Matrix	PCEA	Y	Y	N	N	N	N
2	FB	Matrix	PCEA	N	N	N	N	N	N
3	Std	PCEA	PCEA	Y	Y	Top and Center	Center	Top and Center	Top and Center
4	FB	Matrix	PCEA	Y	Y	Center	N	N	N
5	Std	Matrix	PCEA	Y	Y	Center	N	Center	Center
6	FB	Matrix	PCEA	N	N	N	N	N	N
7	Std	Matrix	PCEA	Y	Y	Center	Center	Top and Center	Top and Center
8	Std	IG-110	IG-110	Y	Y	Top and Center	Center	Center and Bottom	Center and Bottom
9	FB	Matrix	IG-110	N	N	N	N	N	N
10	Std	PCEA	PCEA	Y	Y	Top and Center	N	Center and Bottom	Center and Bottom
11	FB	Matrix	PCEA	N	N	N	N	N	N
12	Std	Matrix	PCEA	Y	Y	N	N	Center and Bottom	Center and Bottom
Y: yes N: no									

Selected steps from and equipment used in HFEF-LI-0162 will be discussed at a high level in the following paragraphs. The first step in the physical sampling process was to fill the ring with epoxy. Epoxy stabilized the ring and prevented cracking and loss of material during milling. At HFEF, the irradiated rings were placed on a piece of rigid tape, and epoxy was poured into the ring's center. Masterbond EP21LV epoxy was used because it was found to bond tightly to the ring without excessively infiltrating or seeping into or through the bulk of the ring. Severe seepage was a problem with very low-viscosity epoxies that were evaluated in out-of-cell testing using unirradiated materials. The rings were weighed before and after filling with epoxy. Figure 5 shows two different views of an unirradiated matrix ring fill with epoxy. The image on the right in Figure 5 shows the ring after milling off the top 1 cm of the matrix material.

Figure 6 shows a simplified illustration of the equipment used to mill the rings. Figure 7 shows a simplified illustration of the vacuum and cyclone separator used to collect the fines as they are milled off the rings. Figure 8 shows photos of these components during Phase II equipment qualifications outside of the hot cell. Epoxy-filled rings were mounted in a rotating chuck beneath the endmill. Using a 10.00-cm wide bit, the endmill removed material from the rings in 11 to 15 steps or cuts. The thickness of the initial cut (at the ring outer surface) and the final cut (at the ring inner surface) was slightly different for each ring because each ring had slightly different inner and outer diameters. Except for the initial cut and final cut, for most rings, each cut depth was 0.508 mm (0.020 in) around the circumference of the ring. The exception was the Capsule 3 OR, which used a series of 0.381 mm (0.015 in) deep cuts. The depth or

thickness of the cuts was verified from the vertical dial indicator shown in Figure 8. This dial indicator was a Starrett 25-2041J, which featured 0.0254 mm (0.001-in) graduations.

A funnel connected to the cyclone separator via a hose was placed around the sample and sucked in fines as the milling progressed (see Figure 9). A tared sample vial was used to collect the fines from each of the cuts. Figure 10 shows the Capsule 8 IR at several points during the collection of the 14 samples (sometimes referred to as cuts or segments). The rightmost image in Figure 10 shows the white epoxy core that remains after all ring material has been removed. Another example in Figure 11 shows what remains of the Capsule 7 IR after milling the axial top and center.

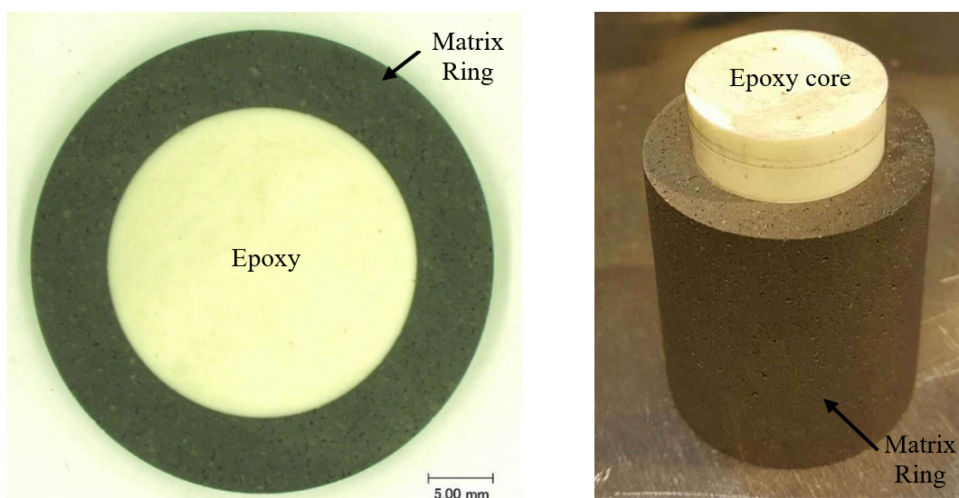


Figure 5. Left: the end of an unirradiated graphitic matrix ring after filling the center with epoxy. Right: unirradiated matrix ring showing the epoxy core after milling the top 1 cm of the ring.

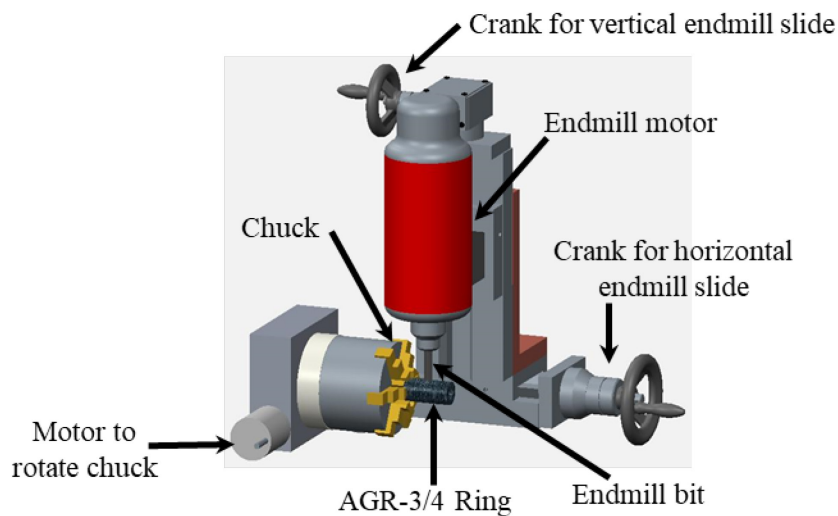


Figure 6. Simplified illustration of endmill.

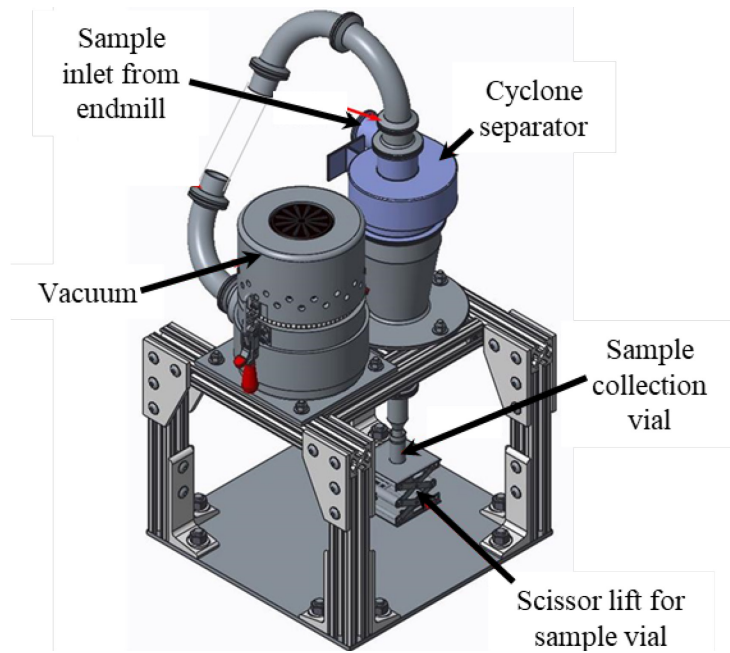


Figure 7. Simplified illustration of cyclone separator.

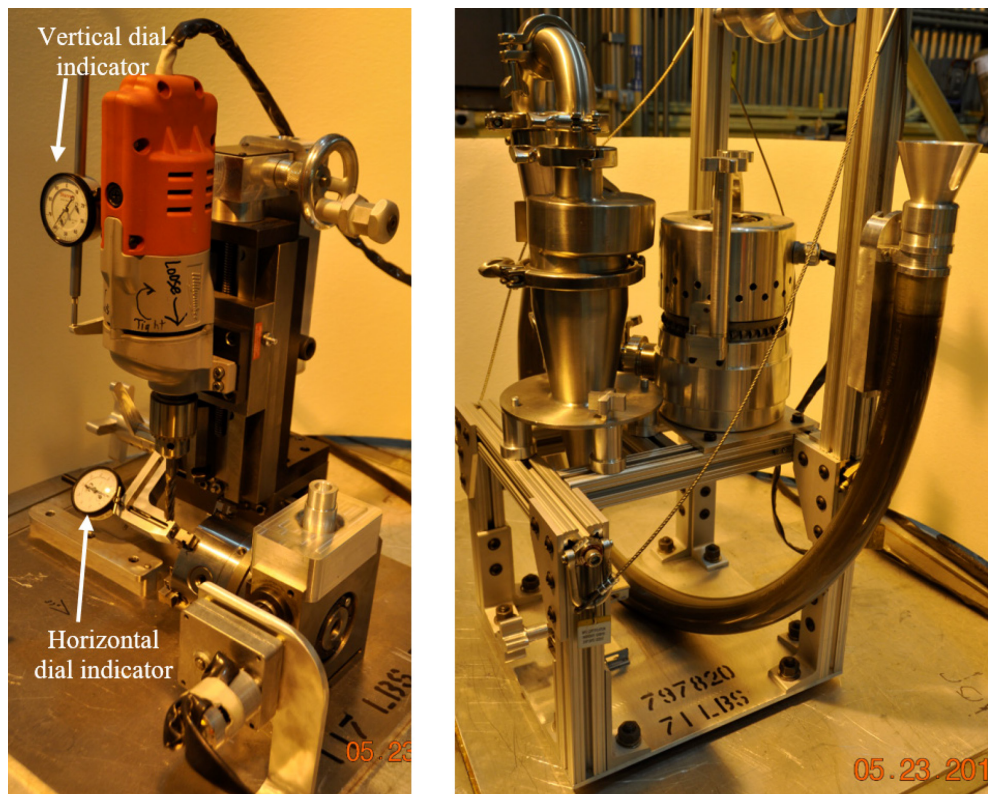


Figure 8. Photos of the endmill (left) and vacuum and cyclone separator (right).

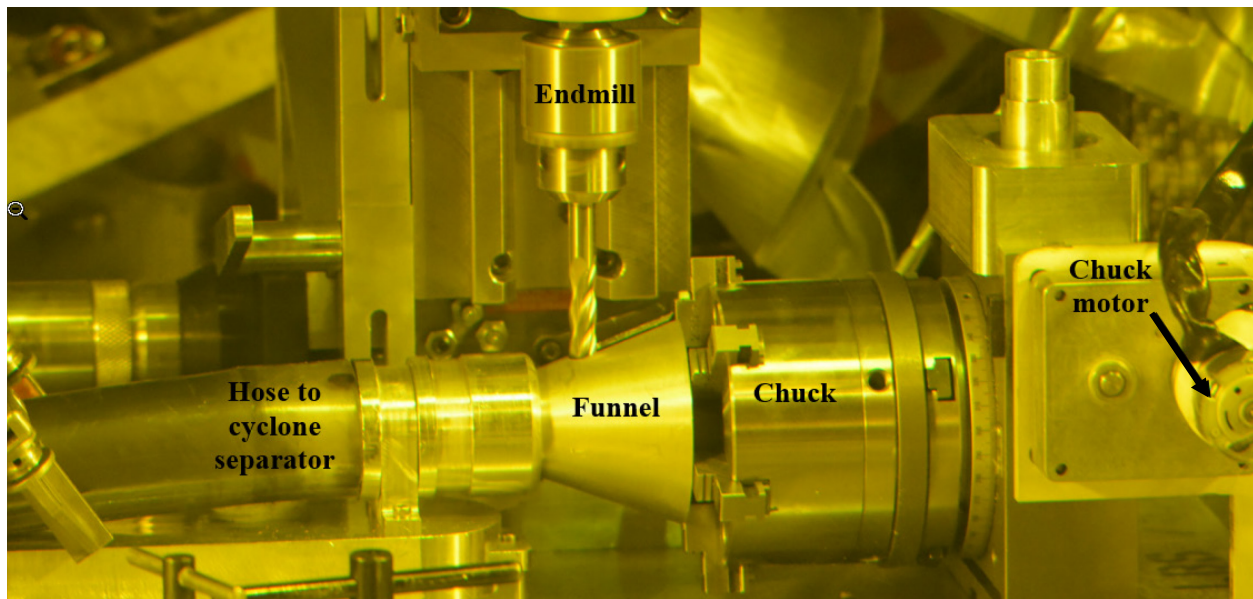


Figure 9. Photo of the funnel, hose to the cyclone separator, chuck, chuck motor, and endmill during Phase III equipment qualifications at HFEF prior to sampling irradiated material.

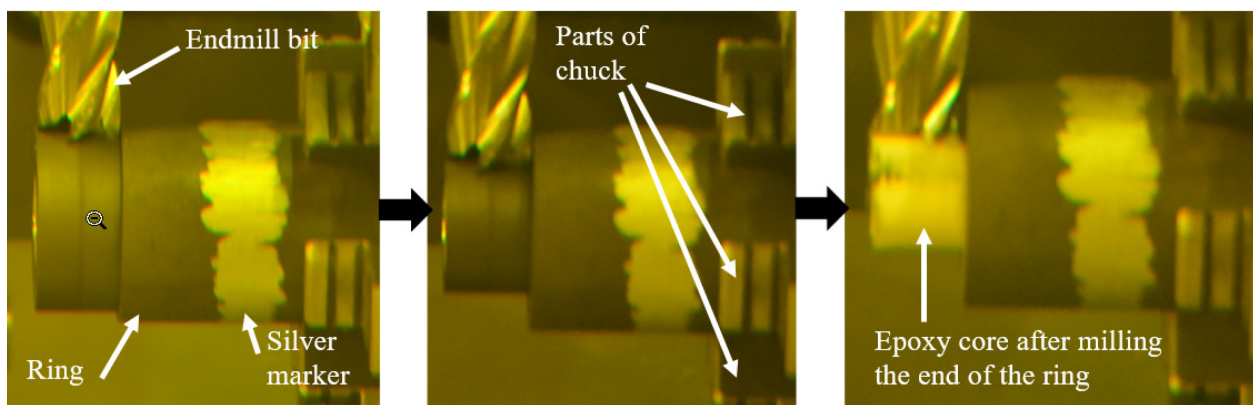


Figure 10. Photos taken after the first, seventh, and fourteenth (final) cuts on the IR from Capsule 8. Note that silver marker was used to indicate when the endmill bit was just in contact with the ring for the initial cut. Silver marker is shown in these images where the ring's axial center was to be milled.

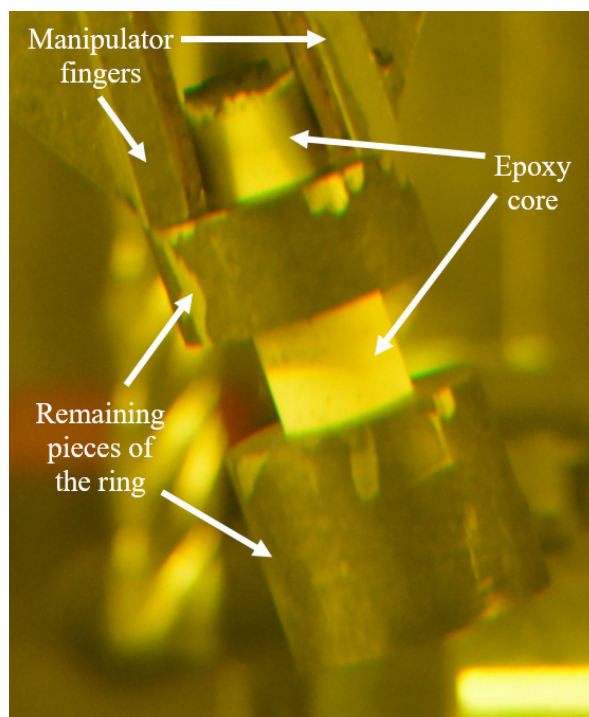


Figure 11. Capsule 7 IR after milling the axial top and center.

To judge hot cell contamination and the potential for cross-contamination from one ring to the next, other samples were taken both before and after sampling each ring. The “environmental” sample was a vial containing about 1 g of clean, unirradiated graphite fines that was left open to the HFEF hot cell atmosphere during sampling. A different environmental sample was left exposed to the hot cell atmosphere during sampling of each ring. Next, a “pre-sample” was taken by using the endmill to machine about 1 g of graphite from clean, unirradiated graphite and using the cyclone separator to collect the fines. This sample was used to judge potential contamination within the cyclone separator prior to the start of sampling the irradiated rings. After setting up the environmental sample and taking the pre-samples, the irradiated ring was sampled. The ORs in some capsules had nubs on their surfaces to maintain gas gaps during irradiation. For example, Figure 12 shows a cross sectional drawing of the Capsule 3 OR. The ORs in Capsules 7, 10, and 12 also had nubs near their ends. Prior to taking circumferential samples of the top or bottom ends of the ORs in Capsules 3, 7, 10, and 12, the nubs at the end of interest were milled and collected in a vial specifically for the nubs. Circumferential sampling at the axial center of the rings was not affected by nubs. The Capsule 5 OR had very small nubs (<0.25 mm tall) at its ends; however, since samples were only taken from the axial center of the Capsule 5 OR, no separate nub samples were collected. The Capsule 8 OR also had very small nubs (~ 0.5 mm tall) that were not sampled separately. They were sampled along with the first segment at the bottom of the ring.

After the environmental sample, pre-samples, and any required nub samples were acquired, the irradiated rings were milled around their circumferences in multiple steps until the entire thickness of the ring had been milled. After all circumferential samples had been taken, three “post-samples” were taken by thrice milling clean unirradiated graphite and collecting it into tared vials via the cyclone separator. Each post-sample was about 1 g of clean graphite fines. The environmental sample, pre-sample, any nub samples, circumferential samples, and all post-samples were sent from INL to Pacific Northwest National Laboratory (PNNL) for radiochemical analyses.

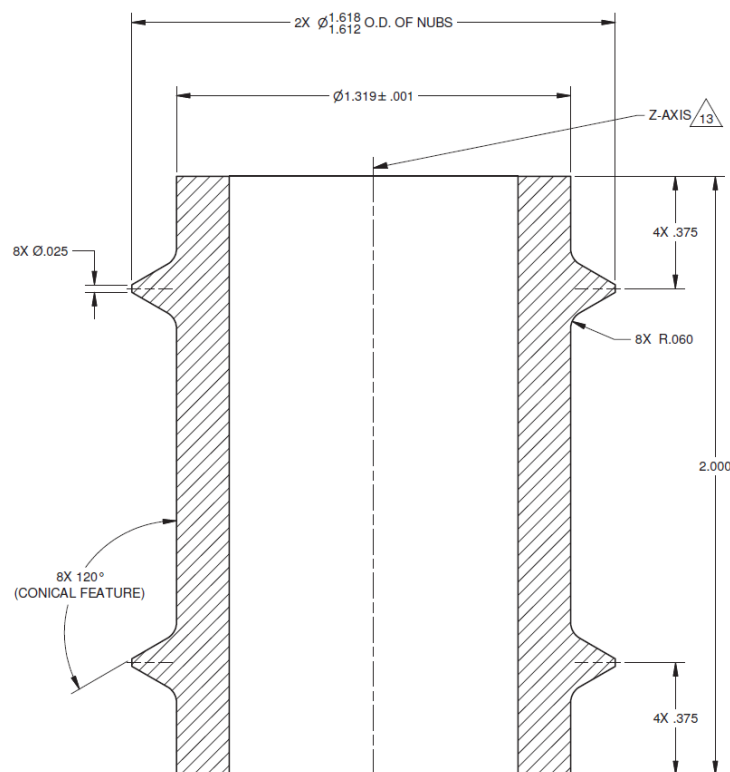


Figure 12. Cross sectional drawing of the Capsule 3 OR (INL, 2011). Certain other outer rings had smaller nubs at similar axial locations.

2.3 Radiochemical Analyses at PNNL

The fines generated from the physical sampling processes were sent to PNNL for analysis. PNNL assigned informal “batch” numbers to the ring samples, and certain batches contained samples from more than one ring. The PNNL radiochemistry report numbers for the different batches of AGR-3/4 ring samples are summarized in Appendix A, Table A-1. Upon receiving the samples at PNNL, the samples were gamma counted for key isotopes such as Ag-110m, Cs-134, Cs-137, Ce-144, Eu-154, and Eu-155. After gamma counting the solid samples (i.e., the fines from milling), the samples were transferred to fused silica beakers and oxidized in a muffle furnace at 750°C for 24 hours. The ash and residue remaining in the beaker was dissolved with HNO₃. In instances where solids did not dissolve using only HNO₃, small amounts of concentrated HF in HNO₃ were used. PNNL reported that solutions with residual solids were centrifuged, the supernate was decanted, and HF and HNO₃ were added. This process was repeated until all solids were dissolved. All the solutions for a given sample were combined. A Sr-90 separation process using an Eichrom strontium resin was then performed for the solutions. After the Sr-90 separation, Sr-90 was quantified by liquid scintillation counting. PNNL counts the separated fraction shortly after separation and then again, several days later, to account for the ingrowth of Y-90 from Sr-90 decay. If the increase in beta activity matches the expected ingrowth, then it is concluded that the separated samples were contaminated by other beta emitters. In the Spring of 2021, PNNL data reviews found that the Sr-90 values initially reported were done so without correcting for ingrowth of Y-90. It was found that the ingrowth of Y-90 was incorrect and indicated the presence of interfering beta emitters. The best approach would have been to perform another Sr-90 separation and recount the samples; however, the samples had been disposed of. Using both the first and second counts, the data were recalculated and the interfering isotopes canceled-out algebraically. In Finally, the solutions were analyzed using inductively coupled plasma-mass spectrometry (ICP-MS) for mass-to-charge ratios (m/z) ranging from 90 to 115.

2.4 General Data Processing

2.4.1 Radionuclide Data and Decay Corrections

Measured radioisotope activities were decay-corrected to April 13, 2014 at 5:00 AM MDT. This date corresponds to the end of the AGR-3/4 irradiation plus one day (end-of-irradiation [EOI]+1). Decay corrections were made using the following equation:

$$A = A_o e^{-\lambda t} \quad (1)$$

where A is the activity at time t , A_o is the activity at $t=0$, and λ is the decay constant. The decay constant is defined as $\lambda = \ln(2)/t_{1/2}$, where $t_{1/2}$ is the half-life. Half-lives for each isotope were taken from the ENDF/B-VII.1 library downloaded on July 9, 2013 (Chadwick et al. 2011). In instances where no activity was detected for a given isotope, minimum detectable activities (MDAs) were determined. These MDAs were also decay-corrected and should be considered an upper bound on the activity of a given component.

A common metric for evaluating the accuracy of physics predictions and/or estimating the release or retention of fission products from the fuel or the graphite rings is to compute the measured-to-calculated ratio (M/C) for isotopes of interest. For example, to determine the fraction of the Cs-134 inventory produced in Capsule X that was measured in that capsule's IR, the measured Cs-134 activity in IR-X was decay-corrected to EOI+1 and divided by the total activity of that isotope predicted from physics calculations to have been produced in Capsule X during irradiation (Sterbentz 2015). Since 20 DTF particles per compact (80 DTF particles per capsule) were incorporated into the AGR-3/4 experiment, it is also useful to consider the ratio of the measured isotopic inventories to the calculated inventory predicted to have been produced in an average particle in a given capsule. This ratio is referred to using the term "particle equivalents." With approximately 1,918 particles per compact (~7,672 particles per capsule), a capsule fraction of $1.30\text{E}-4$ corresponds to a single particle's inventory, and a capsule fraction of $2.6\text{E}-3$ would correspond to 20 particle equivalents (the inventory in 20 particles).

2.4.2 Milled Graphite Ring Dimensions and Volumes

An important result from the ring sampling is the activity concentration of various radionuclides as a function of radius in the ring. To get this quantity, the activity, and the volume of the ring in which that activity was measured, must be known. The isotope activities in the fines collected from each step of milling the rings were determined as described in Section 2.3. Figure 13 illustrates a cut with a certain thickness and width taken around the circumference of a ring at its axial center. The width (w) was determined from the known width of the endmill bit (1 cm), and the depth or thickness (t) of the cut was measured for each cut via the vertical dial indicator used with the endmill (see Figure 8). For cut number n (numbered from the outside in), the volume of that cut V_n is given by the following equation, where r_n is the outer radius of the cut and r_{n+1} is the inner radius of the cut.

$$V_n = \pi w (r_n^2 - r_{n+1}^2) \quad (2)$$

For the first cut on a ring ($n = 1$), r_1 is the outer radius of the ring as determined by PIE metrology reported in Section 5.2 of Stempien et al. 2016. Then, r_2 is given by r_1 minus the cut thickness, t , which was recorded from reading the vertical dial indicator shown in Figure 8. For the second cut ($n = 2$), r_2 was computed previously when calculating V_1 , and r_3 is given by r_2 minus the second cut thickness again determined from the vertical dial indicator. The volumes of each successive cut were calculated in this manner. For the final cut, in order to ensure that all ring material at the ring inner surface was sampled, the cut thickness was set to be thicker than the remaining ring material. If "final" is the total number of cuts used to sample across the entire thickness of a ring, then the final cut volume, V_{final} , is given by the following equation, where r_{final} is the inner radius of the ring reported in Section 5.2 of Stempien et al. 2016, and $r_{final-1}$ is the current outer radius of the ring that resulted from the previous $n = final - 1$ cuts.

$$V_{final} = \pi w (r_{final-1}^2 - r_{final}^2) \quad (3)$$

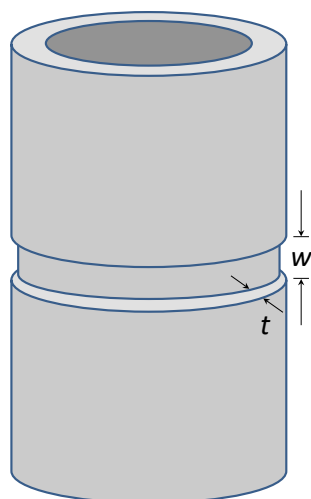


Figure 13. Depiction of a cut of thickness t and width w at the axial center of a ring. Not to scale.

2.4.3 Cyclone Separator Collections Efficiencies

During out-of-cell qualification testing of the equipment used for physical sampling, the cyclone separator collection efficiencies were measured for each of the carbonaceous materials (i.e., graphitic matrix, IG-110, and PCEA). This was performed by first weighing an unirradiated piece of carbonaceous material, then milling it and collecting the fines using the cyclone separator. The milled piece was then weighed to give its mass after it had been milled. The mass of the fines collected was measured and divided by the difference between the starting mass of the unirradiated piece of carbonaceous material and the mass after milling. The resultant fraction was the collection efficiency. This process was repeated 10 times to give an average collection efficiency for each type of material. Table 4 summarizes the collection efficiencies for the three types of carbonaceous materials sampled.

For each section of an irradiated ring that was milled and subjected to radiochemical analysis, the measured activities in that segment were divided by the collection efficiency (expressed as a fraction rather than as a percentage in this case). This was done to account for the loss of material within the cyclone separator.

Table 4. Measured cyclone separator collection efficiencies.

Material	Cyclone Separator Collection Efficiency (%)	Standard Deviation (\pm %)
Graphitic Matrix	99.49	0.43
IG-110	99.44	0.51
PCEA	99.84	0.09

2.4.4 Uncertainty Evaluation

There are several sources of uncertainty in measuring the radial fission product concentration profiles. Some of these are related to the gamma counting and Sr-90 measurements, and some of these are related to the uncertainty in the volume of the milled ring material. The fission product concentrations, the average radial locations at which the concentrations were measured, and the uncertainty of the concentrations are tabulated in Appendix B. An analysis of the potential for cross-contamination is given in Appendix C, where it is concluded that cross-contamination does not significantly affect the results.

The radiochemical analyses were performed at PNNL, and the PNNL data reports give estimated 1- σ uncertainties which account for the statistical counting uncertainties and systematic uncertainties. The measurement uncertainties can vary, but PNNL states that the minimum possible uncertainty in these methods was estimated to be 2%. These uncertainties apply to the activities measured in each sample.

The fission product concentration profiles take the measured activities and normalize them by the volume of the sample in which the concentration was measured. The volume of carbonaceous material that was milled in each segment has five components that comprise its uncertainty. Figure 14 depicts the uncertainties that affect the volume determination for each milled segment. The first component is the uncertainty in the plunge depth of the end mill bit. The depth of the plunge was determined via a Starrett dial indicator with 0.001-in graduations. The endmill bit itself had an “h10” tolerance, which for a 10-mm diameter bit, means it is 10.00 mm +0 mm/-0.058 mm. Note that this tolerance is asymmetrical. The bit can be no larger than 10.00 mm and no smaller than 9.942 mm. There is also an uncertainty in finding the absolute end for milling at the top or bottom end of the ring. For example, the endmill could be positioned so that a small portion of the mill hangs off the end of the ring, or conversely, the endmill could be positioned slightly toward the center of the ring. The end of the ring was located using a Dorsey Metrology International dial indicator with 0.0005-in graduations. The inner and outer diameters of the ring were measured in PIE (Stempien et al. 2016), and they have their own uncertainties associated with them.

For the thickness of each milled segment, which is determined from the Starrett vertical dial indicator on the milling apparatus (see Figure 8), the equivalent standard deviation was taken to be equal to the size of the graduation of the dial (0.001-in) divided by $2\sqrt{3}$. This approach was based on guidance from the Joint Committee for Guides on Metrology (JCGM 2008). For milling the first segment on a ring, for example, the diameter is reduced by two times the depth of the plunge, as determined by the vertical dial indicator. The new outer diameter is the initial ring outer diameter (determined by PIE) minus two times the depth of the plunge. The uncertainty of the new outer diameter is the sum in quadrature of the uncertainty in the depth of the plunge (based on the Starrett dial indicator) and the uncertainty in the initial ring outer diameter based on PIE metrology. With each successive segment that is milled, this uncertainty propagates.

The volume of each segment was determined according to Equation 1, and the uncertainties in the ring radii (and diameters) were propagated along with the uncertainty in the width of the segment that was milled. For samples taken at the axial center of a ring, the uncertainty in the width of the segment is based solely on the tolerance of the end mill bit. For samples taken at the end of a ring, the uncertainty in the width of the segment includes the endmill bit tolerance and the uncertainty in the positioning of the bit with the horizontal dial indicator. In this case, the equivalent standard deviation on the horizontal positioning of the endmill bit was taken to be equal to the size of the graduation of the Dorsey Metrology International dial, 0.0005-in (0.0127-mm), divided by $2\sqrt{3}$ (JCGM 2008). Based on its manufactured tolerance, the narrowest the endmill bit could be is 9.942 mm. Subtracting from that the uncertainty of the horizontal placement of the bit, the smallest effective width of the milled segment of the ring would be 9.938 mm. If the endmill bit were a full 10.00 mm wide and the bit was positioned $0.0127\text{-mm}/2\sqrt{3}$ inside the very end of the ring, the largest the effective width of the endmill bit could be is 10.004-mm. The assumption here is that the 0.004-mm-thick sliver at the end of the ring would break off and be collected during sampling. These upper and lower bounds on the effective width of the endmill were also accounted for in the uncertainty of the volume of the milled material. In actuality, this volume uncertainty is relatively small, ranging from about 0.2 to 2%. This volume uncertainty was propagated to the radiochemical measurement uncertainty to give an overall uncertainty for the concentration of a given isotope.

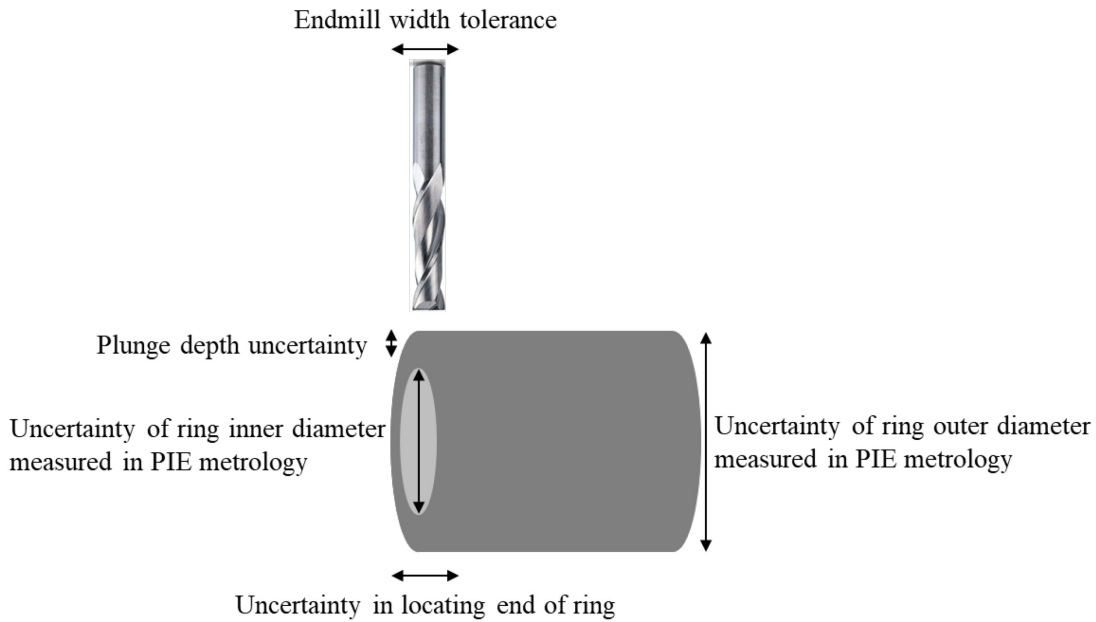


Figure 14. Contributors to the uncertainty in the volume of ring material milled.

2.4.5 Concentration Profile Descriptions and Comparisons

A detailed multiphysics model was constructed to predict the fission product profiles throughout the AGR-3/4 rings (Humrickhouse et al. 2016). Using output from that model as “simulated data,” it was determined that the steady-state solution to diffusion in a cylindrical annulus generally does fit the radial fission product profiles in the AGR-3/4 rings. The transient solution for diffusion through a cylindrical annulus required assumptions on the time-dependent boundary conditions, but it fits these simulated data much better.

Simplified descriptions of the shapes and features of the measured fission product profiles will be used in this report to compare the behavior of different isotopes among the different rings. Some cursory visual comparisons between the model profiles and the measured profiles will be made. However, detailed comparisons and analyses of all the profiles to derive transport parameters for different isotopes at different temperatures using the approach discussed in two papers by Humrickhouse et al. (Humrickhouse et al. 2016, 2018) will be the subject of a future report and/or article.^a

3. CAPSULE 3 INNER AND OUTER RING FISSION PRODUCT PROFILES

Figure 15 and Figure 16 give the radial profiles of select fission product concentrations for the IR and OR at the axial top and axial center of the rings, respectively. Appendix B features tabularized summaries of the fission product concentrations, ring segment volumes, and uncertainties. In Capsule 3, both the IR and OR were made of PCEA graphite. In the as-fabricated condition, the gap between the two rings was 0.057 mm, and PIE measurements showed that the gap increased to 0.42 mm at the EOI (Stempien et al. 2016). The average compact-to-IR gap increased from 0.062 mm to 0.16 mm over the course of the irradiation. This was due to a combination of compact diametric shrinkage and ring volumetric shrinkage where the ring inner diameter increased, and the ring outer diameter decreased.

^a Note that Humrickhouse et al. did not make model predictions for Eu-154 due to a lack of legacy Eu transport parameters. Some preliminary diffusion coefficients were previously determined for Eu-154 and Sr-90 using physical sampling data from Capsules 3 and 7 (Humrickhouse et al. 2018).

The first milling activities were completed at the top and then at the center of the ring. While milling the second IR-03 center sample (IR3-C2), it was noticed that the ring moved slightly toward the bottom of the ring. This was corrected by resecuring the ring in the chuck before the milling was completed as usual. This apparent movement did not give any unusual fission product concentrations compared to any of the other samples taken from the ring.

The Capsule 3 OR had four nubs on its outer surface that were centered 0.375 in. from the top of the ring (see Figure 12). Prior to collecting the radial samples from the top of the ring, the portion of the four nubs that interfered with the top cuts of the ring were removed and collected in a dedicated vial (see Figure 17). The fission product inventories in the nubs were kept separate from that of the bulk of the ring and will be discussed in Section 9.

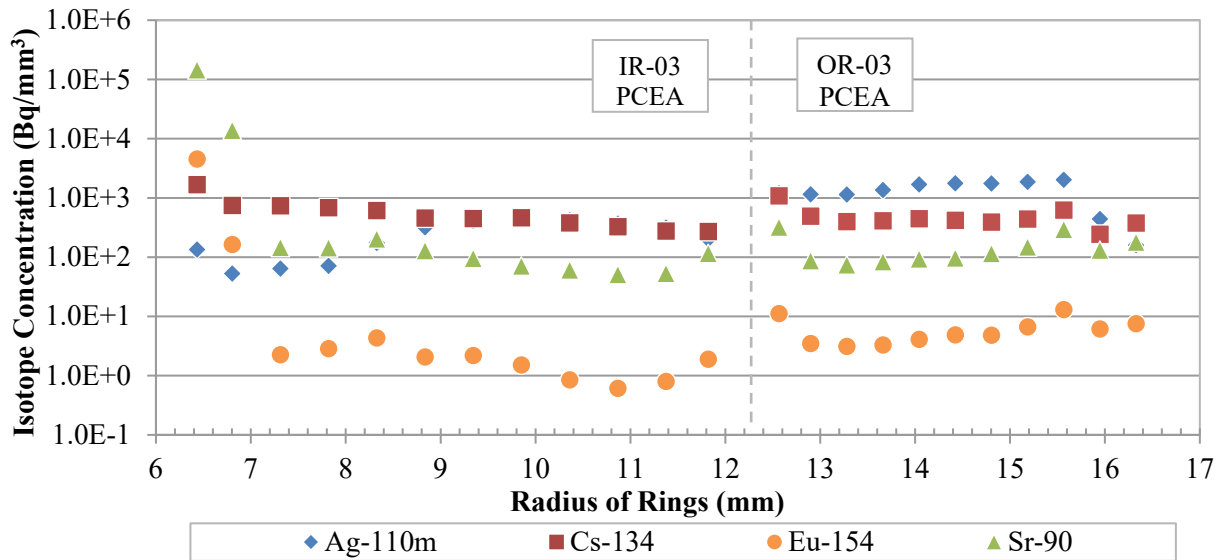


Figure 15. Radial profiles for select fission products at the axial top of the Capsule 3 rings.

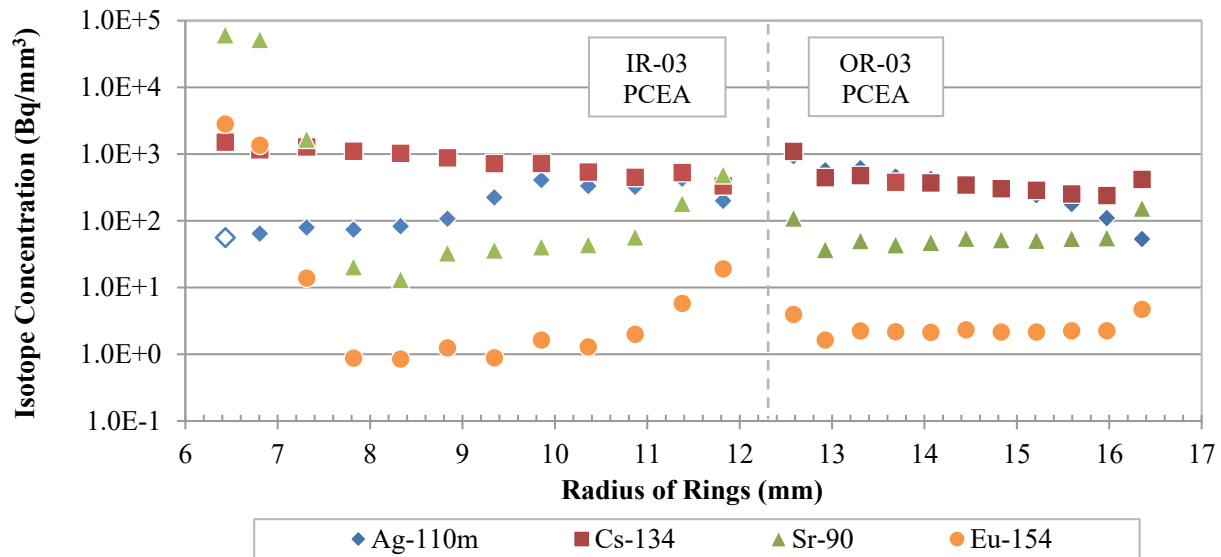


Figure 16. Radial profiles for select fission products at the axial center of the Capsule 3 IRs and ORs. The open symbol for Ag-110m at $x = 6.4$ mm denotes a value derived from an MDA.

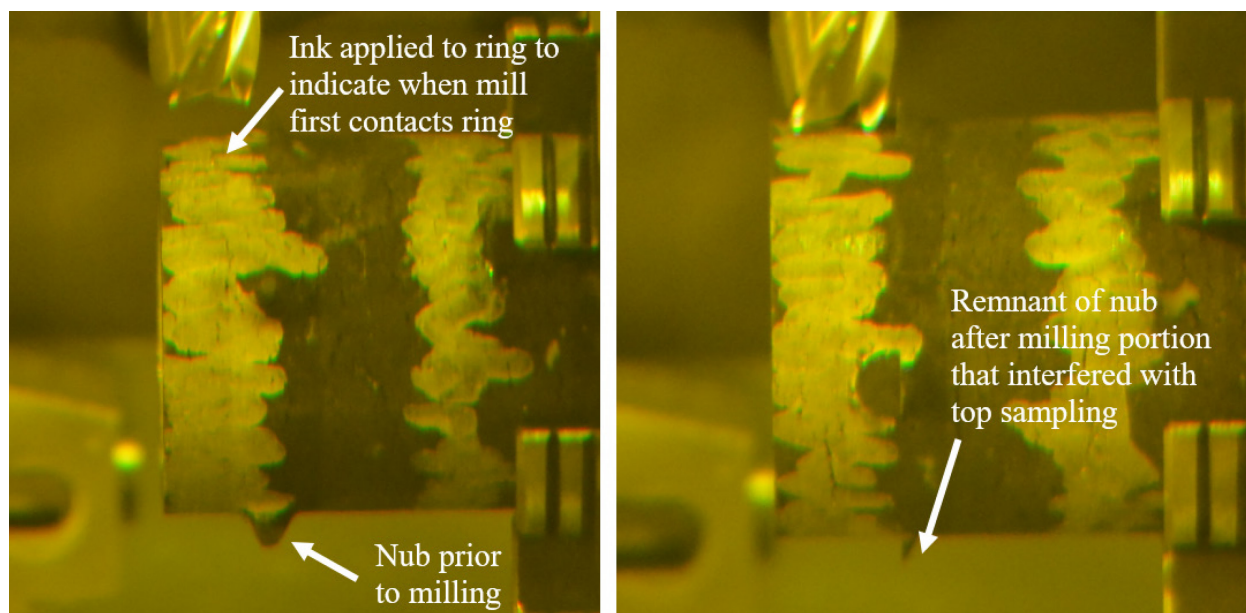


Figure 17. OR-03 in the chuck prior to milling off the nub at the top of the ring (left). OR-03 after the portions of nubs that would interfere with radial sampling at the top had been removed (right).

3.1 Cs-134 in Capsule 3

Figure 18 shows a plot of the Cs-134 profiles in the Capsule 3 IR and OR. The profile at the top of IR-03 decreases sharply from the innermost point to the adjacent point. After that drop, the Cs-134 concentration decreases approximately linearly from the inside out. The IR-03 center profile also decreases approximately linearly with a less pronounced drop after the innermost point.^b

The profiles for the OR are more complicated than for the IR. In the OR, the concentrations are highest at or near the inner and outer surfaces of the ring. The data points away from the surface show an approximately flat (constant concentration) profile at the top of OR-03. For the OR-03 Center profile, if the inner surface and outer surface points are neglected, the profile is approximately linear.

The concentration increases from the outermost point of the IR to the innermost point of the OR. This agrees with the model predictions. Humrickhouse et al. discussed that if the IR and OR materials are the same (in this case they are both PCEA graphite), there should be a step increase in the concentration for the OR due to the lower temperature of the OR (Humrickhouse et al. 2016). The OR had a TAVA irradiation temperature of 962°C compared to 1026°C for the IR.

The elevated concentrations on the OR outer surfaces, combined with the generally linearly decreasing profiles at the interior of the OR, suggest that some effect other than simple diffusion is taking place. One hypothesis is that Cs-134 could transport in the small gaps between the IR and the OR and between the OR and the sink ring such that it bypasses diffusion through the ring itself.

^b Recall that Section 2.4.5 discussed the transient solution for diffusion through a cylindrical annulus is the most appropriate and generally applicable function to fit to these profiles. The term “linear” is used here to refer to a profile that visually approximates a line. It is not being used in a mathematically rigorous way, and different functions may fit. For example, if the innermost point of the IR-03 top profile is neglected, both linear and exponential fits to the remaining points return R-squared values >0.95. If the innermost point is included, an exponential function fits this profile better than a linear profile. Both a linear and exponential function fit to the IR-03 center profile with nearly identical R-squared values of ~ 0.95.

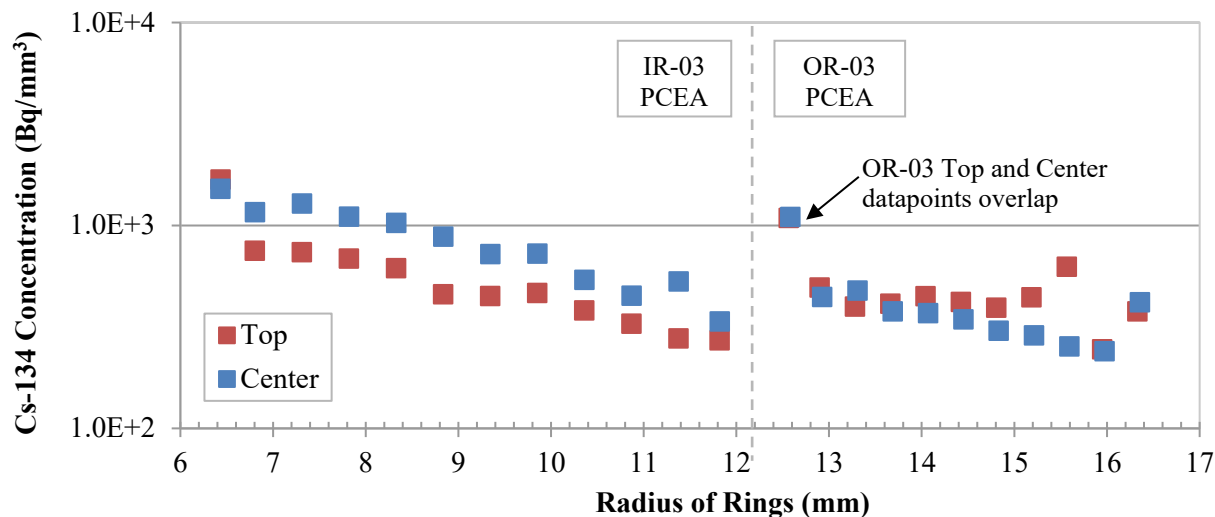


Figure 18. Cs-134 concentrations in the Capsule 3 IR and OR.

3.2 Sr-90 and Eu-154 in Capsule 3

The Sr-90 and Eu-154 concentration profiles are similar; therefore, they will be discussed in the same section. Figure 19 and Figure 20 show the Sr-90 and Eu-154 profiles, respectively. Moving from the inside out in the IR, both isotopes have their highest concentrations at the inner surface, drop sharply within three segments, and the concentrations are relatively constant across the rest of the ring. This is indicative of a transport process where the isotopes are sorbed on the inner surface of the ring, but diffusion into the ring from that surface is quite slow. In the top profile, the modest increases in the Eu-154 and Sr-90 concentrations across the IR-OR gap is consistent with the model prediction (Humrickhouse et al. 2016). In contrast, the concentration drops across the gap at the ring's axial center.

There is an increase in the Sr-90 and Eu-154 concentrations at the outer surfaces of both the IR and OR. This is another indication that a short-circuit pathway existed whereby transport in the gaps between the compacts and the IR and the IR and OR occurred.

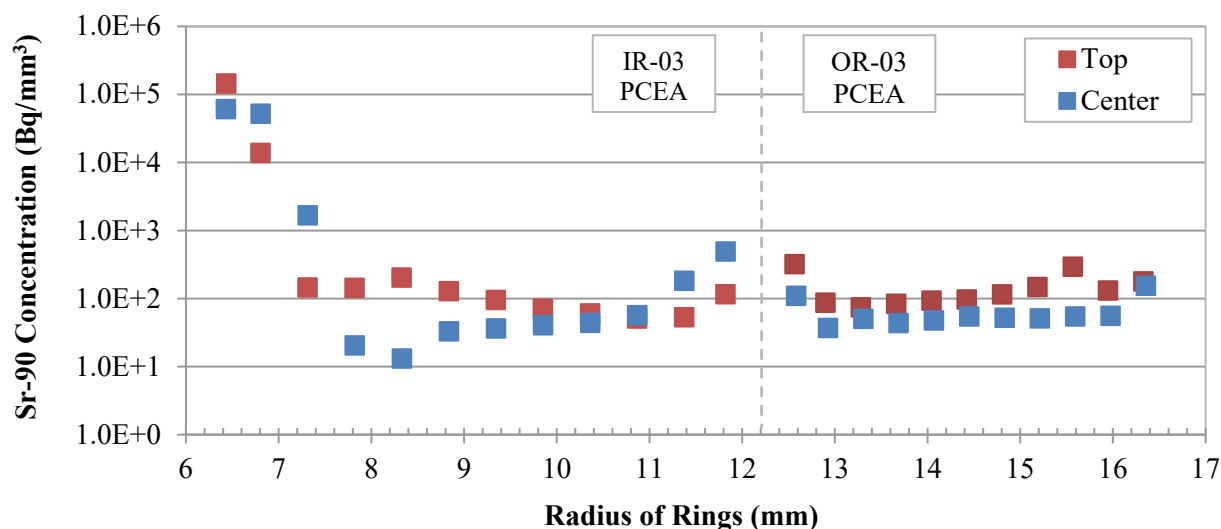


Figure 19. Sr-90 concentrations in the Capsule 3 IR and OR.

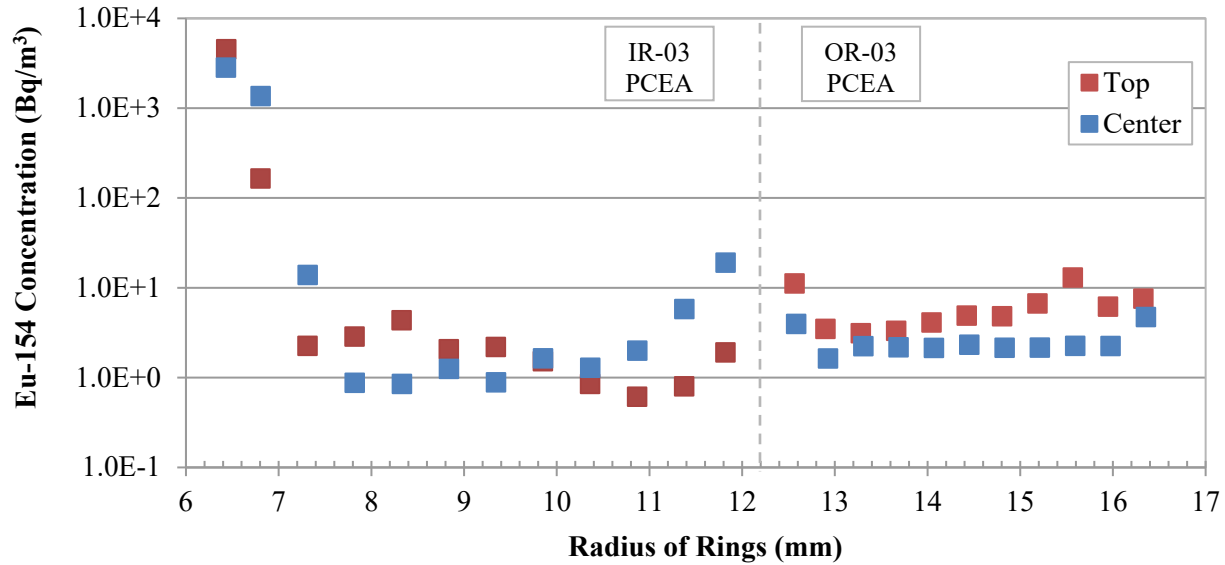


Figure 20. Eu-154 concentrations in the Capsule 3 IR and OR.

3.3 Ag-110m in Capsule 3

The Ag-110m profiles measured at the top and center of the IR and OR are given in Figure 21. In the IR, the top and center profiles are similar. They both have a sigmoidal shape and have maxima on the outer half of the ring. This sort of inverse profile (higher toward the outside of the ring than toward the inside of the ring where the fuel was) is difficult to explain. Here again, this may be evidence of a short-circuit pathway where Ag-110m transported in the gap between the compacts and the IR to the gap between the IR and OR. In the OR, the top and center profiles have similar values on the inner and outer surfaces, but very different behaviors in the bulk of the ring. The center profile decreases from inside to outside, which is indicative of primarily diffusion processes. The OR top profile increases from the inside toward the outside before ultimately dropping sharply in the two outermost segments. The maximum concentration in the OR top profile occurs two segments in from the ring's outer surface. It is not known exactly why these two OR profiles differ in these ways, but it is notable that, in agreement with the data presented here from physical sampling, the axial PGS gamma scans prior to physical sampling showed noticeably higher Ag-110m activity at the top of the OR than at the center (Harp et al. 2020).

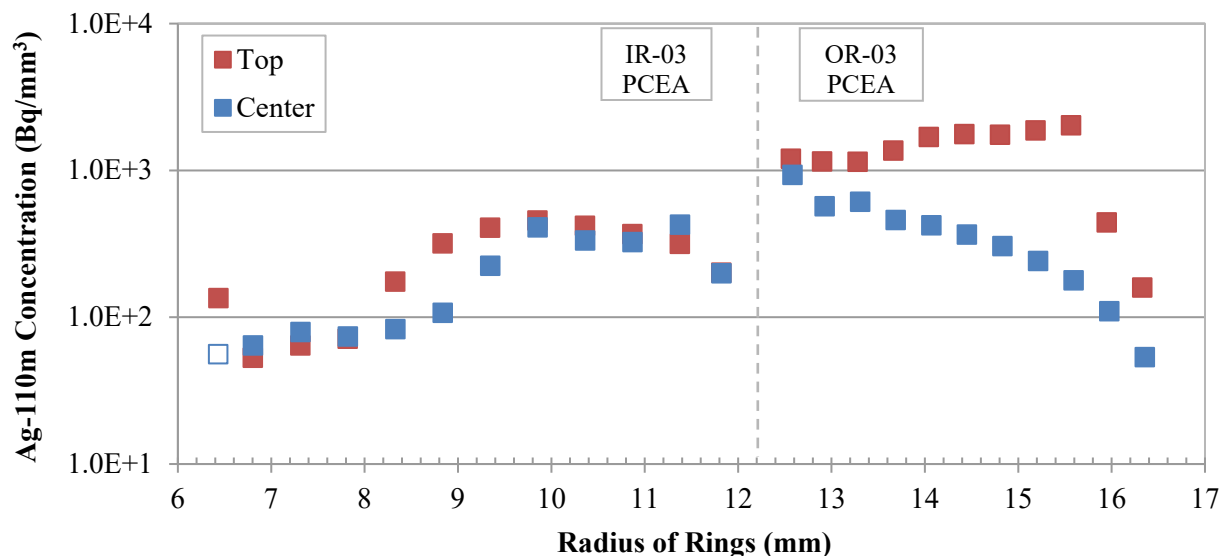


Figure 21. Ag-110m concentrations in the Capsule 3 IR and OR. The open symbol denotes a value derived from an MDA.

4. CAPSULE 5 INNER AND OUTER RING FISSION PRODUCT PROFILES

Pre-sampling gamma scanning of the Capsule 5 rings via PGS showed that the highest activities of gamma emitters were at the axial center of the ring and the ends of the ring had very little activity; therefore, the Capsule 5 rings were sampled only at their axial centers. Figure 22 gives the radial profiles of select fission product concentrations for the IR and OR at the rings' axial centers. In Capsule 5, the IR was made of graphitic matrix material, and the OR was made of PCEA. Capsules 7 and 12 also had matrix IRs with PCEA ORs. This is notable because the legacy diffusion coefficients and sorptivities are known to be different for matrix material and graphite (Humrickhouse et al. 2016). For example, the Sr diffusivity is greater in graphite than in matrix. In contrast, the Ag and Cs diffusivities in graphite are less than in matrix than in graphite at temperatures above about 500°C and 600°C, respectively. The Cs sorptivity is lower in graphite than in matrix.

In the as-fabricated condition, the gap between the two rings was 0.060 mm, and PIE measurements showed the gap increased to 0.40 mm at the EOI (Stempien et al. 2016). The average compact-to-IR gap increased from 0.067 mm to 0.25 mm over the course of the irradiation. Appendix B features tabularized summaries of the fission product concentrations, ring segment volumes, and uncertainties.

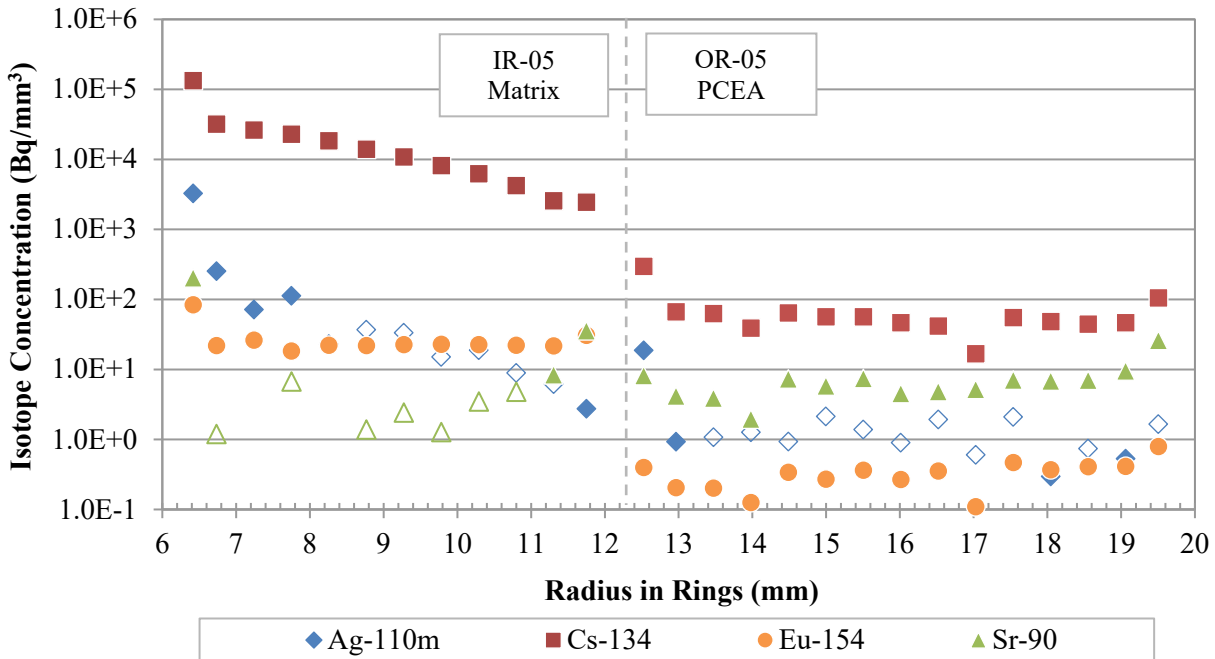


Figure 22. Radial profiles for select fission products at the axial center of the Capsule 5 IR and OR. The open symbols denote values derived from MDAs.

4.1 Cs-134 in Capsule 5

Some of the characteristics of the Capsule 3 Cs-134 concentration profile are seen here for Capsule 5 in Figure 23. For example, as with IR-03, there is a noticeable drop from the innermost point to the adjacent point in IR-05. From cursory curve fitting, it appears that an exponential fits the overall IR-05 Cs-134 profile best (i.e., with highest R-squared). If the innermost and outermost points are neglected, an exponential still seems to fit best, but a linear function fits reasonably well across the middle of the ring thickness too. The Cs-134 profile in IR-05 has a more negative slope than in IR-03, but the shape of the IR-05 profile and the behavior at the inner and outer surfaces are similar to those seen in IR-03.

The Capsule 3 and 5 ORs, which are cooler than the IRs, also have similar features with maxima at the inner and outer surfaces and flat or gradually decreasing profiles across the center. A notable difference is that the concentration on the inner surface of OR-05 is less than at the outer surface of IR-05. This agrees with the model prediction and is evidence of the lower Cs sorptivity in the OR PCEA graphite than in the IR matrix material.

All major components of Capsule 5 had lower TAVA irradiation temperatures than Capsule 3. The Capsule 5 fuel compacts were about 150°C cooler, the IR was about 200°C cooler, and the OR was nearly 300°C cooler (see Figure 3 and Figure 4). The more steeply negative slope in the IR-05 profile could be due to significant transport of Cs-134 from the compacts to the IR inner surface with slower diffusion through the cooler Capsule 5 IR compared to IR-03. Despite cooler temperatures in Capsule 5, more Cs-134 was measured overall in IR-05 than in IR-03 (Stempien et al. 2018). This could be related to the fact that the Capsule 5 compacts had been stuck inside the IR and could not be simply pushed out without an arbor press (Stempien et al. 2016). It is possible that hard contact between the compacts and the IR reduced short-circuit gas-gap transport to the outside of the IR. It could also have caused enhanced transport from the compacts to the inside of the IR if there was no longer a compact-IR gap. Based on the IR-05 outer surface concentration departing somewhat from the linearity across the interior of the ring and the local maximum in concentration at the OR-05 outer surface, some gas-gap transport may still be occurring.

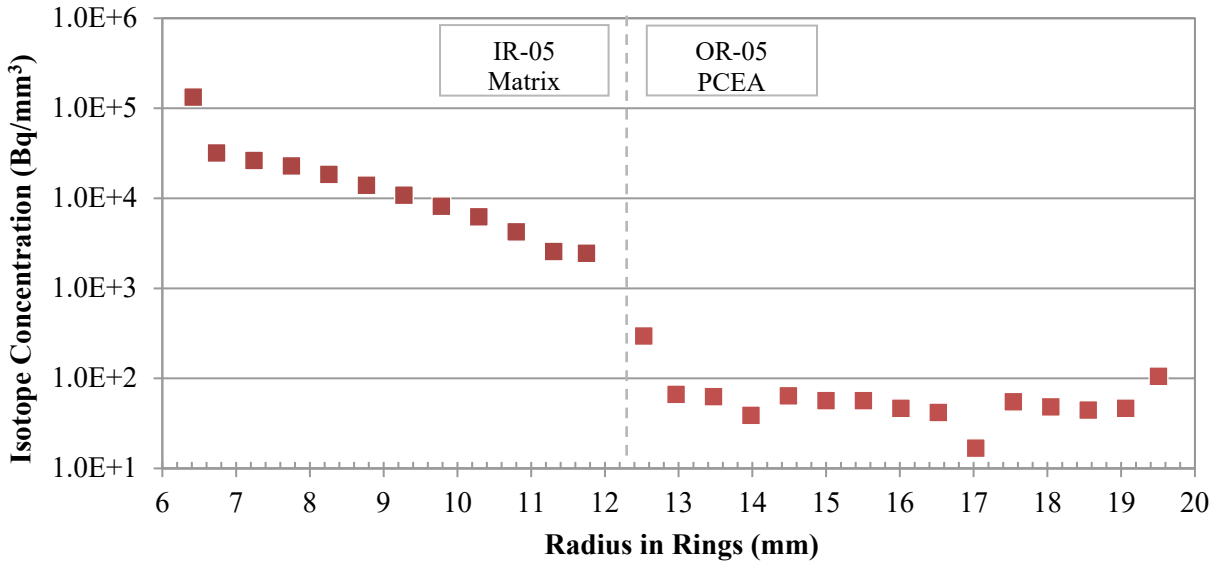


Figure 23. Cs-134 concentrations at the axial centers of the Capsule 5 rings.

4.2 Sr-90 and Eu-154 in Capsule 5

Figure 24 highlights the Sr-90 and Eu-154 profiles. Sr-90 IR data points exist only at the inner and outer surfaces because there was very little change in the first and second scintillation counts at PNNL, meaning that the beta activity was overwhelmingly from beta emitter(s) other than Sr-90 (see Section 2.3). Attempting to mathematically correct for this resulted in very high uncertainties, and the open symbols represent what amount to MDAs. There are no points for IR5-C8 or IR5-C10 because the attempts to correct for interfering beta emitters results in non-physical negative values.

In the IR, there are Eu-154 maxima at the inner and outer surfaces, and the Eu-154 profile across the bulk of the ring is flat (i.e., roughly constant in concentration). The IR-03 and IR-05 Eu-154 profiles are qualitatively similar. The available IR-05 Sr-90 data points suggest a maximum at the inner surface and a local maximum at the outer surface. In IR-03, the Sr-90 profile has similar maxima. The high concentration on the inner surface of the IR, followed by much lower interior concentrations that have a much flatter profile, indicate Eu-154 and Sr-90 are sorbed on the inner surface of the ring, but diffusion into the ring from that surface is quite slow by comparison.

As with the Capsule 3 IR, the Capsule 5 IR also shows local concentration maxima on the outer surface. This is further evidence of a short-circuit path whereby fission products could have been transported from the fuel through the gaps between the fuel and rings rather than having to first diffuse through the IR. The model predicts the Sr-90 concentration will quickly decrease by five orders of magnitude from the inner surface of IR-05 to about one-tenth of the way through the ring. The physical sampling results, however, show a decrease of only one order of magnitude over the same distance. Unlike the model, which shows a very sharp reduction in concentration, the measured concentration is relatively constant in the outward direction.

In contrast to the Capsule 3 IR, the Capsule 5 IR seems to have markedly smaller differences between the concentrations at the surfaces and in the bulk. The surface concentrations in IR-03 were up to three orders of magnitude higher than in the bulk. In IR-05, they were one order of magnitude higher at most. This is likely a consequence of overall less Eu-154 and Sr-90 being transported from the cooler Capsule 5 fuel (1015°C TAVA in Capsule 5 versus 1177°C in Capsule 3) to the Capsule 5 IR (Stempien et al. 2018). Also, in contrast to Capsule 3, there is a step drop in concentration across the Capsule 5 IR-OR gap. This could indicate lower sorptivities in graphite than in matrix.

The Capsule 5 OR has flat Eu-154 and Sr-90 profiles similar to Capsule 3 OR. With maxima in concentration at the OR outer surface, the hypothesis again is that some short-circuit, gap transport is occurring.

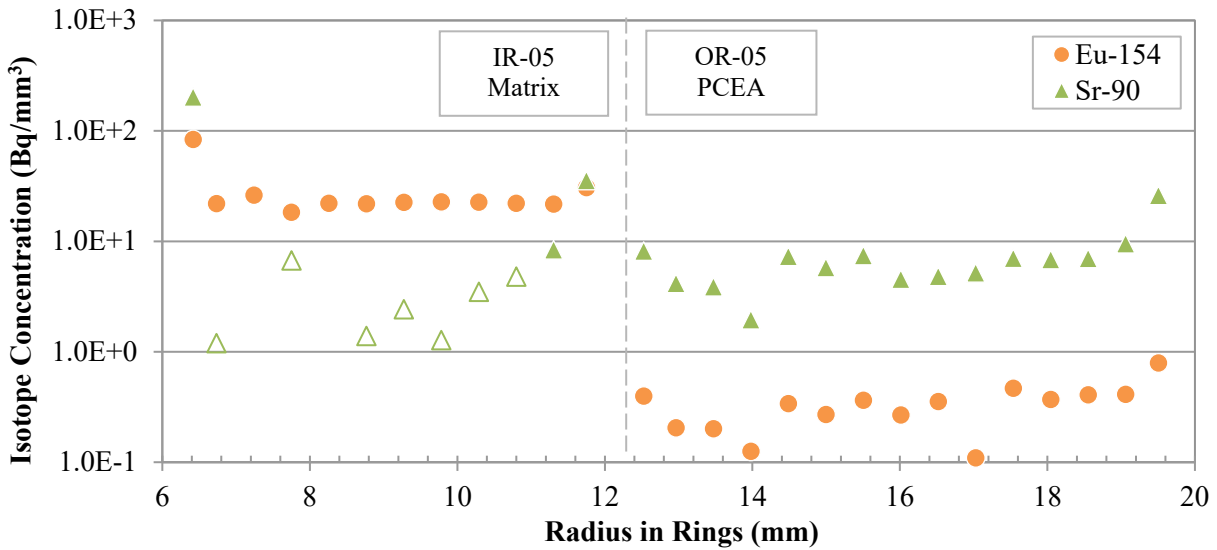


Figure 24. Eu-154 and Sr-90 concentrations at the axial centers of the Capsule 5 rings. Open symbols denote values derived from MDAs.

4.3 Ag-110m in Capsule 5

Figure 25 shows the radial concentration profiles for Ag-110m in Capsule 5. There were a number of samples where Ag-110m was not detected. MDAs were determined for those samples, and upper-bound estimates on the Ag-110m concentrations were made using those MDAs. Neglecting the open symbols, the concentrations are highest on both rings' inner surfaces and lowest at or near both rings' outer surface. The shape of these profiles is about what was expected for radial transport where the source of the Ag-110m was the compacts at the capsule center. For comparison, the Capsule 3 Ag-110m profiles were more complicated and harder to interpret. In Capsule 3, only the OR-03 center profile had concentrations that decreased from the inner surface toward the outer surface.

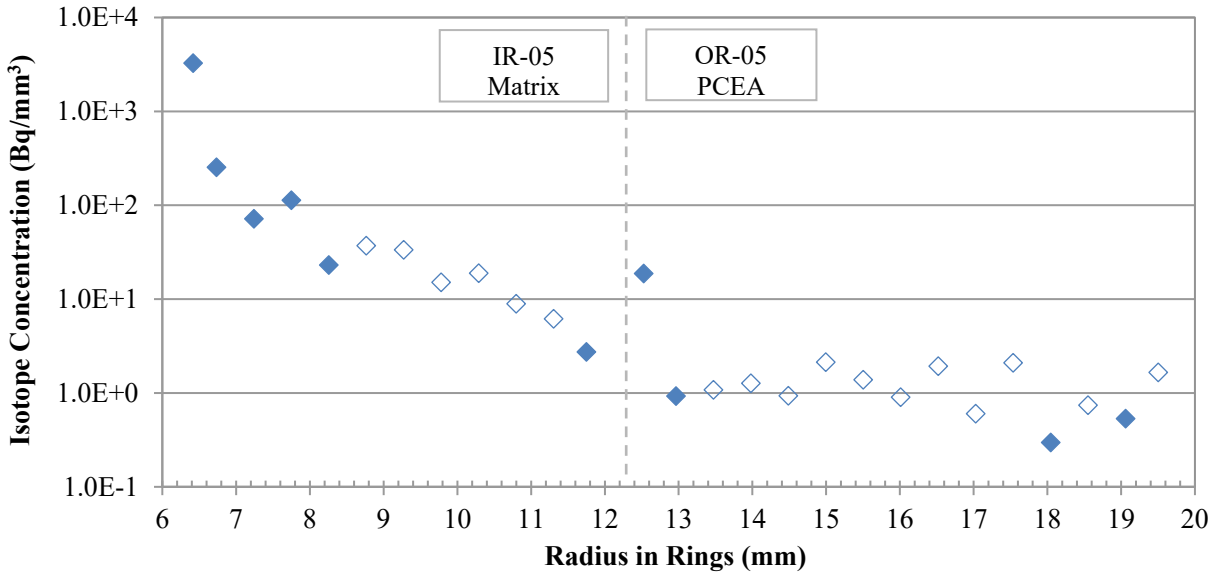


Figure 25. Ag-110m concentrations at the axial center of the Capsule 5 IR and OR. Open symbols indicate values estimated from MDAs.

5. CAPSULE 7 INNER AND OUTER RING FISSION PRODUCT PROFILES

Figure 26 and Figure 27 give the radial profiles of select fission product concentrations for the IR and OR at the axial top and axial center of the rings, respectively. Appendix B features tabularized summaries of the fission product concentrations, ring segment volumes, and uncertainties. Capsule 7 was, on average, the hottest capsule in any of the AGR experiments except for AGR-5/6/7 Capsule 3. Capsule 7 also had the highest inventory of fission products in the sink ring (the outermost ring in a capsule), indicating that Capsule 7 experienced more radial transport than other capsules (Stempien et al. 2018).

In Capsule 7, the IR and OR were made of matrix and PCEA, respectively. The OR had nubs a little smaller than the ones shown in Figure 17 for Capsule 3. These nubs were also removed and collected in a separate container. In the as-fabricated condition, the gap between the IR and OR was 0.0767 mm, and PIE measurements showed the gap increased to 0.63 mm at the EOI (Stempien et al. 2016). The average compact-to-IR gap increased from 0.068 mm to 0.334 mm over the course of the irradiation.

The vial containing the IR7-C4 sample (the fourth sample at the axial center of the Capsule 7 IR) was dropped, and a small amount was lost onto a piece of paper under the vial. A photo of the lost material confirms that it was very small, likely on the order of a hundredth of a gram. This material was not included in the analysis because it was so small and could have picked up hot cell contamination.

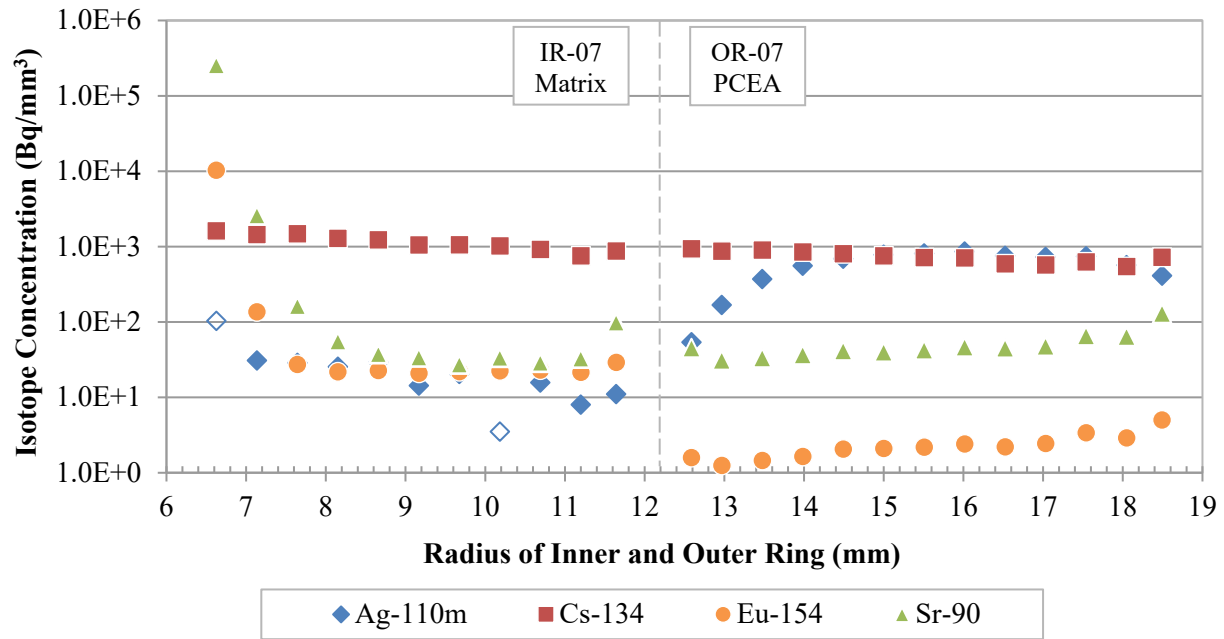


Figure 26. Radial profiles for select fission products at the axial top of the Capsule 7 IR and OR. The open symbols denote values derived from MDAs.

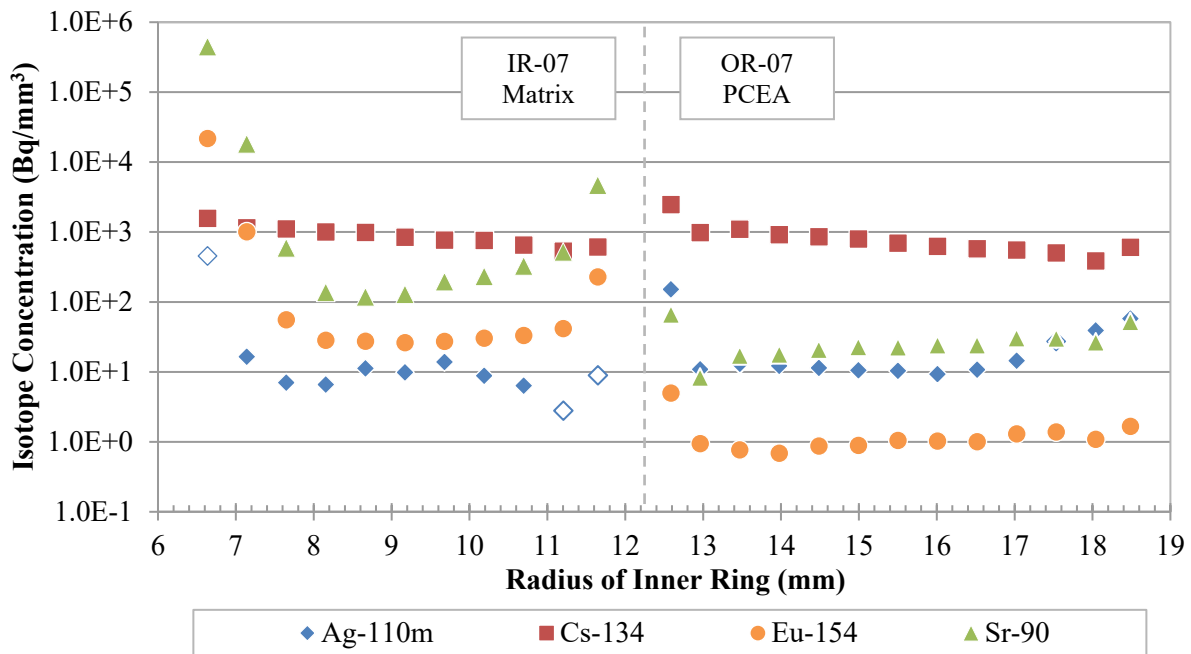


Figure 27. Radial profiles for select fission products at the axial center of the Capsule 7 IR and OR. The open symbols denote values derived from MDAs.

5.1 Cs-134 in Capsule 7

Figure 28 shows the radial concentration profile for Cs-134 at the top and center of the Capsule 7 rings. In both rings, the profiles at the top and center are very similar, and most of the points fall on a somewhat linear or exponential shape. The Cs-134 profiles in the Capsule 7 matrix IR are similar to what has been observed for the Capsule 3 PCEA and Capsule 5 matrix IRs.

The Cs-134 profiles in the Capsule 7 PCEA OR decrease approximately linearly. This is especially true if the innermost and outermost points are neglected. This is different than the Cs-134 OR profiles in other capsules. Except for the Cs-134 profile at the center of the Capsule 3 OR which decreased in the outward direction with some linearity, the other Cs-134 profiles in the Capsule 3 and 5 ORs were roughly flat. The OR-07 linearity could be a consequence of the high-irradiation temperature in Capsule 7 which caused significantly more Cs-134 transport beyond the IR and OR than in Capsules 3 and 5.

Based on the generally lower Cs sorptivity on graphite than on matrix, the AGR-3/4 fission product transport model predicted a significant drop in Cs-134 concentration across the IR-OR gap. However, the physical sampling data show a similar concentration across the gap at the top of the rings and a large increase in concentration across the gap at the center of the Capsule 7 rings. This could be due to the fact that the difference in irradiation temperatures between the Capsule 7 IR and OR was one of the biggest in the AGR-3/4 experiment, possibly making the temperature difference more significant than the difference in material (i.e., matrix versus PCEA).

Also evident in the Capsule 7 Cs-134 profiles are the local maxima at the ring outer surfaces. While are not drastically out of line compared to the overall linear trends, they may be evidence of some gap transport.

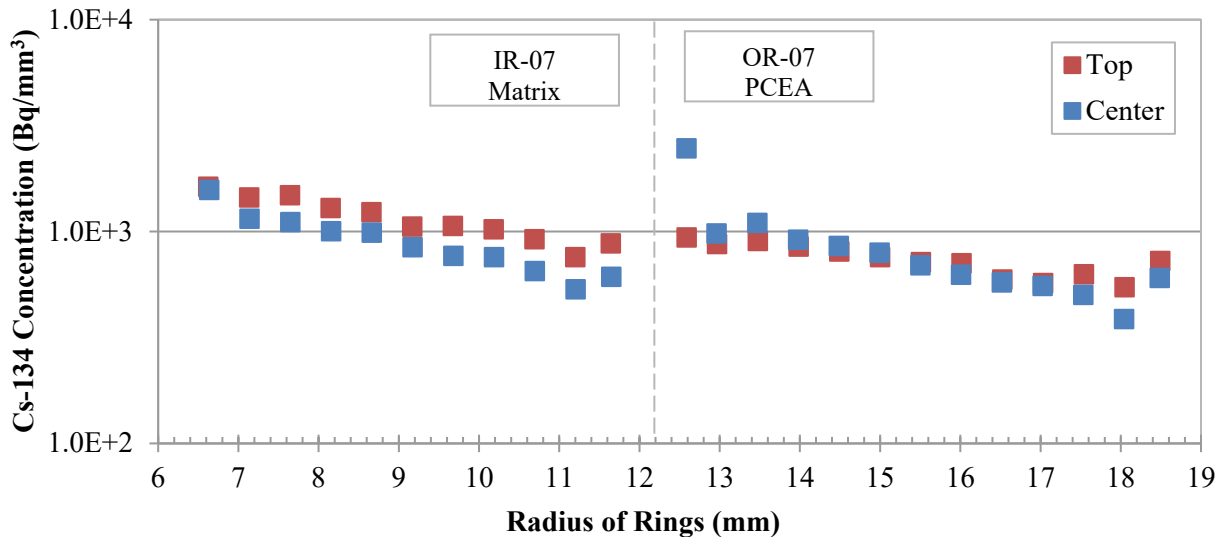


Figure 28. Concentrations of Cs-134 at the axial top and center of the Capsule 7 IR and OR.

5.2 Eu-154 and Sr-90 in Capsule 7

Figure 29 shows the concentration profiles for both Eu-154 and Sr-90 at the axial top and center of the Capsule 7 rings. Both isotopes have similar profiles, and both the tops and centers of each ring give similar profiles. The IR profiles tend to have a minimum near the center of the ring wall and a maximum or local maximum at the inner or outer surfaces. By comparison, the OR profiles are considerably flatter and tend to increase in concentration in the outward direction. These shapes are similar to the Eu and Sr profiles in the Capsules 3 and 5 rings. As with those rings, the conclusion is this indicates a transport process where the isotopes are sorbed on the inner surface, but diffusion into the ring from that surface is quite slow relative to that sorption. The qualitative shapes of these Sr-90 profiles do not compare well with the model (which shows concentrations steadily decreasing in the outward direction), but the observed step drop in the Sr-90 concentration across the IR-OR gap is consistent with the model.

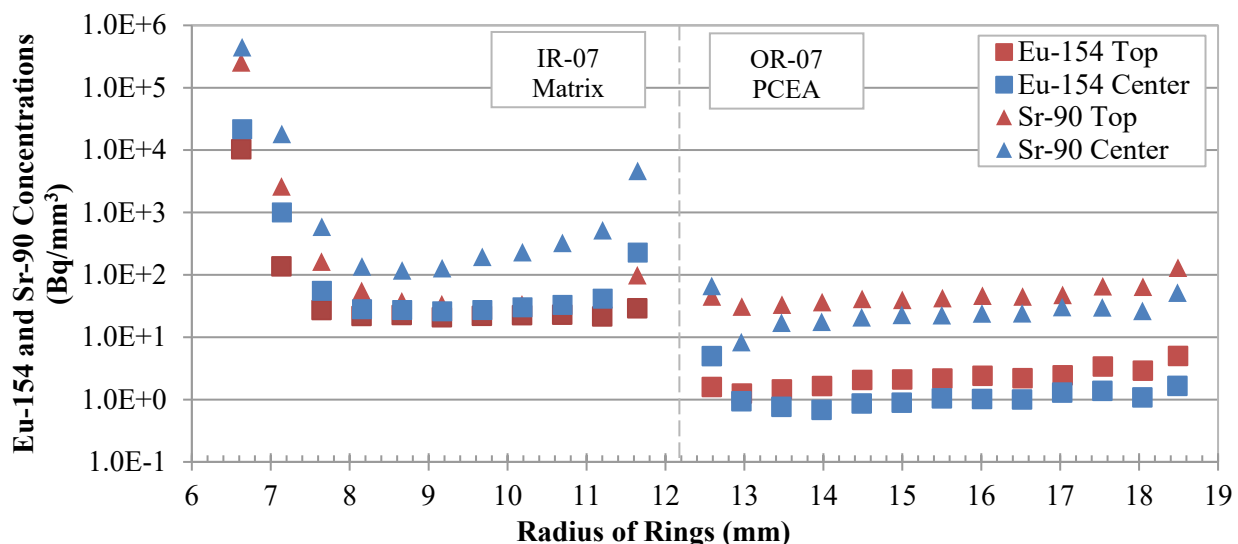


Figure 29. Eu-154 and Sr-90 concentrations in the Capsule 7 IR and OR.

5.3 Ag-110m in Capsule 7

Figure 30 shows the radial fission product concentration profiles for Ag-110m at the top and center of the Capsule 7 rings. Some points in the plot are estimates derived from MDAs. The IR-07 top profile shows some linearity and decreases in the outward direction. The IR-07 center profile also generally decreases in the outward direction, but it has a little more scatter.

The OR-07 profiles have somewhat opposing shapes: the top profile is concave down and the center profile is concave up. It is not clear why the OR-07 top profile has a maximum at its center and drops at the inner and outer surface. Perhaps, this could occur if Ag-110m was rapidly transported to both inner and outer surfaces with rapid diffusion toward the middle of the ring thickness, but in that case, Ag-110m would have to diffuse from the outer surface up the temperature gradient toward the inner surface, which seems unlikely. It is also possible that the very top rim of the ring sorbed more Ag-110m than the inner and outer surfaces.

The OR-07 center profile has high concentrations on the inner and outer surfaces with a flat profile across the middle of the ring. In that respect, it is reminiscent of the Eu-154 and Sr-90 profiles. There is a linearly increasing profile toward the outer surface in the OR-07 center profile, which suggests possible diffusion into the middle of the ring from the outer surface.

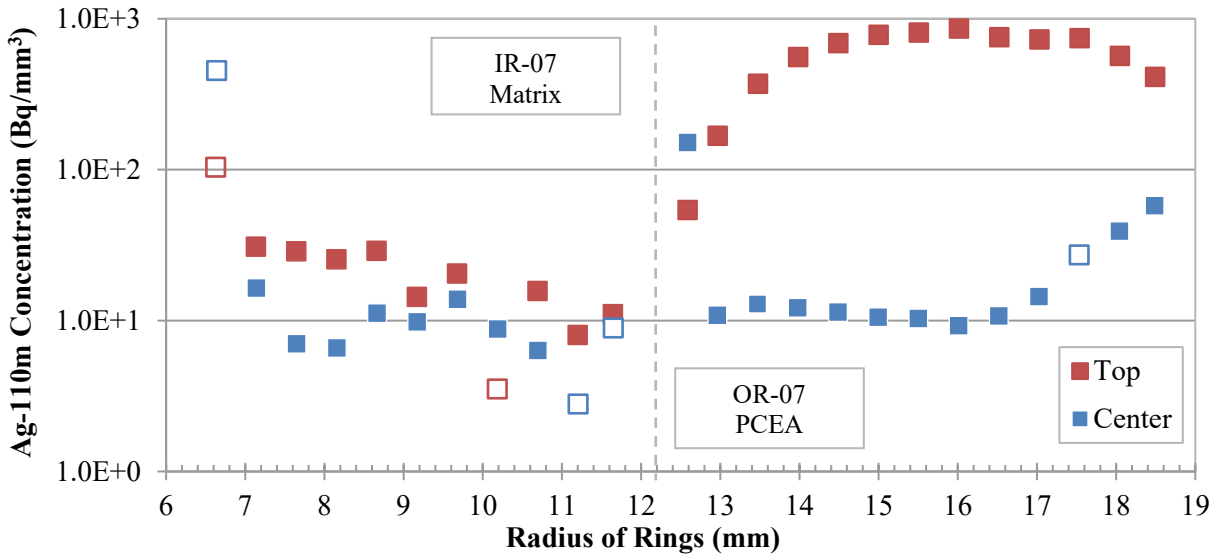


Figure 30. Concentration profiles of Ag-110m at the axial top and center of the Capsule 7 rings. Open symbols denote estimates made from MDAs.

6. CAPSULE 8 INNER AND OUTER RING FISSION PRODUCT PROFILES

Figure 31 and Figure 32 give the radial profiles of select fission product concentrations for the IR and OR at the axial center and bottom of the rings, respectively. Both the IR and OR in this capsule were made of IG-110 graphite. In the as-fabricated condition, the gap between the IR and OR was 0.070 mm, and the PIE measurements showed the gap increased to 0.35 mm at the EOI (Stempien et al. 2016). The average compact-to-IR gap increased from 0.064 mm to 0.234 mm over the course of the irradiation. Appendix B features tabularized summaries of the fission product concentrations, ring segment volumes, and uncertainties.

Very small nubs existed on the outer surface of OR-08, but these were so small that they were not collected separately from the initial cut at the bottom of the ring. During sampling of the 11th segment at the bottom of the OR (i.e., OR8-B11), pieces of the ring broke off and were put into a separate vial for analysis. (This vial had already been labeled as OR8-N1; however, it was not used for the OR-08 nubs.) Figure 33 shows the ring after sample OR8-B11 had been taken. Shards had broken off while OR8-B11 was being milled, but the shards were recovered (see middle of Figure 33). The thickness of the shards was not uniform, and the shards appear to have come from only about half the circumference of the ring. The shards gave a tapered thickness at the top of the ring that was apparent from looking at how the ring evolved from OR8-B11 to after OR8-B13 had been taken (see image at right in Figure 33). Given the irregular thickness of the shards, the fission product inventory measured in the shards could not be specifically assigned to any of the segments OR8-B11 through OR8-B14 (the innermost segment). As a result, the concentrations in OR8-B11 through OR8-B14 have greater uncertainty and are likely underestimated. These points are within the gray-shaded box in Figure 32. Due to the tapered thickness of the shards, the underestimations in segment OR8-B11 will be more severe than for OR8-B14. The affected samples are listed in order of supposed increasing underestimation: OR8-B14, OR8-B13, OR8-B12, and OR8-B11. A viable option for dealing with the results from segments OR8-B11 through OR8-B14 is to take the total activity measured from these segments, add the activity measured in the shards, and normalize that by the total volume represented by those segments. That would give one large section at the inner surface of OR-08 with known volume and activity. The activity concentrations from doing this are summarized in Table 5.

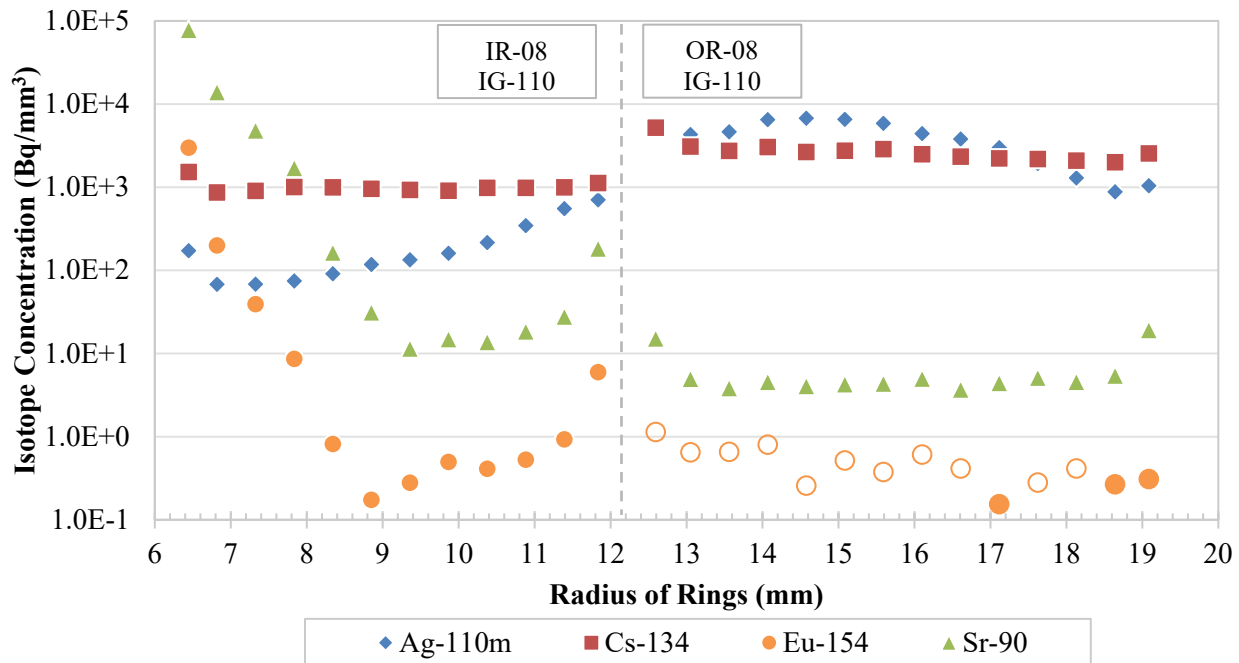


Figure 31. Radial profiles for select fission products at the axial center of the Capsule 8 IR and OR. The open symbols denote values derived from MDAs.

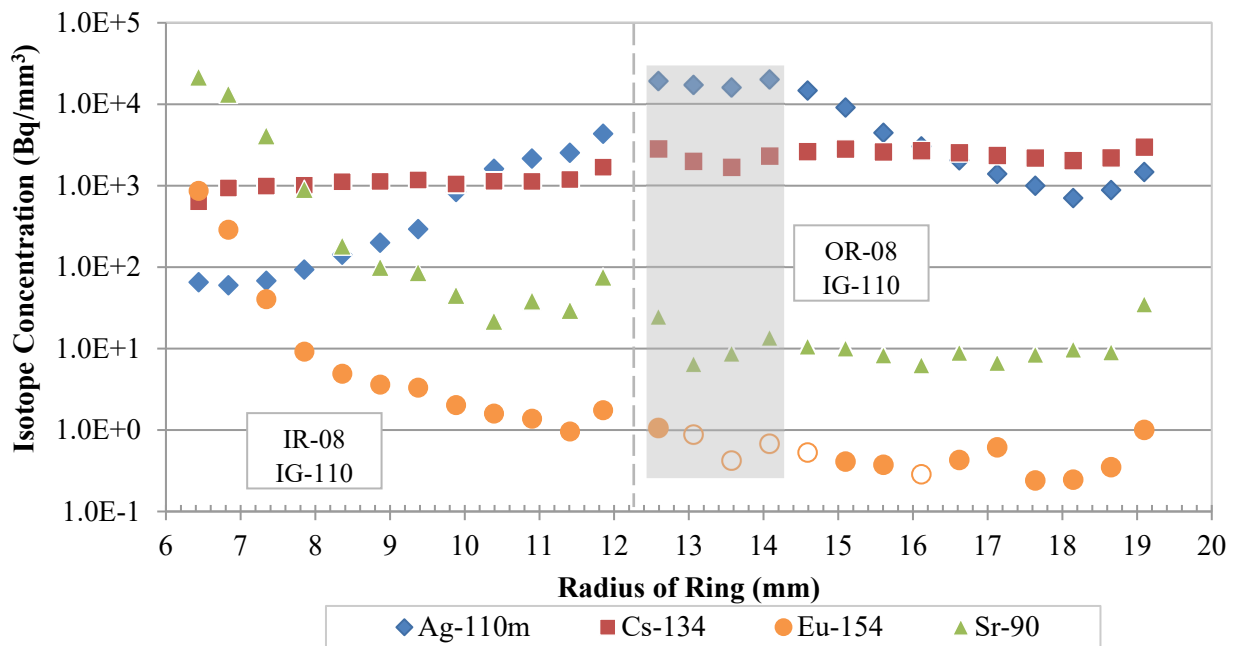


Figure 32. Radial profiles for select fission products at the axial bottom of the Capsule 8 IR and OR. The open symbols denote values derived from MDAs. Gray shading highlights points with greater uncertainty from ring cracking during sampling.

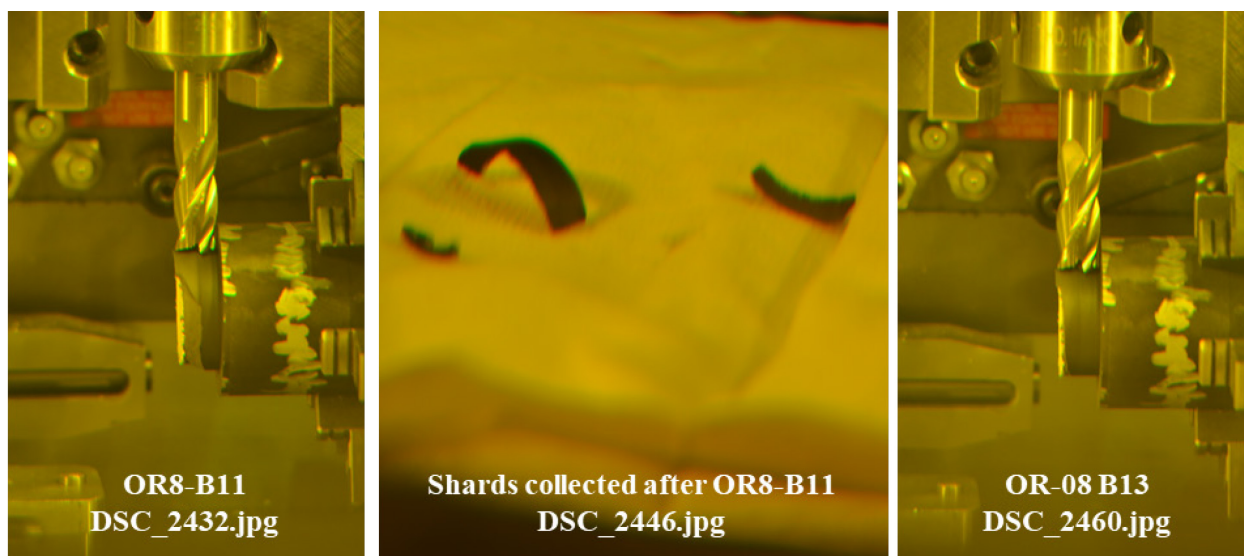


Figure 33. Images of the Capsule 8 OR after the OR8-B11 segment was milled (left), the shards that broke off from the ring (middle), and after the penultimate segment had been milled from the ring (right).

Table 5. Activity concentrations for selected isotopes from the combination of the activities measured in the segments (OR8-B11 through OR8-B14) and the shards. The dimensions and errors are also given.

OR-08 Bottom (Bq/mm ³)	Segments OR8-B11 through OR8-B14 plus the shards collected separately (see Figure 33)	Relative Error of Concentration (%)
Ag-110m	2.58E+4	1.0
Ce-144	<1.98E+2	N/A
Cs-134	3.04E+3	1.0
Cs-137	2.60E+3	1.0
Eu-154	*6.25E-1	15.3
Eu-155	<3.46E+0	N/A
Ru-106	<1.31E+2	N/A
Sb-125	3.58E+2	1.1
Sr-90	2.79E+1	2.2
Segment Volume (mm ³)	1638.39	N/A
Segment Volume Error (+ mm ³)	8.14	N/A
Segment Volume Error (– mm ³)	9.59	N/A
Average Segment Radius (mm)	13.33	N/A
Average Segment Radius Error (mm)	0.094	N/A
*Sum includes only the values > MDA from OR8-B14 and the shards.		

6.1 Cs-134 in Capsule 8

Figure 34 shows the Cs-134 profiles at the center and bottom of the Capsule 8 IR and OR. While the top and bottom profiles in a given Capsule 8 ring are similar to each other, the IR profiles are different than the profiles in other capsules and differ from the model predictions. In other capsules (and in the Capsule 8 model prediction), the IR Cs-134 profiles are generally decreasing from left to right. In Capsule 8, however, the IR profiles are quite flat with a gradual increase in the outward direction. The Capsule 8 OR profile shows Cs-134 concentrations noticeably higher than in the IR at nearly all locations. This is not consistent with the model prediction and is unusual compared to other capsules except for the bottom profile from the Capsule 10 OR, which is similar to the observations in Capsule 8. The model does predict an increase in concentration across the IR-OR gap, which is seen in the measured concentrations; however, the model predicts that the OR concentrations should eventually drop below those of the IR. A consideration is Capsule 8 is notably different than other capsules; it is the only capsule with an IG-110 IR, and it is the only physically sampled capsule with an IG-110 OR.

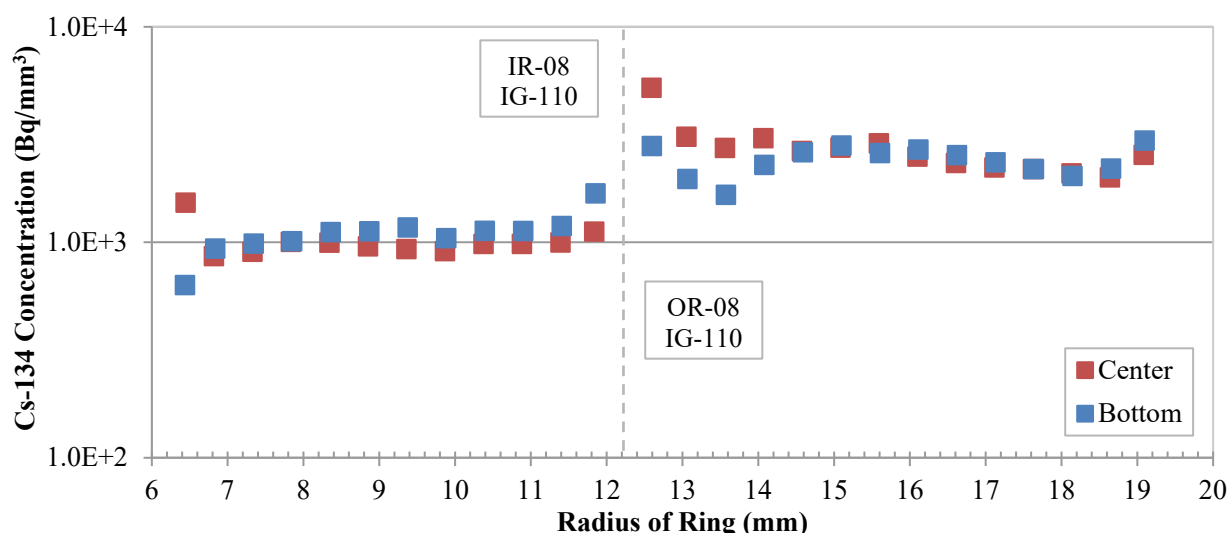


Figure 34. Cs-134 concentration profiles across the center and bottom of the Capsule 8 rings.

6.2 Eu-154 and Sr-90 in Capsule 8

Figure 35 and Figure 36 show the Eu-154 and Sr-90 profiles, respectively. In each case, the center profile is generally similar to the bottom profile. These profiles have characteristics seen in the Eu-154 and Sr-90 profiles from other capsules. In the IR, the concentrations are highest at the inner surface, decrease quickly, and are flatter toward the middle. This indicates a transport process where the isotopes are sorbed on the inner surface of the ring, but diffusion into the ring from that surface is relatively slow. There is a noticeable increase in the concentrations of Sr-90 and Eu-154 at the outer surface of the inner ring. This is another indication that a short-circuit pathway allowed transport in the gaps between the compacts and the IR and the IR and OR. In the OR, the profiles are flat, with maxima and local maxima occurring at the inner and outer surfaces. The observed step drop in Sr-90 concentration across the gap between the rings disagrees with the model, but if gap transport to the IR outer surface was a strong effect in this capsule, that might explain this discrepancy.

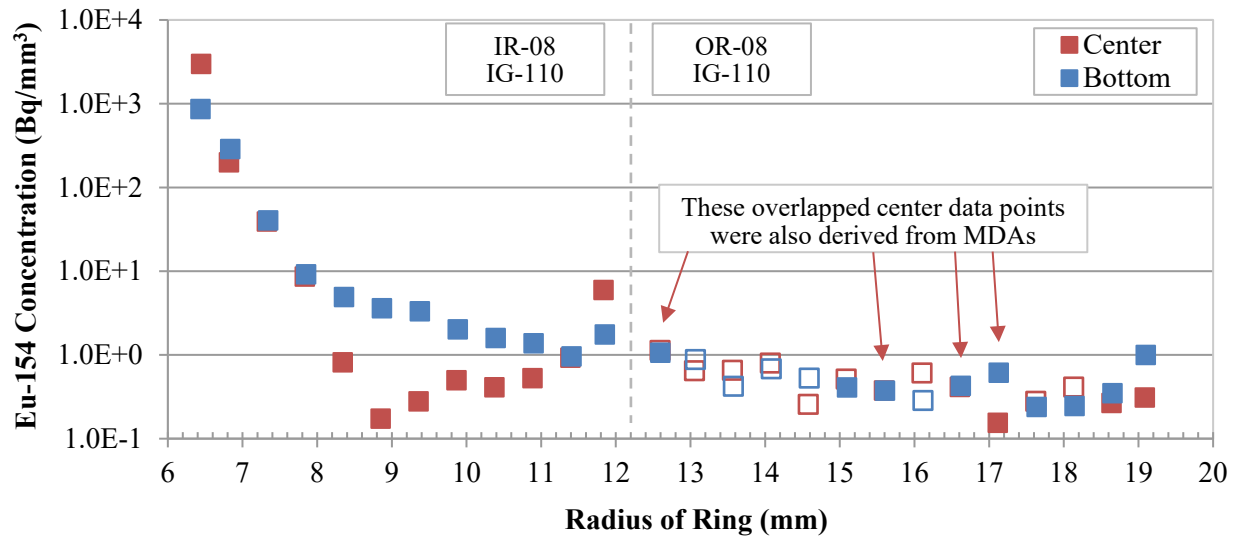


Figure 35. Eu-154 concentration profiles at the axial center and bottom of the Capsule 8 rings. Open symbols denote values derived from MDAs.

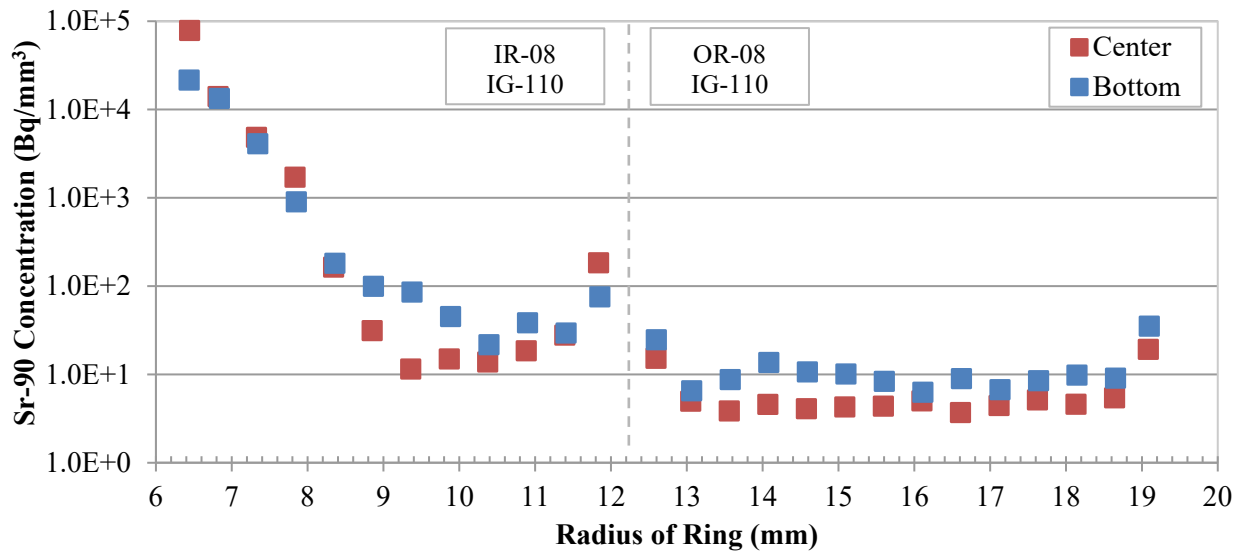


Figure 36. Sr-90 concentration profiles at the axial center and bottom of the Capsule 8 rings.

6.3 Ag-110m in Capsule 8

Figure 37 shows the Ag-110m profiles for Capsule 8. The Capsule 8 IR profiles are similar to those in Capsules 3 and 10 since they increase from the inner surface to the outer surface. This is counterintuitive given the source of the Ag-110m was the fuel compacts in the hollow center of this ring. A short-circuit, gap transport path may explain why the IRs' outer surfaces have higher concentrations than the inner surfaces. The OR profiles both decrease radially outward and are qualitatively similar to the model predictions, including being higher in concentration than the IR profile. The only other OR Ag-110m profile to clearly exhibit this physically reasonable decrease in the radial direction is the axial center profile from the OR of Capsule 3.

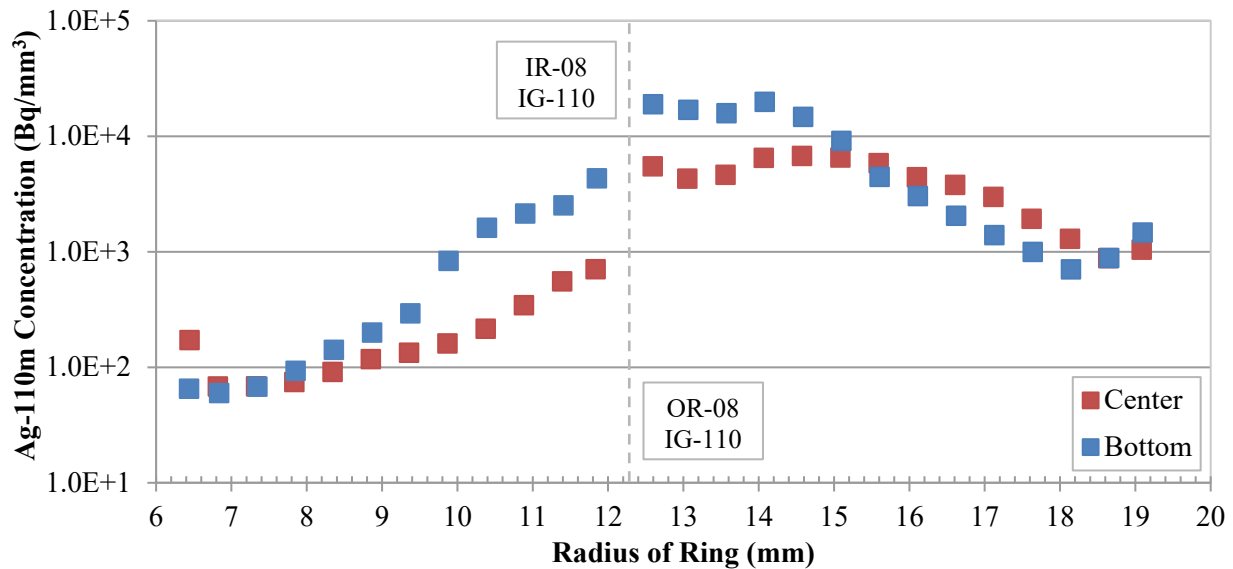


Figure 37. Ag-110m concentration profiles at the axial center and bottom of the Capsule 8 rings.

7. CAPSULE 10 INNER AND OUTER RING FISSION PRODUCT PROFILES

Figure 38 and Figure 39 give the radial profiles of select fission product concentrations for the IR and OR at the axial center and bottom of the rings, respectively. Appendix B features tabularized summaries of the fission product concentrations, ring segment volumes, and uncertainties. Both the IR and OR in this capsule were made of PCEA graphite. In the as-fabricated condition, the gap between the IR and OR was 0.051 mm, and the PIE measurements showed the gap increased to 0.39 mm at the EOI (Stempien et al. 2016). The average compact-to-IR gap increased from 0.076 mm to 0.22 mm over the course of the irradiation.

OR-10 had four small nubs toward its top and bottom ends totaling eight nubs with the same dimensions as the OR-07 nubs. Those nubs were sampled separately from the first ring segment taken from the bottom of the ring and were collected in the OR10-N1 vial. After sampling the 7th segment at the bottom of the OR, it was apparent through the hot cell window that the ring had moved in the chuck. After reviewing the photos taken at the end of each milling step, it appears the ring may have started to move slightly in the chuck during the 3rd through 5th segments. The largest movements were during the 6th and 7th segments. Thus, Segments 3 through 7 from sampling the bottom of OR-10 were collected a little farther (perhaps about 3 mm farther) toward the axial center of the ring than the rest of the bottom samples from OR-10. Figure 40 shows the axial locations of the cuts. After the 7th sample was taken, the ring was repositioned properly, and the material toward the very bottom that was missed in the 3rd through 7th cuts was collected into the unused nub vial from IR-10, labeled IR10-N1. No attempts were made to correct the values in the 3rd through 7th segments for the ring movement, and the material collected in IR10-N1 was not utilized in the analyses presented here. The gray, shaded box in Figure 39 shows Segments 3 through 7 that were affected by movement of the ring. Fortunately, these segments are at radii where the profiles seem to be flat rather than at the surfaces where concentration gradients tend to be steeper. Thus, the concentrations measured in Segments 3 through 7 are not expected to be significantly different due to the shifted position of the ring.

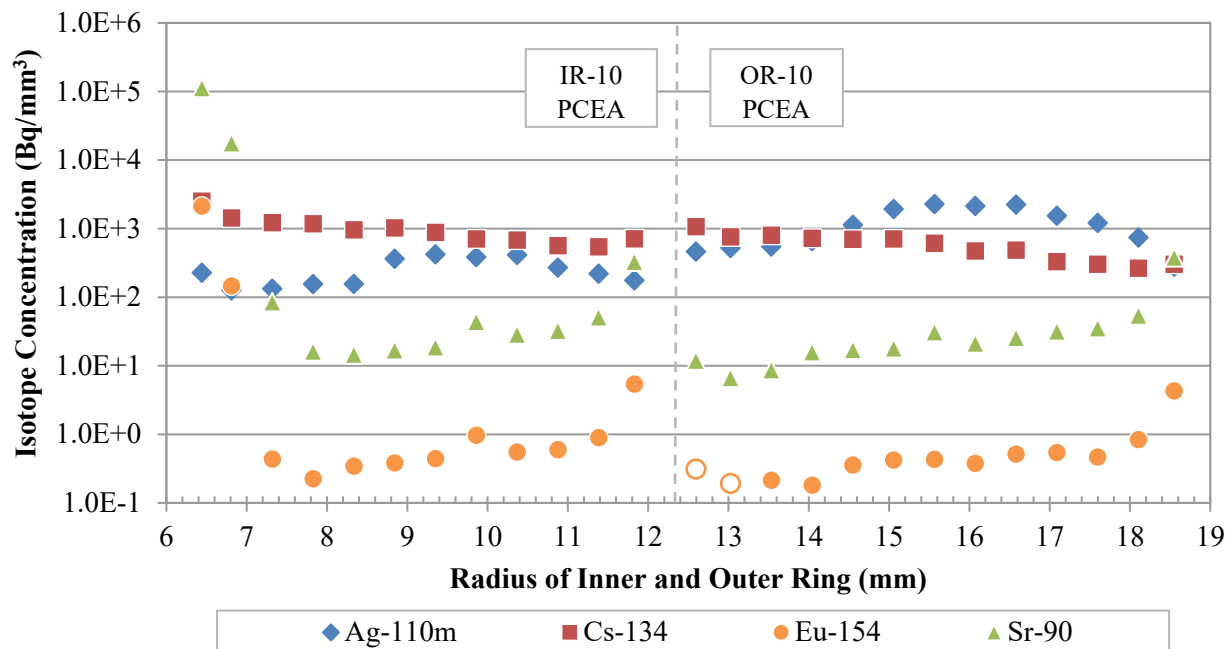


Figure 38. Radial profiles for select fission products at the axial center of the Capsule 10 IR and OR. The open symbols denote values derived from MDAs.

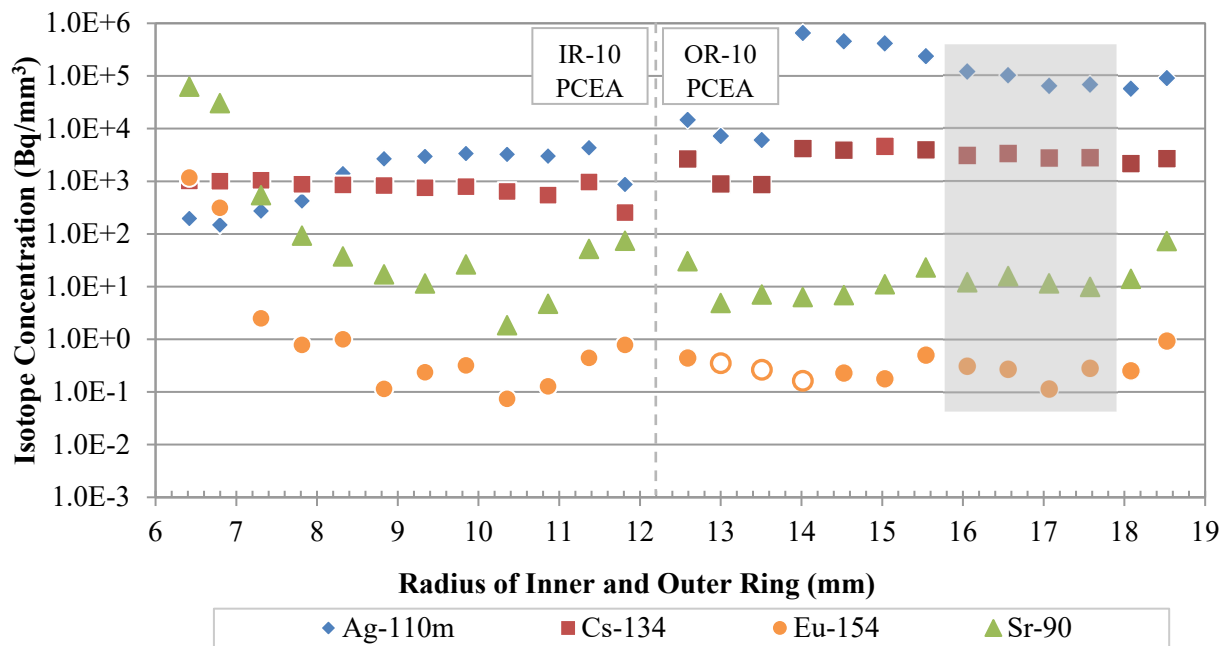
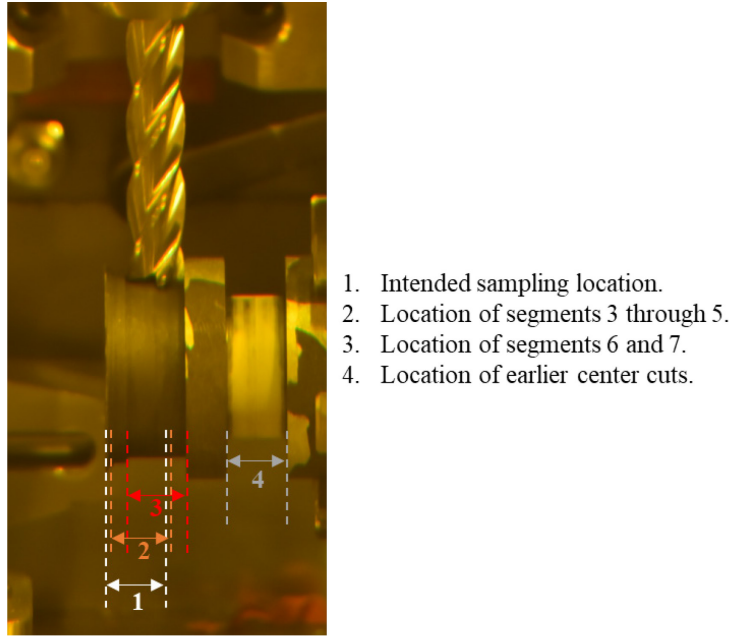


Figure 39. Radial profiles for select fission products at the axial bottom of the Capsule 10 IR and OR. The open symbols denote values derived from MDAs. Gray shading highlights the points with greater uncertainty from ring movement during sampling.



1. Intended sampling location.
2. Location of segments 3 through 5.
3. Location of segments 6 and 7.
4. Location of earlier center cuts.

Figure 40. Photograph of OR-10 after the 7th segment was milled at the top of the ring. The intended sampling location is compared to the actual sampling locations.

7.1 Cs-134 in Capsule 10

Figure 41 shows the center and bottom Cs-134 profiles in Capsule 10. The center and bottom IR profiles generally show very similar values. These are somewhat linear profiles, except on the inner and outer surfaces where the center profile has some increases in concentration on the surfaces. These features are very similar to what was seen in the Capsules 3, 5, and 7 IRs.

In the Capsule 10 OR, the center and bottom profiles are very similar at the inner surface, but they diverge abruptly starting at $r \sim 14$ mm. After that, the shapes of the bottom and center profiles are similar except the bottom profile is suddenly at a higher concentration. The reason for the sudden jump in the OR-10 bottom profile is unknown; however, PGS scans of the OR show that the Cs-134 content at the bottom of the ring is roughly 50% higher than at the center (Harp et al. 2020). The linearity and surface behavior of the Capsule 10 OR center radial profile is most like the Capsule 7 OR center profile. The Capsule 3 OR center profile is also similar, but it has a little more pronounced increases at the surfaces. Not only are the OR profiles similar among these three capsules, but the irradiation temperatures in these ORs were similar as well. The TAVA temperatures for the ORs were 962°C, 1025°C, and 971°C for Capsules 3, 7, and 10, respectively. The behavior across the IR-OR gap is consistent with the model.

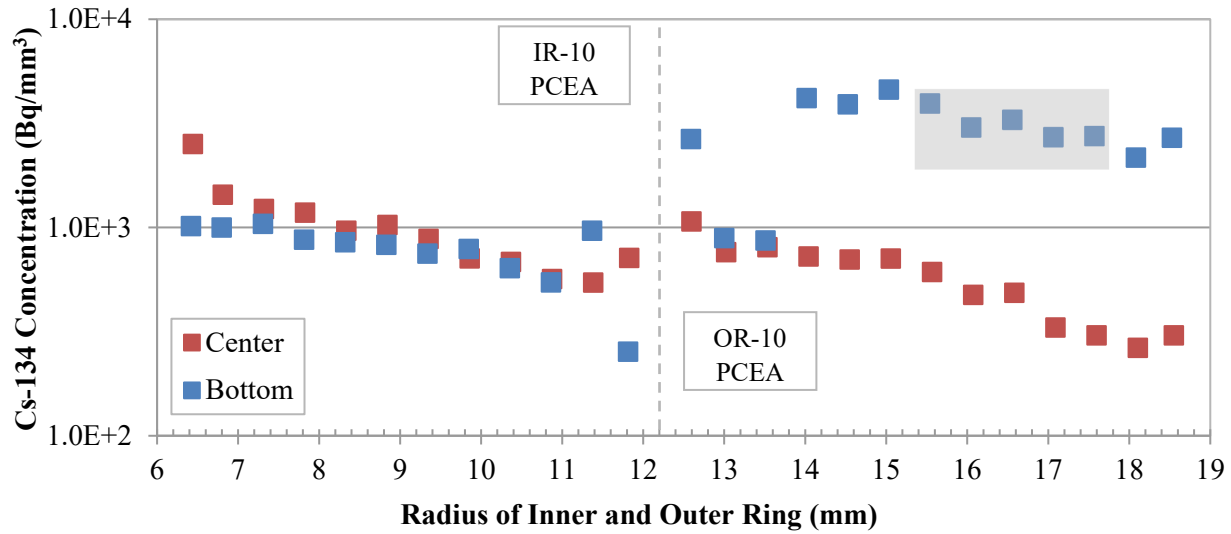


Figure 41. Cs-134 concentration profiles across the center and bottom of the Capsule 10 rings. Gray shading denotes segments affected by ring movement during sampling.

7.2 Eu-154 and Sr-90 in Capsule 10

Figure 42 shows the center and bottom profiles for Eu-154, and Figure 43 shows the center and bottom profiles for Sr-90. Generally, the center and bottom profiles are very similar for both Sr-90 and Eu-154 in both the IR and OR. Both the shape and the values of the IR Eu-154 concentration profiles in Capsule 10 are very similar to those in the Capsule 3 IR. This appears to be a consistent result since the irradiation temperatures of the fuel and the IR and OR were nearly identical in Capsules 3 and 10, and all the rings were made of the same material (PCEA).

In the IR, the Eu-154 and Sr-90 profiles are characterized by high-inner surface concentrations and much lower concentrations across the middle of the ring. Again, this indicates that diffusion of these isotopes through the PCEA IR is much slower than sorption on the inner surface. There are also local maxima at the IR outer surface, which suggests a short-circuit pathway through the gaps between the fuel compacts and rings. As with Capsule 8, the observed step drop in Sr-90 concentration across the gap between the Capsule 10 rings disagrees with the model, but if gap transport to the IR outer surface was a strong effect in this capsule, that might explain this discrepancy. The OR profiles are generally flat and feature maxima on the outer surface of the ring. This is similar to what was seen in all the other capsules.

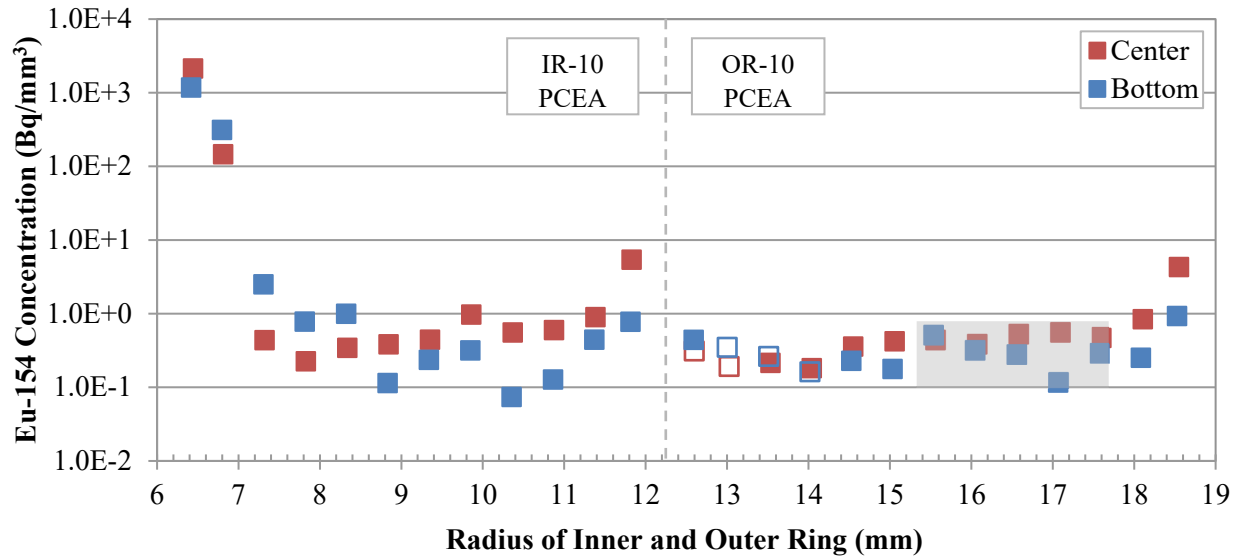


Figure 42. Eu-154 concentration profiles across the center and bottom of the Capsule 10 rings. Open symbols denote values derived from MDAs. Gray shading denotes the bottom segments affected by ring movement during sampling.

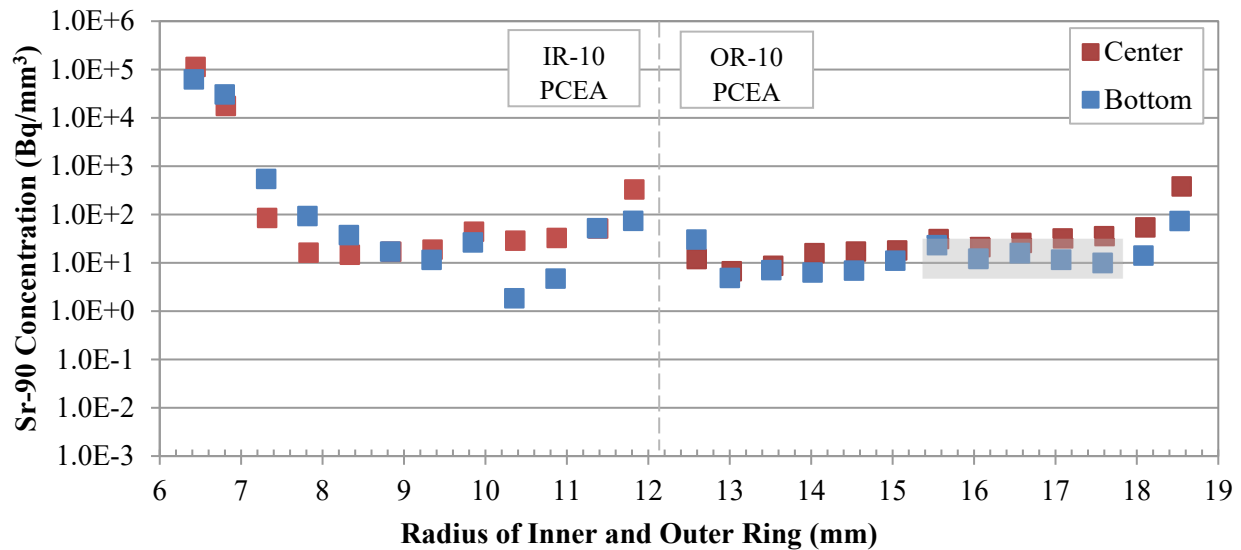


Figure 43. Sr-90 concentration profiles across the center and bottom of the Capsule 10 rings. Gray shading denotes the bottom segments affected by ring movement during sampling.

7.3 Ag-110m in Capsule 10

Figure 44 shows the Ag-110m profiles at the center and bottom locations in the Capsule 10 rings. The bottom profiles have higher concentrations than the center profiles. Similar to Cs-134, pre-sampling gamma scanning via PGS showed that the Ag-110m concentrations were highest at the top and bottom ends of the Capsule 10 rings (Harp et al. 2020); therefore, it is consistent that the radial profiles at the bottoms of the rings have higher concentrations than the center profiles. While the concentrations are different, the shapes of the Capsule 10 IR profiles are similar and closely match those for Ag-110m in the Capsule 3 IR. Both the Capsule 10 and 3 IRs had very similar TAVA irradiation temperatures: IR-10 at

1028°C and IR-03 at 1026°C. The Ag-110m profiles in the Capsule 10 and Capsule 3 IRs increase from the inner surface toward the outer surface and goes through an inflection point roughly halfway through the ring. The Capsule 8 IR also had a very similar TAVA temperature of 1021°C. Its Ag-110m profile increases from inside to outside, but it does so in a more linear fashion. Perhaps the differences in the profile shapes could be related to the fact that IR-08 is made of IG-110 and both IR-03 and IR-10 are made of PCEA. It is not clear why the IRs in Capsules 3, 8 and 10 have concentration profiles that increase with distance from the inner surface.

The Capsule 10 OR Ag-110m profiles are quite different at the center and the bottom of the ring. There are some similarities to the OR profiles in Capsule 3 and Capsule 8. The biggest difference is in the OR-10 bottom profile which increases sharply after the three innermost points before following a shape similar to the bottom of OR-08. The Cs-134 concentration (see Figure 41) was also comparatively low for those three points before increasing sharply at higher radii. It is not known why these three inner points are so different from the other points.

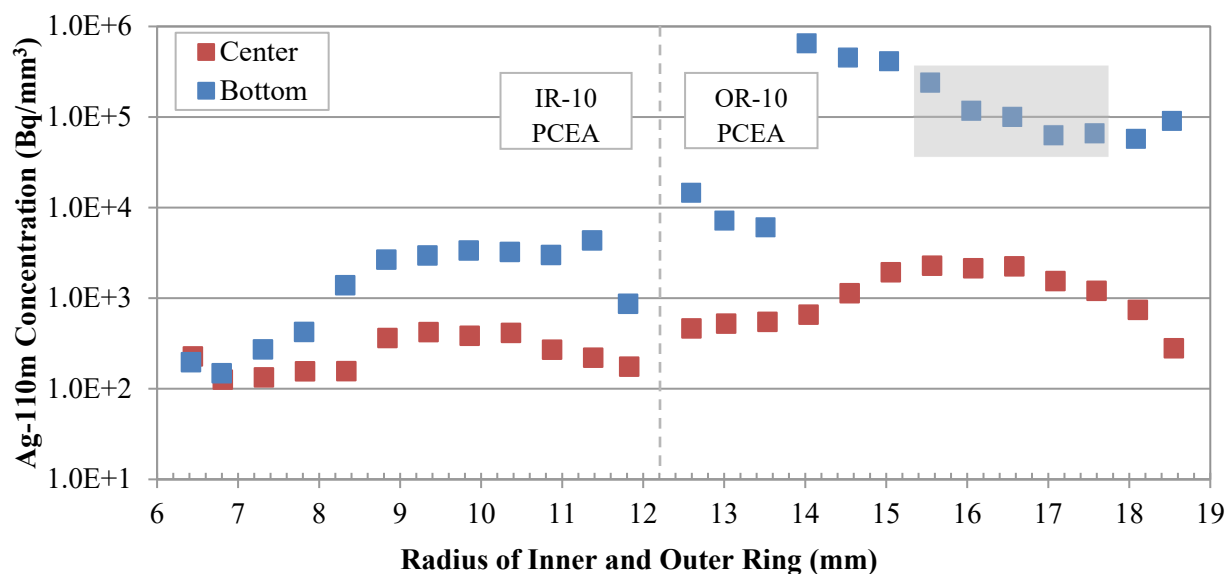


Figure 44. Ag-110m concentration profiles at the axial top and center of the Capsule 10 rings. Gray shading denotes bottom segments affected by ring movement during sampling.

8. CAPSULE 12 INNER AND OUTER RING FISSION PRODUCT PROFILES

Figure 45 and Figure 46 give the radial profiles of select fission product concentrations for the IR and OR at the axial center and bottom of the rings, respectively. Appendix B features tabularized summaries of the fission product concentrations, ring segment volumes, and uncertainties. The IR was made of graphitic matrix, and the OR was made of PCEA graphite. The nubs on the outside of the OR were milled and collected separately from the radial segments. In the as-fabricated condition, the gap between the IR and OR was 0.089 mm, and the PIE measurements showed the gap increased to 0.14 mm at the EOI (Stempien et al. 2016). The average compact-to-IR gap increased from 0.069 mm to 0.10 mm over the course of the irradiation.

Because the equipment had not been used for about one year, some additional clean, unirradiated graphite was milled at various points before and after the Capsule 12 milling activities. This served to further sweep out the cyclone separator and was used as practice for the hot cell technicians to refamiliarize themselves with the sampling processes. Prior to taking the first samples on the bottom end of the Capsule 12 IR, a vial of clean graphite fines was placed at the outlet from the cyclone separator, and the cyclone separator was run for 5 minutes. Then, the usual pre-sampling activity was performed by milling about 1 gram of clean, unirradiated graphite and collecting it in the cyclone separator. After completing milling of the Capsule 12 IR (and before beginning milling of the OR), the usual three post-sampling cuts of clean graphite were performed, followed by an additional three clean graphite samples. Then, two pre-sampling activities involving milling and collecting clean graphite (instead of the usual one) were performed prior beginning sampling of the bottom end of the OR.

While sampling the axial center of the IR, after the second segment (IR12-C2) had been milled, the vial for that segment was inadvertently left at the cyclone separator, and approximately 0.4 g of the expected 0.6 g from the third segment (IR12-C3) was collected in the IR12-C2 vial. The third vial (IR12-C3) was then placed at the cyclone separator, and the remaining ~0.2 g of the third segment was collected in it. Thus, in Figure 45, the segment at about $x = 11.4$ mm is artificially high, and the segment near $x = 10.8$ mm is artificially low. Since the exact volume of material from the third segment that was captured in the second segment is not known, no attempts were made to correct the concentrations of these two data points. Instead, the total activity measured from the samples collected from these two segments was summed and normalized by the total volume of these two segments. The activity concentrations from combining the IR12-C2 and IR12-C3 segments are given in Table 6 for select isotopes.

Table 6. Activity concentrations for selected isotopes from the combination of the activities measured in segments IR12-C2 and IR12-C3. The dimensions and errors are also given.

	Concentration from Combining Segments IR12-C2 and IR12-C3 (Bq/mm ³)	Relative Error of Concentration (%)
Ag-110m	<3.61E+0	N/A
Ce-144	3.32E+2	1.9
Cs-134	3.73E+0	1.6
Cs-137	1.51E+1	1.7
Eu-154	1.67E+1	1.4
Eu-155	9.54E+0	1.4
Ru-106	1.03E+1	2.8
Sb-125	5.03E-1	1.9
Sr-90	5.59E+0	9.2
Segment Volume (mm ³)	706.83	N/A
Segment Volume Error (+ mm ³)	1.27	N/A
Segment Volume Error (– mm ³)	3.33	N/A
Average Segment Radius (mm)	11.072	N/A
Average Segment Radius Error (mm)	0.019	N/A

When sampling the axial center of the OR, some extra material was sampled as part of segment OR12-C8 (at about $x = 13.6$ in Figure 45). This happened when the 10-mm diameter end mill was accidentally plunged 0.254-mm too deep straight into the ring. The mill was retracted (pulled straight back) to the correct position and then the sample was taken from around the circumference of the ring. The volume of the OR12-C8 segment included the intended sampling volume plus the extra material (0.254-mm deep and 10-mm in diameter) from the initial plunge that was too deep. This extra volume was subtracted from what was to be the nominal volume of segment nine (at $x = 13.2$ in Figure 45). Thus, the concentrations for Segments 8 (OR12-C8) and 9 (OR12-C9) were corrected for the sampling mistake.

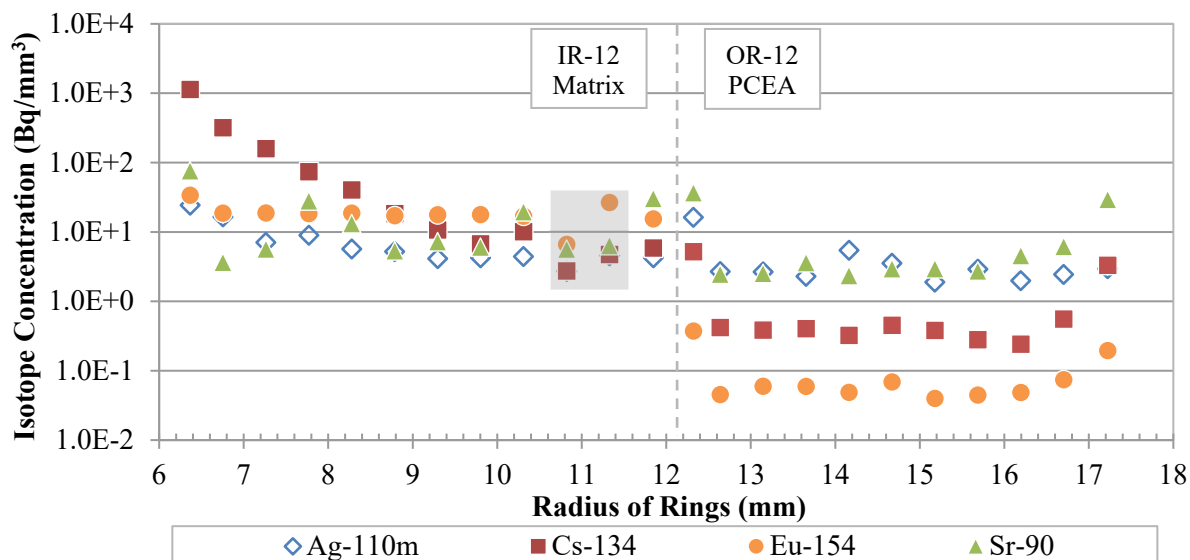


Figure 45. Radial profiles for select fission products at the axial center of the Capsule 12 IR and OR. The open symbols denote values derived from MDAs. Gray shading shows the IR-12 segments where roughly 60% of the third segment (around $x = 10.8$ mm) was collected in the vial for the second segment (around $x = 11.4$ mm).

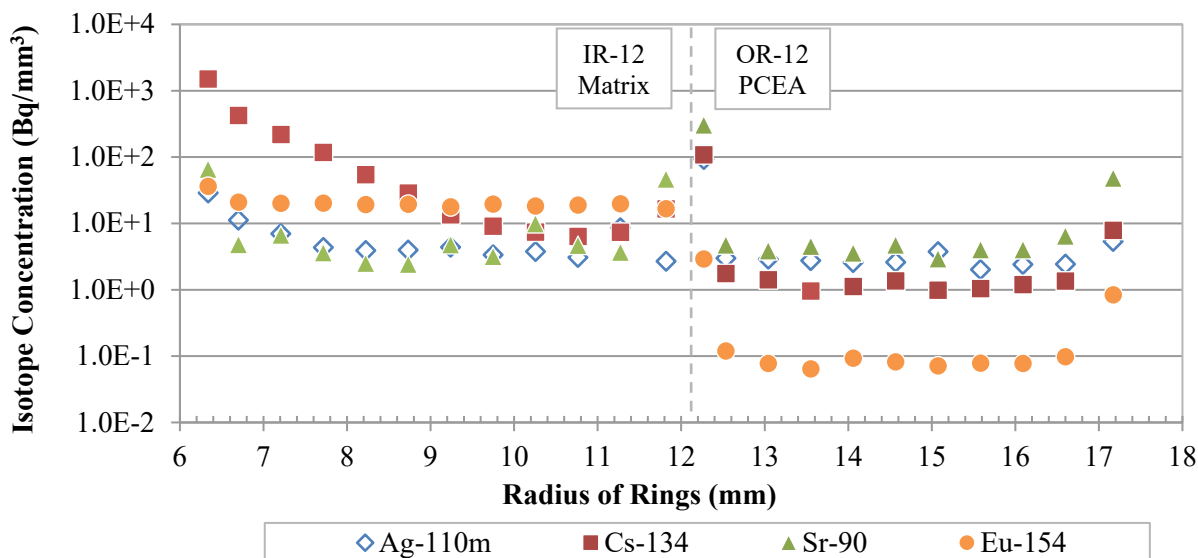


Figure 46. Radial profiles for select fission products at the axial bottom of the Capsule 12 IR and OR. The open symbols denote values derived from MDAs.

8.1 Cs-134 in Capsule 12

Figure 47 shows the Cs-134 profiles from the axial center and bottom of the rings. The IR profiles decrease linearly from the inside toward the outside, except at the outer surface where the concentration begins to increase again. The increase at the IR outer surface again suggests some Cs-134 transported in the gaps. Despite the Capsule 12 IR having the coldest irradiation temperature of all the rings to undergo physical sampling (782°C), the shape of the Cs-134 profile in the ring is similar to what was seen in Capsules 3, 5, 7 and 10. One notable difference between the Capsule 12 IR and the other IRs is that the difference between the maximum and minimum Cs-134 concentrations in IR-12 is more than two orders of magnitude. The difference between the max and min Cs-134 concentrations in IR-05 was a little less than two orders of magnitude, and in the other capsules, this difference was less than one order of magnitude. This suggests there was significant transport from the compacts to the IR, but the solid-state diffusion was considerably slower at the lower temperatures in Capsule 12.

The OR concentration profiles are quite flat across the middle and peaked on the inner and outer surfaces. The model predicts they should decrease sharply in the radial direction. The peaked concentrations at the inner and outer surfaces are common with many of the OR profiles in the other capsules. The flat profile across the middle portion of the OR was not predicted by the model and was only seen in one other capsule (i.e., Capsule 5). Of the rings to undergo physical sampling, the Capsule 5 and 12 ORs had the lowest irradiation temperatures. In fact, the Capsule 5 OR was lowest at 677°C versus 741°C for OR-12.

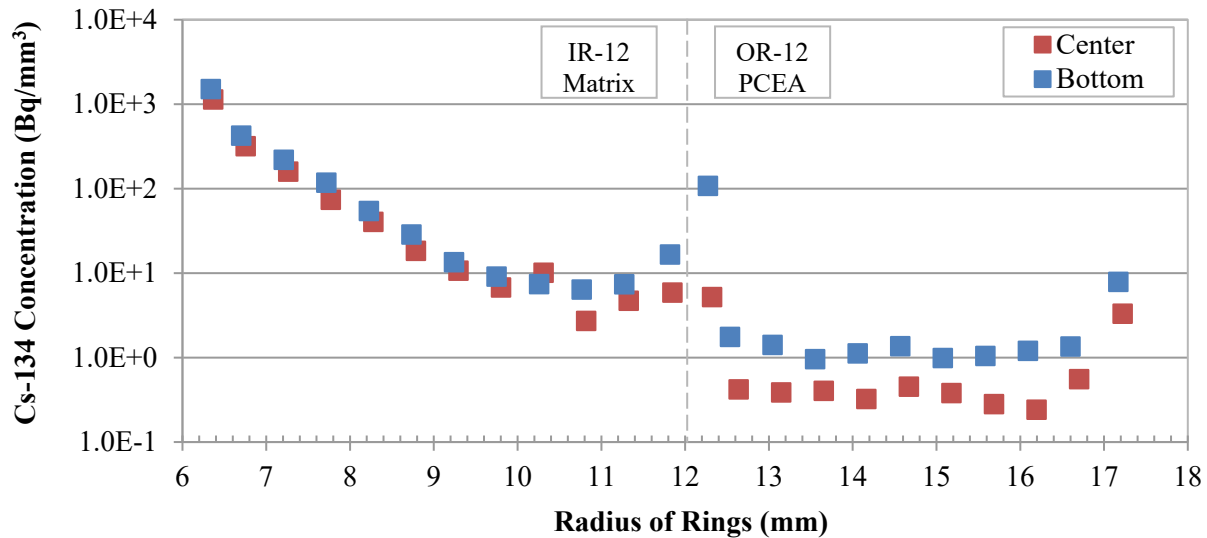


Figure 47. Concentrations of Cs-134 at the axial center and bottom of the Capsule 12 rings.

8.2 Eu-154 and Sr-90 in Capsule 12

Figure 48 shows the Eu-154 radial profiles for the center and bottom of the Capsule 12 rings. The IR profile has a maximum on the inner surface, and then it is virtually flat across its thickness to the outer surface. Here, there is no local maximum at the outer surface. The Capsule 5 IR Eu-154 profile is the only other IR that bears some resemblance to this, but IR-05 has a local maximum at its outer surface that IR-12 does not have.

In the Capsule 12 OR, there is an Eu-154 maximum at the OR inner surface, a flat profile across the middle, and then a local maximum at the outer surface. The concentration at the middle of the OR is over two orders of magnitude lower than in the IR. Only Capsule 5 (which also had a relatively low-OR

irradiation temperature) had a similar decrease from the IR to the OR. The local maximum on the OR-12 outer surface is evidence of gap transport.

Figure 49 shows the Sr-90 profiles for the centers and bottoms of the Capsule 12 rings. The OR Sr-90 profile closely resembles the shape of the OR Eu-154 profile. The Sr-90 IR profiles are generally peaked at the inner and outer surface, and on average, they are roughly flat across the middle. However, there is noticeable up and down variation in the Sr-90 concentration across the middle of the IR that was not seen in the other Capsule 12 IR and OR profiles. The model predicts very little Sr-90 in the IR (and virtually no Sr-90 in the OR) with very little penetration into the IR. These measurements seem to indicate the model underpredicts Sr-90 transport in the Capsule 12 rings.

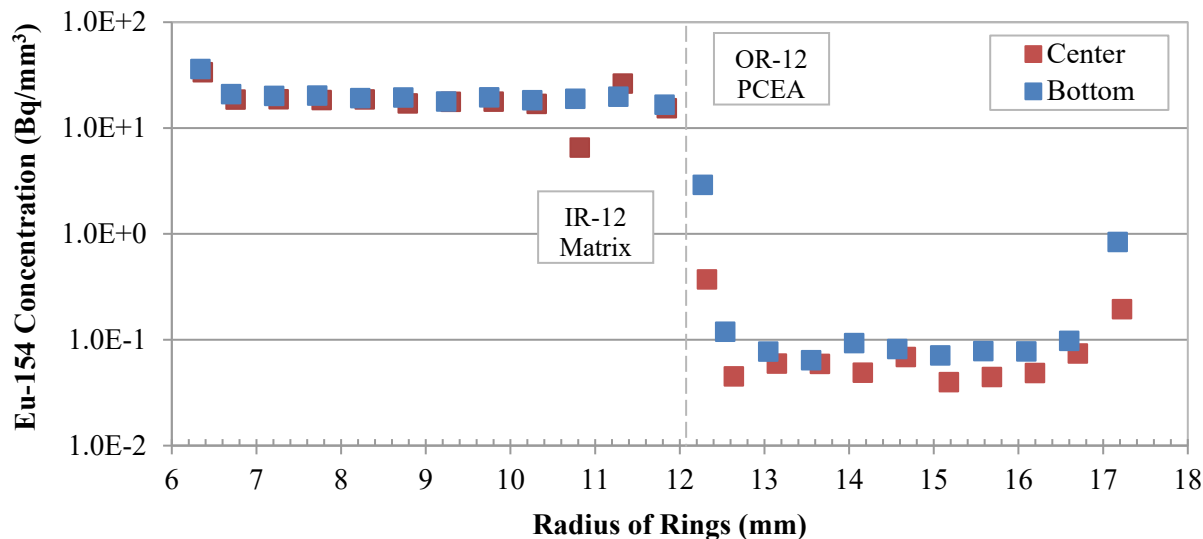


Figure 48. Concentrations of Eu-154 at the axial center and bottom of the Capsule 12 rings.

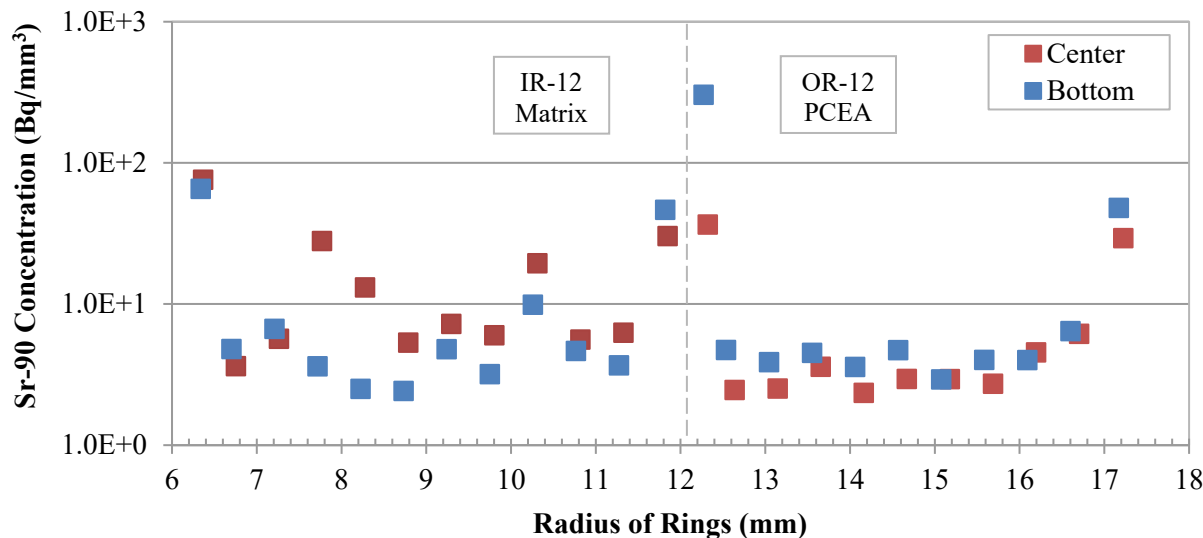


Figure 49. Concentrations of Sr-90 at the axial center and bottom of the Capsule 12 IR and OR.

8.3 Ag-110m in Capsule 12

Given the decay time between the end of the AGR-3/4 irradiation and the Capsule 12 physical sampling was almost 10 half-lives of Ag-110m, no Ag-110m was detected in any of the Capsule 12 samples. The Ag-110m points in Figure 45 and Figure 46 were all derived from MDAs.

9. EVALUATION OF NUB INVENTORIES AS AN INDICATION OF THE STRENGTH OF SHORT-CIRCUIT TRANSPORT VERSUS DIFFUSIVE TRANSPORT

The nubs from the ORs of Capsules 3, 7, 10, and 12 were sampled and analyzed separately from the purely circumferential segments. Table 7 gives the decay-corrected activities of select fission products in the nubs. Table 7 also compares the activity concentrations in the nubs to the activity concentrations measured in the outermost circumferential segments of the rings. The nubs contained substantial activity. In Capsules 3, 10, and 12, the concentrations of the isotopes (except Ag-110m) were higher in the nubs than in the outermost segments of the rings. This supports the hypothesis that short-circuit, gap transport occurred causing relatively high surface concentrations on the outer surfaces of the rings. The ratio of the fission product concentrations in the nubs to those in the outermost segment of the ORs was generally highest for the coldest ring (Capsule 12), lower for the medium-temperature rings from Capsules 3 and 10, and lowest of all for the hottest OR from Capsule 7. This suggests gap transport was less significant at the high temperatures in Capsule 7 where diffusive transport was rapid enough to compete with the gas-phase gap transport. Gap transport was more significant in the cooler capsules where diffusive, solid-state transport was slower than in the hot capsules.

In Capsule 7, all the isotope concentrations in the nubs were less than in the outermost ring segment. The exception was Sr-90, which had a nub concentration 18% higher than in the outermost radial segment. This could be evidence of significant Sr-90 transport via a gaseous precursor and a highly volatile intermediate. In this case, the gaseous precursor is the noble gas Kr-90, and the volatile intermediate is Rb-90. Kr-90 produced from fission rapidly decays ($t_{1/2} = 32$ seconds) to Rb-90, which rapidly decays ($t_{1/2} = 2.6$ minutes) to Sr-90 ($t_{1/2} = 28.8$ years). As a noble gas, Kr-90 will transport more rapidly than Sr-90. The intermediate Rb-90 is much more volatile than Sr given that its melting point is 32°C compared to 777°C for Sr. In fact, comparing the direct fission yields of Sr-90, Rb-90, and Kr-90, it is apparent that most of the long-lived Sr-90 was produced from the decay of Kr-90 and Rb-90. The independent fission yield of Sr-90 is $0.01\% < \text{fission yield} \leq 0.1\%$, the independent fission yield of Kr-90 is considerably higher at $> 3.0\%$, and the fission yield for Rb-90 is $0.1\% < \text{fission yield} \leq 1\%$ (Baum et al. 2009). The elevated concentration of Sr-90 on the Capsule 7 OR nubs could be the result of rapid, gas-gap transport of gaseous Kr-90 and volatile Rb-90 prior to their decaying to Sr-90.

This same mechanism for Sr-90 would be active in the other capsules as well, but its effect is harder to discern from comparing the nub concentrations with the outer segment concentrations. Capsule 7 was the only case where the Sr-90 concentration was higher in the nubs, *and* the other isotopes concentrations were lower in the nubs. This could be due to the rapid initial transport of the short-lived Kr-90 and Rb-90 precursors at the high temperatures of Capsule 7. At the lower temperatures in the other capsules, these short-lived precursors may have transported slower and decayed to Sr-90 prior to transporting as far as in Capsule 7. The distinct similarities in the shapes of the Eu-154 and Sr-90 profiles across rings in all capsules suggests that the dominant mechanism of Sr-90 transport is similar to that of Eu-154, and therefore, the transport of short-lived Sr-90 precursors is not a major effect.

Table 7. Activities, activity concentrations, and comparisons of nub and first segment concentrations of select fission products. Nub volume approximated by dividing collected nub mass by material density.

	OR-03 Nubs	OR-07 Nubs	OR-10 Nubs	OR-12 Nubs	OR-03 Nubs	OR-07 Nubs	OR-10 Nubs	OR-12 Nubs
Material	PCEA	PCEA	PCEA	PCEA				
Density (g/cm ³)	1.84	1.84	1.84	1.84				
Mass (g)	0.161	0.0565	0.0396	0.0577				
Volume (mm ³)	87.50	30.71	21.52	31.36				
	Nub Decay-corrected Activities (Bq)				Nub Activity Concentration (Bq/mm ³)			
Ag-110m	9.71E+3	9.90E+1	4.71E+5	8.39E+2	1.11E+2	3.22E+0	2.19E+4	2.68E+1
Ce-144	1.99E+4	7.16E+2	5.02E+7	9.40E+6	2.28E+2	2.33E+1	2.33E+6	3.00E+5
Cs-134	7.08E+4	8.77E+2	7.61E+4	3.20E+3	8.09E+2	2.86E+1	3.54E+3	1.02E+2
Cs-137	8.28E+4	3.36E+3	3.25E+4	4.82E+4	9.46E+2	1.09E+2	1.51E+3	1.54E+3
Eu-154	4.12E+3	7.51E+1	2.61E+2	2.45E+2	4.71E+1	2.45E+0	1.21E+1	7.82E+0
Eu-155	2.94E+3	5.10E+1	2.55E+2	2.20E+2	3.36E+1	1.66E+0	1.19E+1	7.02E+0
Ru-106	7.07E+2	1.19E+2	1.27E+5	1.93E+4	8.09E+0	3.89E+0	5.89E+3	6.15E+2
Sb-125	7.43E+2	6.45E+1	2.32E+3	2.10E+2	8.49E+0	2.10E+0	1.08E+2	6.70E+0
Sr-90	7.88E+4	4.57E+3	1.76E+4	1.76E+4	9.01E+2	1.49E+2	8.18E+2	5.61E+2
	Ratio of Nub to First Segment Inventory				Ratio of Nub Concentration to First Segment Concentration			
Ag-110m	0.16	5.4E-4	9.1E-3	0.23	0.69	0.01	0.19	5.00
Ce-144	0.56	1.5E-2	1.58	0.90	2.51	0.22	32.5	19.7
Cs-134	0.48	2.7E-3	4.9E-2	0.59	2.14	0.04	1.02	12.9
Cs-137	0.52	1.1E-2	8.9E-2	0.52	2.31	0.16	1.83	11.5
Eu-154	1.39	3.4E-2	0.49	0.43	6.20	0.48	10.1	9.31
Eu-155	1.54	1.7E-2	0.38	1.15	6.90	0.24	7.75	25.2
Ru-106	0.20	3.8E-2	0.26	0.41	0.88	0.54	5.29	8.98
Sb-125	0.46	1.1E-2	0.17	0.52	2.05	0.16	3.42	11.4
Sr-90	1.13	7.9E-2	0.54	0.53	5.04	1.14	11.17	11.70
	Shading indicates MDA in the nubs measurements only.							
	Shading indicates MDA in both the first segment and nub measurements.							
	Shading indicates MDA in the first segment measurements, but a measurable value in the nubs.							

10. ESTIMATION OF SR-90 INVENTORY IN THE RINGS

The total inventories of key gamma-emitting fission products in the AGR-3/4 IR and OR were quantified via non-destructive gamma scanning (Harp et al. 2020), and they comprise an important part of the total AGR-3/4 fission product mass balance (Stempien et al. 2018). That mass balance can also be used to adjust the predicted particle and/or compact releases used in the AGR-3/4 fission product transport model (Humrickhouse et al. 2016). To fully quantify beta-emitting Sr-90, the destructive burn-leach process followed by a Sr-90 separation and counting is necessary. Only the portions of the AGR-3/4 rings that were physically sampled have been through the burn-leach process to quantify Sr-90. None of the inner or outer AGR-3/4 rings have been through burn-leach in their entirety. Thus, the Sr-90 inventory has not been quantified for any of the AGR-3/4 IR and OR. This quantification has not been performed because it was decided to keep the unsampled remnants (see Figure 11 for an example) of the rings for possible future heating tests in inert or oxidizing atmospheres. However, estimates of the Sr-90 inventories in the rings can be made using the results of the physical sampling.

The Capsule 5 rings were only sampled at their axial centers, accounting for just under 20% of the total ring volume. The remaining 80% has not been analyzed for Sr-90. To estimate the total Sr-90 inventory in the Capsule 5 rings, it was assumed that the average Sr-90 concentration in the center segment was the same throughout the ring. The activity measured in each of the radial segments taken from the axial center were summed and divided by the total volume represented by those segments to give an average concentration. Then, the Capsule 5 Sr-90 inventory in the rings was estimated by multiplying that concentration by the total volume of the ring.

Rings from Capsules 3, 7, 8, 10, and 12 were sampled at one of the axial ends and at the axial center. This sampled material accounted for about 40% of the volume of the ring. The remaining 60% has not been analyzed for Sr-90. Figure 50 depicts the process for estimating the total Sr-90 inventory in a ring that was sampled at its center and at one of its ends. Both the volumetric concentration and the Sr-90 inventory (i.e., activity) are known for the 1-cm tall segment at the end and the 1-cm tall segment at the axial center. There is a 1.04-cm tall segment that was not sampled in between the end segment and the center segment (also see Figure 11 for an example). Knowing the concentrations and axial locations of the end segment and the center segment, linear interpolation was used to estimate the concentration in the unsampled segment. Multiplying this concentration by the volume of that segment gives the Sr-90 inventory in that segment. The ORs from Capsules 3, 7, 10, and 12 had a total of eight substantial nubs on their surfaces. Four of these nubs were toward the axial top and four were toward the axial bottom end of the rings. Since only one of the ends (top or bottom) of these rings was sampled, only four of the nubs from that one end were sampled. These nub samples were collected in separate vials and analyzed for Sr-90. Based on PGS of the rings that showed generally axially symmetric fission product distributions for the gamma emitters, it was assumed the axial distribution of Sr-90 would also be axially symmetric. Accordingly, the estimated total Sr-90 inventory in a Capsule 3, 7, 10, or 12 OR (I_{total}) is given by Equation 4, where I_{end} is the measured inventory in the end; I_{nubs} is the inventory in the four nubs at one of the ends; I_{center} is the measured inventory in the axial center; and $I_{interpolated}$ is the estimated inventory in the unsampled segment between the center and end segments:

$$I_{total} = 2(I_{end} + I_{interpolated} + I_{nubs}) + I_{center} \quad (4)$$

None of the IRs had nubs, and the Capsule 8 OR had nubs that were so small they were not sampled separately. For the Capsules 3, 7, 8, 10, and 12 IRs and the Capsule 8 OR, the estimated total Sr-90 inventory is given by Equation 5.

$$I_{total} = 2(I_{end} + I_{interpolated}) + I_{center} \quad (5)$$

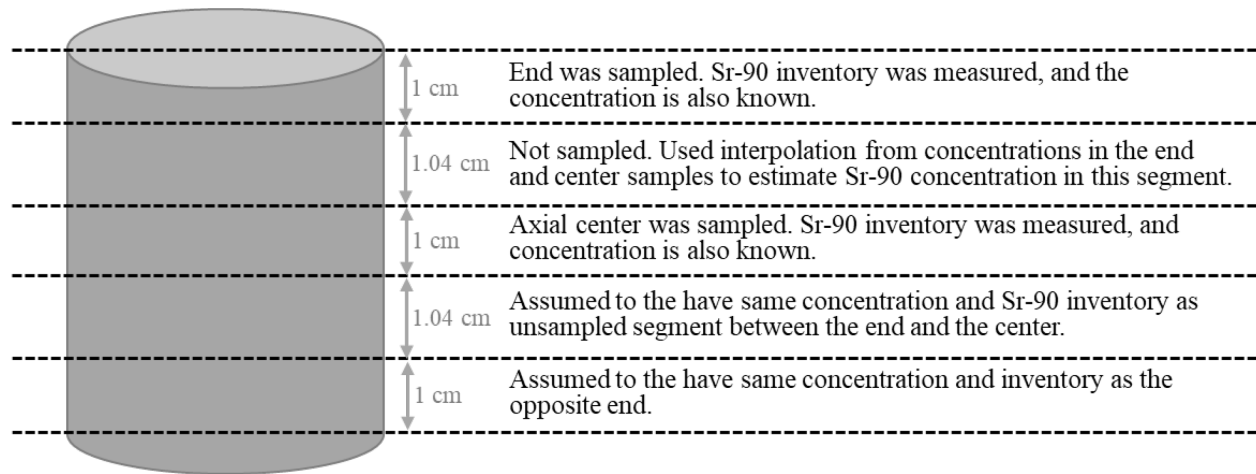


Figure 50. Process used to estimate the Sr-90 inventory in a ring sampled at its center and one of its ends.

Table 8 and Table 9 give two estimates of the total Sr-90 content in the rings that were subject to physical sampling. Table 8 gives Sr-90 inventory estimates if the inventory in the nubs on the ORs are neglected. Table 9 gives an estimate that includes the contribution from the nubs. The green shading in Table 9 indicates values where nub inventories were included. Due to significant interference from other beta emitters, most of the Sr-90 concentrations in IR-05 are represented by MDAs (see Section 4.2). The values given in Table 8 and Table 9 only account for actual measured values. If the IR-05 MDAs are also used to estimate the activity of Sr-90, the upper bound on the possible Sr-90 inventory in IR-05 is $<1.51\text{E}5$ Bq.

Table 8. Estimated inventory of Sr-90 in the IR and OR of the AGR-3/4 capsules that were physically sampled. The estimate in this table neglects the contribution from any nubs that were sampled separately from the rest of the ring. The activity was decay-corrected to EOI + 1 day.

Not Including Nubs	Activity (Bq)			Capsule Fraction			Particle Equivalents		
Capsule	IR	OR	Total	IR	OR	Total	IR	OR	Total
3	8.78E+7	2.14E+6	9.00E+7	3.98E-3	9.71E-5	4.08E-3	3.06E+1	7.45E-1	3.13E+1
5	1.19E+5	3.08E+5	4.27E+5	4.67E-6	1.21E-5	1.67E-5	3.59E-2	9.25E-2	1.28E-1
7	3.69E+8	1.33E+6	3.71E+8	1.44E-2	5.16E-5	1.44E-2	1.10E+2	3.96E-1	1.11E+2
8	4.59E+7	3.23E+5	4.62E+7	1.83E-3	1.29E-5	1.85E-3	1.41E+1	9.91E-2	1.42E+1
10	6.99E+7	9.51E+5	7.09E+7	3.35E-3	3.70E-5	3.39E-3	2.57E+1	2.84E-1	2.60E+1
12	2.19E+5	2.41E+5	4.60E+5	2.19E-5	2.41E-5	4.61E-5	1.68E-1	1.85E-1	3.53E-1

Table 9. Estimated inventory of Sr-90 in the IR and OR of the AGR-3/4 capsules that were physically sampled. The estimate in this table includes the contribution from the nubs sampled separately from the ORs of Capsules 3, 7, 10, and 12. Green shading denotes values including the contributions from nubs. The activity was decay-corrected to EOI + 1 day.

Including Nubs	Activity (Bq)			Capsule Fraction			Particle Equivalents		
Capsule	IR	OR	Total	IR	OR	Total	IR	OR	Total
3	8.78E+7	2.30E+6	9.01E+7	3.98E-3	1.04E-4	4.09E-3	3.06E+1	7.99E-1	3.14E+1
5	1.19E+5	3.08E+5	4.27E+5	4.67E-6	1.21E-5	1.67E-5	3.59E-2	9.25E-2	1.28E-1
7	3.69E+8	1.33E+6	3.71E+8	1.44E-2	5.20E-5	1.44E-2	1.10E+2	3.99E-1	1.11E+2
8	4.59E+7	3.23E+5	4.62E+7	1.83E-3	1.29E-5	1.85E-3	1.41E+1	9.91E-2	1.42E+1
10	6.99E+7	9.51E+5	7.09E+7	3.35E-3	3.70E-5	3.39E-3	2.57E+1	2.84E-1	2.60E+1
12	2.19E+5	2.76E+5	4.95E+5	2.19E-5	2.76E-5	4.96E-5	1.68E-1	2.12E-1	3.80E-1

11. CONCLUSIONS

Radial fission product concentration profiles were measured for gamma-emitting fission products (e.g., Ag-110m, Cs-134, and Eu-154) and beta-emitting Sr-90 in the inner and outer carbon rings from six different AGR-3/4 irradiation capsules. Two of the IRs were PCEA graphite. Three of the IRs were graphitic matrix material similar to the historic German A3-27 matrix formulation. One of the IRs was IG-110 graphite. Five of the ORs were PCEA graphite, and one of the ORs was IG-110 graphite. In future work, these profiles will be compared in detail to simulations of AGR-3/4 fission product transport and to non-destructive measurements. The ultimate goal of this work is the extraction of new fission product transport parameters (e.g., diffusivity and sorptivity) from these data. The immediate conclusions are as follows:

- Elevated concentrations of Ag, Cs, Eu, and Sr were detected on the outer surfaces of some IRs and ORs. This indicates a short-circuit pathway may exist whereby gas-phase fission product transport occurred in the gaps between the compacts and the IR and the IR and OR. This complicates the analysis because it means that 1D diffusive transport was not the only transport mechanism.
- Ag-110m profiles had the most variation. Some profiles were peaked at an inner or outer surface. Some were peaked at the middle of the ring wall thickness. Some went through inflection points. Some increased radially outward. Some decreased radially outward. In some instances, the concentrations varied significantly depending on whether the ring was sampled at the axial center or at one of the ends. The axial non-uniformities are generally consistent with observations in non-destructive gamma scanning of the rings, which also showed non-uniform axial distributions for Ag-110m. This may adversely impact the ability to extract reasonable diffusion coefficients for this isotope.
- In many cases, the IR Cs-134 profiles decrease somewhat linearly from the inside to the outside, and the qualitative shape of these profiles compared reasonably with the model. The step changes in concentration across the IR-OR gap were generally consistent with the model predictions as well. The ORs tend to have flatter Cs-134 profiles, but there are also OR profiles (particularly in the hotter capsules) that decrease noticeably in the outward radial direction. Local increases in concentration at the OR's inner and outer surfaces are more pronounced than for the IRs. This combined with the flatter, though in some cases still linear, profiles in the ORs suggest that some effect (i.e., gap transport) in addition to simple diffusion is taking place.
- Eu-154 and Sr-90 profiles tend to have very similar shapes. This suggests that they transport via the same mechanisms and have the same rate-limiting steps. In the IRs, both isotopes have their highest concentrations at the inner surface and drop sharply moving radially outward where they are relatively flat across the rest of the IR. This indicates a transport process where the isotopes are sorbed on the inner surface of the ring, but diffusion into the ring from that surface is quite slow. By comparison, the OR profiles are largely flat and feature maxima at the inner and/or outer surfaces of the OR. There are frequently local maxima at IR outer surfaces as well. These local maxima on the outer surfaces could indicate that gap transport has a minor, but noticeable, effect. In some capsules, the qualitative Sr-90 behavior across the ring gaps was consistent with the model (using legacy Sr-90 transport parameters), but in other capsules, the model was inconsistent with the measurements and seemed to underestimate the amount of Sr-90 in the ORs.

- The analysis of the small nubs on the outer surfaces of some of the ORs revealed fission product concentrations in the nubs that were often higher than in the outermost segments of the rings. This supports the hypothesis that short-circuit, gap transport occurred, causing relatively high surface concentrations on the outer surfaces of the rings. Comparing the ratios of the fission product concentrations in the nubs to those in the outermost segment of the ORs suggests that gap transport was less significant at high temperatures where diffusive transport was rapid enough to clearly overpower gas-phase gap transport and more significant at lower irradiation temperatures in the cooler capsules, where diffusive, solid-state transport is not as rapid.
- Some Sr-90 transport via a gaseous precursor (Kr-90) and a highly volatile intermediate (Rb-90) likely occurred in all capsules. This was most noticeable in the hottest capsule, Capsule 7, which was the only capsule where the Sr-90 concentration was higher in the nubs than in the OR segment; while at the same time, the other isotopes concentrations were lower in the nubs than in the OR segment. However, the distinct similarities in the shapes of the Eu-154 and Sr-90 profiles across rings in all capsules suggests that the dominant mechanism of Sr-90 transport is similar to that of Eu-154 and that the transport of short-lived Sr-90 precursors is not a major effect.
- Total Sr-90 inventories were estimated in the rings based on the results from the physical sampling. These results will be used to adjust the predicted particle and/or compact releases used in the AGR-3/4 fission product transport model.
- Given the different irradiation temperatures among the capsules and the rings, it was not possible to discern fundamental differences in the transport of isotopes within the different carbon materials (i.e., graphitic matrix, IG-110, or PCEA). It may be possible to do this while determining diffusion coefficients and sorptivities from the concentration profiles. Future work will also rigorously compare the model predictions with the measured concentration profiles.

12. REFERENCES

- Baum, E. M., et al. 2010. *Nuclides and Isotopes Chart of the Nuclides 17th Edition*. Schenectady: Knolls Atomic Power Laboratory, Bechtel.
- Chadwick, M. B., et al. 2011. “ENDF/B-VII.1 Nuclear Data for Science and Technology: Cross-Sections, Covariances, Fission Product Yields and Decay Data.” Nuclear Data Sheets 112, no. 12 (December): 2887–2996. <https://doi.org/10.1016/j.nds.2011.11.002>.
- Collin, B.P., et al. 2018. “The AGR-3/4 Fission Product Transport Irradiation Experiment.” Nuclear Engineering and Design 327 (February): 212–227. <https://doi.org/10.1016/j.nucengdes.2017.12.016>.
- Collin, B. P. 2015a. “AGR-3/4 Irradiation Test Final As-Run Report.” INL/EXT-15-35550, Rev. 0, Idaho National Laboratory. <https://doi.org/10.2172/1196553>.
- Collin, B. P. 2015b “AGR-3/4 Irradiation Experiment Test Plan.” PLN-3867, Rev. 1, Idaho National Laboratory.
- Demkowicz, P. A. 2017. “AGR-3/4 Phase 2 Post-Irradiation Examination Plan.” PLN-5382, Idaho National Laboratory.
- Hawkes, G. et al. 2016. “AGR-3/4 Daily As-Run Thermal Analyses.” ECAR-2807, Rev. 1, Idaho National Laboratory.
- Harp, J. M., J. D. Stempien, and P. A. Demkowicz. 2020. “Gamma Spectrometry Examination of the AGR-3/4 Irradiation.” INL/EXT-20-58254, Rev. 0, Idaho National Laboratory.
- Humrickhouse, P. W., et al. 2018. “Preliminary Estimation of Fission Product Diffusion Coefficients from AGR-3/4 Data.” Paper presented at the 9th *International Topical Meeting on High Temperature Reactor Technology (HTR-2018)*, Warsaw, Poland, October 2018.

- Humrickhouse, P. W., et al. 2016. “Modeling and Analysis of Fission Product Transport in the AGR-3/4 Experiment.” Paper 18693 presented at the *International Topical Meeting on High Temperature Reactor Technology (HTR-2016)*, Las Vegas, NV, USA, November 6-10, 2016.
- Hunn, J. D., et al. 2014. “Fabrication and Characterization of Driver Fuel Particles, Designed-to-Fail Fuel Particles, and Fuel Compacts for the US AGR-3/4 Irradiation Test.” *Nuclear Engineering and Design* 271 (May): 123–130. <https://doi.org/10.1016/j.nucengdes.2013.11.020>.
- Hunn, J. D., M. P. Trammel, and F. C. Montgomery. 2011. “Data Compilation for AGR-3/4 Matrix Ring Blank Lot ARB-B1.” ORNL/TM-2011/272, Oak Ridge National Laboratory. <https://doi.org/10.2172/1606046>.
- Hunn, J. D. and R. A. Lowden. 2007. “Data Compilation for AGR-3/4 Driver Fuel Coated Particle Composite LEU03-09T.” ORNL/TM-2007/019, Oak Ridge National Laboratory. <https://doi.org/10.2172/931362>.
- Hunn, J. D. and J. H. Miller. 2009. “Data Compilation for AGR-3/4 Designed-to-Fail (DTF) Fuel Particle Batch LEU04-02DTF.” Oak Ridge National Laboratory, ORNL/TM-2008/193. <https://doi.org/10.2172/940336>.
- Hunn, J., M. P. Trammell, and F. C. Montgomery. 2011. “Data Compilation for AGR-3/4 Designed-to-Fail (DTF) Fuel Compact Lot (LEU03-10TOP2/LEU03-07DTF-OP1)-Z.” ORNL/TM-2011/124, Oak Ridge National Laboratory.
- INL. 2020. “Technical Program Plan for INL Advanced Reactor Technologies Advanced Gas Reactor Fuel Development and Qualification Program,” PLN-3636, INL/MIS-10-20662, Rev. 9, Idaho National Laboratory.
- INL. 2017. “AGR-3/4 Ring Sampling.” HFEF-LI-0162, Rev. 1, Idaho National Laboratory.
- INL. 2011. “ATR Advanced Gas Reactor (AGR-3/4) Capsule 3 Assembly and Details.” DWG-602703, Rev. 3, Idaho National Laboratory.
- JCGM. 2008. “Evaluation of measurement data – Guide to the expression of uncertainty in measurement,” JCGM 100:2008, Joint Committee for Guides in Metrology. https://ncc.nesdis.noaa.gov/documents/documentation/JCGM_100_2008_E.pdf.
- Kercher, A. K., et al. 2011. “Data Compilation for AGR-3/4 Designed-to-Fail (DTF) Fuel Particle Batch LEU03-07DTF.” ORNL/TM-2011/109, Oak Ridge National Laboratory. <https://doi.org/10.2172/1649083>.
- Kercher, A. K. and J. D. Hunn. 2006. “Results from ORNL Characterization of Nominal 350 μm LEUCO Kernels (LEU03) from the BWXT G73V-20-69303 Composite.” ORNL/TM-2006/552, Oak Ridge National Laboratory. <https://doi.org/10.2172/974612>.
- Stempien, J. D., et al. 2018. “AGR-3/4 Experiment Preliminary Mass Balance.” INL/EXT-18-46049, Rev. 0, Idaho National Laboratory. <https://doi.org/10.2172/1558760>.
- Stempien, J. D., et al. 2016. “AGR-3/4 Irradiation Test Train Disassembly and Component Metrology First Look Report.” Rev. 1, INL/EXT-16-38005, Idaho National Laboratory.
- Sterbentz, J. W. 2015. “JMOCUP As-Run Daily Physics Depletion Calculation for the AGR-3/4 TRISO Particle Experiment in ATR Northeast Flux Trap.” ECAR-2753, Rev. 1, Idaho National Laboratory.

Appendix A

PNNL Report Numbers

Table A-1. PNNL radiochemical analyses report numbers. Note that revised Sr-90 results were sent from PNNL to INL in May 2021 and that these revised results are separate from the gamma spectroscopy and ICP-MS results sent previously. Only the Sr-90 results were affected by these revisions.

Batch	Ring Sample in Batch	PNNL Report Numbers
1	IR-07	ASR 0411
2	IR-07 and IR-03	ASR 0450
3	IR-03 and OR-07	ASR 0455
4	OR-07	ASR 0460
5	OR-07 and OR-03	ASR 0468
6	OR-03 and IR-08	ASR 0475
7	IR-08	ASR 0480
8	IR-05 and IR-08	ASR 0502
9	IR-05 and OR-05	ASR 0510
10	OR-05 and OR-08	ASR 0523
11	IR-07 and OR-08	ASR 0534
12	OR-10	ASR 0755
13	OR-10	ASR 0756
14	IR-10	ASR 0759
15	IR-10	ASR 0760
16	OR-12	ASR 1016
17	IR-12 and OR-12	ASR 1019
18	IR-12	ASR 1022
19	IR-12 and OR-12	ASR 1028

Appendix B

Fission Product Concentrations, Ring Dimensions, and Uncertainties

Table B-1. Capsule 3 IR, axial top: decay-corrected concentrations (Bq per mm³) of selected fission products for each radial segment sampled at the axial top of the Capsule 3 IR. The volume and average radius $[(r_{\text{inner}} + r_{\text{outer}})/2]$ of each segment are also given. Shading indicates a value derived from an MDA.

IR-03 Top (Bq/mm ³)	IR3-T1	IR3-T2	IR3-T3	IR3-T4	IR3-T5	IR3-T6	IR3-T7	IR3-T8	IR3-T9	IR3-T10	IR3-T11	IR3-T12
Ag-110m	2.01E+2	3.16E+2	3.68E+2	4.20E+2	4.56E+2	4.07E+2	3.19E+2	1.75E+2	7.13E+1	6.43E+1	5.30E+1	1.35E+2
Ce-144	1.00E+2	4.27E+1	3.01E+1	3.86E+1	4.47E+1	3.63E+1	1.41E+1	3.75E+1	2.39E+1	4.13E+1	6.33E+1	4.36E+2
Cs-134	2.71E+2	2.78E+2	3.28E+2	3.81E+2	4.65E+2	4.49E+2	4.59E+2	6.16E+2	6.87E+2	7.38E+2	7.50E+2	1.68E+3
Cs-137	4.58E+2	3.39E+2	3.71E+2	4.31E+2	5.31E+2	5.16E+2	5.09E+2	6.85E+2	7.69E+2	8.20E+2	8.32E+2	2.02E+3
Eu-154	1.91E+0	7.99E-1	6.12E-1	8.51E-1	1.52E+0	2.20E+0	2.07E+0	4.35E+0	2.87E+0	2.26E+0	1.65E+2	4.54E+3
Eu-155	1.32E+0	7.19E-1	8.20E-1	1.38E+0	1.17E+0	1.25E+0	1.31E+0	3.05E+0	2.01E+0	1.80E+0	1.10E+2	3.14E+3
Ru-106	7.74E+0	2.06E+1	2.26E+1	3.03E+1	1.71E+1	4.83E-4	1.48E+1	2.00E+1	1.07E+1	1.95E+1	2.88E+1	5.30E+1
Sb-125	2.94E+1	1.63E+1	5.63E-1	2.65E+1	3.55E+1	3.50E+1	3.30E+1	4.30E+1	4.49E+1	4.59E+1	4.54E+1	2.69E+2
Sr-90	1.16E+2	5.33E+1	5.10E+1	6.06E+1	7.10E+1	9.55E+1	1.29E+2	2.03E+2	1.44E+2	1.46E+2	1.38E+4	1.45E+5
Segment Volume (mm ³)	282.95	363.07	346.86	330.64	314.43	298.22	282.00	265.79	249.57	233.36	217.14	93.28
Average Segment Radius (mm)	11.82	11.38	10.87	10.36	9.85	9.34	8.84	8.33	7.82	7.31	6.80	6.43

Table B-2. Capsule 3 IR, axial top: decay-corrected concentrations (particle equivalents per mm³) of selected fission products for each radial segment sampled at the axial top of the Capsule 3 IR. The volume and average radius $[(r_{\text{inner}} + r_{\text{outer}})/2]$ of each segment are also given. Shading indicates a value derived from an MDA.

IR-03 Top (Particle Equivalents/mm ³)	IR3-T1	IR3-T2	IR3-T3	IR3-T4	IR3-T5	IR3-T6	IR3-T7	IR3-T8	IR3-T9	IR3-T10	IR3-T11	IR3-T12
Ag-110m	5.62E-3	8.81E-3	1.03E-2	1.17E-2	1.27E-2	1.14E-2	8.89E-3	4.88E-3	1.99E-3	1.79E-3	1.93E+2	4.91E+2
Ce-144	2.00E-6	8.53E-7	6.02E-7	7.71E-7	8.94E-7	7.26E-7	2.81E-7	7.49E-7	4.78E-7	8.26E-7	1.65E-1	1.14E+0
Cs-134	7.63E-5	7.80E-5	9.23E-5	1.07E-4	1.31E-4	1.26E-4	1.29E-4	1.73E-4	1.93E-4	2.08E-4	2.75E+1	6.17E+1
Cs-137	1.39E-4	1.03E-4	1.13E-4	1.31E-4	1.61E-4	1.57E-4	1.55E-4	2.08E-4	2.34E-4	2.49E-4	3.29E+1	7.99E+1
Eu-154	1.64E-5	6.87E-6	5.26E-6	7.32E-6	1.31E-5	1.89E-5	1.78E-5	3.74E-5	2.47E-5	1.94E-5	1.85E+2	5.09E+3
Eu-155	1.68E-5	9.15E-6	1.04E-5	1.76E-5	1.49E-5	1.59E-5	1.66E-5	3.88E-5	2.56E-5	2.29E-5	1.82E+2	5.21E+3
Ru-106	7.44E-7	1.98E-6	2.17E-6	2.92E-6	1.64E-6	4.64E-11	1.43E-6	1.92E-6	1.03E-6	1.87E-6	3.61E-1	6.63E-1
Sb-125	1.16E-4	6.39E-5	2.21E-6	1.04E-4	1.40E-4	1.37E-4	1.30E-4	1.69E-4	1.77E-4	1.81E-4	2.33E+1	1.38E+2
Sr-90	4.05E-5	1.86E-5	1.77E-5	2.11E-5	2.47E-5	3.32E-5	4.48E-5	7.08E-5	5.01E-5	5.08E-5	6.28E+2	6.59E+3
Segment Volume (mm ³)	282.95	363.07	346.86	330.64	314.43	298.22	282.00	265.79	249.57	233.36	217.14	93.28
Average Segment Radius (mm)	11.82	11.38	10.87	10.36	9.85	9.34	8.84	8.33	7.82	7.31	6.80	6.43

Table B-3. Relative uncertainties in the concentrations reported in Table B-1 and Table B-2. Absolute uncertainties in the segment volumes and average radii of the segments. N/A denotes a case where an isotope was not detected, and therefore, no uncertainty is available.

IR-03 Top	Units	IR3-T1	IR3-T2	IR3-T3	IR3-T4	IR3-T5	IR3-T6	IR3-T7	IR3-T8	IR3-T9	IR3-T10	IR3-T11	IR3-T12
Ag-110m Concentration	+	2.0%	2.0%	2.0%	2.0%	2.1%	2.1%	2.2%	2.2%	2.3%	2.5%	2.6%	2.8%
	–	2.1%	2.1%	2.1%	2.1%	2.2%	2.2%	2.3%	2.3%	2.4%	2.5%	2.7%	2.9%
Ce-144 Concentration	+	15.0%	9.0%	N/A	19.0%	27.0%	8.0%	35.0%	13.0%	48.0%	N/A	N/A	15.1%
	–	15.0%	9.0%	N/A	19.0%	27.0%	8.1%	35.0%	13.1%	48.0%	N/A	N/A	15.1%
Cs-134 Concentration	+	2.0%	2.0%	2.0%	2.0%	2.1%	2.1%	2.2%	2.2%	2.3%	2.5%	2.6%	2.8%
	–	2.1%	2.1%	2.1%	2.1%	2.2%	2.2%	2.3%	2.3%	2.4%	2.5%	2.7%	2.9%
Cs-137 Concentration	+	2.0%	2.0%	2.0%	2.0%	2.1%	2.1%	2.2%	2.2%	2.3%	2.5%	2.6%	2.8%
	–	2.1%	2.1%	2.1%	2.1%	2.2%	2.2%	2.3%	2.3%	2.4%	2.5%	2.7%	2.9%
Eu-154 Concentration	+	2.0%	5.0%	6.0%	7.0%	5.0%	2.1%	3.1%	2.2%	2.3%	2.5%	2.6%	2.8%
	–	2.1%	5.0%	6.0%	7.0%	5.1%	2.2%	3.2%	2.3%	2.4%	2.5%	2.7%	2.9%
Eu-155 Concentration	+	9.0%	N/A	N/A	N/A	19.0%	3.1%	10.0%	3.2%	6.1%	17.1%	2.6%	3.6%
	–	9.0%	N/A	N/A	N/A	19.0%	3.1%	10.1%	3.2%	6.2%	17.1%	2.7%	3.6%
Ru-106 Concentration	+	23.0%	N/A	N/A	N/A	N/A	N/A	N/A	N/A	N/A	N/A	N/A	28.1%
	–	23.0%	N/A	N/A	N/A	N/A	N/A	N/A	N/A	N/A	N/A	N/A	28.1%
Sb-125 Concentration	+	2.0%	2.0%	2.0%	2.0%	2.1%	2.1%	1.3%	2.2%	2.3%	2.5%	2.6%	2.8%
	–	2.1%	2.1%	2.1%	2.1%	2.2%	2.2%	1.4%	2.3%	2.4%	2.5%	2.7%	2.9%
Sr-90 Concentration	+	3.0%	3.0%	3.0%	3.0%	3.0%	3.1%	3.1%	3.2%	3.2%	3.3%	3.4%	2.8%
	–	3.1%	3.1%	3.1%	3.1%	3.1%	3.1%	3.2%	3.2%	3.3%	3.4%	3.5%	2.9%
Segment Volume (mm ³)	+ mm ³	0.34	0.73	1.04	1.36	1.69	2.02	2.35	2.68	3.01	3.34	3.67	1.81
	– mm ³	1.77	2.35	2.38	2.45	2.57	2.73	2.92	3.14	3.38	3.63	3.91	1.90
Average Radius of Segment (mm)	+/- mm	0.009	0.016	0.023	0.030	0.037	0.044	0.052	0.059	0.066	0.074	0.081	0.088

Table B-4. Capsule 3 IR, axial center: decay-corrected concentrations (Bq per mm³) of selected fission products for each radial segment sampled at the axial center of the Capsule 3 IR. The volume and average radius [(r_{inner} + r_{outer})/2] of each segment are also given. Shading indicates a value derived from an MDA.

IR-03 Center (Bq/mm ³)	IR3-C1	IR3-C2	IR3-C3	IR3-C4	IR3-C5	IR3-C6	IR3-C7	IR3-C8	IR3-C9	IR3-C10	IR3-C11	IR3-C12
Ag-110m	1.99E+2	4.27E+2	3.25E+2	3.33E+2	4.09E+2	2.24E+2	1.07E+2	8.30E+1	7.39E+1	7.92E+1	6.42E+1	5.61E+1
Ce-144	1.36E+2	3.58E+1	2.33E+1	2.49E+1	3.08E+1	4.03E+1	8.25E+1	7.55E+1	3.61E+1	8.95E+1	1.26E+2	2.25E+2
Cs-134	3.36E+2	5.29E+2	4.50E+2	5.39E+2	7.27E+2	7.23E+2	8.81E+2	1.03E+3	1.10E+3	1.28E+3	1.16E+3	1.52E+3
Cs-137	4.94E+2	5.96E+2	4.90E+2	5.96E+2	7.98E+2	7.87E+2	9.62E+2	1.12E+3	1.20E+3	1.38E+3	1.27E+3	1.79E+3
Eu-154	1.91E+1	5.80E+0	2.00E+0	1.29E+0	1.64E+0	8.86E-1	1.25E+0	8.50E-1	8.76E-1	1.39E+1	1.37E+3	2.83E+3
Eu-155	1.30E+1	3.45E+0	9.61E-1	7.15E-1	6.92E-1	9.47E-1	2.30E+0	2.15E+0	9.79E-1	8.14E+0	8.69E+2	1.89E+3
Ru-106	1.13E+1	3.18E+1	1.86E+1	1.08E+1	1.95E+1	2.02E+1	5.73E+1	5.26E+1	2.46E+1	6.22E+1	4.75E+1	1.34E+2
Sb-125	2.64E+1	2.91E+1	2.68E+1	3.46E+1	5.02E+1	4.77E+1	5.76E+1	6.18E+1	6.54E+1	7.29E+1	6.59E+1	2.67E+2
Sr-90	4.91E+2	1.83E+2	5.72E+1	4.40E+1	4.07E+1	3.64E+1	3.30E+1	1.32E+1	2.05E+1	1.68E+3	5.23E+4	6.11E+4
Segment Volume (mm ³)	282.99	363.13	346.92	330.70	314.49	298.28	282.06	265.85	249.63	233.42	217.20	96.57
Average Segment Radius (mm)	11.82	11.38	10.87	10.36	9.85	9.34	8.84	8.33	7.82	7.31	6.80	6.43

Table B-5. Capsule 3 IR, axial center: decay-corrected concentrations (particle equivalents per mm³) of selected fission products for each radial segment sampled at the axial center of the Capsule 3 IR. The volume and average radius [(r_{inner} + r_{outer})/2] of each segment are also given. Shading indicates a value derived from an MDA.

IR-03 Center (Particle equivalents /mm ³)	IR3-C1	IR3-C2	IR3-C3	IR3-C4	IR3-C5	IR3-C6	IR3-C7	IR3-C8	IR3-C9	IR3-C10	IR3-C11	IR3-C12
Ag-110m	5.56E-3	1.19E-2	9.07E-3	9.29E-3	1.14E-2	6.25E-3	2.99E-3	2.32E-3	2.06E-3	2.21E-3	2.33E+2	2.04E+2
Ce-144	2.73E-6	7.15E-7	4.65E-7	4.97E-7	6.16E-7	8.05E-7	1.65E-6	1.51E-6	7.21E-7	1.79E-6	3.28E-1	5.87E-1
Cs-134	9.45E-5	1.49E-4	1.27E-4	1.51E-4	2.04E-4	2.03E-4	2.48E-4	2.89E-4	3.10E-4	3.60E-4	4.26E+1	5.55E+1
Cs-137	1.50E-4	1.81E-4	1.49E-4	1.81E-4	2.42E-4	2.39E-4	2.92E-4	3.41E-4	3.66E-4	4.21E-4	5.02E+1	7.09E+1
Eu-154	1.64E-4	4.98E-5	1.72E-5	1.11E-5	1.41E-5	7.62E-6	1.07E-5	7.30E-6	7.53E-6	1.19E-4	1.53E+3	3.17E+3
Eu-155	1.65E-4	4.39E-5	1.22E-5	9.10E-6	8.81E-6	1.21E-5	2.92E-5	2.74E-5	1.25E-5	1.04E-4	1.44E+3	3.14E+3
Ru-106	1.08E-6	3.06E-6	1.79E-6	1.03E-6	1.88E-6	1.94E-6	5.51E-6	5.06E-6	2.37E-6	5.97E-6	5.95E-1	1.68E+0
Sb-125	1.04E-4	1.14E-4	1.05E-4	1.36E-4	1.97E-4	1.87E-4	2.26E-4	2.43E-4	2.57E-4	2.87E-4	3.38E+1	1.37E+2
Sr-90	1.71E-4	6.35E-5	1.99E-5	1.53E-5	1.42E-5	1.27E-5	1.15E-5	4.59E-6	7.14E-6	5.83E-4	2.37E+3	2.77E+3
Segment Volume (mm ³)	282.99	363.13	346.92	330.70	314.49	298.28	282.06	265.85	249.63	233.42	217.20	96.57
Average Segment Radius (mm)	11.82	11.38	10.87	10.36	9.85	9.34	8.84	8.33	7.82	7.31	6.80	6.43

Table B-6. Relative uncertainties in the concentrations reported in Table B-4 and Table B-5. Absolute uncertainties in the segment volumes and average radii of the segments. N/A denotes a case where an isotope was not detected, and therefore, no uncertainty is available.

IR-03 Center	Units	IR3-C1	IR3-C2	IR3-C3	IR3-C4	IR3-C5	IR3-C6	IR3-C7	IR3-C8	IR3-C9	IR3-C10	IR3-C11	IR3-C12
Ag-110m Concentration	+	2.0%	2.0%	2.0%	2.0%	2.1%	2.1%	2.2%	3.2%	3.2%	4.2%	3.4%	N/A
	–	2.1%	2.1%	2.1%	2.1%	2.2%	2.2%	2.3%	3.2%	3.3%	4.3%	3.5%	N/A
Ce-144 Concentration	+	9.0%	22.0%	21.0%	N/A	N/A	N/A	N/A	N/A	N/A	N/A	N/A	N/A
	–	9.0%	22.0%	21.0%	N/A	N/A	N/A	N/A	N/A	N/A	N/A	N/A	N/A
Cs-134 Concentration	+	2.0%	2.0%	2.0%	2.0%	2.1%	2.1%	2.2%	2.2%	2.3%	2.5%	2.6%	2.8%
	–	2.1%	2.1%	2.1%	2.1%	2.2%	2.2%	2.3%	2.3%	2.4%	2.5%	2.7%	2.9%
Cs-137 Concentration	+	2.0%	2.0%	2.0%	2.0%	2.1%	2.1%	2.2%	2.2%	2.3%	2.5%	2.6%	2.8%
	–	2.1%	2.1%	2.1%	2.1%	2.2%	2.2%	2.3%	2.3%	2.4%	2.5%	2.7%	2.9%
Eu-154 Concentration	+	2.0%	5.0%	4.0%	4.0%	3.0%	8.0%	19.0%	26.0%	11.1%	2.5%	2.6%	2.8%
	–	2.1%	5.0%	4.1%	4.1%	3.1%	8.1%	19.0%	26.0%	11.1%	2.5%	2.7%	2.9%
Eu-155 Concentration	+	2.0%	21.0%	N/A	N/A	N/A	N/A	N/A	N/A	N/A	10.1%	2.6%	7.3%
	–	2.1%	21.0%	N/A	N/A	N/A	N/A	N/A	N/A	N/A	10.1%	2.7%	7.3%
Ru-106 Concentration	+	N/A	N/A	N/A	N/A	N/A	N/A	N/A	N/A	N/A	N/A	N/A	N/A
	–	N/A	N/A	N/A	N/A	N/A	N/A	N/A	N/A	N/A	N/A	N/A	N/A
Sb-125 Concentration	+	2.0%	2.0%	2.0%	3.0%	2.1%	2.1%	2.2%	2.2%	2.3%	2.5%	2.6%	2.8%
	–	2.1%	2.1%	2.1%	3.1%	2.2%	2.2%	2.3%	2.3%	2.4%	2.5%	2.7%	2.9%
Sr-90 Concentration	+	3.0%	2.0%	2.0%	2.0%	3.0%	3.1%	3.1%	4.1%	3.2%	2.5%	2.6%	2.8%
	–	3.1%	2.1%	2.1%	2.1%	3.1%	3.1%	3.2%	4.2%	3.3%	2.5%	2.7%	2.9%
Segment Volume (mm ³)	+ mm ³	0.39	0.78	1.08	1.39	1.71	2.04	2.36	2.69	3.02	3.35	3.68	1.88
	– mm ³	1.79	2.37	2.39	2.47	2.58	2.74	2.93	3.15	3.39	3.65	3.92	1.97
Average Radius of Segment (mm)	+/- mm	0.011	0.017	0.024	0.031	0.038	0.045	0.052	0.059	0.067	0.074	0.081	0.088

Table B-7. Capsule 3 OR, axial top: decay-corrected concentrations (Bq per mm³) of selected fission products for each radial segment sampled at the axial top of the Capsule 3 OR. The volume and average radius $[(r_{\text{inner}} + r_{\text{outer}})/2]$ of each segment are also given. Shading indicates a value derived from an MDA.

OR-03 Top (Bq/mm ³)	OR3-T1	OR3-T2	OR3-T3	OR3-T4	OR3-T5	OR3-T6	OR3-T7	OR3-T8	OR3-T9	OR3-T10	OR3-T11
Ag-110m	1.59E+2	4.42E+2	2.03E+3	1.87E+3	1.75E+3	1.77E+3	1.69E+3	1.36E+3	1.15E+3	1.15E+3	1.20E+3
Ce-144	9.06E+1	1.38E+1	4.51E+1	1.54E+1	2.80E+1	5.65E+1	2.02E+1	3.64E+1	1.60E+1	2.11E+1	7.97E+1
Cs-134	3.77E+2	2.45E+2	6.26E+2	4.43E+2	3.93E+2	4.20E+2	4.48E+2	4.12E+2	3.99E+2	4.95E+2	1.09E+3
Cs-137	4.08E+2	2.50E+2	6.30E+2	4.49E+2	4.06E+2	4.34E+2	4.71E+2	4.32E+2	4.20E+2	5.30E+2	1.19E+3
Eu-154	7.57E+0	6.18E+0	1.30E+1	6.70E+0	4.83E+0	4.90E+0	4.11E+0	3.32E+0	3.12E+0	3.49E+0	1.12E+1
Eu-155	4.85E+0	4.49E+0	8.24E+0	4.85E+0	4.07E+0	3.14E+0	3.03E+0	2.15E+0	1.96E+0	2.62E+0	6.03E+0
Ru-106	9.11E+0	1.05E+1	3.47E+1	1.17E+1	8.31E+0	4.39E+1	2.57E+1	1.29E+1	4.84E+0	1.07E+1	2.73E+1
Sb-125	4.13E+0	1.95E+0	9.14E+0	1.10E+1	1.00E+1	1.57E+1	1.94E+1	1.93E+1	2.13E+1	3.09E+1	1.49E+2
Sr-90	1.79E+2	1.31E+2	2.95E+2	1.48E+2	1.16E+2	9.69E+1	9.33E+1	8.41E+1	7.43E+1	8.70E+1	3.21E+2
Segment Volume (mm ³)	390.88	381.76	372.64	363.52	354.40	345.28	336.16	327.04	317.92	308.79	227.48
Average Segment Radius (mm)	16.33	15.95	15.57	15.19	14.80	14.42	14.04	13.66	13.28	12.90	12.56

Table B-8. Capsule 3 OR, axial top: decay-corrected concentrations (particle equivalents per mm³) of selected fission products for each radial segment sampled at the axial top of the Capsule 3 OR. The volume and average radius $[(r_{\text{inner}} + r_{\text{outer}})/2]$ of each segment are also given. Shading indicates a value derived from an MDA.

OR-03 Top (Particle Equivalents/mm ³)	OR3-T1	OR3-T2	OR3-T3	OR3-T4	OR3-T5	OR3-T6	OR3-T7	OR3-T8	OR3-T9	OR3-T10	OR3-T11
Ag-110m	4.44E-3	1.23E-2	5.66E-2	5.22E-2	4.88E-2	4.93E-2	4.71E-2	3.80E-2	3.20E-2	3.21E-2	3.35E-2
Ce-144	1.81E-6	2.75E-7	9.01E-7	3.08E-7	5.60E-7	1.13E-6	4.03E-7	7.28E-7	3.20E-7	4.21E-7	1.59E-6
Cs-134	1.06E-4	6.89E-5	1.76E-4	1.24E-4	1.11E-4	1.18E-4	1.26E-4	1.16E-4	1.12E-4	1.39E-4	3.06E-4
Cs-137	1.24E-4	7.61E-5	1.91E-4	1.36E-4	1.23E-4	1.32E-4	1.43E-4	1.31E-4	1.28E-4	1.61E-4	3.62E-4
Eu-154	6.50E-5	5.31E-5	1.12E-4	5.76E-5	4.15E-5	4.22E-5	3.53E-5	2.85E-5	2.69E-5	3.00E-5	9.62E-5
Eu-155	6.17E-5	5.72E-5	1.05E-4	6.18E-5	5.18E-5	4.00E-5	3.85E-5	2.73E-5	2.50E-5	3.34E-5	7.67E-5
Ru-106	8.76E-7	1.01E-6	3.34E-6	1.12E-6	7.98E-7	4.22E-6	2.47E-6	1.24E-6	4.65E-7	1.03E-6	2.63E-6
Sb-125	1.62E-5	7.68E-6	3.59E-5	4.30E-5	3.93E-5	6.16E-5	7.62E-5	7.60E-5	8.39E-5	1.21E-4	5.84E-4
Sr-90	6.22E-5	4.57E-5	1.03E-4	5.17E-5	4.02E-5	3.37E-5	3.25E-5	2.93E-5	2.58E-5	3.03E-5	1.12E-4
Segment Volume (mm ³)	390.88	381.76	372.64	363.52	354.40	345.28	336.16	327.04	317.92	308.79	227.48
Average Segment Radius (mm)	16.33	15.95	15.57	15.19	14.80	14.42	14.04	13.66	13.28	12.90	12.56

Table B-9. Relative uncertainties in the concentrations reported in Table B-7 and Table B-8. Absolute uncertainties in the segment volumes and average radii of the segments. N/A denotes a case where an isotope was not detected, and therefore, no uncertainty is available.

OR-03 Top	Units	OR3-T1	OR3-T2	OR3-T3	OR3-T4	OR3-T5	OR3-T6	OR3-T7	OR3-T8	OR3-T9	OR3-T10	OR3-T11
Ag-110m Concentration	+	2.0%	2.0%	2.0%	2.0%	2.0%	2.0%	2.1%	2.1%	2.1%	2.2%	2.2%
	–	2.1%	2.1%	2.1%	2.1%	2.1%	2.1%	2.2%	2.2%	2.2%	2.2%	2.3%
Ce-144 Concentration	+	13.0%	N/A	N/A	33.0%	N/A	N/A	28.0%	43.0%	30.0%	N/A	8.1%
	–	13.0%	N/A	N/A	33.0%	N/A	N/A	28.0%	43.0%	30.0%	N/A	8.1%
Cs-134 Concentration	+	2.0%	2.0%	2.0%	2.0%	2.0%	2.0%	2.1%	2.1%	2.1%	2.2%	2.2%
	–	2.1%	2.1%	2.1%	2.1%	2.1%	2.1%	2.2%	2.2%	2.2%	2.2%	2.3%
Cs-137 Concentration	+	2.0%	2.0%	2.0%	2.0%	2.0%	2.0%	2.1%	2.1%	2.1%	2.2%	2.2%
	–	2.1%	2.1%	2.1%	2.1%	2.1%	2.1%	2.2%	2.2%	2.2%	2.2%	2.3%
Eu-154 Concentration	+	2.0%	2.0%	2.0%	2.0%	2.0%	2.0%	2.1%	2.1%	2.1%	2.2%	2.2%
	–	2.1%	2.1%	2.1%	2.1%	2.1%	2.1%	2.2%	2.2%	2.2%	2.2%	2.3%
Eu-155 Concentration	+	3.0%	4.0%	7.0%	3.0%	7.0%	5.0%	16.0%	4.0%	2.1%	8.0%	4.1%
	–	3.1%	4.0%	7.0%	3.1%	7.0%	5.1%	16.0%	4.1%	2.2%	8.1%	4.1%
Ru-106 Concentration	+	N/A	N/A	N/A	N/A	N/A	N/A	N/A	N/A	N/A	N/A	N/A
	–	N/A	N/A	N/A	N/A	N/A	N/A	N/A	N/A	N/A	N/A	N/A
Sb-125 Concentration	+	3.0%	19.0%	3.0%	2.0%	3.0%	2.0%	2.1%	2.1%	2.1%	2.2%	2.2%
	–	3.1%	19.0%	3.1%	2.1%	3.1%	2.1%	2.2%	2.2%	2.2%	2.2%	2.3%
Sr-90 Concentration	+	4.0%	4.0%	4.0%	4.0%	4.0%	4.0%	4.0%	3.1%	3.1%	3.1%	3.1%
	–	4.0%	4.0%	4.1%	4.1%	4.1%	4.1%	4.1%	3.1%	3.1%	3.2%	3.2%
Segment Volume (mm ³)	+ mm ³	0.37	0.57	0.79	1.03	1.27	1.52	1.76	2.01	2.25	2.50	2.08
	– mm ³	2.43	2.42	2.43	2.46	2.53	2.61	2.72	2.84	2.98	3.14	2.50
Average Radius of Segment (mm)	+/- mm	0.010	0.016	0.023	0.030	0.037	0.045	0.052	0.059	0.066	0.074	0.081

Table B-10. Capsule 3 OR, axial center: decay-corrected concentrations (Bq per mm³) of selected fission products for each radial segment sampled at the axial center of the Capsule 3 OR. The volume and average radius $[(r_{\text{inner}} + r_{\text{outer}})/2]$ of each segment are also given. Shading indicates a value derived from an MDA.

OR-03 Center (Bq/mm ³)	OR3-C1	OR3-C2	OR3-C3	OR3-C4	OR3-C5	OR3-C6	OR3-C7	OR3-C8	OR3-C9	OR3-C10	OR3-C11
Ag-110m	5.35E+1	1.10E+2	1.78E+2	2.42E+2	3.05E+2	3.65E+2	4.23E+2	4.59E+2	6.11E+2	5.70E+2	9.31E+2
Ce-144	2.95E+2	1.17E+1	6.38E+0	1.11E+1	1.25E+1	1.63E+1	1.75E+1	1.55E+1	7.31E+0	1.64E+1	5.95E+1
Cs-134	4.19E+2	2.40E+2	2.54E+2	2.87E+2	3.03E+2	3.45E+2	3.70E+2	3.77E+2	4.77E+2	4.44E+2	1.10E+3
Cs-137	5.19E+2	2.43E+2	2.58E+2	2.98E+2	3.10E+2	3.61E+2	3.89E+2	3.97E+2	5.08E+2	4.71E+2	1.21E+3
Eu-154	4.72E+0	2.25E+0	2.26E+0	2.16E+0	2.15E+0	2.33E+0	2.14E+0	2.18E+0	2.24E+0	1.63E+0	3.97E+0
Eu-155	3.73E+0	1.55E+0	1.41E+0	2.06E+0	1.19E+0	1.95E+0	1.82E+0	2.05E+0	1.13E+0	9.61E-1	2.45E+0
Ru-106	1.77E+1	8.64E+0	3.93E+0	6.59E+0	1.11E+1	7.01E+0	1.05E+1	6.59E+0	1.25E+1	8.40E+0	2.98E+0
Sb-125	3.33E+0	4.22E+0	6.53E+0	8.18E+0	1.07E+1	1.30E+1	1.56E+1	1.63E+1	2.22E+1	2.03E+1	1.04E+2
Sr-90	1.55E+2	5.57E+1	5.46E+1	5.11E+1	5.22E+1	5.47E+1	4.76E+1	4.37E+1	5.04E+1	3.70E+1	1.10E+2
Segment Volume (mm ³)	391.52	382.40	373.28	364.16	355.04	345.92	336.80	327.68	318.56	309.44	241.53
Average Segment Radius (mm)	16.36	15.97	15.59	15.21	14.83	14.45	14.07	13.69	13.31	12.93	12.58

Table B-11. Capsule 3 OR, axial center: decay-corrected concentrations (particle equivalents per mm³) of selected fission products for each radial segment sampled at the axial center of the Capsule 3 OR. The volume and average radius $[(r_{\text{inner}} + r_{\text{outer}})/2]$ of each segment are also given. Shading indicates a value derived from an MDA.

OR-03 Center (Particle Equivalents/mm ³)	OR3-C1	OR3-C2	OR3-C3	OR3-C4	OR3-C5	OR3-C6	OR3-C7	OR3-C8	OR3-C9	OR3-C10	OR3-C11
Ag-110m	1.49E-3	3.06E-3	4.98E-3	6.74E-3	8.51E-3	1.02E-2	1.18E-2	1.28E-2	1.70E-2	1.59E-2	2.60E-2
Ce-144	5.88E-6	2.33E-7	1.27E-7	2.22E-7	2.49E-7	3.27E-7	3.49E-7	3.09E-7	1.46E-7	3.27E-7	1.19E-6
Cs-134	1.18E-4	6.75E-5	7.12E-5	8.08E-5	8.51E-5	9.69E-5	1.04E-4	1.06E-4	1.34E-4	1.25E-4	3.09E-4
Cs-137	1.58E-4	7.39E-5	7.84E-5	9.05E-5	9.43E-5	1.10E-4	1.18E-4	1.21E-4	1.54E-4	1.43E-4	3.67E-4
Eu-154	4.06E-5	1.94E-5	1.94E-5	1.85E-5	1.85E-5	2.00E-5	1.84E-5	1.87E-5	1.92E-5	1.41E-5	3.41E-5
Eu-155	4.74E-5	1.97E-5	1.80E-5	2.63E-5	1.51E-5	2.48E-5	2.31E-5	2.61E-5	1.44E-5	1.22E-5	3.11E-5
Ru-106	1.70E-6	8.30E-7	3.78E-7	6.33E-7	1.07E-6	6.74E-7	1.01E-6	6.34E-7	1.20E-6	8.07E-7	2.87E-7
Sb-125	1.31E-5	1.66E-5	2.57E-5	3.21E-5	4.19E-5	5.12E-5	6.14E-5	6.42E-5	8.72E-5	7.96E-5	4.10E-4
Sr-90	5.39E-5	1.94E-5	1.90E-5	1.78E-5	1.82E-5	1.90E-5	1.66E-5	1.52E-5	1.75E-5	1.29E-5	3.83E-5
Segment Volume (mm ³)	391.52	382.40	373.28	364.16	355.04	345.92	336.80	327.68	318.56	309.44	241.53
Average Segment Radius (mm)	16.36	15.97	15.59	15.21	14.83	14.45	14.07	13.69	13.31	12.93	12.58

Table B-12. Estimated relative uncertainties in the concentrations reported in Table B-10 and Table B-11. Absolute uncertainties in the segment volumes and average radii of the segments. N/A denotes a case where an isotope was not detected, and therefore, no uncertainty is available.

OR-03 Center	Units	OR3-C1	OR3-C2	OR3-C3	OR3-C4	OR3-C5	OR3-C6	OR3-C7	OR3-C8	OR3-C9	OR3-C10	OR3-C11
Ag-110m Concentration	+	2.1%	2.0%	2.0%	2.0%	2.0%	2.1%	2.1%	2.1%	2.1%	2.2%	2.2%
	–	2.2%	2.1%	2.1%	2.1%	2.1%	2.1%	2.2%	2.2%	2.2%	2.2%	2.3%
Ce-144 Concentration	+	4.2%	16.7%	14.4%	21.8%	N/A	N/A	N/A	N/A	24.9%	N/A	N/A
	–	4.3%	16.7%	14.5%	21.8%	N/A	N/A	N/A	N/A	24.9%	N/A	N/A
Cs-134 Concentration	+	2.0%	2.0%	2.0%	2.0%	2.0%	2.1%	2.1%	2.1%	2.1%	2.2%	2.2%
	–	2.1%	2.1%	2.1%	2.1%	2.1%	2.1%	2.2%	2.2%	2.2%	2.2%	2.3%
Cs-137 Concentration	+	2.0%	2.0%	2.0%	2.0%	2.0%	2.1%	2.1%	2.1%	2.1%	2.2%	2.2%
	–	2.1%	2.1%	2.1%	2.1%	2.1%	2.1%	2.2%	2.2%	2.2%	2.2%	2.3%
Eu-154 Concentration	+	2.0%	2.0%	2.0%	2.0%	2.0%	2.3%	2.4%	2.3%	1.8%	2.2%	2.6%
	–	2.1%	2.1%	2.1%	2.1%	2.1%	2.4%	2.5%	2.3%	1.9%	2.2%	2.7%
Eu-155 Concentration	+	2.1%	2.0%	2.0%	11.3%	4.0%	12.6%	4.1%	8.1%	4.2%	5.1%	6.3%
	–	2.2%	2.1%	2.1%	11.3%	4.0%	12.6%	4.2%	8.1%	4.2%	5.1%	6.4%
Ru-106 Concentration	+	6.3%	N/A	N/A	N/A	N/A	N/A	N/A	N/A	N/A	N/A	N/A
	–	6.3%	N/A	N/A	N/A	N/A	N/A	N/A	N/A	N/A	N/A	N/A
Sb-125 Concentration	+	6.8%	1.8%	2.0%	2.0%	2.0%	1.6%	2.1%	2.1%	2.1%	2.2%	2.2%
	–	6.8%	1.9%	2.1%	2.1%	2.1%	1.7%	2.2%	2.2%	2.2%	2.2%	2.3%
Sr-90 Concentration	+	3.0%	3.0%	3.0%	3.0%	3.0%	3.0%	3.0%	3.1%	3.1%	3.1%	3.1%
	–	3.1%	3.1%	3.1%	3.1%	3.1%	3.1%	3.1%	3.1%	3.1%	3.2%	3.2%
Segment Volume (mm ³)	+ mm ³	0.52	0.67	0.87	1.09	1.32	1.56	1.80	2.04	2.28	2.53	2.22
	– mm ³	2.47	2.45	2.46	2.50	2.56	2.64	2.75	2.87	3.01	3.17	2.68
Average Radius of Segment (mm)	+/- mm	0.015	0.020	0.026	0.032	0.039	0.046	0.053	0.060	0.067	0.075	0.082

Table B-13. Capsule 5 IR, axial center: decay-corrected concentrations (Bq per mm³) of selected fission products for each radial segment sampled at the axial center of the Capsule 5 IR. The volume and average radius $[(r_{\text{inner}} + r_{\text{outer}})/2]$ of each segment are also given. Shading indicates a value derived from an MDA. Interferences from other beta-emitting isotopes made it impossible to estimate an MDA for two of the Sr-90 points. Those points are denoted by “N/A”.

IR-05 Center (Bq/mm ³)	IR5-C1	IR5-C2	IR5-C3	IR5-C4	IR5-C5	IR5-C6	IR5-C7	IR5-C8	IR5-C9	IR5-C10	IR5-C11	IR5-C12
Ag-110m	2.74E+0	6.16E+0	8.91E+0	1.88E+1	1.51E+1	3.34E+1	3.69E+1	2.30E+1	1.13E+2	7.17E+1	2.54E+2	3.27E+3
Ce-144	4.46E+1	6.95E+1	9.09E+1	2.39E+2	1.87E+2	3.75E+2	3.95E+2	3.13E+2	3.75E+2	3.47E+2	3.21E+2	2.61E+3
Cs-134	2.45E+3	2.57E+3	4.24E+3	6.25E+3	8.17E+3	1.08E+4	1.40E+4	1.85E+4	2.29E+4	2.63E+4	3.20E+4	1.33E+5
Cs-137	1.65E+3	1.65E+3	2.74E+3	4.21E+3	5.54E+3	7.30E+3	9.56E+3	1.27E+4	1.62E+4	1.84E+4	2.34E+4	1.01E+5
Eu-154	3.08E+1	2.18E+1	2.21E+1	2.27E+1	2.29E+1	2.26E+1	2.19E+1	2.22E+1	1.84E+1	2.62E+1	2.20E+1	8.39E+1
Eu-155	2.04E+1	1.49E+1	1.38E+1	1.65E+1	1.54E+1	2.31E+1	1.52E+1	1.42E+1	8.59E+0	1.81E+1	9.11E+0	4.86E+1
Ru-106	2.01E+1	4.41E+1	6.07E+1	1.38E+2	1.07E+2	2.20E+2	2.32E+2	1.82E+2	2.22E+2	2.07E+2	1.77E+2	1.40E+3
Sb-125	1.92E+0	3.65E+0	4.82E+0	4.60E+0	8.97E+0	1.87E+1	1.97E+1	1.53E+1	1.86E+1	1.73E+1	1.67E+1	1.26E+2
Sr-90	3.56E+1	8.39E+0	4.81E+0	3.50E+0	1.28E+0	2.43E+0	1.39E+0	N/A	6.72E+0	N/A	1.20E+0	2.03E+2
Segment Volume (mm ³)	281.29	360.86	344.64	328.43	312.22	296.00	279.79	263.57	247.36	231.14	214.93	50.98
Average Segment Radius (mm)	11.75	11.31	10.80	10.29	9.78	9.27	8.77	8.26	7.75	7.24	6.73	6.42

Table B-14. Capsule 5 IR, axial center: decay-corrected concentrations (particle equivalents per mm³) of selected fission products for each radial segment sampled at the axial center of the Capsule 5 IR. The volume and average radius $[(r_{\text{inner}} + r_{\text{outer}})/2]$ of each segment are also given. Shading indicates a value derived from an MDA. Interferences from other beta-emitting isotopes made it impossible to estimate an MDA for two of the Sr-90 points. Those points are denoted by “N/A”.

IR-05 Center (Particle equivalents/mm ³)	IR5-C1	IR5-C2	IR5-C3	IR5-C4	IR5-C5	IR5-C6	IR5-C7	IR5-C8	IR5-C9	IR5-C10	IR5-C11	IR5-C12
Ag-110m	4.56E-5	1.02E-4	1.48E-4	3.13E-4	2.50E-4	5.55E-4	6.14E-4	3.83E-4	1.88E-3	1.19E-3	4.23E-3	5.44E-2
Ce-144	7.73E-7	1.20E-6	1.57E-6	4.13E-6	3.23E-6	6.49E-6	6.84E-6	5.41E-6	6.50E-6	6.00E-6	5.55E-6	4.51E-5
Cs-134	4.72E-4	4.94E-4	8.15E-4	1.20E-3	1.57E-3	2.08E-3	2.68E-3	3.55E-3	4.41E-3	5.06E-3	6.15E-3	2.56E-2
Cs-137	4.23E-4	4.24E-4	7.03E-4	1.08E-3	1.42E-3	1.88E-3	2.46E-3	3.27E-3	4.17E-3	4.72E-3	6.02E-3	2.59E-2
Eu-154	1.90E-4	1.35E-4	1.37E-4	1.40E-4	1.41E-4	1.40E-4	1.36E-4	1.37E-4	1.14E-4	1.62E-4	1.36E-4	5.19E-4
Eu-155	1.93E-4	1.41E-4	1.31E-4	1.56E-4	1.45E-4	2.19E-4	1.44E-4	1.35E-4	8.13E-5	1.71E-4	8.62E-5	4.60E-4
Ru-106	1.45E-6	3.18E-6	4.38E-6	9.99E-6	7.72E-6	1.59E-5	1.67E-5	1.31E-5	1.60E-5	1.49E-5	1.28E-5	1.01E-4
Sb-125	6.18E-6	1.17E-5	1.55E-5	1.48E-5	2.89E-5	6.02E-5	6.33E-5	4.91E-5	5.99E-5	5.58E-5	5.37E-5	4.07E-4
Sr-90	1.07E-5	2.52E-6	1.45E-6	1.05E-6	3.84E-7	7.32E-7	4.19E-7	N/A	2.02E-6	N/A	3.61E-7	6.11E-5
Segment Volume (mm ³)	281.29	360.86	344.64	328.43	312.22	296.00	279.79	263.57	247.36	231.14	214.93	50.98
Average Segment Radius (mm)	11.75	11.31	10.80	10.29	9.78	9.27	8.77	8.26	7.75	7.24	6.73	6.42

Table B-15. Estimated relative uncertainties in the concentrations reported in Table B-13 and Table B-14. Absolute uncertainties in the segment volumes and average radii of the segments. N/A denotes a case where an isotope was not detected, and therefore, no uncertainty is available.

IR-05 Center	Units	IR5-C1	IR5-C2	IR5-C3	IR5-C4	IR5-C5	IR5-C6	IR5-C7	IR5-C8	IR5-C9	IR5-C10	IR5-C11	IR5-C12
Ag-110m Concentration	+	14.0%	N/A	N/A	N/A	N/A	N/A	N/A	13.0%	6.1%	4.3%	2.6%	2.8%
	–	14.0%	N/A	N/A	N/A	N/A	N/A	N/A	13.1%	6.2%	4.3%	2.7%	2.9%
Ce-144 Concentration	+	N/A	N/A	N/A	N/A	N/A	N/A	N/A	N/A	N/A	N/A	N/A	N/A
	–	N/A	N/A	N/A	N/A	N/A	N/A	N/A	N/A	N/A	N/A	N/A	N/A
Cs-134 Concentration	+	2.0%	2.0%	2.0%	2.0%	2.1%	2.1%	2.2%	2.2%	2.3%	2.5%	2.6%	2.8%
	–	2.1%	2.1%	2.1%	2.1%	2.2%	2.2%	2.3%	2.3%	2.4%	2.5%	2.7%	2.9%
Cs-137 Concentration	+	2.0%	2.0%	2.0%	2.0%	2.1%	2.1%	2.2%	2.2%	2.3%	2.5%	2.6%	2.8%
	–	2.1%	2.1%	2.1%	2.1%	2.2%	2.2%	2.3%	2.3%	2.4%	2.5%	2.7%	2.9%
Eu-154 Concentration	+	2.0%	2.0%	2.0%	2.0%	2.1%	2.1%	2.2%	2.2%	3.2%	2.5%	2.6%	2.8%
	–	2.1%	2.1%	2.1%	2.1%	2.2%	2.2%	2.3%	2.3%	3.3%	2.5%	2.7%	2.9%
Eu-155 Concentration	+	3.0%	3.0%	3.0%	4.0%	4.0%	9.0%	8.0%	6.1%	23.0%	9.1%	27.1%	N/A
	–	3.1%	3.1%	3.1%	4.1%	4.1%	9.0%	8.1%	6.1%	23.0%	9.1%	27.1%	N/A
Ru-106 Concentration	+	N/A	N/A	N/A	N/A	N/A	N/A	N/A	N/A	N/A	N/A	N/A	N/A
	–	N/A	N/A	N/A	N/A	N/A	N/A	N/A	N/A	N/A	N/A	N/A	N/A
Sb-125 Concentration	+	19.0%	N/A	N/A	40.0%	N/A	N/A	N/A	N/A	N/A	N/A	15.1%	10.2%
	–	19.0%	N/A	N/A	40.0%	N/A	N/A	N/A	N/A	N/A	N/A	15.1%	10.2%
Sr-90 Concentration	+	4.0%	3.0%	N/A	N/A	N/A	N/A	N/A	N/A	N/A	N/A	N/A	3.6%
	–	4.0%	3.1%	N/A	N/A	N/A	N/A	N/A	N/A	N/A	N/A	N/A	3.6%
Segment Volume (mm ³)	+ mm ³	0.37	0.76	1.06	1.38	1.70	2.03	2.36	2.69	3.02	3.35	3.68	0.99
	– mm ³	1.77	2.35	2.38	2.45	2.57	2.73	2.92	3.14	3.38	3.64	3.91	1.04
Average Radius of Segment (mm)	+/- mm	0.011	0.017	0.023	0.030	0.038	0.045	0.052	0.059	0.066	0.074	0.081	0.088

Table B-16. Capsule 5 OR, axial center: decay-corrected concentrations (Bq per mm³) of selected fission products for each radial segment sampled at the axial center of the Capsule 5 OR. The volume and average radius $[(r_{\text{inner}} + r_{\text{outer}})/2]$ of each segment are also given. Shading indicates a value derived from an MDA.

OR-05 Center (Bq/mm ³)	OR5-C1	OR5-C2	OR5-C3	OR5-C4	OR5-C5	OR5-C6	OR5-C7	OR5-C8	OR5-C9	OR5- C10	OR5- C11	OR5- C12	OR5- C13	OR5- C14	OR5- C15
Ag-110m	1.65E+0	5.33E-1	7.41E-1	2.97E-1	2.09E+0	6.01E-1	1.93E+0	8.98E-1	1.38E+0	2.12E+0	9.32E-1	1.26E+0	1.08E+0	9.28E-1	1.88E+1
Ce-144	1.67E+2	1.32E+1	5.59E+0	6.05E+0	5.58E+0	1.09E+0	4.95E+0	4.04E+0	6.35E+0	5.25E+0	6.44E+0	3.44E+0	3.70E+0	3.65E+0	8.69E+0
Cs-134	1.05E+2	4.66E+1	4.45E+1	4.83E+1	5.50E+1	1.68E+1	4.18E+1	4.65E+1	5.66E+1	5.67E+1	6.41E+1	3.90E+1	6.29E+1	6.66E+1	2.96E+2
Cs-137	1.11E+2	3.52E+1	3.26E+1	3.51E+1	3.90E+1	1.18E+1	2.99E+1	3.19E+1	3.89E+1	3.90E+1	5.06E+1	2.65E+1	4.38E+1	4.45E+1	2.03E+2
Eu-154	7.93E-1	4.13E-1	4.09E-1	3.71E-1	4.69E-1	1.10E-1	3.55E-1	2.69E-1	3.64E-1	2.71E-1	3.40E-1	1.26E-1	2.02E-1	2.05E-1	3.99E-1
Eu-155	6.46E-1	2.75E-1	2.67E-1	2.36E-1	2.91E-1	6.28E-2	1.07E-1	2.24E-1	2.15E-1	1.69E-1	1.75E-1	8.46E-2	1.94E-1	1.51E-1	3.03E-1
Ru-106	8.00E+0	2.65E+0	1.69E+0	3.76E+0	5.86E+0	1.30E+0	5.54E+0	2.18E+0	3.03E+0	6.25E+0	2.22E+0	2.84E+0	2.47E+0	2.92E+0	5.08E+0
Sb-125	1.35E+0	3.79E-1	3.37E-1	2.92E-1	3.64E-1	5.81E-2	1.54E-1	2.79E-1	2.88E-1	1.63E-1	1.15E-1	8.21E-2	2.34E-1	2.16E-1	3.36E-1
Sr-90	2.61E+1	9.53E+0	7.00E+0	6.84E+0	7.03E+0	5.19E+0	4.83E+0	4.54E+0	7.44E+0	5.80E+0	7.32E+0	1.96E+0	3.88E+0	4.16E+0	8.17E+0
Segment Volume (mm ³)	466.92	608.37	592.15	575.94	559.72	543.51	527.29	511.08	494.87	478.65	462.44	446.22	430.01	413.79	289.00
Average Segment Radius (mm)	19.50	19.06	18.55	18.04	17.54	17.03	16.52	16.01	15.50	15.00	14.49	13.98	13.47	12.96	12.53

Table B-17. Capsule 5 OR, axial center: decay-corrected concentrations (particle equivalents per mm³) of selected fission products for each radial segment sampled at the axial center of the Capsule 5 OR. The volume and average radius [(r_{inner} + r_{outer})/2] of each segment are also given. Shading indicates a value derived from an MDA.

OR-05 Center (Particle equivalents/mm ³)	OR5-C1	OR5-C2	OR5-C3	OR5-C4	OR5-C5	OR5-C6	OR5-C7	OR5-C8	OR5-C9	OR5- C10	OR5- C11	OR5- C12	OR5- C13	OR5- C14	OR5- C15
Ag-110m	2.75E-5	8.87E-6	1.23E-5	4.93E-6	3.48E-5	1.00E-5	3.20E-5	1.49E-5	2.30E-5	3.53E-5	1.55E-5	2.10E-5	1.79E-5	1.54E-5	3.12E-4
Ce-144	2.90E-6	2.28E-7	9.68E-8	1.05E-7	9.66E-8	1.88E-8	8.56E-8	6.99E-8	1.10E-7	9.10E-8	1.11E-7	5.96E-8	6.41E-8	6.33E-8	1.50E-7
Cs-134	2.03E-5	8.95E-6	8.54E-6	9.27E-6	1.06E-5	3.23E-6	8.03E-6	8.94E-6	1.09E-5	1.09E-5	1.23E-5	7.49E-6	1.21E-5	1.28E-5	5.69E-5
Cs-137	2.85E-5	9.05E-6	8.38E-6	9.00E-6	1.00E-5	3.02E-6	7.67E-6	8.20E-6	9.99E-6	1.00E-5	1.30E-5	6.81E-6	1.13E-5	1.14E-5	5.21E-5
Eu-154	4.91E-6	2.56E-6	2.53E-6	2.30E-6	2.90E-6	6.80E-7	2.20E-6	1.66E-6	2.25E-6	1.68E-6	2.10E-6	7.79E-7	1.25E-6	1.27E-6	2.47E-6
Eu-155	6.12E-6	2.60E-6	2.52E-6	2.23E-6	2.75E-6	5.94E-7	1.02E-6	2.12E-6	2.04E-6	1.60E-6	1.65E-6	8.00E-7	1.84E-6	1.42E-6	2.87E-6
Ru-106	5.77E-7	1.91E-7	1.22E-7	2.72E-7	4.22E-7	9.39E-8	4.00E-7	1.57E-7	2.19E-7	4.51E-7	1.60E-7	2.05E-7	1.78E-7	2.11E-7	3.67E-7
Sb-125	4.35E-6	1.22E-6	1.08E-6	9.41E-7	1.17E-6	1.87E-7	4.97E-7	8.98E-7	9.26E-7	5.25E-7	3.72E-7	2.64E-7	7.53E-7	6.95E-7	1.08E-6
Sr-90	7.84E-6	2.87E-6	2.11E-6	2.06E-6	2.12E-6	1.56E-6	1.45E-6	1.37E-6	2.24E-6	1.74E-6	2.20E-6	5.88E-7	1.17E-6	1.25E-6	2.46E-6
Segment Volume (mm ³)	466.92	608.37	592.15	575.94	559.72	543.51	527.29	511.08	494.87	478.65	462.44	446.22	430.01	413.79	289.00
Average Segment Radius (mm)	19.50	19.06	18.55	18.04	17.54	17.03	16.52	16.01	15.50	15.00	14.49	13.98	13.47	12.96	12.53

Table B-18. Estimated relative uncertainties in the concentrations reported in for OR-05 Center in Table B-16 and Table B-17. Absolute uncertainties in the segment volumes and average radii of the segments. N/A denotes a case where an isotope was not detected, and therefore, no uncertainty is available.

OR-05 Center	Units	OR5-C1	OR5-C2	OR5-C3	OR5-C4	OR5-C5	OR5-C6	OR5-C7	OR5-C8	OR5-C9	OR5-C10	OR5-C11	OR5-C12	OR5-C13	OR5-C14	OR5-C15
Ag-110m Concentration	+	N/A	27.0%	N/A	33.0%	N/A	N/A	N/A	N/A	N/A	N/A	N/A	N/A	N/A	18.0%	2.4%
	–	N/A	27.0%	N/A	33.0%	N/A	N/A	N/A	N/A	N/A	N/A	N/A	N/A	N/A	18.0%	2.4%
Ce-144 Concentration	+	4.0%	11.0%	8.0%	N/A	N/A	48.0%	N/A	N/A	8.0%	N/A	38.0%	N/A	N/A	N/A	N/A
	–	4.0%	11.0%	8.0%	N/A	N/A	48.0%	N/A	N/A	8.0%	N/A	38.0%	N/A	N/A	N/A	N/A
Cs-134 Concentration	+	2.0%	2.0%	2.0%	2.0%	2.0%	2.0%	2.0%	2.1%	2.1%	2.1%	2.2%	2.2%	2.2%	2.3%	2.4%
	–	2.1%	2.1%	2.1%	2.1%	2.1%	2.1%	2.1%	2.2%	2.2%	2.2%	2.2%	2.3%	2.3%	2.4%	2.4%
Cs-137 Concentration	+	2.0%	2.0%	2.0%	2.0%	2.0%	2.0%	2.0%	2.1%	2.1%	2.1%	2.2%	2.2%	2.2%	2.3%	2.4%
	–	2.1%	2.1%	2.1%	2.1%	2.1%	2.1%	2.1%	2.2%	2.2%	2.2%	2.2%	2.3%	2.3%	2.4%	2.4%
Eu-154 Concentration	+	3.0%	2.0%	2.0%	3.0%	2.0%	4.0%	3.0%	2.1%	2.1%	3.1%	3.1%	4.1%	3.2%	6.1%	3.2%
	–	3.1%	2.1%	2.1%	3.1%	2.1%	4.1%	3.1%	2.2%	2.2%	3.1%	3.2%	4.1%	3.2%	6.1%	3.3%
Eu-155 Concentration	+	17.0%	12.0%	4.0%	15.0%	15.0%	10.0%	12.0%	4.0%	5.0%	10.0%	7.0%	8.0%	5.1%	7.1%	4.2%
	–	17.0%	12.0%	4.1%	15.0%	15.0%	10.0%	12.0%	4.1%	5.1%	10.0%	7.1%	8.1%	5.1%	7.1%	4.2%
Ru-106 Concentration	+	7.0%	N/A	N/A	N/A	N/A	N/A	N/A	N/A	N/A	N/A	N/A	N/A	N/A	N/A	N/A
	–	7.0%	N/A	N/A	N/A	N/A	N/A	N/A	N/A	N/A	N/A	N/A	N/A	N/A	N/A	N/A
Sb-125 Concentration	+	4.0%	4.0%	5.0%	7.0%	7.0%	48.0%	N/A	12.0%	6.0%	20.0%	18.0%	15.0%	N/A	12.1%	N/A
	–	4.0%	4.0%	5.0%	7.0%	7.0%	48.0%	N/A	12.0%	6.1%	20.0%	18.0%	15.0%	N/A	12.1%	N/A
Sr-90 Concentration	+	2.0%	2.0%	2.0%	2.0%	2.0%	2.0%	2.0%	2.1%	2.1%	2.1%	2.2%	2.2%	2.2%	2.3%	4.2%
	–	2.1%	2.1%	2.1%	2.1%	2.1%	2.1%	2.1%	2.2%	2.2%	2.2%	2.2%	2.3%	2.3%	2.4%	4.2%
Segment Volume (mm ³)	+ mm ³	0.31	0.71	1.03	1.35	1.68	2.01	2.34	2.67	3.00	3.33	3.66	3.99	4.32	4.65	3.60
	– mm ³	2.90	3.82	3.79	3.80	3.84	3.91	4.00	4.13	4.28	4.45	4.64	4.84	5.07	5.30	4.01
Average Radius of Segment (mm)	+/- mm	0.009	0.016	0.023	0.030	0.037	0.044	0.052	0.059	0.066	0.074	0.081	0.088	0.095	0.103	0.110

Table B-19. Capsule 7 IR, axial top: decay-corrected concentrations (Bq per mm³) of selected fission products for each radial segment sampled at the axial top of the Capsule 7 IR. The volume and average radius $[(r_{\text{inner}} + r_{\text{outer}})/2]$ of each segment are also given. Shading indicates a value derived from an MDA.

IR-07 Top (Bq/mm ³)	IR7-T1	IR7-T2	IR7-T3	IR7-T4	IR7-T5	IR7-T6	IR7-T7	IR7-T8	IR7-T9	IR7-T10	IR7-T11
Ag-110m	1.10E+1	8.03E+0	1.57E+1	3.52E+0	2.05E+1	1.43E+1	2.90E+1	2.55E+1	2.88E+1	3.09E+1	1.04E+2
Ce-144	5.19E+1	2.45E+1	3.05E+1	3.83E+1	7.30E+1	1.13E+2	1.56E+2	4.77E+1	3.74E+1	1.87E+1	4.34E-4
Cs-134	8.78E+2	7.57E+2	9.19E+2	1.02E+3	1.06E+3	1.05E+3	1.23E+3	1.29E+3	1.48E+3	1.45E+3	1.63E+3
Cs-137	7.71E+2	6.00E+2	7.48E+2	8.30E+2	8.71E+2	8.77E+2	1.02E+3	1.07E+3	1.24E+3	1.23E+3	1.52E+3
Eu-154	2.92E+1	2.15E+1	2.30E+1	2.26E+1	2.20E+1	2.09E+1	2.27E+1	2.19E+1	2.74E+1	1.37E+2	1.03E+4
Eu-155	1.84E+1	1.23E+1	1.62E+1	1.53E+1	1.35E+1	1.85E+1	1.68E+1	1.51E+1	1.90E+1	9.32E+1	6.93E+3
Ru-106	9.11E+0	1.16E+1	1.34E+1	1.91E+1	4.96E+1	6.80E+1	6.80E+1	3.70E+1	2.06E+1	8.69E+0	2.44E+2
Sb-125	1.40E+1	7.50E+0	9.92E+0	1.96E+1	1.95E+1	2.15E+1	2.20E+1	2.68E+1	3.37E+1	3.55E+1	2.10E+2
Sr-90	9.89E+1	3.30E+1	2.90E+1	3.37E+1	2.74E+1	3.40E+1	3.78E+1	5.55E+1	1.63E+2	2.62E+3	2.56E+5
Segment Volume (mm ³)	278.73	357.45	341.23	325.02	308.80	292.59	276.38	260.16	243.95	227.73	213.00
Average Segment Radius (mm)	11.64	11.20	10.69	10.18	9.67	9.17	8.66	8.15	7.64	7.13	6.62

Table B-20. Capsule 7 IR, axial top: decay-corrected concentrations (particle equivalents per mm³) of selected fission products for each radial segment sampled at the axial top of the Capsule 7 IR. The volume and average radius $[(r_{\text{inner}} + r_{\text{outer}})/2]$ of each segment are also given. Shading indicates a value derived from an MDA.

IR-07 Top (Particle equivalents/mm ³)	IR7-T1	IR7-T2	IR7-T3	IR7-T4	IR7-T5	IR7-T6	IR7-T7	IR7-T8	IR7-T9	IR7-T10	IR7-T11
Ag-110m	1.80E-4	1.31E-4	2.56E-4	5.74E-5	3.34E-4	2.34E-4	4.73E-4	4.15E-4	4.69E-4	5.04E-4	1.69E-3
Ce-144	8.93E-7	4.22E-7	5.24E-7	6.58E-7	1.25E-6	1.94E-6	2.69E-6	8.20E-7	6.44E-7	3.22E-7	7.46E-12
Cs-134	1.68E-4	1.45E-4	1.76E-4	1.96E-4	2.03E-4	2.01E-4	2.36E-4	2.47E-4	2.83E-4	2.77E-4	3.10E-4
Cs-137	1.97E-4	1.53E-4	1.91E-4	2.12E-4	2.22E-4	2.24E-4	2.60E-4	2.73E-4	3.17E-4	3.13E-4	3.88E-4
Eu-154	1.81E-4	1.34E-4	1.43E-4	1.40E-4	1.37E-4	1.30E-4	1.41E-4	1.36E-4	1.70E-4	8.49E-4	6.43E-2
Eu-155	1.73E-4	1.16E-4	1.53E-4	1.44E-4	1.27E-4	1.74E-4	1.58E-4	1.43E-4	1.79E-4	8.80E-4	6.54E-2
Ru-106	6.53E-7	8.34E-7	9.59E-7	1.37E-6	3.56E-6	4.88E-6	4.88E-6	2.66E-6	1.48E-6	6.24E-7	1.75E-5
Sb-125	4.47E-5	2.40E-5	3.17E-5	6.27E-5	6.24E-5	6.86E-5	7.02E-5	8.56E-5	1.08E-4	1.13E-4	6.71E-4
Sr-90	2.95E-5	9.85E-6	8.65E-6	1.01E-5	8.19E-6	1.02E-5	1.13E-5	1.66E-5	4.88E-5	7.82E-4	7.64E-2
Segment Volume (mm ³)	278.73	357.45	341.23	325.02	308.80	292.59	276.38	260.16	243.95	227.73	213.00
Average Segment Radius (mm)	11.64	11.20	10.69	10.18	9.67	9.17	8.66	8.15	7.64	7.13	6.62

Table B-21. Estimated relative uncertainties in the concentrations reported in Table B-19 and Table B-20. Absolute uncertainties in the segment volumes and average radii of the segments. N/A denotes a case where an isotope was not detected, and therefore, no uncertainty is available.

IR-07 Top	Units	IR7-T1	IR7-T2	IR7-T3	IR7-T4	IR7-T5	IR7-T6	IR7-T7	IR7-T8	IR7-T9	IR7-T10	IR7-T11
Ag-110m Concentration	+	5.0%	7.0%	5.0%	N/A	8.0%	13.0%	25.0%	3.2%	2.4%	2.5%	N/A
	–	5.0%	7.0%	5.1%	N/A	8.1%	13.0%	25.0%	3.3%	2.5%	2.6%	N/A
Ce-144 Concentration	+	25.0%	N/A	N/A	N/A	N/A	N/A	N/A	N/A	N/A	26.0%	N/A
	–	25.0%	N/A	N/A	N/A	N/A	N/A	N/A	N/A	N/A	26.1%	N/A
Cs-134 Concentration	+	2.0%	2.0%	2.1%	2.1%	2.1%	2.2%	2.2%	2.3%	2.4%	2.5%	2.7%
	–	2.1%	2.1%	2.1%	2.2%	2.2%	2.2%	2.3%	2.4%	2.5%	2.6%	2.8%
Cs-137 Concentration	+	2.0%	2.0%	2.1%	2.1%	2.1%	2.2%	2.2%	2.3%	2.4%	2.5%	2.7%
	–	2.1%	2.1%	2.1%	2.2%	2.2%	2.2%	2.3%	2.4%	2.5%	2.6%	2.8%
Eu-154 Concentration	+	2.0%	2.0%	2.1%	2.1%	2.1%	2.2%	2.2%	2.3%	2.4%	2.5%	2.7%
	–	2.1%	2.1%	2.1%	2.2%	2.2%	2.2%	2.3%	2.4%	2.5%	2.6%	2.8%
Eu-155 Concentration	+	3.0%	5.0%	3.0%	6.0%	8.0%	4.1%	6.1%	9.1%	2.4%	2.5%	2.7%
	–	3.1%	5.1%	3.1%	6.1%	8.1%	4.1%	6.1%	9.1%	2.5%	2.6%	2.8%
Ru-106 Concentration	+	N/A	N/A	N/A	N/A	N/A	N/A	N/A	N/A	N/A	N/A	N/A
	–	N/A	N/A	N/A	N/A	N/A	N/A	N/A	N/A	N/A	N/A	N/A
Sb-125 Concentration	+	3.0%	3.0%	5.0%	2.1%	2.1%	3.1%	5.1%	2.3%	2.4%	2.5%	2.7%
	–	3.1%	3.1%	5.1%	2.2%	2.2%	3.2%	5.1%	2.4%	2.5%	2.6%	2.8%
Sr-90 Concentration	+	5.0%	7.0%	5.0%	5.0%	3.1%	3.1%	5.1%	6.1%	5.2%	4.3%	4.4%
	–	5.0%	7.0%	5.1%	5.1%	3.1%	3.2%	5.1%	6.1%	5.2%	4.3%	4.4%
Segment Volume (mm ³)	+ mm ³	0.96	1.41	1.59	1.82	2.08	2.35	2.64	2.94	3.24	3.55	3.89
	– mm ³	1.97	2.61	2.64	2.71	2.81	2.96	3.14	3.34	3.57	3.82	4.11
Average Radius of Segment (mm)	+/- mm	0.028	0.031	0.035	0.040	0.046	0.052	0.058	0.065	0.071	0.078	0.085

Table B-22. Capsule 7 IR, axial center: decay-corrected concentrations (Bq per mm³) of selected fission products for each radial segment sampled at the axial center of the Capsule 7 IR. The volume and average radius $[(r_{\text{inner}} + r_{\text{outer}})/2]$ of each segment are also given. Shading indicates a value derived from an MDA.

IR-07 Center (Bq/mm ³)	IR7-C1	IR7-C2	IR7-C3	IR7-C4	IR7-C5	IR7-C6	IR7-C7	IR7-C8	IR7-C9	IR7-C10	IR7-C11
Ag-110m	8.94E+0	2.80E+0	6.35E+0	8.80E+0	1.39E+1	9.83E+0	1.12E+1	6.60E+0	7.03E+0	1.64E+1	4.54E+2
Ce-144	1.44E+2	2.58E+1	1.55E+1	2.32E+1	1.51E+1	4.08E+1	6.78E+1	3.45E+1	2.52E+1	5.77E+1	1.70E+3
Cs-134	6.11E+2	5.33E+2	6.50E+2	7.57E+2	7.68E+2	8.42E+2	9.87E+2	1.00E+3	1.11E+3	1.15E+3	1.57E+3
Cs-137	7.82E+2	4.59E+2	5.57E+2	6.41E+2	6.55E+2	7.19E+2	8.57E+2	8.64E+2	9.80E+2	1.02E+3	1.68E+3
Eu-154	2.29E+2	4.17E+1	3.32E+1	3.03E+1	2.74E+1	2.62E+1	2.75E+1	2.83E+1	5.57E+1	1.01E+3	2.18E+4
Eu-155	1.51E+2	2.62E+1	2.37E+1	2.07E+1	1.66E+1	1.70E+1	1.76E+1	1.84E+1	3.82E+1	6.34E+2	1.40E+4
Ru-106	1.94E+1	1.32E+1	5.56E+0	8.49E+0	7.14E+0	2.65E+1	4.60E+1	1.13E+1	1.10E+1	2.05E+1	9.78E+2
Sb-125	1.80E+1	6.22E+0	6.56E+0	2.28E+1	4.03E+1	1.21E+1	1.57E+1	2.27E+0	1.65E+1	2.32E+1	1.51E+2
Sr-90	4.66E+3	5.20E+2	3.26E+2	2.31E+2	1.95E+2	1.28E+2	1.18E+2	1.37E+2	5.93E+2	1.82E+4	4.47E+5
Segment Volume (mm ³)	278.83	357.59	341.37	325.16	308.94	292.73	276.51	260.30	244.09	227.87	207.25
Average Segment Radius (mm)	11.65	11.20	10.70	10.19	9.68	9.17	8.66	8.16	7.65	7.14	6.64

Table B-23. Capsule 7 IR, axial center: decay-corrected concentrations (particle equivalents per mm³) of selected fission products for each radial segment sampled at the axial center of the Capsule 7 IR. The volume and average radius [(r_{inner} + r_{outer})/2] of each segment are also given. Shading indicates a value derived from an MDA.

IR-07 Center (Particle equivalents/mm ³)	IR7-C1	IR7-C2	IR7-C3	IR7-C4	IR7-C5	IR7-C6	IR7-C7	IR7-C8	IR7-C9	IR7-C10	IR7-C11
Ag-110m	1.46E-4	4.57E-5	1.03E-4	1.43E-4	2.26E-4	1.60E-4	1.82E-4	1.08E-4	1.15E-4	2.68E-4	7.40E-3
Ce-144	2.48E-6	4.44E-7	2.66E-7	4.00E-7	2.59E-7	7.02E-7	1.17E-6	5.94E-7	4.32E-7	9.92E-7	2.92E-5
Cs-134	1.17E-4	1.02E-4	1.24E-4	1.45E-4	1.47E-4	1.61E-4	1.88E-4	1.92E-4	2.12E-4	2.19E-4	3.00E-4
Cs-137	1.99E-4	1.17E-4	1.42E-4	1.64E-4	1.67E-4	1.83E-4	2.18E-4	2.20E-4	2.50E-4	2.59E-4	4.29E-4
Eu-154	1.42E-3	2.59E-4	2.06E-4	1.88E-4	1.70E-4	1.62E-4	1.71E-4	1.76E-4	3.46E-4	6.25E-3	1.35E-1
Eu-155	1.42E-3	2.47E-4	2.24E-4	1.96E-4	1.57E-4	1.61E-4	1.66E-4	1.73E-4	3.61E-4	5.98E-3	1.32E-1
Ru-106	1.39E-6	9.48E-7	3.99E-7	6.09E-7	5.12E-7	1.90E-6	3.30E-6	8.09E-7	7.90E-7	1.47E-6	7.02E-5
Sb-125	5.75E-5	1.99E-5	2.10E-5	7.30E-5	1.29E-4	3.85E-5	5.03E-5	7.26E-6	5.26E-5	7.43E-5	4.83E-4
Sr-90	1.39E-3	1.55E-4	9.73E-5	6.91E-5	5.82E-5	3.83E-5	3.52E-5	4.08E-5	1.77E-4	5.43E-3	1.33E-1
Segment Volume (mm ³)	278.83	357.59	341.37	325.16	308.94	292.73	276.51	260.30	244.09	227.87	207.25
Average Segment Radius (mm)	11.65	11.20	10.70	10.19	9.68	9.17	8.66	8.16	7.65	7.14	6.64

Table B-24. Estimated relative uncertainties in the concentrations reported for IR-07 center in Table B-22 and Table B-23. Absolute uncertainties in the segment volumes and average radii of the segments. N/A denotes a case where an isotope was not detected, and therefore, no uncertainty is available.

IR-07 Center	Units	IR7-C1	IR7-C2	IR7-C3	IR7-C4	IR7-C5	IR7-C6	IR7-C7	IR7-C8	IR7-C9	IR7-C10	IR7-C11
Ag-110m Concentration	+	N/A	N/A	28.0%	4.0%	3.1%	9.0%	30.0%	6.1%	10.1%	9.1%	N/A
	–	N/A	N/A	28.0%	4.1%	3.1%	9.0%	30.0%	6.1%	10.1%	9.1%	N/A
Ce-144 Concentration	+	14.0%	N/A	N/A	N/A	N/A	N/A	N/A	N/A	N/A	N/A	N/A
	–	14.0%	N/A	N/A	N/A	N/A	N/A	N/A	N/A	N/A	N/A	N/A
Cs-134 Concentration	+	2.0%	2.0%	2.0%	2.1%	2.1%	2.1%	2.2%	2.3%	2.4%	2.5%	2.7%
	–	2.1%	2.1%	2.1%	2.1%	2.2%	2.2%	2.3%	2.3%	2.4%	2.6%	2.7%
Cs-137 Concentration	+	2.0%	2.0%	2.0%	2.1%	2.1%	2.1%	2.2%	2.3%	2.4%	2.5%	2.7%
	–	2.1%	2.1%	2.1%	2.1%	2.2%	2.2%	2.3%	2.3%	2.4%	2.6%	2.7%
Eu-154 Concentration	+	2.0%	2.0%	2.0%	2.1%	2.1%	2.1%	2.2%	2.3%	2.4%	2.5%	2.7%
	–	2.1%	2.1%	2.1%	2.1%	2.2%	2.2%	2.3%	2.3%	2.4%	2.6%	2.7%
Eu-155 Concentration	+	7.0%	2.0%	2.0%	2.1%	2.1%	4.1%	6.1%	4.1%	2.4%	2.5%	2.7%
	–	7.0%	2.1%	2.1%	2.1%	2.2%	4.1%	6.1%	4.2%	2.4%	2.6%	2.7%
Ru-106 Concentration	+	N/A	N/A	N/A	N/A	N/A	N/A	N/A	N/A	N/A	N/A	N/A
	–	N/A	N/A	N/A	N/A	N/A	N/A	N/A	N/A	N/A	N/A	N/A
Sb-125 Concentration	+	2.0%	3.0%	4.0%	2.1%	2.1%	5.1%	3.1%	N/A	3.3%	2.5%	2.7%
	–	2.1%	3.1%	4.1%	2.1%	2.2%	5.1%	3.2%	N/A	3.3%	2.6%	2.7%
Sr-90 Concentration	+	2.0%	2.0%	6.0%	4.0%	5.0%	7.0%	2.2%	6.1%	5.2%	4.3%	3.5%
	–	2.1%	2.1%	6.0%	4.1%	5.1%	7.1%	2.3%	6.1%	5.2%	4.3%	3.5%
Segment Volume (mm ³)	+ mm ³	0.56	0.94	1.20	1.49	1.79	2.10	2.42	2.74	3.07	3.39	3.64
	– mm ³	1.81	2.40	2.42	2.50	2.62	2.77	2.96	3.18	3.42	3.67	3.86
Average Radius of Segment (mm)	+/- mm	0.016	0.021	0.026	0.033	0.039	0.046	0.053	0.060	0.068	0.075	0.082

Table B-25. Capsule 7 OR, axial top: decay-corrected concentrations (Bq per mm³) of selected fission products for each radial segment sampled at the axial top of the Capsule 7 OR. The volume and average radius $[(r_{\text{inner}} + r_{\text{outer}})/2]$ of each segment are also given. Shading indicates a value derived from an MDA.

OR-07 Top (Bq/mm ³)	OR7-T1	OR7-T2	OR7-T3	OR7-T4	OR7-T5	OR7-T6	OR7-T7	OR7-T8	OR7-T9	OR7-T10	OR7-T11	OR7-T12	OR7-T13
Ag-110m	4.12E+2	5.68E+2	7.45E+2	7.30E+2	7.56E+2	8.61E+2	8.11E+2	7.83E+2	6.90E+2	5.57E+2	3.71E+2	1.68E+2	5.40E+1
Ce-144	1.06E+2	1.13E+1	1.08E+1	1.39E+1	1.36E+1	1.39E+1	2.68E+1	1.91E+1	1.52E+1	1.38E+1	2.18E+1	1.56E+1	2.49E+1
Cs-134	7.25E+2	5.45E+2	6.29E+2	5.71E+2	5.93E+2	7.08E+2	7.17E+2	7.56E+2	8.05E+2	8.49E+2	9.01E+2	8.73E+2	9.37E+2
Cs-137	6.99E+2	4.52E+2	5.07E+2	4.68E+2	4.94E+2	5.84E+2	5.95E+2	6.32E+2	6.74E+2	7.19E+2	7.64E+2	7.49E+2	8.26E+2
Eu-154	5.03E+0	2.91E+0	3.41E+0	2.45E+0	2.21E+0	2.42E+0	2.18E+0	2.11E+0	2.07E+0	1.65E+0	1.46E+0	1.25E+0	1.59E+0
Eu-155	6.80E+0	1.75E+0	2.31E+0	1.46E+0	1.82E+0	1.73E+0	1.53E+0	1.34E+0	2.15E+0	1.57E+0	1.04E+0	2.17E+0	1.87E+0
Ru-106	7.11E+0	7.98E+0	1.11E+1	7.58E+0	7.43E+0	1.13E+1	1.69E+1	9.95E+0	6.83E+0	1.83E+1	3.74E+0	1.12E+1	1.11E+1
Sb-125	1.33E+1	8.07E+0	1.09E+1	1.14E+1	1.28E+1	1.81E+1	1.86E+1	2.20E+1	2.28E+1	3.00E+1	3.33E+1	2.79E+1	9.70E+1
Sr-90	1.30E+2	6.44E+1	6.56E+1	4.76E+1	4.50E+1	4.65E+1	4.25E+1	3.99E+1	4.13E+1	3.67E+1	3.34E+1	3.11E+1	4.52E+1
Segment Volume (mm ³)	442.68	576.05	559.84	543.62	527.41	511.19	494.98	478.76	462.55	446.33	430.12	413.90	199.01
Average Segment Radius (mm)	18.49	18.05	17.54	17.03	16.52	16.02	15.51	15.00	14.49	13.98	13.48	12.97	12.59

Table B-26. Capsule 7 OR, axial top: decay-corrected concentrations (particle equivalents per mm³) of selected fission products for each radial segment sampled at the axial top of the Capsule 7 OR. The volume and average radius $[(r_{\text{inner}} + r_{\text{outer}})/2]$ of each segment are also given. Shading indicates a value derived from an MDA.

OR-07 Top (Particle equivalents/mm ³)	OR7-T1	OR7-T2	OR7-T3	OR7-T4	OR7-T5	OR7-T6	OR7-T7	OR7-T8	OR7-T9	OR7-T10	OR7-T11	OR7-T12	OR7-T13
Ag-110m	6.71E-3	9.25E-3	1.21E-2	1.19E-2	1.23E-2	1.40E-2	1.32E-2	1.28E-2	1.12E-2	9.08E-3	6.05E-3	2.84E-3	9.14E-4
Ce-144	1.82E-6	1.95E-7	1.86E-7	2.39E-7	2.34E-7	2.40E-7	4.60E-7	3.29E-7	2.62E-7	2.37E-7	3.74E-7	2.78E-7	4.44E-7
Cs-134	1.39E-4	1.04E-4	1.20E-4	1.09E-4	1.13E-4	1.35E-4	1.37E-4	1.45E-4	1.54E-4	1.62E-4	1.72E-4	1.73E-4	1.86E-4
Cs-137	1.78E-4	1.15E-4	1.29E-4	1.19E-4	1.26E-4	1.49E-4	1.52E-4	1.61E-4	1.72E-4	1.83E-4	1.95E-4	1.98E-4	2.19E-4
Eu-154	3.12E-5	1.81E-5	2.12E-5	1.52E-5	1.37E-5	1.50E-5	1.36E-5	1.31E-5	1.28E-5	1.03E-5	9.06E-6	8.08E-6	1.03E-5
Eu-155	6.42E-5	1.65E-5	2.18E-5	1.38E-5	1.72E-5	1.63E-5	1.45E-5	1.26E-5	2.03E-5	1.48E-5	9.83E-6	2.13E-5	1.83E-5
Ru-106	5.10E-7	5.73E-7	7.96E-7	5.44E-7	5.33E-7	8.11E-7	1.21E-6	7.14E-7	4.90E-7	1.31E-6	2.68E-7	8.36E-7	8.26E-7
Sb-125	4.25E-5	2.58E-5	3.49E-5	3.63E-5	4.11E-5	5.80E-5	5.94E-5	7.05E-5	7.29E-5	9.60E-5	1.06E-4	9.25E-5	3.22E-4
Sr-90	3.89E-5	1.92E-5	1.96E-5	1.42E-5	1.34E-5	1.39E-5	1.27E-5	1.19E-5	1.23E-5	1.10E-5	9.98E-6	9.64E-6	1.40E-5
Segment Volume (mm ³)	442.68	576.05	559.84	543.62	527.41	511.19	494.98	478.76	462.55	446.33	430.12	413.90	199.01
Average Segment Radius (mm)	18.49	18.05	17.54	17.03	16.52	16.02	15.51	15.00	14.49	13.98	13.48	12.97	12.59

Table B-27. Estimated relative uncertainties in the concentrations reported for OR-07 Top in Table B-25 and Table B-26. Absolute uncertainties in the segment volumes and average radii of the segments. N/A denotes a case where an isotope was not detected, and therefore, no uncertainty is available.

OR-07 Top	Units	OR7-T1	OR7-T2	OR7-T3	OR7-T4	OR7-T5	OR7-T6	OR7-T7	OR7-T8	OR7-T9	OR7-T10	OR7-T11	OR7-T12	OR7-T13
Ag-110m Concentration	+	2.0%	2.0%	2.0%	2.1%	2.1%	2.1%	2.1%	2.1%	2.2%	2.2%	2.2%	2.3%	2.3%
	–	2.1%	2.1%	2.1%	2.1%	2.2%	2.2%	2.2%	2.2%	2.2%	2.3%	2.3%	2.4%	2.4%
Ce-144 Concentration	+	11.0%	46.0%	19.0%	N/A	N/A	16.0%	N/A	N/A	N/A	N/A	N/A	N/A	12.1%
	–	11.0%	46.0%	19.0%	N/A	N/A	16.0%	N/A	N/A	N/A	N/A	N/A	N/A	12.1%
Cs-134 Concentration	+	2.0%	2.0%	2.0%	2.1%	2.1%	2.1%	2.1%	2.1%	2.2%	2.2%	2.2%	2.3%	2.3%
	–	2.1%	2.1%	2.1%	2.1%	2.2%	2.2%	2.2%	2.2%	2.2%	2.3%	2.3%	2.4%	2.4%
Cs-137 Concentration	+	2.0%	2.0%	2.0%	2.1%	2.1%	2.1%	2.1%	2.1%	2.2%	2.2%	2.2%	2.3%	2.3%
	–	2.1%	2.1%	2.1%	2.1%	2.2%	2.2%	2.2%	2.2%	2.2%	2.3%	2.3%	2.4%	2.4%
Eu-154 Concentration	+	2.0%	2.0%	2.0%	2.1%	2.1%	2.1%	3.1%	2.1%	2.2%	3.1%	2.2%	2.3%	2.3%
	–	2.1%	2.1%	2.1%	2.1%	2.2%	2.2%	3.1%	2.2%	2.2%	3.2%	2.3%	2.4%	2.4%
Eu-155 Concentration	+	2.0%	6.0%	8.0%	4.0%	8.0%	6.0%	5.0%	5.1%	7.0%	6.1%	12.0%	8.1%	4.2%
	–	2.1%	6.0%	8.0%	4.1%	8.0%	6.1%	5.1%	5.1%	7.1%	6.1%	12.1%	8.1%	4.2%
Ru-106 Concentration	+	N/A	N/A	N/A	N/A	N/A	N/A	N/A	N/A	N/A	N/A	35.0%	N/A	N/A
	–	N/A	N/A	N/A	N/A	N/A	N/A	N/A	N/A	N/A	N/A	35.0%	N/A	N/A
Sb-125 Concentration	+	2.0%	2.0%	2.0%	2.1%	2.1%	2.1%	2.1%	2.1%	2.2%	2.2%	2.2%	2.3%	2.3%
	–	2.1%	2.1%	2.1%	2.1%	2.2%	2.2%	2.2%	2.2%	2.2%	2.3%	2.3%	2.4%	2.4%
Sr-90 Concentration	+	2.0%	2.0%	2.0%	2.1%	2.1%	2.1%	2.1%	2.1%	2.2%	2.2%	2.2%	2.3%	2.3%
	–	2.1%	2.1%	2.1%	2.1%	2.2%	2.2%	2.2%	2.2%	2.2%	2.3%	2.3%	2.4%	2.4%
Segment Volume (mm ³)	+ mm ³	1.74	2.38	2.50	2.65	2.83	3.03	3.26	3.50	3.76	4.03	4.31	4.59	2.41
	– mm ³	3.23	4.27	4.26	4.27	4.31	4.37	4.46	4.58	4.72	4.88	5.05	5.25	2.71
Average Radius of Segment (mm)	+/- mm	0.051	0.053	0.055	0.058	0.062	0.067	0.072	0.077	0.083	0.089	0.095	0.101	0.108

Table B-28. Capsule 7 OR, axial center: decay-corrected concentrations (Bq per mm³) of selected fission products for each radial segment sampled at the axial center of the Capsule 7 OR. The volume and average radius $[(r_{\text{inner}} + r_{\text{outer}})/2]$ of each segment are also given. Shading indicates a value derived from an MDA.

OR-07 Center (Bq/mm ³)	OR7-C1	OR7-C2	OR7-C3	OR7-C4	OR7-C5	OR7-C6	OR7-C7	OR7-C8	OR7-C9	OR7-C10	OR7-C11	OR7-C12	OR7-C13
Ag-110m	5.78E+1	3.92E+1	2.73E+1	1.44E+1	1.07E+1	9.27E+0	1.03E+1	1.06E+1	1.14E+1	1.22E+1	1.29E+1	1.09E+1	1.52E+2
Ce-144	7.29E+1	1.03E+1	1.41E+1	2.31E+1	1.54E+1	1.38E+1	2.76E+1	2.24E+1	2.49E+1	2.30E+1	6.03E+1	3.59E+1	1.85E+2
Cs-134	6.03E+2	3.86E+2	5.02E+2	5.53E+2	5.75E+2	6.25E+2	6.92E+2	7.94E+2	8.54E+2	9.15E+2	1.10E+3	9.79E+2	2.47E+3
Cs-137	5.12E+2	2.99E+2	3.91E+2	4.35E+2	4.54E+2	5.01E+2	5.59E+2	6.41E+2	6.85E+2	7.42E+2	8.86E+2	7.83E+2	2.03E+3
Eu-154	1.66E+0	1.09E+0	1.38E+0	1.30E+0	1.01E+0	1.03E+0	1.05E+0	8.92E-1	8.70E-1	6.87E-1	7.68E-1	9.45E-1	5.00E+0
Eu-155	1.19E+0	1.00E+0	8.54E-1	6.85E-1	1.38E+0	1.00E+0	7.17E-1	1.62E+0	1.44E+0	1.90E+0	1.39E+0	1.59E+0	5.23E+0
Ru-106	1.17E+1	5.67E+0	9.63E+0	1.69E+1	7.95E+0	7.00E+0	1.41E+1	1.17E+1	1.33E+1	1.30E+1	4.62E+1	4.63E+1	1.49E+2
Sb-125	9.15E+0	5.67E+0	9.29E+0	1.20E+1	1.42E+1	1.65E+1	2.03E+1	2.34E+1	2.48E+1	2.68E+1	3.24E+1	2.49E+1	1.46E+2
Sr-90	5.20E+1	2.65E+1	3.01E+1	3.05E+1	2.41E+1	2.41E+1	2.26E+1	2.28E+1	2.08E+1	1.77E+1	1.71E+1	8.35E+0	6.64E+1
Segment Volume (mm ³)	442.53	575.85	559.64	543.42	527.21	510.99	494.78	478.56	462.35	446.13	429.92	413.70	191.53
Average Segment Radius (mm)	18.49	18.04	17.53	17.03	16.52	16.01	15.50	14.99	14.49	13.98	13.47	12.96	12.59

Table B-29. Capsule 7 OR, axial center: decay-corrected concentrations (particle equivalents per mm³) of selected fission products for each radial segment sampled at the axial center of the Capsule 7 OR. The volume and average radius $[(r_{\text{inner}} + r_{\text{outer}})/2]$ of each segment are also given. Shading indicates a value derived from an MDA.

OR-07 Center (Particle equivalents/mm ³)	OR7-C1	OR7-C2	OR7-C3	OR7-C4	OR7-C5	OR7-C6	OR7-C7	OR7-C8	OR7-C9	OR7-C10	OR7-C11	OR7-C12	OR7-C13
Ag-110m	9.41E-4	6.38E-4	4.45E-4	2.35E-4	1.75E-4	1.51E-4	1.68E-4	1.72E-4	1.86E-4	1.98E-4	2.10E-4	1.77E-4	2.47E-3
Ce-144	1.25E-6	1.78E-7	2.43E-7	3.96E-7	2.64E-7	2.38E-7	4.74E-7	3.86E-7	4.28E-7	3.96E-7	1.04E-6	6.17E-7	3.17E-6
Cs-134	1.15E-4	7.38E-5	9.59E-5	1.06E-4	1.10E-4	1.19E-4	1.32E-4	1.52E-4	1.63E-4	1.75E-4	2.10E-4	1.87E-4	4.72E-4
Cs-137	1.31E-4	7.64E-5	9.97E-5	1.11E-4	1.16E-4	1.28E-4	1.42E-4	1.64E-4	1.75E-4	1.89E-4	2.26E-4	2.00E-4	5.18E-4
Eu-154	1.03E-5	6.75E-6	8.59E-6	8.06E-6	6.25E-6	6.37E-6	6.51E-6	5.54E-6	5.41E-6	4.27E-6	4.77E-6	5.87E-6	3.10E-5
Eu-155	1.13E-5	9.46E-6	8.07E-6	6.46E-6	1.30E-5	9.44E-6	6.77E-6	1.52E-5	1.36E-5	1.79E-5	1.31E-5	1.50E-5	4.93E-5
Ru-106	8.43E-7	4.06E-7	6.91E-7	1.21E-6	5.70E-7	5.02E-7	1.01E-6	8.37E-7	9.52E-7	9.33E-7	3.31E-6	3.32E-6	1.07E-5
Sb-125	2.93E-5	1.81E-5	2.97E-5	3.85E-5	4.54E-5	5.26E-5	6.50E-5	7.47E-5	7.94E-5	8.57E-5	1.04E-4	7.95E-5	4.67E-4
Sr-90	1.55E-5	7.92E-6	8.98E-6	9.10E-6	7.21E-6	7.20E-6	6.74E-6	6.82E-6	6.23E-6	5.30E-6	5.11E-6	2.49E-6	1.98E-5
Segment Volume (mm ³)	442.53	575.85	559.64	543.42	527.21	510.99	494.78	478.56	462.35	446.13	429.92	413.70	191.53
Average Segment Radius (mm)	18.49	18.04	17.53	17.03	16.52	16.01	15.50	14.99	14.49	13.98	13.47	12.96	12.59

Table B-30. Estimated relative uncertainties in the concentrations reported for OR-07 center in Table B-28 and Table B-29. Absolute uncertainties in the segment volumes and average radii of the segments. N/A denotes a case where an isotope was not detected, and therefore, no uncertainty is available.

OR-07 Center	Units	OR7-C1	OR7-C2	OR7-C3	OR7-C4	OR7-C5	OR7-C6	OR7-C7	OR7-C8	OR7-C9	OR7-C10	OR7-C11	OR7-C12	OR7-C13
Ag-110m Concentration	+	2.0%	2.0%	3.0%	5.0%	3.0%	7.0%	4.0%	4.1%	7.0%	18.0%	N/A	34.0%	5.1%
	–	2.1%	2.1%	3.1%	5.1%	3.1%	7.0%	4.1%	4.1%	7.1%	18.0%	N/A	34.0%	5.2%
Ce-144 Concentration	+	9.0%	N/A	N/A	N/A	N/A	N/A	N/A	N/A	N/A	N/A	N/A	N/A	N/A
	–	9.0%	N/A	N/A	N/A	N/A	N/A	N/A	N/A	N/A	N/A	N/A	N/A	N/A
Cs-134 Concentration	+	2.0%	2.0%	2.0%	2.0%	2.0%	2.1%	2.1%	2.1%	2.1%	2.2%	2.2%	2.2%	2.3%
	–	2.1%	2.1%	2.1%	2.1%	2.1%	2.1%	2.2%	2.2%	2.2%	2.2%	2.3%	2.3%	2.4%
Cs-137 Concentration	+	2.0%	2.0%	2.0%	2.0%	2.0%	2.1%	2.1%	2.1%	2.1%	2.2%	2.2%	2.2%	2.3%
	–	2.1%	2.1%	2.1%	2.1%	2.1%	2.1%	2.2%	2.2%	2.2%	2.2%	2.3%	2.3%	2.4%
Eu-154 Concentration	+	2.0%	2.0%	3.0%	2.0%	3.0%	4.0%	7.0%	5.0%	2.1%	4.1%	7.1%	8.1%	6.1%
	–	2.1%	2.1%	3.1%	2.1%	3.1%	4.1%	7.0%	5.1%	2.2%	4.1%	7.1%	8.1%	6.1%
Eu-155 Concentration	+	13.0%	10.0%	11.0%	13.0%	4.0%	9.0%	14.0%	10.0%	9.0%	7.0%	N/A	20.0%	9.1%
	–	13.0%	10.0%	11.0%	13.0%	4.1%	9.0%	14.0%	10.0%	9.1%	7.1%	N/A	20.0%	9.1%
Ru-106 Concentration	+	N/A	N/A	N/A	N/A	N/A	N/A	N/A	N/A	N/A	N/A	N/A	N/A	N/A
	–	N/A	N/A	N/A	N/A	N/A	N/A	N/A	N/A	N/A	N/A	N/A	N/A	N/A
Sb-125 Concentration	+	2.0%	2.0%	2.0%	2.0%	2.0%	2.1%	2.1%	2.1%	2.1%	2.2%	2.2%	2.2%	2.3%
	–	2.1%	2.1%	2.1%	2.1%	2.1%	2.1%	2.2%	2.2%	2.2%	2.2%	2.3%	2.3%	2.4%
Sr-90 Concentration	+	2.0%	2.0%	2.0%	2.0%	2.0%	2.1%	4.0%	4.1%	4.1%	4.1%	4.1%	5.1%	4.2%
	–	2.1%	2.1%	2.1%	2.1%	2.1%	2.1%	4.1%	4.1%	4.1%	4.1%	4.2%	5.1%	4.2%
Segment Volume (mm ³)	+ mm ³	1.16	1.65	1.81	2.01	2.24	2.50	2.77	3.05	3.34	3.64	3.95	4.26	2.17
	– mm ³	2.96	3.91	3.89	3.91	3.95	4.02	4.12	4.25	4.39	4.57	4.75	4.96	2.47
Average Radius of Segment (mm)	+/- mm	0.034	0.036	0.040	0.044	0.050	0.055	0.061	0.067	0.074	0.081	0.087	0.094	0.101

Table B-31. Capsule 8 IR, axial center: decay-corrected concentrations (Bq per mm³) of selected fission products for each radial segment sampled at the axial center of the Capsule 8 IR. The volume and average radius $[(r_{\text{inner}} + r_{\text{outer}})/2]$ of each segment are also given. Shading indicates a value derived from an MDA.

IR-08 Center (Bq/mm ³)	IR8-C1	IR8-C2	IR8-C3	IR8-C4	IR8-C5	IR8-C6	IR8-C7	IR8-C8	IR8-C9	IR8-C10	IR8-C11	IR8-C12
Ag-110m	7.06E+2	5.54E+2	3.45E+2	2.16E+2	1.61E+2	1.34E+2	1.18E+2	9.12E+1	7.47E+1	6.83E+1	6.81E+1	1.72E+2
Ce-144	8.94E+1	4.53E+1	3.70E+1	3.09E+1	3.63E+1	2.79E+1	2.81E+1	3.70E+1	3.52E+1	1.00E+1	1.84E+1	3.86E+2
Cs-134	1.12E+3	9.99E+2	9.83E+2	9.83E+2	9.10E+2	9.30E+2	9.57E+2	9.96E+2	1.01E+3	9.04E+2	8.63E+2	1.53E+3
Cs-137	1.09E+3	9.07E+2	9.23E+2	9.25E+2	8.60E+2	9.14E+2	9.22E+2	9.69E+2	9.88E+2	9.00E+2	8.72E+2	1.58E+3
Eu-154	5.97E+0	9.29E-1	5.29E-1	4.10E-1	4.98E-1	2.79E-1	1.74E-1	8.16E-1	8.64E+0	3.92E+1	2.00E+2	2.99E+3
Eu-155	3.45E+0	1.66E+0	1.51E+0	1.74E+0	1.82E+0	4.16E-1	1.70E+0	1.79E+0	6.84E+0	2.60E+1	1.30E+2	1.93E+3
Ru-106	4.81E+1	2.96E+1	1.59E+1	1.50E+1	2.05E+1	1.25E+1	1.09E+1	1.80E+1	1.32E+1	6.33E+0	2.49E+1	5.96E+1
Sb-125	1.28E+2	1.24E+2	1.40E+2	1.58E+2	1.92E+2	1.84E+2	1.95E+2	2.38E+2	2.46E+2	2.70E+2	3.02E+2	7.83E+2
Sr-90	1.84E+2	2.79E+1	1.85E+1	1.38E+1	1.49E+1	1.15E+1	3.13E+1	1.64E+2	1.71E+3	4.83E+3	1.40E+4	7.85E+4
Segment Volume (mm ³)	283.32	363.57	347.36	331.14	314.93	298.71	282.50	266.28	250.07	233.86	217.64	97.19
Average Segment Radius (mm)	11.84	11.39	10.88	10.37	9.87	9.36	8.85	8.34	7.83	7.33	6.82	6.44

Table B-32. Capsule 8 IR, axial center: decay-corrected concentrations (particle equivalents per mm³) of selected fission products for each radial segment sampled at the axial center of the Capsule 8 IR. The volume and average radius [(r_{inner} + r_{outer})/2] of each segment are also given. Shading indicates a value derived from an MDA.

IR-08 Center (Particle equivalents/mm ³)	IR8-C1	IR8-C2	IR8-C3	IR8-C4	IR8-C5	IR8-C6	IR8-C7	IR8-C8	IR8-C9	IR8-C10	IR8-C11	IR8-C12
Ag-110m	1.27E-2	9.98E-3	6.22E-3	3.89E-3	2.90E-3	2.41E-3	2.12E-3	1.64E-3	1.35E-3	1.23E-3	1.23E-3	3.10E-3
Ce-144	1.58E-6	8.00E-7	6.54E-7	5.45E-7	6.41E-7	4.92E-7	4.96E-7	6.52E-7	6.21E-7	1.77E-7	3.26E-7	6.82E-6
Cs-134	2.32E-4	2.06E-4	2.03E-4	2.03E-4	1.88E-4	1.92E-4	1.98E-4	2.06E-4	2.08E-4	1.87E-4	1.78E-4	3.15E-4
Cs-137	2.86E-4	2.39E-4	2.43E-4	2.43E-4	2.26E-4	2.41E-4	2.42E-4	2.55E-4	2.60E-4	2.37E-4	2.29E-4	4.15E-4
Eu-154	3.93E-5	6.11E-6	3.48E-6	2.70E-6	3.28E-6	1.84E-6	1.14E-6	5.37E-6	5.69E-5	2.58E-4	1.32E-3	1.97E-2
Eu-155	3.44E-5	1.65E-5	1.51E-5	1.73E-5	1.81E-5	4.14E-6	1.70E-5	1.78E-5	6.80E-5	2.58E-4	1.30E-3	1.92E-2
Ru-106	3.66E-6	2.25E-6	1.20E-6	1.14E-6	1.56E-6	9.50E-7	8.29E-7	1.36E-6	1.00E-6	4.81E-7	1.89E-6	4.53E-6
Sb-125	4.25E-4	4.13E-4	4.66E-4	5.23E-4	6.37E-4	6.12E-4	6.47E-4	7.90E-4	8.16E-4	8.95E-4	1.00E-3	2.60E-3
Sr-90	5.63E-5	8.54E-6	5.67E-6	4.24E-6	4.58E-6	3.53E-6	9.60E-6	5.03E-5	5.24E-4	1.48E-3	4.29E-3	2.41E-2
Segment Volume (mm ³)	283.32	363.57	347.36	331.14	314.93	298.71	282.50	266.28	250.07	233.86	217.64	97.19
Average Segment Radius (mm)	11.84	11.39	10.88	10.37	9.87	9.36	8.85	8.34	7.83	7.33	6.82	6.44

Table B-33. Estimated relative uncertainties in the concentrations reported for IR-08 center in Table B-31 and Table B-32. Absolute uncertainties in the segment volumes and average radii of the segments. N/A denotes a case where an isotope was not detected, and therefore, no uncertainty is available.

IR-08 Center	Units	IR8-C1	IR8-C2	IR8-C3	IR8-C4	IR8-C5	IR8-C6	IR8-C7	IR8-C8	IR8-C9	IR8-C10	IR8-C11	IR8-C12
Ag-110m Concentration	+	2.0%	2.0%	2.0%	2.0%	2.1%	2.1%	2.2%	2.2%	2.3%	2.5%	2.6%	2.8%
	–	2.1%	2.1%	2.1%	2.1%	2.2%	2.2%	2.3%	2.3%	2.4%	2.5%	2.7%	2.9%
Ce-144 Concentration	+	25.0%	N/A	N/A	N/A	N/A	N/A	N/A	N/A	N/A	35.0%	39.0%	7.3%
	–	25.0%	N/A	N/A	N/A	N/A	N/A	N/A	N/A	N/A	35.0%	39.0%	7.3%
Cs-134 Concentration	+	2.0%	2.0%	2.0%	2.0%	2.1%	2.1%	2.2%	2.2%	2.3%	2.5%	2.6%	2.8%
	–	2.1%	2.1%	2.1%	2.1%	2.2%	2.2%	2.3%	2.3%	2.4%	2.5%	2.7%	2.9%
Cs-137 Concentration	+	2.0%	2.0%	2.0%	2.0%	2.1%	2.1%	2.2%	2.2%	2.3%	2.5%	2.6%	2.8%
	–	2.1%	2.1%	2.1%	2.1%	2.2%	2.2%	2.3%	2.3%	2.4%	2.5%	2.7%	2.9%
Eu-154 Concentration	+	2.0%	6.0%	3.0%	7.0%	6.0%	12.0%	6.1%	4.1%	2.3%	2.5%	2.6%	2.8%
	–	2.1%	6.0%	3.1%	7.0%	6.1%	12.0%	6.1%	4.2%	2.4%	2.5%	2.7%	2.9%
Eu-155 Concentration	+	5.0%	18.0%	11.0%	9.0%	9.0%	N/A	11.0%	13.0%	4.2%	2.5%	2.6%	2.8%
	–	5.0%	18.0%	11.0%	9.0%	9.0%	N/A	11.1%	13.1%	4.2%	2.5%	2.7%	2.9%
Ru-106 Concentration	+	5.0%	N/A	N/A	N/A	N/A	N/A	N/A	N/A	N/A	36.0%	N/A	N/A
	–	5.0%	N/A	N/A	N/A	N/A	N/A	N/A	N/A	N/A	36.0%	N/A	N/A
Sb-125 Concentration	+	2.0%	2.0%	2.0%	2.0%	2.1%	2.1%	2.2%	2.2%	2.3%	2.5%	2.0%	2.8%
	–	2.1%	2.1%	2.1%	2.1%	2.2%	2.2%	2.3%	2.3%	2.4%	2.5%	2.1%	2.9%
Sr-90 Concentration	+	2.0%	2.0%	2.0%	2.0%	2.1%	2.1%	2.2%	2.2%	3.2%	2.5%	2.6%	2.8%
	–	2.1%	2.1%	2.1%	2.1%	2.2%	2.2%	2.3%	2.3%	3.3%	2.5%	2.7%	2.9%
Segment Volume (mm ³)	+ mm ³	0.55	0.93	1.19	1.48	1.79	2.10	2.42	2.74	3.06	3.39	3.72	1.91
	– mm ³	1.83	2.43	2.45	2.52	2.64	2.79	2.98	3.19	3.43	3.68	3.95	2.00
Average Radius of Segment (mm)	+/- mm	0.016	0.021	0.026	0.033	0.039	0.046	0.053	0.060	0.068	0.075	0.082	0.089

Table B-34. Capsule 8 IR, axial bottom: decay-corrected concentrations (Bq per mm³) of selected fission products for each radial segment sampled at the axial bottom of the Capsule 8 IR. The volume and average radius $[(r_{\text{inner}} + r_{\text{outer}})/2]$ of each segment are also given. Shading indicates a value derived from an MDA.

IR-08 Bottom (Bq/mm ³)	IR8-B1	IR8-B2	IR8-B3	IR8-B4	IR8-B5	IR8-B6	IR8-B7	IR8-B8	IR8-B9	IR8-B10	IR8-B11	IR8-B12
Ag-110m	4.33E+3	2.53E+3	2.15E+3	1.61E+3	8.35E+2	2.93E+2	2.00E+2	1.42E+2	9.31E+1	6.80E+1	5.98E+1	6.53E+1
Ce-144	7.02E+1	2.74E+1	2.77E+1	5.04E+1	2.95E+1	3.11E+1	5.72E+1	3.11E+1	3.01E+1	5.50E+1	7.39E+1	3.17E+2
Cs-134	#DIV/0!	#DIV/0!	#DIV/0!	#DIV/0!	#DIV/0!	#DIV/0!	#DIV/0!	#DIV/0!	#DIV/0!	#DIV/0!	#DIV/0!	#DIV/0!
Cs-137	1.69E+3	1.19E+3	1.13E+3	1.13E+3	1.05E+3	1.17E+3	1.12E+3	1.12E+3	1.01E+3	9.87E+2	9.35E+2	6.33E+2
Eu-154	1.55E+3	1.05E+3	1.03E+3	1.02E+3	9.82E+2	1.07E+3	1.03E+3	1.03E+3	9.60E+2	9.39E+2	8.98E+2	6.79E+2
Eu-155	1.75E+0	9.60E-1	1.38E+0	1.59E+0	2.02E+0	3.32E+0	3.62E+0	4.91E+0	9.20E+0	4.04E+1	2.88E+2	8.64E+2
Ru-106	1.91E+1	1.20E+1	1.30E+1	3.41E+1	1.35E+1	2.07E+1	3.50E+1	1.19E+1	1.79E+1	3.93E+1	4.89E+1	2.80E+1
Sb-125	2.36E+2	1.50E+2	1.70E+2	1.90E+2	1.90E+2	2.12E+2	2.47E+2	2.50E+2	2.76E+2	3.09E+2	3.71E+2	4.92E+2
Sr-90	7.56E+1	2.95E+1	3.84E+1	2.17E+1	4.51E+1	8.56E+1	9.93E+1	1.81E+2	9.00E+2	4.09E+3	1.33E+4	2.15E+4
Segment Volume (mm ³)	283.72	364.11	347.90	331.68	315.47	299.25	283.04	266.82	250.61	234.39	218.18	116.75
Average Segment Radius (mm)	11.85	11.41	10.90	10.39	9.88	9.38	8.87	8.36	7.85	7.34	6.84	6.44

Table B-35. Capsule 8 IR, axial bottom: decay-corrected concentrations (particle equivalents per mm³) of selected fission products for each radial segment sampled at the axial bottom of the Capsule 8 IR. The volume and average radius [(r_{inner} + r_{outer})/2] of each segment are also given. Shading indicates a value derived from an MDA.

IR-08 Bottom (Particle equivalents/mm ³)	IR8-B1	IR8-B2	IR8-B3	IR8-B4	IR8-B5	IR8-B6	IR8-B7	IR8-B8	IR8-B9	IR8-B10	IR8-B11	IR8-B12
Ag-110m	7.80E-2	4.55E-2	3.87E-2	2.91E-2	1.50E-2	5.27E-3	3.60E-3	2.55E-3	1.68E-3	1.23E-3	1.08E-3	1.18E-3
Ce-144	1.24E-6	4.85E-7	4.88E-7	8.90E-7	5.21E-7	5.50E-7	1.01E-6	5.48E-7	5.31E-7	9.72E-7	1.31E-6	5.59E-6
Cs-134	3.48E-4	2.46E-4	2.33E-4	2.33E-4	2.16E-4	2.42E-4	2.32E-4	2.30E-4	2.09E-4	2.04E-4	1.93E-4	1.31E-4
Cs-137	4.07E-4	2.75E-4	2.70E-4	2.68E-4	2.58E-4	2.82E-4	2.71E-4	2.71E-4	2.53E-4	2.47E-4	2.36E-4	1.79E-4
Eu-154	1.15E-5	6.32E-6	9.08E-6	1.05E-5	1.33E-5	2.18E-5	2.38E-5	3.23E-5	6.05E-5	2.66E-4	1.89E-3	5.69E-3
Eu-155	6.10E-6	5.26E-6	4.20E-6	9.18E-6	1.80E-5	1.27E-5	3.00E-5	3.43E-5	5.64E-5	2.63E-4	1.85E-3	5.55E-3
Ru-106	1.45E-6	9.15E-7	9.88E-7	2.59E-6	1.02E-6	1.58E-6	2.66E-6	9.00E-7	1.36E-6	2.98E-6	3.72E-6	2.13E-6
Sb-125	7.83E-4	5.00E-4	5.63E-4	6.29E-4	6.32E-4	7.03E-4	8.19E-4	8.29E-4	9.15E-4	1.03E-3	1.23E-3	1.63E-3
Sr-90	2.32E-5	9.03E-6	1.18E-5	6.65E-6	1.38E-5	2.63E-5	3.05E-5	5.56E-5	2.76E-4	1.26E-3	4.08E-3	6.60E-3
Segment Volume (mm ³)	283.72	364.11	347.90	331.68	315.47	299.25	283.04	266.82	250.61	234.39	218.18	116.75
Average Segment Radius (mm)	11.85	11.41	10.90	10.39	9.88	9.38	8.87	8.36	7.85	7.34	6.84	6.44

Table B-36. Estimated relative uncertainties in the concentrations reported for IR-08 bottom in Table B-34 and Table B-35. Absolute uncertainties in the segment volumes and average radii of the segments. N/A denotes a case where an isotope was not detected, and therefore, no uncertainty is available.

IR-08 Bottom	Units	IR8-B1	IR8-B2	IR8-B3	IR8-B4	IR8-B5	IR8-B6	IR8-B7	IR8-B8	IR8-B9	IR8-B10	IR8-B11	IR8-B12
Ag-110m Concentration	+	2.0%	2.0%	2.1%	2.1%	2.1%	2.2%	2.2%	2.3%	2.4%	2.5%	3.5%	2.9%
	–	2.1%	2.1%	2.2%	2.2%	2.2%	2.3%	2.3%	2.4%	2.5%	2.6%	3.6%	2.9%
Ce-144 Concentration	+	9.0%	N/A	N/A	N/A	N/A	N/A	N/A	N/A	N/A	N/A	N/A	7.3%
	–	9.0%	N/A	N/A	N/A	N/A	N/A	N/A	N/A	N/A	N/A	N/A	7.3%
Cs-134 Concentration	+	2.0%	2.0%	2.1%	2.1%	2.1%	2.2%	2.2%	2.3%	2.4%	2.5%	2.7%	2.9%
	–	2.1%	2.1%	2.2%	2.2%	2.2%	2.3%	2.3%	2.4%	2.5%	2.6%	2.8%	2.9%
Cs-137 Concentration	+	2.0%	2.0%	2.1%	2.1%	2.1%	2.2%	2.2%	2.3%	2.4%	2.5%	2.7%	2.9%
	–	2.1%	2.1%	2.2%	2.2%	2.2%	2.3%	2.3%	2.4%	2.5%	2.6%	2.8%	2.9%
Eu-154 Concentration	+	4.0%	3.0%	2.1%	2.1%	2.1%	2.2%	2.2%	2.3%	2.4%	2.5%	2.7%	2.9%
	–	4.1%	3.1%	2.2%	2.2%	2.2%	2.3%	2.3%	2.4%	2.5%	2.6%	2.8%	2.9%
Eu-155 Concentration	+	N/A	N/A	N/A	17.0%	10.0%	12.0%	6.1%	2.3%	3.3%	3.4%	2.7%	2.9%
	–	N/A	N/A	N/A	17.0%	10.0%	12.0%	6.1%	2.4%	3.3%	3.4%	2.8%	2.9%
Ru-106 Concentration	+	N/A	N/A	N/A	N/A	N/A	N/A	N/A	N/A	N/A	N/A	N/A	20.1%
	–	N/A	N/A	N/A	N/A	N/A	N/A	N/A	N/A	N/A	N/A	N/A	20.1%
Sb-125 Concentration	+	2.0%	2.0%	2.1%	2.1%	2.1%	2.2%	2.2%	2.3%	2.4%	2.5%	2.7%	2.9%
	–	2.1%	2.1%	2.2%	2.2%	2.2%	2.3%	2.3%	2.4%	2.5%	2.6%	2.8%	2.9%
Sr-90 Concentration	+	2.0%	2.0%	2.1%	2.1%	2.1%	2.2%	2.2%	2.3%	2.4%	2.5%	2.7%	2.9%
	–	2.1%	2.1%	2.2%	2.2%	2.2%	2.3%	2.3%	2.4%	2.5%	2.6%	2.8%	2.9%
Segment Volume (mm ³)	+ mm ³	1.15	1.64	1.80	2.00	2.24	2.49	2.77	3.05	3.34	3.65	3.95	2.42
	– mm ³	2.09	2.78	2.80	2.86	2.96	3.10	3.27	3.46	3.68	3.92	4.17	2.52
Average Radius of Segment (mm)	+/- mm	0.034	0.036	0.040	0.044	0.049	0.055	0.061	0.067	0.074	0.080	0.087	0.094

Table B-37. Capsule 8 OR, axial center: decay-corrected concentrations (Bq per mm³) of selected fission products for each radial segment sampled at the axial center of the Capsule 8 OR. The volume and average radius $[(r_{\text{inner}} + r_{\text{outer}})/2]$ of each segment are also given. Shading indicates a value derived from an MDA.

OR-08 Center (Bq/mm ³)	OR8-C1	OR8-C2	OR8-C3	OR8-C4	OR8-C5	OR8-C6	OR8-C7	OR8-C8	OR8-C9	OR8-C10	OR8-C11	OR8-C12	OR8-C13	OR8-C14
Ag-110m	1.04E+3	8.81E+2	1.29E+3	1.93E+3	2.99E+3	3.80E+3	4.43E+3	5.86E+3	6.56E+3	6.75E+3	6.50E+3	4.64E+3	4.30E+3	5.50E+3
Ce-144	1.78E+2	5.15E+1	1.56E+2	1.63E+2	6.43E+1	1.29E+2	1.88E+2	1.91E+2	1.47E+2	7.21E+1	2.25E+2	1.96E+2	2.20E+2	3.50E+2
Cs-134	2.55E+3	2.00E+3	2.09E+3	2.19E+3	2.22E+3	2.34E+3	2.50E+3	2.88E+3	2.75E+3	2.66E+3	3.04E+3	2.74E+3	3.09E+3	5.21E+3
Cs-137	2.17E+3	1.69E+3	1.77E+3	1.87E+3	1.89E+3	1.99E+3	2.16E+3	2.49E+3	2.39E+3	2.30E+3	2.66E+3	2.39E+3	2.70E+3	4.64E+3
Eu-154	3.10E-1	2.67E-1	4.15E-1	2.81E-1	1.55E-1	4.15E-1	6.11E-1	3.77E-1	5.18E-1	2.58E-1	8.02E-1	6.58E-1	6.49E-1	1.14E+0
Eu-155	2.68E+0	8.26E-1	2.49E+0	2.25E+0	9.22E-1	1.94E+0	3.01E+0	3.09E+0	2.35E+0	1.17E+0	3.65E+0	2.32E+0	3.50E+0	5.67E+0
Ru-106	9.78E+1	2.82E+1	8.45E+1	9.03E+1	3.22E+1	6.98E+1	1.05E+2	1.11E+2	8.43E+1	4.02E+1	1.29E+2	1.15E+2	1.19E+2	1.96E+2
Sb-125	2.15E+1	5.84E+0	7.38E+0	1.26E+1	1.90E+1	3.09E+1	5.26E+1	9.09E+1	1.18E+2	1.57E+2	2.35E+2	2.51E+2	3.13E+2	7.23E+2
Sr-90	1.92E+1	5.43E+0	4.59E+0	5.14E+0	4.45E+0	3.69E+0	5.01E+0	4.37E+0	4.29E+0	4.08E+0	4.57E+0	3.86E+0	4.97E+0	1.52E+1
Segment Volume (mm ³)	456.85	594.94	578.73	562.51	546.30	530.08	513.87	497.65	481.44	465.23	449.01	432.80	416.58	324.48
Average Segment Radius (mm)	19.08	18.64	18.13	17.62	17.12	16.61	16.10	15.59	15.08	14.58	14.07	13.56	13.05	12.59

Table B-38. Capsule 8 OR, axial center: decay-corrected concentrations (particle equivalents per mm³) of selected fission products for each radial segment sampled at the axial center of the Capsule 8 OR. The volume and average radius $[(r_{\text{inner}} + r_{\text{outer}})/2]$ of each segment are also given. Shading indicates a value derived from an MDA.

OR-08 Center (Particle equivalents/mm ³)	OR8-C1	OR8-C2	OR8-C3	OR8-C4	OR8-C5	OR8-C6	OR8-C7	OR8-C8	OR8-C9	OR8-C10	OR8-C11	OR8-C12	OR8-C13	OR8-C14
Ag-110m	1.88E-2	1.59E-2	2.33E-2	3.48E-2	5.39E-2	6.84E-2	7.97E-2	1.06E-1	1.18E-1	1.22E-1	1.17E-1	8.36E-2	7.75E-2	7.72E-2
Ce-144	3.14E-6	9.09E-7	2.76E-6	2.87E-6	1.14E-6	2.27E-6	3.32E-6	3.37E-6	2.59E-6	1.27E-6	3.98E-6	3.45E-6	3.89E-6	4.82E-6
Cs-134	5.25E-4	4.13E-4	4.31E-4	4.51E-4	4.59E-4	4.82E-4	5.16E-4	5.95E-4	5.68E-4	5.48E-4	6.28E-4	5.66E-4	6.38E-4	8.38E-4
Cs-137	5.71E-4	4.45E-4	4.66E-4	4.91E-4	4.98E-4	5.24E-4	5.69E-4	6.54E-4	6.29E-4	6.05E-4	7.00E-4	6.28E-4	7.12E-4	9.51E-4
Eu-154	2.04E-6	1.76E-6	2.73E-6	1.85E-6	1.02E-6	2.73E-6	4.02E-6	2.48E-6	3.41E-6	1.70E-6	5.28E-6	4.33E-6	4.27E-6	5.83E-6
Eu-155	2.67E-5	8.22E-6	2.48E-5	2.23E-5	9.17E-6	1.93E-5	3.00E-5	3.07E-5	2.34E-5	1.16E-5	3.63E-5	2.30E-5	3.48E-5	4.40E-5
Ru-106	7.43E-6	2.14E-6	6.42E-6	6.86E-6	2.45E-6	5.30E-6	8.00E-6	8.40E-6	6.40E-6	3.05E-6	9.82E-6	8.77E-6	9.01E-6	1.16E-5
Sb-125	7.13E-5	1.94E-5	2.45E-5	4.17E-5	6.30E-5	1.03E-4	1.75E-4	3.02E-4	3.92E-4	5.22E-4	7.80E-4	8.35E-4	1.04E-3	1.87E-3
Sr-90	5.89E-6	1.67E-6	1.41E-6	1.57E-6	1.36E-6	1.13E-6	1.54E-6	1.34E-6	1.31E-6	1.25E-6	1.40E-6	1.18E-6	1.52E-6	3.63E-6
Segment Volume (mm ³)	456.85	594.94	578.73	562.51	546.30	530.08	513.87	497.65	481.44	465.23	449.01	432.80	416.58	324.48
Average Segment Radius (mm)	19.08	18.64	18.13	17.62	17.12	16.61	16.10	15.59	15.08	14.58	14.07	13.56	13.05	12.59

Table B-39. Estimated relative uncertainties in the concentrations reported for OR-08 center in Table B-37 and Table B-38. Absolute uncertainties in the segment volumes and average radii of the segments. N/A denotes a case where an isotope was not detected, and therefore, no uncertainty is available.

OR-08 Center	Units	OR8-C1	OR8-C2	OR8-C3	OR8-C4	OR8-C5	OR8-C6	OR8-C7	OR8-C8	OR8-C9	OR8-C10	OR8-C11	OR8-C12	OR8-C13	OR8-C14
Ag-110m Concentration	+	2.0%	2.0%	2.0%	2.0%	2.0%	2.0%	2.1%	2.1%	2.1%	2.1%	2.2%	2.2%	2.3%	2.3%
	–	2.1%	2.1%	2.1%	2.1%	2.1%	2.1%	2.1%	2.2%	2.2%	2.2%	2.3%	2.3%	2.3%	2.4%
Ce-144 Concentration	+	N/A	N/A	N/A	N/A	N/A	N/A	N/A	N/A	N/A	N/A	N/A	N/A	N/A	N/A
	–	N/A	N/A	N/A	N/A	N/A	N/A	N/A	N/A	N/A	N/A	N/A	N/A	N/A	N/A
Cs-134 Concentration	+	2.0%	2.0%	2.0%	2.0%	2.0%	2.0%	2.1%	2.1%	2.1%	2.1%	2.2%	2.2%	2.3%	2.3%
	–	2.1%	2.1%	2.1%	2.1%	2.1%	2.1%	2.1%	2.2%	2.2%	2.2%	2.3%	2.3%	2.3%	2.4%
Cs-137 Concentration	+	2.0%	2.0%	2.0%	2.0%	2.0%	2.0%	2.1%	2.1%	2.1%	2.1%	2.2%	2.2%	2.3%	2.3%
	–	2.1%	2.1%	2.1%	2.1%	2.1%	2.1%	2.1%	2.2%	2.2%	2.2%	2.3%	2.3%	2.3%	2.4%
Eu-154 Concentration	+	14.0%	19.0%	N/A	N/A	10.0%	N/A	N/A	N/A	N/A	N/A	N/A	N/A	N/A	N/A
	–	14.0%	19.0%	N/A	N/A	10.0%	N/A	N/A	N/A	N/A	N/A	N/A	N/A	N/A	N/A
Eu-155 Concentration	+	N/A	N/A	N/A	N/A	N/A	N/A	N/A	N/A	N/A	N/A	N/A	N/A	N/A	N/A
	–	N/A	N/A	N/A	N/A	N/A	N/A	N/A	N/A	N/A	N/A	N/A	N/A	N/A	N/A
Ru-106 Concentration	+	N/A	N/A	N/A	N/A	N/A	N/A	N/A	N/A	N/A	N/A	N/A	N/A	N/A	N/A
	–	N/A	N/A	N/A	N/A	N/A	N/A	N/A	N/A	N/A	N/A	N/A	N/A	N/A	N/A
Sb-125 Concentration	+	3.0%	4.0%	7.0%	8.0%	2.0%	2.0%	2.1%	2.1%	2.1%	2.1%	2.2%	2.2%	2.3%	2.3%
	–	3.1%	4.1%	7.0%	8.0%	2.1%	2.1%	2.1%	2.2%	2.2%	2.2%	2.3%	2.3%	2.3%	2.4%
Sr-90 Concentration	+	4.0%	5.0%	5.0%	5.0%	5.0%	6.0%	5.0%	2.1%	6.0%	6.0%	5.1%	6.1%	5.1%	4.2%
	–	4.0%	5.0%	5.0%	5.0%	5.0%	6.0%	5.1%	2.2%	6.1%	6.1%	5.1%	6.1%	5.1%	4.2%
Segment Volume (mm ³)	+ mm ³	0.66	1.05	1.28	1.56	1.85	2.15	2.46	2.77	3.09	3.41	3.74	4.06	4.39	3.80
	– mm ³	2.89	3.82	3.79	3.80	3.84	3.91	4.01	4.14	4.29	4.46	4.65	4.86	5.08	4.30
Average Radius of Segment (mm)	+/- mm	0.019	0.023	0.028	0.034	0.041	0.047	0.054	0.061	0.068	0.075	0.083	0.090	0.097	0.104

Table B-40. Capsule 8 OR, axial bottom: decay-corrected concentrations (Bq per mm³) of selected fission products for each radial segment sampled at the axial bottom of the Capsule 8 OR. The volume and average radius [(r_{inner} + r_{outer})/2] of each segment are also given. Shading indicates a value derived from an MDA. Shaded column headings denote segments with greater (but unknown) uncertainty due to ring cracking during sampling.

OR-08 Bottom (Bq/mm ³)	OR8-B1	OR8-B2	OR8-B3	OR8-B4	OR8-B5	OR8-B6	OR8-B7	OR8-B8	OR8-B9	OR8-B10	OR8-B11	OR8-B12	OR8-B13	OR8-B14
Ag-110m	1.47E+3	8.84E+2	7.04E+2	9.97E+2	1.40E+3	2.05E+3	3.03E+3	4.46E+3	9.12E+3	1.47E+4	1.99E+4	1.58E+4	1.70E+4	1.89E+4
Ce-144	1.81E+2	1.48E+2	4.81E+1	1.14E+2	7.89E+1	8.58E+1	1.03E+2	8.62E+1	1.09E+2	5.78E+1	1.61E+2	7.45E+1	1.43E+2	2.05E+2
Cs-134	2.97E+3	2.20E+3	2.03E+3	2.19E+3	2.35E+3	2.54E+3	2.69E+3	2.60E+3	2.81E+3	2.62E+3	2.29E+3	1.66E+3	1.97E+3	2.80E+3
Cs-137	2.45E+3	1.82E+3	1.66E+3	1.78E+3	1.93E+3	2.11E+3	2.24E+3	2.10E+3	2.36E+3	2.17E+3	1.93E+3	1.41E+3	1.66E+3	2.46E+3
Eu-154	1.00E+0	3.49E-1	2.46E-1	2.40E-1	6.12E-1	4.28E-1	2.87E-1	3.75E-1	4.09E-1	5.31E-1	6.84E-1	4.24E-1	8.84E-1	1.06E+0
Eu-155	2.86E+0	2.56E+0	8.40E-1	1.78E+0	1.29E+0	1.49E+0	1.83E+0	1.60E+0	1.96E+0	1.54E+0	3.11E+0	1.18E+0	2.65E+0	3.01E+0
Ru-106	1.05E+2	8.16E+1	2.68E+1	6.98E+1	4.79E+1	4.89E+1	5.94E+1	5.62E+1	6.48E+1	6.78E+1	1.15E+2	4.74E+1	1.01E+2	1.21E+2
Sb-125	1.57E+1	5.31E+0	6.98E+0	1.67E+1	2.40E+1	3.44E+1	5.67E+1	8.22E+1	1.15E+2	1.49E+2	1.58E+2	1.60E+2	2.22E+2	5.59E+2
Sr-90	3.53E+1	9.06E+0	9.81E+0	8.47E+0	6.72E+0	8.94E+0	6.29E+0	8.34E+0	1.01E+1	1.07E+1	1.37E+1	8.74E+0	6.52E+0	2.47E+1
Segment Volume (mm ³)	457.16	595.36	579.15	562.93	546.72	530.50	514.29	498.07	481.86	465.64	449.43	433.21	417.00	338.75
Average Segment Radius (mm)	19.10	18.65	18.14	17.64	17.13	16.62	16.11	15.60	15.10	14.59	14.08	13.57	13.06	12.60

Table B-41. Capsule 8 OR, axial bottom: decay-corrected concentrations (particle equivalents per mm³) of selected fission products for each radial segment sampled at the axial bottom of the Capsule 8 OR. The volume and average radius $[(r_{\text{inner}} + r_{\text{outer}})/2]$ of each segment are also given. Shaded column headings denote segments with greater (but unknown) uncertainty due to ring cracking during sampling.

OR-08 Bottom (Particle equivalents/mm ³)	OR8-B1	OR8-B2	OR8-B3	OR8-B4	OR8-B5	OR8-B6	OR8-B7	OR8-B8	OR8-B9	OR8-B10	OR8-B11	OR8-B12	OR8-B13	OR8-B14
Ag-110m	2.65E-2	1.59E-2	1.27E-2	1.80E-2	2.51E-2	3.69E-2	5.47E-2	8.03E-2	1.64E-1	2.65E-1	3.58E-1	2.85E-1	3.06E-1	3.41E-1
Ce-144	3.19E-6	2.61E-6	8.49E-7	2.02E-6	1.39E-6	1.51E-6	1.82E-6	1.52E-6	1.92E-6	1.02E-6	2.84E-6	1.32E-6	2.52E-6	3.62E-6
Cs-134	6.13E-4	4.54E-4	4.20E-4	4.52E-4	4.85E-4	5.24E-4	5.56E-4	5.36E-4	5.80E-4	5.41E-4	4.72E-4	3.43E-4	4.06E-4	5.78E-4
Cs-137	6.44E-4	4.78E-4	4.37E-4	4.69E-4	5.08E-4	5.56E-4	5.88E-4	5.54E-4	6.21E-4	5.70E-4	5.09E-4	3.72E-4	4.38E-4	6.47E-4
Eu-154	6.59E-6	2.30E-6	1.62E-6	1.58E-6	4.03E-6	2.81E-6	1.89E-6	2.47E-6	2.69E-6	3.49E-6	4.50E-6	2.79E-6	5.82E-6	7.00E-6
Eu-155	2.85E-5	2.55E-5	8.36E-6	1.77E-5	1.28E-5	1.48E-5	1.82E-5	1.59E-5	1.95E-5	1.53E-5	3.09E-5	1.18E-5	2.64E-5	2.99E-5
Ru-106	8.00E-6	6.20E-6	2.03E-6	5.30E-6	3.64E-6	3.72E-6	4.51E-6	4.27E-6	4.92E-6	5.15E-6	8.75E-6	3.60E-6	7.64E-6	9.18E-6
Sb-125	5.21E-5	1.76E-5	2.32E-5	5.55E-5	7.97E-5	1.14E-4	1.88E-4	2.73E-4	3.81E-4	4.95E-4	5.25E-4	5.33E-4	7.36E-4	1.86E-3
Sr-90	1.08E-5	2.78E-6	3.01E-6	2.60E-6	2.06E-6	2.74E-6	1.93E-6	2.56E-6	3.10E-6	3.27E-6	4.19E-6	2.68E-6	2.00E-6	7.58E-6
Segment Volume (mm ³)	457.16	595.36	579.15	562.93	546.72	530.50	514.29	498.07	481.86	465.64	449.43	433.21	417.00	338.75
Average Segment Radius (mm)	19.10	18.65	18.14	17.64	17.13	16.62	16.11	15.60	15.10	14.59	14.08	13.57	13.06	12.60

Table B-42. Estimated relative uncertainties in the concentrations reported for OR-08 bottom in Table B-40 and Table B-41. Absolute uncertainties in the segment volumes and average radii of the segments. N/A denotes a case where an isotope was not detected, and therefore, no uncertainty is available. Shaded column headings denote segments with greater (but unknown) uncertainty due to ring cracking during sampling.

OR-08 Bottom	Units	OR8-B1	OR8-B2	OR8-B3	OR8-B4	OR8-B5	OR8-B6	OR8-B7	OR8-B8	OR8-B9	OR8-B10	OR8-B11	OR8-B12	OR8-B13	OR8-B14
Ag-110m Concentration	+	2.0%	2.0%	2.0%	2.0%	2.0%	2.0%	2.1%	2.1%	2.1%	2.1%	2.2%	2.2%	2.3%	2.3%
	–	2.1%	2.1%	2.1%	2.1%	2.1%	2.1%	2.1%	2.2%	2.2%	2.2%	2.3%	2.3%	2.3%	2.4%
Ce-144 Concentration	+	N/A	N/A	N/A	N/A	N/A	N/A	N/A	N/A	N/A	22.0%	N/A	N/A	N/A	N/A
	–	N/A	N/A	N/A	N/A	N/A	N/A	N/A	N/A	N/A	22.0%	N/A	N/A	N/A	N/A
Cs-134 Concentration	+	2.0%	2.0%	2.0%	2.0%	2.0%	2.0%	2.1%	2.1%	2.1%	2.1%	2.2%	2.2%	2.3%	2.3%
	–	2.1%	2.1%	2.1%	2.1%	2.1%	2.1%	2.1%	2.2%	2.2%	2.2%	2.3%	2.3%	2.3%	2.4%
Cs-137 Concentration	+	2.0%	2.0%	2.0%	2.0%	2.0%	2.0%	2.1%	2.1%	2.1%	2.1%	2.2%	2.2%	2.3%	2.3%
	–	2.1%	2.1%	2.1%	2.1%	2.1%	2.1%	2.1%	2.2%	2.2%	2.2%	2.3%	2.3%	2.3%	2.4%
Eu-154 Concentration	+	6.0%	24.0%	5.0%	41.0%	4.0%	4.0%	N/A	10.0%	27.0%	N/A	N/A	N/A	N/A	34.0%
	–	6.0%	24.0%	5.0%	41.0%	4.1%	4.1%	N/A	10.0%	27.0%	N/A	N/A	N/A	N/A	34.0%
Eu-155 Concentration	+	N/A	N/A	N/A	N/A	N/A	N/A	N/A	N/A	N/A	N/A	N/A	N/A	N/A	N/A
	–	N/A	N/A	N/A	N/A	N/A	N/A	N/A	N/A	N/A	N/A	N/A	N/A	N/A	N/A
Ru-106 Concentration	+	N/A	N/A	N/A	N/A	N/A	N/A	N/A	N/A	N/A	N/A	N/A	N/A	N/A	N/A
	–	N/A	N/A	N/A	N/A	N/A	N/A	N/A	N/A	N/A	N/A	N/A	N/A	N/A	N/A
Sb-125 Concentration	+	4.0%	12.0%	4.0%	3.0%	2.0%	2.0%	2.1%	2.1%	2.1%	2.1%	2.2%	2.2%	2.3%	2.3%
	–	4.1%	12.0%	4.1%	3.1%	2.1%	2.1%	2.1%	2.2%	2.2%	2.2%	2.3%	2.3%	2.3%	2.4%
Sr-90 Concentration	+	4.0%	4.0%	4.0%	4.0%	5.0%	4.0%	5.0%	5.0%	4.1%	4.1%	4.1%	5.1%	5.1%	4.2%
	–	4.1%	4.1%	4.1%	4.1%	5.0%	4.1%	5.1%	5.1%	4.1%	4.1%	4.1%	5.1%	5.1%	4.2%
Segment Volume (mm ³)	+ mm ³	0.75	1.16	1.37	1.63	1.91	2.20	2.51	2.82	3.13	3.45	3.77	4.09	4.41	3.99
	– mm ³	2.91	3.84	3.82	3.83	3.87	3.94	4.04	4.16	4.31	4.48	4.67	4.88	5.10	4.50
Average Radius of Segment (mm)	+/- mm	0.022	0.025	0.030	0.036	0.042	0.048	0.055	0.062	0.069	0.076	0.083	0.090	0.097	0.105

Table B-43. Capsule 10 IR, axial center: decay-corrected concentrations (Bq per mm³) of selected fission products for each radial segment sampled at the axial center of the Capsule 10 IR. The volume and average radius $[(r_{\text{inner}} + r_{\text{outer}})/2]$ of each segment are also given. Shading indicates a value derived from an MDA.

IR-10 Center (Bq/mm ³)	IR10-C1	IR10-C2	IR10-C3	IR10-C4	IR10-C5	IR10-C6	IR10-C7	IR10-C8	IR10-C9	IR10-C10	IR10-C11	IR10-C12
Ag-110m	1.75E+2	2.20E+2	2.70E+2	4.14E+2	3.85E+2	4.23E+2	3.63E+2	1.56E+2	1.55E+2	1.33E+2	1.26E+2	2.27E+2
Ce-144	1.18E+3	1.13E+2	1.21E+2	1.06E+3	2.16E+2	6.66E+2	2.96E+2	3.03E+2	7.66E+2	4.58E+2	1.38E+3	4.06E+3
Cs-134	7.14E+2	5.44E+2	5.66E+2	6.84E+2	7.10E+2	8.82E+2	1.03E+3	9.64E+2	1.18E+3	1.23E+3	1.44E+3	2.52E+3
Cs-137	9.58E+2	5.92E+2	6.33E+2	7.53E+2	7.95E+2	9.64E+2	1.05E+3	1.09E+3	1.31E+3	1.37E+3	1.61E+3	2.91E+3
Eu-154	5.41E+0	8.99E-1	6.00E-1	5.54E-1	9.73E-1	4.44E-1	3.85E-1	3.44E-1	2.25E-1	4.36E-1	1.46E+2	2.13E+3
Eu-155	3.25E+0	1.01E+0	2.87E-1	1.01E+0	7.67E-1	1.33E+0	5.31E-1	6.99E-1	1.22E+0	9.16E-1	1.01E+2	1.44E+3
Ru-106	4.94E+1	1.84E+1	1.82E+1	5.55E+1	3.09E+1	6.88E+1	4.45E+1	2.39E+1	7.02E+1	3.34E+1	1.11E+2	2.98E+2
Sb-125	5.15E+1	2.94E+1	3.04E+1	5.69E+1	1.29E+2	6.26E+1	6.53E+1	6.44E+1	7.66E+1	6.90E+1	7.21E+1	2.41E+2
Sr-90	3.29E+2	5.10E+1	3.26E+1	2.86E+1	4.41E+1	1.88E+1	1.69E+1	1.46E+1	1.62E+1	8.48E+1	1.76E+4	1.13E+5
Segment Volume (mm ³)	283.14	363.33	347.12	330.90	314.69	298.47	282.26	266.05	249.83	233.62	217.40	94.10
Average Segment Radius (mm)	11.83	11.38	10.88	10.37	9.86	9.35	8.84	8.34	7.83	7.32	6.81	6.44

Table B-44. Capsule 10 IR, axial center: decay-corrected concentrations (particle equivalents per mm³) of selected fission products for each radial segment sampled at the axial center of the Capsule 10 IR. The volume and average radius [(r_{inner} + r_{outer})/2] of each segment are also given. Shading indicates a value derived from an MDA.

IR-10 Center (Particle equivalents/mm ³)	IR10-C1	IR10-C2	IR10-C3	IR10-C4	IR10-C5	IR10-C6	IR10-C7	IR10-C8	IR10-C9	IR10-C10	IR10-C11	IR10-C12
Ag-110m	5.92E-3	7.42E-3	9.10E-3	1.39E-2	1.30E-2	1.42E-2	1.22E-2	5.28E-3	5.24E-3	4.49E-3	4.24E-3	7.66E-3
Ce-144	2.48E-5	2.39E-6	2.56E-6	2.23E-5	4.57E-6	1.41E-5	6.25E-6	6.40E-6	1.62E-5	9.67E-6	2.92E-5	8.57E-5
Cs-134	2.34E-4	1.78E-4	1.85E-4	2.24E-4	2.32E-4	2.88E-4	3.36E-4	3.15E-4	3.86E-4	4.02E-4	4.70E-4	8.23E-4
Cs-137	3.10E-4	1.92E-4	2.05E-4	2.44E-4	2.58E-4	3.12E-4	3.41E-4	3.54E-4	4.25E-4	4.45E-4	5.22E-4	9.43E-4
Eu-154	5.37E-5	8.91E-6	5.95E-6	5.50E-6	9.66E-6	4.40E-6	3.82E-6	3.41E-6	2.23E-6	4.33E-6	1.45E-3	2.11E-2
Eu-155	4.67E-5	1.46E-5	4.13E-6	1.46E-5	1.10E-5	1.92E-5	7.63E-6	1.00E-5	1.75E-5	1.32E-5	1.45E-3	2.07E-2
Ru-106	5.31E-6	1.97E-6	1.95E-6	5.97E-6	3.32E-6	7.39E-6	4.78E-6	2.56E-6	7.55E-6	3.59E-6	1.19E-5	3.20E-5
Sb-125	2.18E-4	1.25E-4	1.29E-4	2.41E-4	5.46E-4	2.65E-4	2.77E-4	2.73E-4	3.25E-4	2.93E-4	3.06E-4	1.02E-3
Sr-90	1.21E-4	1.88E-5	1.20E-5	1.05E-5	1.62E-5	6.90E-6	6.23E-6	5.38E-6	5.96E-6	3.12E-5	6.49E-3	4.15E-2
Segment Volume (mm ³)	283.14	363.33	347.12	330.90	314.69	298.47	282.26	266.05	249.83	233.62	217.40	94.10
Average Segment Radius (mm)	11.83	11.38	10.88	10.37	9.86	9.35	8.84	8.34	7.83	7.32	6.81	6.44

Table B-45. Estimated relative uncertainties in the concentrations reported for IR-10 center in Table B-43 and Table B-44. Absolute uncertainties in the segment volumes and average radii of the segments. N/A denotes a case where an isotope was not detected, and therefore, no uncertainty is available.

IR-10 Center	Units	IR10-C1	IR10-C2	IR10-C3	IR10-C4	IR10-C5	IR10-C6	IR10-C7	IR10-C8	IR10-C9	IR10-C10	IR10-C11	IR10-C12
Ag-110m Concentration	+	2.2%	2.0%	2.0%	2.1%	1.9%	2.1%	2.2%	2.4%	3.2%	3.4%	4.4%	5.2%
	–	2.3%	2.1%	2.1%	2.1%	2.0%	2.2%	2.3%	2.5%	3.3%	3.5%	4.4%	5.2%
Ce-144 Concentration	+	2.2%	27.8%	4.9%	2.5%	17.0%	9.3%	9.9%	4.3%	3.3%	4.2%	9.7%	10.7%
	–	2.3%	27.8%	4.9%	2.6%	17.0%	9.3%	9.9%	4.3%	3.4%	4.3%	9.8%	10.7%
Cs-134 Concentration	+	2.0%	2.0%	2.0%	2.1%	2.1%	2.1%	2.2%	2.3%	2.4%	2.5%	2.6%	2.8%
	–	2.1%	2.1%	2.1%	2.1%	2.2%	2.2%	2.3%	2.3%	2.4%	2.6%	2.7%	2.9%
Cs-137 Concentration	+	2.0%	2.0%	2.0%	2.1%	2.1%	2.1%	2.2%	2.3%	2.4%	2.5%	2.6%	2.8%
	–	2.1%	2.1%	2.1%	2.1%	2.2%	2.2%	2.3%	2.3%	2.4%	2.6%	2.7%	2.9%
Eu-154 Concentration	+	2.0%	3.2%	5.8%	14.1%	12.0%	9.3%	6.6%	9.8%	15.8%	15.0%	2.6%	2.8%
	–	2.1%	3.3%	5.9%	14.1%	12.0%	9.3%	6.6%	9.9%	15.8%	15.0%	2.7%	2.9%
Eu-155 Concentration	+	8.8%	7.8%	N/A	N/A	N/A	N/A	N/A	N/A	N/A	N/A	2.8%	2.8%
	–	8.8%	7.8%	N/A	N/A	N/A	N/A	N/A	N/A	N/A	N/A	2.9%	2.9%
Ru-106 Concentration	+	N/A	N/A	N/A	N/A	N/A	N/A	2.2%	N/A	N/A	N/A	N/A	N/A
	–	N/A	N/A	N/A	N/A	N/A	N/A	2.3%	N/A	N/A	N/A	N/A	N/A
Sb-125 Concentration	+	2.0%	2.0%	2.0%	2.1%	2.1%	2.1%	1.9%	2.3%	2.4%	2.5%	2.6%	2.8%
	–	2.1%	2.1%	2.1%	2.1%	2.2%	2.2%	2.0%	2.3%	2.4%	2.6%	2.7%	2.9%
Sr-90 Concentration	+	2.0%	2.0%	2.0%	2.1%	2.1%	2.1%	3.1%	3.2%	3.2%	2.5%	2.6%	2.8%
	–	2.1%	2.1%	2.1%	2.1%	2.2%	2.2%	3.2%	3.2%	3.3%	2.6%	2.7%	2.9%
Segment Volume (mm ³)	+ mm ³	0.61	1.00	1.25	1.53	1.82	2.13	2.44	2.76	3.09	3.41	3.74	1.85
	– mm ³	1.85	2.45	2.48	2.55	2.66	2.82	3.00	3.21	3.45	3.70	3.97	1.94
Average Radius of Segment (mm)	+/- mm	0.018	0.022	0.027	0.034	0.040	0.047	0.054	0.061	0.068	0.075	0.082	0.090

Table B-46. Capsule 10 IR, axial bottom: decay-corrected concentrations (Bq per mm³) of selected fission products for each radial segment sampled at the axial bottom of the Capsule 10 IR. The volume and average radius $[(r_{\text{inner}} + r_{\text{outer}})/2]$ of each segment are also given. Shading indicates a value derived from an MDA.

IR-10 Bottom (Bq/mm ³)	IR10-B1	IR10-B2	IR10-B3	IR10-B4	IR10-B5	IR10-B6	IR10-B7	IR10-B8	IR10-B9	IR10-B10	IR10-B11	IR10-B12
Ag-110m	8.67E+2	4.33E+3	2.99E+3	3.24E+3	3.35E+3	2.96E+3	2.67E+3	1.39E+3	4.23E+2	2.72E+2	1.49E+2	1.96E+2
Ce-144	1.98E+3	9.48E+2	2.27E+2	4.79E+2	1.33E+2	1.63E+2	1.73E+2	1.05E+2	3.16E+2	1.26E+2	5.58E+3	1.36E+3
Cs-134	2.54E+2	9.65E+2	5.45E+2	6.38E+2	7.89E+2	7.50E+2	8.26E+2	8.50E+2	8.74E+2	1.04E+3	1.00E+3	1.02E+3
Cs-137	3.30E+2	1.05E+3	6.17E+2	6.67E+2	8.80E+2	8.15E+2	9.17E+2	9.38E+2	9.69E+2	1.15E+3	1.10E+3	1.26E+3
Eu-154	7.78E-1	4.43E-1	1.28E-1	7.39E-2	3.18E-1	2.36E-1	1.14E-1	9.99E-1	7.82E-1	2.50E+0	3.13E+2	1.18E+3
Eu-155	7.46E-1	8.61E-1	7.57E-1	4.62E-1	8.54E-1	4.59E-1	8.13E-1	1.36E+0	1.20E+0	1.55E+0	2.19E+2	8.06E+2
Ru-106	1.95E+1	1.20E+1	2.96E+1	1.56E+1	5.57E+1	2.67E+1	2.77E+1	6.41E+1	4.12E+1	8.44E+1	1.21E+2	2.01E+2
Sb-125	2.52E+1	6.38E+1	4.40E+1	5.09E+1	8.69E+1	7.78E+1	7.88E+1	8.75E+1	8.75E+2	9.49E+1	9.08E+1	2.52E+2
Sr-90	7.40E+1	5.21E+1	4.72E+0	1.84E+0	2.64E+1	1.15E+1	1.70E+1	3.74E+1	9.30E+1	5.45E+2	3.05E+4	6.23E+4
Segment Volume (mm ³)	282.83	362.91	346.70	330.48	314.27	298.06	281.84	265.63	249.41	233.20	216.98	101.28
Average Segment Radius (mm)	11.81	11.37	10.86	10.35	9.85	9.34	8.83	8.32	7.81	7.31	6.80	6.42

Table B-47. Capsule 10 IR, axial bottom: decay-corrected concentrations (particle equivalents per mm³) of selected fission products for each radial segment sampled at the axial bottom of the Capsule 10 IR. The volume and average radius $[(r_{\text{inner}} + r_{\text{outer}})/2]$ of each segment are also given. Shading indicates a value derived from an MDA.

IR-10 Bottom (Particle equivalents/mm ³)	IR10-B1	IR10-B2	IR10-B3	IR10-B4	IR10-B5	IR10-B6	IR10-B7	IR10-B8	IR10-B9	IR10-B10	IR10-B11	IR10-B12
Ag-110m	2.92E-2	1.46E-1	1.01E-1	1.09E-1	1.13E-1	9.97E-2	8.99E-2	4.68E-2	1.43E-2	9.16E-3	5.01E-3	6.61E-3
Ce-144	4.18E-5	2.00E-5	4.78E-6	1.01E-5	2.80E-6	3.44E-6	3.65E-6	2.22E-6	6.67E-6	2.65E-6	1.18E-4	2.87E-5
Cs-134	8.29E-5	3.16E-4	1.78E-4	2.09E-4	2.58E-4	2.45E-4	2.70E-4	2.78E-4	2.86E-4	3.41E-4	3.27E-4	3.32E-4
Cs-137	1.07E-4	3.39E-4	2.00E-4	2.16E-4	2.85E-4	2.64E-4	2.97E-4	3.04E-4	3.14E-4	3.72E-4	3.57E-4	4.09E-4
Eu-154	7.72E-6	4.40E-6	1.27E-6	7.33E-7	3.15E-6	2.34E-6	1.13E-6	9.91E-6	7.76E-6	2.48E-5	3.11E-3	1.17E-2
Eu-155	1.07E-5	1.24E-5	1.09E-5	6.65E-6	1.23E-5	6.59E-6	1.17E-5	1.96E-5	1.73E-5	2.23E-5	3.15E-3	1.16E-2
Ru-106	2.09E-6	1.29E-6	3.18E-6	1.67E-6	5.99E-6	2.86E-6	2.98E-6	6.89E-6	4.43E-6	9.07E-6	1.30E-5	2.16E-5
Sb-125	1.07E-4	2.70E-4	1.86E-4	2.16E-4	3.68E-4	3.30E-4	3.34E-4	3.71E-4	3.71E-3	4.02E-4	3.85E-4	1.07E-3
Sr-90	2.72E-5	1.92E-5	1.74E-6	6.78E-7	9.72E-6	4.22E-6	6.27E-6	1.38E-5	3.42E-5	2.01E-4	1.12E-2	2.29E-2
Segment Volume (mm ³)	282.83	362.91	346.70	330.48	314.27	298.06	281.84	265.63	249.41	233.20	216.98	101.28
Average Segment Radius (mm)	11.81	11.37	10.86	10.35	9.85	9.34	8.83	8.32	7.81	7.31	6.80	6.42

Table B-48. Estimated relative uncertainties in the concentrations reported for IR-10 bottom in Table B-46 and Table B-47. Absolute uncertainties in the segment volumes and average radii of the segments. N/A denotes a case where an isotope was not detected, and therefore, no uncertainty is available.

IR-10 Bottom	Units	IR10-B1	IR10-B2	IR10-B3	IR10-B4	IR10-B5	IR10-B6	IR10-B7	IR10-B8	IR10-B9	IR10-B10	IR10-B11	IR10-B12
Ag-110m Concentration	+	2.0%	2.0%	2.0%	2.0%	2.1%	2.1%	2.2%	2.2%	2.3%	2.2%	3.8%	5.4%
	–	2.1%	2.1%	2.1%	2.1%	2.2%	2.2%	2.3%	2.3%	2.4%	2.3%	3.8%	5.4%
Ce-144 Concentration	+	2.2%	2.3%	5.7%	7.4%	10.8%	9.2%	28.3%	15.4%	25.1%	18.3%	3.7%	16.6%
	–	2.3%	2.4%	5.7%	7.4%	10.9%	9.2%	28.3%	15.4%	25.1%	18.3%	3.8%	16.6%
Cs-134 Concentration	+	2.0%	2.0%	2.0%	2.0%	2.1%	2.1%	2.2%	2.2%	2.3%	2.5%	2.6%	2.8%
	–	2.1%	2.1%	2.1%	2.1%	2.2%	2.2%	2.3%	2.3%	2.4%	2.5%	2.7%	2.9%
Cs-137 Concentration	+	2.0%	2.0%	2.0%	2.0%	2.1%	2.1%	2.2%	2.2%	2.3%	2.5%	2.6%	2.8%
	–	2.1%	2.1%	2.1%	2.1%	2.2%	2.2%	2.3%	2.3%	2.4%	2.5%	2.7%	2.9%
Eu-154 Concentration	+	2.0%	8.8%	N/A	N/A	8.4%	9.1%	N/A	23.5%	9.6%	4.4%	2.6%	2.8%
	–	2.1%	8.8%	N/A	N/A	8.4%	9.1%	N/A	23.5%	9.6%	4.5%	2.7%	2.9%
Eu-155 Concentration	+	4.9%	N/A	N/A	N/A	36.1%	N/A	N/A	N/A	N/A	18.8%	2.8%	2.8%
	–	4.9%	N/A	N/A	N/A	36.2%	N/A	N/A	N/A	N/A	18.8%	2.9%	2.9%
Ru-106 Concentration	+	11.5%	35.4%	N/A	N/A	N/A	N/A	N/A	N/A	N/A	N/A	N/A	N/A
	–	11.5%	35.4%	N/A	N/A	N/A	N/A	N/A	N/A	N/A	N/A	N/A	N/A
Sb-125 Concentration	+	1.5%	2.0%	2.0%	2.0%	2.1%	2.1%	2.2%	2.2%	2.3%	2.5%	2.6%	2.8%
	–	1.7%	2.1%	2.1%	2.1%	2.2%	2.2%	2.3%	2.3%	2.4%	2.5%	2.7%	2.9%
Sr-90 Concentration	+	2.0%	2.0%	2.0%	2.0%	2.1%	2.1%	2.2%	2.2%	2.3%	2.5%	2.6%	2.8%
	–	2.1%	2.1%	2.1%	2.1%	2.2%	2.2%	2.3%	2.3%	2.4%	2.5%	2.7%	2.9%
Segment Volume (mm ³)	+ mm ³	0.43	0.82	1.11	1.41	1.73	2.05	2.37	2.70	3.03	3.36	3.69	1.98
	– mm ³	1.79	2.38	2.40	2.48	2.59	2.75	2.94	3.16	3.40	3.65	3.92	2.08
Average Radius of Segment (mm)	+/- mm	0.012	0.018	0.024	0.031	0.038	0.045	0.052	0.060	0.067	0.074	0.081	0.089

Table B-49. Capsule 10 OR, axial center: decay-corrected concentrations (Bq per mm³) of selected fission products for each radial segment sampled at the axial center of the Capsule 10 OR. The volume and average radius $[(r_{\text{inner}} + r_{\text{outer}})/2]$ of each segment are also given. Shading indicates a value derived from an MDA.

OR-10 Center (Bq/mm ³)	OR10-C1	OR10-C2	OR10-C3	OR10-C4	OR10-C5	OR10-C6	OR10-C7	OR10-C8	OR10-C9	OR10- C10	OR10- C11	OR10- C12	OR10- C13
Ag-110m	2.80E+2	7.43E+2	1.21E+3	1.54E+3	2.25E+3	2.14E+3	2.29E+3	1.93E+3	1.13E+3	6.57E+2	5.48E+2	5.23E+2	4.62E+2
Ce-144	4.87E+3	3.47E+2	2.74E+2	2.23E+2	8.85E+1	1.18E+2	3.77E+2	1.83E+2	1.87E+2	6.37E+2	9.85E+1	1.31E+2	4.50E+2
Cs-134	3.04E+2	2.65E+2	3.04E+2	3.31E+2	4.86E+2	4.74E+2	6.12E+2	7.09E+2	7.02E+2	7.26E+2	8.04E+2	7.62E+2	1.07E+3
Cs-137	5.36E+2	2.80E+2	3.26E+2	3.55E+2	5.47E+2	5.09E+2	6.82E+2	7.80E+2	7.66E+2	7.93E+2	8.80E+2	8.35E+2	1.22E+3
Eu-154	4.31E+0	8.42E-1	4.69E-1	5.44E-1	5.17E-1	3.78E-1	4.31E-1	4.22E-1	3.57E-1	1.82E-1	2.15E-1	1.92E-1	3.12E-1
Eu-155	2.42E+0	4.23E-1	1.16E+0	2.12E-1	1.16E+0	3.08E-1	9.61E-1	5.75E-1	5.50E-1	7.18E-1	7.73E-1	4.24E-1	1.14E+0
Ru-106	1.83E+2	5.16E+1	5.96E+1	1.15E+1	6.79E+1	1.63E+1	5.16E+1	3.09E+1	2.77E+1	3.56E+1	3.89E+1	3.59E+1	5.85E+1
Sb-125	1.00E+1	4.75E+0	7.73E+0	9.52E+0	1.54E+1	1.77E+1	2.47E+1	3.05E+1	2.95E+1	3.38E+1	4.10E+1	3.53E+1	1.15E+2
Sr-90	3.82E+2	5.42E+1	3.55E+1	3.19E+1	2.57E+1	2.12E+1	3.10E+1	1.80E+1	1.71E+1	1.58E+1	8.68E+0	6.68E+0	1.19E+1
Segment Volume (mm ³)	444.06	577.89	561.67	545.46	529.24	513.03	496.81	480.60	464.38	448.17	431.95	415.74	278.55
Average Segment Radius (mm)	18.55	18.11	17.60	17.09	16.58	16.07	15.57	15.06	14.55	14.04	13.53	13.03	12.60

Table B-50. Capsule 10 OR, axial center: decay-corrected concentrations (particle equivalents per mm³) of selected fission products for each radial segment sampled at the axial center of the Capsule 10 OR. The volume and average radius $[(r_{\text{inner}} + r_{\text{outer}})/2]$ of each segment are also given. Shading indicates a value derived from an MDA.

OR-10 Center (Particle equivalents/mm ³)	OR10-C1	OR10-C2	OR10-C3	OR10-C4	OR10-C5	OR10-C6	OR10-C7	OR10-C8	OR10-C9	OR10- C10	OR10- C11	OR10- C12	OR10- C13
Ag-110m	4.56E-3	1.21E-2	1.97E-2	2.52E-2	3.66E-2	3.49E-2	3.72E-2	3.15E-2	1.85E-2	1.07E-2	8.93E-3	8.84E-3	7.82E-3
Ce-144	8.37E-5	5.97E-6	4.72E-6	3.84E-6	1.52E-6	2.02E-6	6.48E-6	3.15E-6	3.21E-6	1.10E-5	1.69E-6	2.34E-6	8.03E-6
Cs-134	5.80E-5	5.05E-5	5.80E-5	6.32E-5	9.28E-5	9.06E-5	1.17E-4	1.35E-4	1.34E-4	1.39E-4	1.54E-4	1.51E-4	2.12E-4
Cs-137	1.37E-4	7.15E-5	8.32E-5	9.05E-5	1.39E-4	1.30E-4	1.74E-4	1.99E-4	1.95E-4	2.02E-4	2.24E-4	2.21E-4	3.24E-4
Eu-154	2.67E-5	5.23E-6	2.91E-6	3.38E-6	3.21E-6	2.35E-6	2.68E-6	2.62E-6	2.22E-6	1.13E-6	1.34E-6	1.24E-6	2.01E-6
Eu-155	2.28E-5	3.99E-6	1.10E-5	2.00E-6	1.10E-5	2.90E-6	9.07E-6	5.43E-6	5.19E-6	6.77E-6	7.29E-6	4.15E-6	1.12E-5
Ru-106	1.31E-5	3.70E-6	4.28E-6	8.23E-7	4.87E-6	1.17E-6	3.70E-6	2.22E-6	1.98E-6	2.55E-6	2.79E-6	2.67E-6	4.35E-6
Sb-125	3.20E-5	1.52E-5	2.47E-5	3.04E-5	4.92E-5	5.65E-5	7.89E-5	9.74E-5	9.43E-5	1.08E-4	1.31E-4	1.17E-4	3.80E-4
Sr-90	1.14E-4	1.62E-5	1.06E-5	9.53E-6	7.68E-6	6.34E-6	9.27E-6	5.39E-6	5.10E-6	4.73E-6	2.59E-6	2.07E-6	3.70E-6
Segment Volume (mm ³)	444.06	577.89	561.67	545.46	529.24	513.03	496.81	480.60	464.38	448.17	431.95	415.74	278.55
Average Segment Radius (mm)	18.55	18.11	17.60	17.09	16.58	16.07	15.57	15.06	14.55	14.04	13.53	13.03	12.60

Table B-51. Estimated relative uncertainties in the concentrations reported for OR-10 center in Table B-49 and Table B-50. Absolute uncertainties in the segment volumes and average radii of the segments. N/A denotes a case where an isotope was not detected, and therefore, no uncertainty is available.

OR-10 Center	Units	OR10-C1	OR10-C2	OR10-C3	OR10-C4	OR10-C5	OR10-C6	OR10-C7	OR10-C8	OR10-C9	OR10-C10	OR10-C11	OR10-C12	OR10-C13
Ag-110m Concentration	+	2.0%	2.0%	2.0%	2.0%	2.0%	2.0%	2.1%	2.1%	2.1%	2.1%	2.2%	2.2%	2.3%
	–	2.1%	2.1%	2.1%	2.1%	2.1%	2.1%	2.2%	2.2%	2.2%	2.2%	2.3%	2.3%	2.4%
Ce-144 Concentration	+	2.0%	2.0%	10.0%	2.9%	53.7%	23.9%	13.6%	17.2%	16.6%	3.3%	17.9%	15.9%	5.9%
	–	2.1%	2.1%	10.0%	2.9%	53.7%	23.9%	13.6%	17.2%	16.6%	3.3%	17.9%	15.9%	5.9%
Cs-134 Concentration	+	2.0%	2.0%	2.0%	2.0%	2.0%	2.0%	2.1%	2.1%	2.1%	2.1%	2.2%	2.2%	2.3%
	–	2.1%	2.1%	2.1%	2.1%	2.1%	2.1%	2.2%	2.2%	2.2%	2.2%	2.3%	2.3%	2.4%
Cs-137 Concentration	+	2.0%	2.0%	2.0%	2.0%	2.0%	2.0%	2.1%	2.1%	2.1%	2.1%	2.2%	2.2%	2.3%
	–	2.1%	2.1%	2.1%	2.1%	2.1%	2.1%	2.2%	2.2%	2.2%	2.2%	2.3%	2.3%	2.4%
Eu-154 Concentration	+	2.0%	2.0%	7.5%	5.9%	14.1%	7.7%	6.4%	13.2%	17.8%	16.1%	16.1%	N/A	N/A
	–	2.1%	2.1%	7.5%	5.9%	14.1%	7.8%	6.4%	13.2%	17.8%	16.1%	16.1%	N/A	N/A
Eu-155 Concentration	+	4.2%	2.0%	N/A	N/A	15.9%	N/A	N/A	N/A	N/A	N/A	N/A	N/A	N/A
	–	4.2%	2.1%	N/A	N/A	15.9%	N/A	N/A	N/A	N/A	N/A	N/A	N/A	N/A
Ru-106 Concentration	+	2.0%	N/A	N/A	N/A	N/A	N/A	N/A	N/A	N/A	N/A	N/A	N/A	N/A
	–	2.1%	N/A	N/A	N/A	N/A	N/A	N/A	N/A	N/A	N/A	N/A	N/A	N/A
Sb-125 Concentration	+	2.3%	2.0%	4.2%	2.1%	2.7%	0.8%	2.1%	2.1%	2.1%	2.1%	2.2%	2.2%	2.3%
	–	2.4%	2.1%	4.2%	2.2%	2.8%	1.0%	2.2%	2.2%	2.2%	2.2%	2.3%	2.3%	2.4%
Sr-90 Concentration	+	2.0%	2.0%	3.0%	3.0%	3.0%	3.0%	3.0%	3.1%	3.1%	3.1%	4.1%	4.1%	3.2%
	–	2.1%	2.1%	3.1%	3.1%	3.1%	3.1%	3.1%	3.1%	3.1%	3.2%	4.1%	4.2%	3.3%
Segment Volume (mm ³)	+ mm ³	0.82	1.23	1.44	1.69	1.96	2.25	2.54	2.85	3.16	3.48	3.79	4.11	3.07
	– mm ³	2.86	3.77	3.75	3.76	3.81	3.88	3.98	4.11	4.27	4.44	4.64	4.85	3.52
Average Radius of Segment (mm)	+/- mm	0.024	0.027	0.032	0.037	0.043	0.050	0.056	0.063	0.070	0.077	0.084	0.091	0.098

Table B-52. Capsule 10 OR, axial bottom: decay-corrected concentrations (Bq per mm³) of selected fission products for each radial segment sampled at the axial bottom of the Capsule 10 OR. The volume and average radius $[(r_{\text{inner}} + r_{\text{outer}})/2]$ of each segment are also given. Shaded cells indicate a value derived from an MDA. Shaded column headings denote segments with greater (but unknown) uncertainty due to ring movement during sampling.

OR-10 Bottom (Bq/mm ³)	OR10-B1	OR10-B2	OR10-B3	OR10-B4	OR10-B5	OR10-B6	OR10-B7	OR10-B8	OR10-B9	OR10- B10	OR10- B11	OR10- B12	OR10- B13
Ag-110m	9.07E+4	5.74E+4	6.61E+4	6.28E+4	9.98E+4	1.17E+5	2.37E+5	4.13E+5	4.54E+5	6.53E+5	6.07E+3	7.20E+3	1.46E+4
Ce-144	5.57E+4	2.52E+4	1.45E+4	7.24E+3	1.15E+4	2.11E+4	1.79E+4	3.28E+4	1.49E+4	1.54E+4	4.61E+2	9.32E+2	1.48E+3
Cs-134	2.70E+3	2.17E+3	2.75E+3	2.72E+3	3.30E+3	3.02E+3	3.95E+3	4.59E+3	3.91E+3	4.18E+3	8.66E+2	8.90E+2	2.66E+3
Cs-137	6.41E+2	4.64E+2	5.97E+2	5.89E+2	7.16E+2	6.53E+2	8.73E+2	1.02E+3	8.55E+2	9.38E+2	9.10E+2	9.57E+2	2.90E+3
Eu-154	9.29E-1	2.52E-1	2.85E-1	1.16E-1	2.74E-1	3.13E-1	4.99E-1	1.78E-1	2.29E-1	1.63E-1	2.63E-1	3.51E-1	4.41E-1
Eu-155	1.19E+0	4.92E-1	6.72E-1	1.12E+0	1.24E+0	6.32E-1	6.63E-1	8.41E-1	1.86E+0	8.71E-1	8.37E-1	1.31E+0	2.63E+0
Ru-106	8.65E+2	3.39E+2	4.93E+2	5.19E+2	9.04E+2	4.56E+2	4.80E+2	5.86E+2	8.73E+2	6.45E+2	4.14E+1	6.57E+1	1.20E+2
Sb-125	2.45E+1	1.07E+1	2.02E+1	2.44E+1	4.22E+1	5.10E+1	6.94E+1	1.01E+2	1.13E+2	1.40E+2	5.33E+1	6.23E+1	4.62E+2
Sr-90	7.32E+1	1.41E+1	9.90E+0	1.16E+1	1.58E+1	1.21E+1	2.31E+1	1.11E+1	6.90E+0	6.30E+0	7.06E+0	4.87E+0	3.03E+1
Segment Volume (mm ³)	443.49	577.13	560.91	544.70	528.48	512.27	496.05	479.84	463.63	447.41	431.20	414.98	248.36
Average Segment Radius (mm)	18.53	18.08	17.57	17.07	16.56	16.05	15.54	15.03	14.53	14.02	13.51	13.00	12.59

Table B-53. Capsule 10 OR, axial bottom: decay-corrected concentrations (particle equivalents per mm³) of selected fission products for each radial segment sampled at the axial bottom of the Capsule 10 OR. The volume and average radius [(r_{inner} + r_{outer})/2] of each segment are also given. Shading indicates a value derived from an MDA. Shaded column headings denote segments with greater (but unknown) uncertainty due to ring movement during sampling.

OR-10 Bottom (Particle equivalents/mm ³)	OR10-B1	OR10-B2	OR10-B3	OR10-B4	OR10-B5	OR10-B6	OR10-B7	OR10-B8	OR10-B9	OR10- B10	OR10- B11	OR10- B12	OR10- B13
Ag-110m	1.48E+0	9.36E-1	1.08E+0	1.02E+0	1.63E+0	1.90E+0	3.86E+0	6.73E+0	7.40E+0	1.06E+1	9.89E-2	1.17E-1	2.38E-1
Ce-144	9.58E-4	4.33E-4	2.49E-4	1.24E-4	1.98E-4	3.62E-4	3.07E-4	5.64E-4	2.57E-4	2.65E-4	7.93E-6	1.60E-5	2.54E-5
Cs-134	5.15E-4	4.14E-4	5.25E-4	5.19E-4	6.30E-4	5.78E-4	7.54E-4	8.77E-4	7.46E-4	7.99E-4	1.65E-4	1.70E-4	5.08E-4
Cs-137	1.63E-4	1.18E-4	1.52E-4	1.50E-4	1.83E-4	1.66E-4	2.23E-4	2.61E-4	2.18E-4	2.39E-4	2.32E-4	2.44E-4	7.38E-4
Eu-154	5.77E-6	1.56E-6	1.77E-6	7.22E-7	1.70E-6	1.94E-6	3.10E-6	1.11E-6	1.42E-6	1.01E-6	1.64E-6	2.18E-6	2.74E-6
Eu-155	1.12E-5	4.64E-6	6.35E-6	1.06E-5	1.17E-5	5.96E-6	6.26E-6	7.94E-6	1.76E-5	8.22E-6	7.90E-6	1.23E-5	2.48E-5
Ru-106	6.20E-5	2.43E-5	3.54E-5	3.72E-5	6.48E-5	3.27E-5	3.44E-5	4.20E-5	6.26E-5	4.63E-5	2.97E-6	4.71E-6	8.62E-6
Sb-125	7.85E-5	3.41E-5	6.45E-5	7.80E-5	1.35E-4	1.63E-4	2.22E-4	3.21E-4	3.61E-4	4.48E-4	1.70E-4	1.99E-4	1.48E-3
Sr-90	2.19E-5	4.20E-6	2.96E-6	3.45E-6	4.72E-6	3.62E-6	6.91E-6	3.31E-6	2.06E-6	1.88E-6	2.11E-6	1.45E-6	9.05E-6
Segment Volume (mm ³)	443.49	577.13	560.91	544.70	528.48	512.27	496.05	479.84	463.63	447.41	431.20	414.98	248.36
Average Segment Radius (mm)	18.53	18.08	17.57	17.07	16.56	16.05	15.54	15.03	14.53	14.02	13.51	13.00	12.59

Table B-54. Estimated relative uncertainties in the concentrations reported for OR-10 Bottom in Table B-52 and Table B-53. Absolute uncertainties in the segment volumes and average radii of the segments. N/A denotes a case where an isotope was not detected, and therefore, no uncertainty is available. Shaded column headings denote segments with greater (but unknown) uncertainty due to ring movement during sampling.

OR-10 Bottom	Units	OR10-B1	OR10-B2	OR10-B3	OR10-B4	OR10-B5	OR10-B6	OR10-B7	OR10-B8	OR10-B9	OR10-B10	OR10-B11	OR10-B12	OR10-B13
Ag-110m Concentration	+	2.0%	2.0%	2.0%	2.1%	2.0%	2.1%	2.1%	2.1%	2.1%	2.2%	2.2%	2.2%	2.3%
	–	2.1%	2.1%	2.1%	2.2%	2.1%	2.1%	2.2%	2.2%	2.2%	2.2%	2.3%	2.3%	2.4%
Ce-144 Concentration	+	12.2%	6.8%	3.0%	44.2%	22.1%	7.7%	3.9%	5.2%	5.5%	20.9%	3.4%	3.1%	3.2%
	–	12.2%	6.8%	3.1%	44.2%	22.1%	7.8%	3.9%	5.2%	5.5%	20.9%	3.4%	3.2%	3.3%
Cs-134 Concentration	+	2.0%	2.0%	2.0%	2.0%	2.0%	2.1%	2.1%	2.1%	2.1%	2.2%	2.2%	2.2%	2.3%
	–	2.1%	2.1%	2.1%	2.1%	2.1%	2.1%	2.2%	2.2%	2.2%	2.2%	2.3%	2.3%	2.4%
Cs-137 Concentration	+	2.0%	2.0%	2.0%	2.0%	2.0%	2.1%	2.1%	2.1%	2.1%	2.2%	2.2%	2.2%	2.3%
	–	2.1%	2.1%	2.1%	2.1%	2.1%	2.1%	2.2%	2.2%	2.2%	2.2%	2.3%	2.3%	2.4%
Eu-154 Concentration	+	17.2%	11.1%	2.6%	16.0%	3.5%	6.7%	4.5%	31.8%	16.9%	N/A	N/A	N/A	14.1%
	–	17.2%	11.1%	2.7%	16.1%	3.6%	6.7%	4.6%	31.8%	17.0%	N/A	N/A	N/A	14.1%
Eu-155 Concentration	+	N/A	N/A	N/A	0.3%	N/A	N/A	N/A	11.8%	28.0%	N/A	N/A	N/A	N/A
	–	N/A	N/A	N/A	0.7%	N/A	N/A	N/A	11.8%	28.0%	N/A	N/A	N/A	N/A
Ru-106 Concentration	+	N/A	N/A	N/A	N/A	N/A	N/A	N/A	N/A	N/A	N/A	N/A	N/A	N/A
	–	N/A	N/A	N/A	N/A	N/A	N/A	N/A	N/A	N/A	N/A	N/A	N/A	N/A
Sb-125 Concentration	+	3.5%	2.3%	1.8%	2.7%	1.7%	2.1%	2.1%	2.1%	2.1%	2.2%	2.2%	2.2%	2.3%
	–	3.5%	2.4%	1.9%	2.7%	1.8%	2.1%	2.2%	2.2%	2.2%	2.2%	2.3%	2.3%	2.4%
Sr-90 Concentration	+	4.0%	3.0%	3.0%	3.0%	3.0%	3.0%	3.0%	3.1%	4.1%	4.1%	4.1%	5.1%	3.2%
	–	4.1%	3.1%	3.1%	3.1%	3.1%	3.1%	3.1%	3.1%	4.1%	4.1%	4.1%	5.1%	3.3%
Segment Volume (mm ³)	+ mm ³	1.05	1.51	1.68	1.90	2.14	2.41	2.69	2.98	3.28	3.58	3.89	4.20	2.79
	– mm ³	2.92	3.86	3.84	3.85	3.89	3.97	4.07	4.19	4.35	4.52	4.71	4.92	3.18
Average Radius of Segment (mm)	+/- mm	0.031	0.033	0.037	0.042	0.047	0.053	0.059	0.066	0.072	0.079	0.086	0.093	0.100

Table B-55. Capsule 12 IR, axial center: decay-corrected concentrations (Bq per mm³) of selected fission products for each radial segment sampled at the axial center of the Capsule 12 IR. The volume and average radius $[(r_{\text{inner}} + r_{\text{outer}})/2]$ of each segment are also given. Shading indicates a value derived from an MDA.

IR-12 Center (Bq/mm ³)	IR12-C1	IR12-C2	IR12-C3	IR12-C4	IR12-C5	IR12-C6	IR12-C7	IR12-C8	IR12-C9	IR12-C10	IR12-C11	IR12-C12
Ag-110m	4.24E+0	4.50E+0	2.68E+0	4.43E+0	4.24E+0	4.13E+0	5.20E+0	5.67E+0	8.96E+0	7.07E+0	1.65E+1	2.43E+1
Ce-144	2.41E+2	2.08E+2	4.63E+2	1.10E+3	5.20E+2	1.71E+2	1.34E+2	1.63E+2	1.63E+2	1.19E+3	1.14E+3	1.16E+3
Cs-134	5.88E+0	4.70E+0	2.71E+0	1.01E+1	6.75E+0	1.07E+1	1.84E+1	4.03E+1	7.39E+1	1.59E+2	3.18E+2	1.14E+3
Cs-137	7.32E+1	1.60E+1	1.42E+1	4.76E+1	2.68E+1	4.57E+1	9.57E+1	1.21E+2	2.01E+2	3.88E+2	7.98E+2	3.19E+3
Eu-154	1.54E+1	2.63E+1	6.55E+0	1.69E+1	1.78E+1	1.77E+1	1.71E+1	1.87E+1	1.84E+1	1.87E+1	1.86E+1	3.38E+1
Eu-155	8.27E+0	1.52E+1	3.58E+0	9.77E+0	9.96E+0	9.69E+0	9.50E+0	1.03E+1	1.00E+1	1.00E+1	9.18E+0	2.01E+1
Ru-106	3.82E+0	3.67E+0	1.72E+1	5.38E+1	8.19E+0	5.79E+0	4.44E+0	7.76E+0	1.63E+1	1.40E+1	5.27E+1	5.18E+1
Sb-125	2.55E-1	3.92E-1	6.20E-1	9.10E-1	3.60E-1	3.22E-1	3.69E-1	2.85E-1	6.13E-1	6.07E-1	1.98E+0	4.18E+0
Sr-90	3.03E+1	6.27E+0	5.60E+0	1.95E+1	6.01E+0	7.24E+0	5.33E+0	1.31E+1	2.79E+1	5.67E+0	3.63E+0	7.61E+1
Segment Volume (mm ³)	397.05	361.52	345.31	329.09	312.88	296.66	280.45	264.23	248.02	231.80	215.59	107.13
Average Segment Radius (mm)	11.85	11.33	10.82	10.31	9.80	9.29	8.79	8.28	7.77	7.26	6.75	6.37

Table B-56. Capsule 12 IR, axial center: decay-corrected concentrations (particle equivalents per mm³) of selected fission products for each radial segment sampled at the axial center of the Capsule 12 IR. The volume and average radius $[(r_{\text{inner}} + r_{\text{outer}})/2]$ of each segment are also given. Shading indicates a value derived from an MDA.

IR-12 Center (Particle equivalents/mm ³)	IR12-C1	IR12-C2	IR12-C3	IR12-C4	IR12-C5	IR12-C6	IR12-C7	IR12-C8	IR12-C9	IR12-C10	IR12-C11	IR12-C12
Ag-110m	1.43E-3	1.52E-3	9.01E-4	1.49E-3	1.43E-3	1.39E-3	1.75E-3	1.91E-3	3.02E-3	2.38E-3	5.54E-3	8.18E-3
Ce-144	1.05E-5	9.09E-6	2.02E-5	4.81E-5	2.27E-5	7.49E-6	5.86E-6	7.12E-6	7.13E-6	5.21E-5	4.98E-5	5.09E-5
Cs-134	1.10E-5	8.78E-6	5.07E-6	1.89E-5	1.26E-5	2.00E-5	3.43E-5	7.54E-5	1.38E-4	2.97E-4	5.95E-4	2.12E-3
Cs-137	5.26E-5	1.15E-5	1.02E-5	3.42E-5	1.93E-5	3.29E-5	6.87E-5	8.66E-5	1.45E-4	2.78E-4	5.73E-4	2.29E-3
Eu-154	8.53E-4	1.46E-3	3.62E-4	9.36E-4	9.83E-4	9.80E-4	9.47E-4	1.03E-3	1.02E-3	1.04E-3	1.03E-3	1.87E-3
Eu-155	3.61E-4	6.65E-4	1.56E-4	4.27E-4	4.35E-4	4.23E-4	4.15E-4	4.52E-4	4.37E-4	4.37E-4	4.01E-4	8.76E-4
Ru-106	1.39E-6	1.34E-6	6.28E-6	1.96E-5	2.99E-6	2.11E-6	1.62E-6	2.83E-6	5.95E-6	5.09E-6	1.92E-5	1.89E-5
Sb-125	2.71E-6	4.17E-6	6.59E-6	9.67E-6	3.82E-6	3.42E-6	3.92E-6	3.03E-6	6.51E-6	6.45E-6	2.11E-5	4.45E-5
Sr-90	2.33E-5	4.82E-6	4.31E-6	1.50E-5	4.62E-6	5.56E-6	4.10E-6	1.01E-5	2.15E-5	4.36E-6	2.79E-6	5.85E-5
Segment Volume (mm ³)	397.05	361.52	345.31	329.09	312.88	296.66	280.45	264.23	248.02	231.80	215.59	107.13
Average Segment Radius (mm)	11.85	11.33	10.82	10.31	9.80	9.29	8.79	8.28	7.77	7.26	6.75	6.37

Table B-57. Estimated relative uncertainties in the concentrations reported for IR-12 Center in Table B-55 and Table B-56. Absolute uncertainties in the segment volumes and average radii of the segments. N/A denotes a case where an isotope was not detected, and therefore, no uncertainty is available.

IR-12 Center	Units	IR12-C1	IR12-C2	IR12-C3	IR12-C4	IR12-C5	IR12-C6	IR12-C7	IR12-C8	IR12-C9	IR12-C10	IR12-C11	IR12-C12
Ag-110m Concentration	+	N/A	N/A	N/A	N/A	N/A	N/A	N/A	N/A	N/A	N/A	N/A	N/A
	–	N/A	N/A	N/A	N/A	N/A	N/A	N/A	N/A	N/A	N/A	N/A	N/A
Ce-144 Concentration	+	3.4%	2.8%	2.0%	2.0%	2.1%	2.1%	3.5%	2.6%	11.0%	2.3%	3.0%	11.3%
	–	3.5%	2.8%	2.1%	2.1%	2.2%	2.2%	3.6%	2.7%	11.0%	2.4%	3.1%	11.3%
Cs-134 Concentration	+	2.0%	2.0%	2.0%	2.0%	2.1%	2.1%	2.2%	2.2%	2.3%	2.5%	2.6%	2.8%
	–	2.1%	2.1%	2.1%	2.1%	2.2%	2.2%	2.3%	2.3%	2.4%	2.5%	2.7%	2.9%
Cs-137 Concentration	+	2.0%	2.0%	2.0%	2.0%	2.1%	2.1%	2.2%	2.2%	2.3%	2.5%	2.6%	2.8%
	–	2.1%	2.1%	2.1%	2.1%	2.2%	2.2%	2.3%	2.3%	2.4%	2.5%	2.7%	2.9%
Eu-154 Concentration	+	2.0%	2.0%	2.0%	2.0%	2.1%	2.1%	2.2%	2.2%	2.3%	2.5%	2.6%	2.8%
	–	2.1%	2.1%	2.1%	2.1%	2.2%	2.2%	2.3%	2.3%	2.4%	2.5%	2.7%	2.9%
Eu-155 Concentration	+	1.6%	2.0%	2.0%	2.0%	2.1%	2.1%	2.2%	2.2%	2.3%	2.5%	4.5%	3.6%
	–	1.7%	2.1%	2.1%	2.1%	2.2%	2.2%	2.3%	2.3%	2.4%	2.5%	4.6%	3.7%
Ru-106 Concentration	+	14.1%	18.9%	2.9%	5.7%	6.6%	8.4%	24.6%	N/A	N/A	N/A	N/A	N/A
	–	14.1%	18.9%	2.9%	5.7%	6.6%	8.4%	24.6%	N/A	N/A	N/A	N/A	N/A
Sb-125 Concentration	+	20.1%	3.5%	2.1%	2.6%	3.9%	4.3%	6.5%	8.5%	N/A	N/A	N/A	N/A
	–	20.1%	3.6%	2.2%	2.7%	3.9%	4.3%	6.5%	8.5%	N/A	N/A	N/A	N/A
Sr-90 Concentration	+	25.0%	10.0%	11.0%	9.0%	11.0%	11.0%	9.0%	7.1%	3.2%	13.1%	8.2%	5.4%
	–	25.0%	10.0%	11.0%	9.0%	11.0%	11.0%	9.1%	7.1%	3.3%	13.1%	8.2%	5.4%
Segment Volume (mm ³)	+ mm ³	0.46	0.73	1.04	1.36	1.69	2.02	2.35	2.68	3.01	3.34	3.67	2.10
	– mm ³	2.49	2.34	2.37	2.44	2.56	2.72	2.91	3.13	3.37	3.63	3.91	2.21
Average Radius of Segment (mm)	+/- mm	0.010	0.016	0.023	0.030	0.037	0.044	0.052	0.059	0.066	0.074	0.081	0.088

Table B-58. Capsule 12 IR, axial bottom: decay-corrected concentrations (Bq per mm³) of selected fission products for each radial segment sampled at the axial bottom of the Capsule 12 IR. The volume and average radius [(r_{inner} + r_{outer})/2] of each segment are also given. Shading indicates a value derived from an MDA.

IR-12 Bottom (Bq/mm ³)	IR12-B1	IR12-B2	IR12-B3	IR12-B4	IR12-B5	IR12-B6	IR12-B7	IR12-B8	IR12-B9	IR12-B10	IR12-B11	IR12-B12
Ag-110m	2.69E+0	8.56E+0	3.07E+0	3.77E+0	3.36E+0	4.38E+0	3.97E+0	3.91E+0	4.33E+0	6.99E+0	1.12E+1	2.88E+1
Ce-144	1.71E+4	1.59E+2	1.54E+2	1.29E+3	1.31E+2	1.54E+2	2.60E+2	2.24E+2	2.06E+2	1.27E+3	2.11E+2	2.86E+3
Cs-134	1.66E+1	7.38E+0	6.38E+0	7.42E+0	9.08E+0	1.35E+1	2.87E+1	5.44E+1	1.18E+2	2.19E+2	4.24E+2	1.51E+3
Cs-137	1.24E+2	1.70E+1	1.53E+1	2.83E+1	2.05E+1	3.20E+1	6.06E+1	1.10E+2	2.40E+2	4.74E+2	9.20E+2	3.51E+3
Eu-154	1.66E+1	1.98E+1	1.89E+1	1.83E+1	1.95E+1	1.78E+1	1.95E+1	1.92E+1	2.03E+1	2.01E+1	2.09E+1	3.62E+1
Eu-155	9.61E+0	1.03E+1	1.06E+1	1.01E+1	1.11E+1	9.96E+0	1.11E+1	1.10E+1	1.22E+1	1.16E+1	1.23E+1	1.99E+1
Ru-106	1.81E+1	2.80E+0	2.22E+0	5.70E+0	2.83E+0	5.29E+0	5.26E+0	3.11E+0	6.73E+0	1.80E+1	3.39E+1	6.41E+1
Sb-125	4.61E-1	3.48E-1	3.51E-1	3.28E-1	4.04E-1	3.68E-1	4.04E-1	3.64E-1	4.86E-1	1.61E-1	1.73E+0	4.81E+0
Sr-90	4.66E+1	3.68E+0	4.66E+0	9.90E+0	3.19E+0	4.78E+0	2.42E+0	2.51E+0	3.62E+0	6.68E+0	4.81E+0	6.55E+1
Segment Volume (mm ³)	433.84	359.82	343.61	327.39	311.18	294.96	278.75	262.53	246.32	230.10	213.89	86.70
Average Segment Radius (mm)	11.82	11.27	10.77	10.26	9.75	9.24	8.73	8.23	7.72	7.21	6.70	6.34

Table B-59. Capsule 12 IR, axial bottom: decay-corrected concentrations (particle equivalents per mm³) of selected fission products for each radial segment sampled at the axial bottom of the Capsule 12 IR. The volume and average radius $[(r_{\text{inner}} + r_{\text{outer}})/2]$ of each segment are also given. Shading indicates a value derived from an MDA.

IR-12 Bottom (Particle equivalents/mm ³)	IR12-B1	IR12-B2	IR12-B3	IR12-B4	IR12-B5	IR12-B6	IR12-B7	IR12-B8	IR12-B9	IR12-B10	IR12-B11	IR12-B12
Ag-110m	9.05E-4	2.88E-3	1.03E-3	1.27E-3	1.13E-3	1.48E-3	1.34E-3	1.32E-3	1.46E-3	2.35E-3	3.77E-3	9.68E-3
Ce-144	7.49E-4	6.97E-6	6.75E-6	5.65E-5	5.75E-6	6.72E-6	1.14E-5	9.77E-6	9.01E-6	5.55E-5	9.23E-6	1.25E-4
Cs-134	3.10E-5	1.38E-5	1.19E-5	1.39E-5	1.70E-5	2.52E-5	5.36E-5	1.02E-4	2.20E-4	4.10E-4	7.93E-4	2.81E-3
Cs-137	8.92E-5	1.22E-5	1.10E-5	2.04E-5	1.47E-5	2.30E-5	4.35E-5	7.92E-5	1.72E-4	3.40E-4	6.61E-4	2.52E-3
Eu-154	9.20E-4	1.09E-3	1.05E-3	1.01E-3	1.08E-3	9.86E-4	1.08E-3	1.06E-3	1.12E-3	1.11E-3	1.16E-3	2.00E-3
Eu-155	4.20E-4	4.49E-4	4.65E-4	4.42E-4	4.84E-4	4.35E-4	4.85E-4	4.80E-4	5.33E-4	5.06E-4	5.35E-4	8.70E-4
Ru-106	6.59E-6	1.02E-6	8.09E-7	2.08E-6	1.03E-6	1.93E-6	1.92E-6	1.13E-6	2.45E-6	6.56E-6	1.23E-5	2.34E-5
Sb-125	4.90E-6	3.70E-6	3.73E-6	3.48E-6	4.29E-6	3.91E-6	4.29E-6	3.87E-6	5.16E-6	1.71E-6	1.84E-5	5.11E-5
Sr-90	3.58E-5	2.83E-6	3.58E-6	7.61E-6	2.45E-6	3.68E-6	1.86E-6	1.93E-6	2.78E-6	5.13E-6	3.70E-6	5.04E-5
Segment Volume (mm ³)	433.84	359.82	343.61	327.39	311.18	294.96	278.75	262.53	246.32	230.10	213.89	86.70
Average Segment Radius (mm)	11.82	11.27	10.77	10.26	9.75	9.24	8.73	8.23	7.72	7.21	6.70	6.34

Table B-60. Estimated relative uncertainties in the concentrations reported for IR-12 bottom in Table B-58 and Table B-59. Absolute uncertainties in the segment volumes and average radii of the segments. N/A denotes a case where an isotope was not detected, and therefore, no uncertainty is available.

IR-12 Bottom	Units	IR12-B1	IR12-B2	IR12-B3	IR12-B4	IR12-B5	IR12-B6	IR12-B7	IR12-B8	IR12-B9	IR12-B10	IR12-B11	IR12-B12
Ag-110m Concentration	+	N/A	N/A	N/A	N/A	N/A	N/A	N/A	N/A	N/A	N/A	N/A	N/A
	–	N/A	N/A	N/A	N/A	N/A	N/A	N/A	N/A	N/A	N/A	N/A	N/A
Ce-144 Concentration	+	2.0%	6.2%	2.7%	1.6%	3.5%	4.7%	2.9%	3.7%	5.2%	2.5%	31.0%	7.3%
	–	2.1%	6.2%	2.7%	1.7%	3.5%	4.8%	3.0%	3.7%	5.2%	2.5%	31.1%	7.3%
Cs-134 Concentration	+	2.0%	2.0%	2.0%	2.0%	2.1%	2.1%	2.2%	2.2%	2.3%	2.5%	2.6%	2.8%
	–	2.1%	2.1%	2.1%	2.1%	2.2%	2.2%	2.3%	2.3%	2.4%	2.5%	2.7%	2.9%
Cs-137 Concentration	+	2.0%	2.0%	2.0%	2.0%	2.1%	2.1%	2.2%	2.2%	2.3%	2.5%	2.0%	2.8%
	–	2.1%	2.1%	2.1%	2.1%	2.2%	2.2%	2.3%	2.3%	2.4%	2.5%	2.1%	2.9%
Eu-154 Concentration	+	2.0%	2.0%	2.0%	2.0%	2.1%	2.1%	2.2%	2.2%	2.3%	2.5%	2.6%	2.8%
	–	2.1%	2.1%	2.1%	2.1%	2.2%	2.2%	2.3%	2.3%	2.4%	2.5%	2.7%	2.9%
Eu-155 Concentration	+	2.0%	2.0%	2.0%	1.6%	2.1%	1.7%	2.2%	2.2%	2.3%	2.3%	2.6%	2.8%
	–	2.1%	2.1%	2.1%	1.7%	2.2%	1.8%	2.3%	2.3%	2.3%	2.4%	2.7%	2.9%
Ru-106 Concentration	+	3.5%	41.3%	15.5%	16.4%	14.8%	N/A	N/A	20.1%	22.3%	N/A	N/A	N/A
	–	3.5%	41.3%	15.6%	16.4%	14.9%	N/A	N/A	20.1%	22.3%	N/A	N/A	N/A
Sb-125 Concentration	+	3.2%	7.5%	2.8%	4.0%	3.0%	17.8%	6.3%	5.4%	5.1%	37.5%	N/A	N/A
	–	3.2%	7.5%	2.9%	4.0%	3.1%	17.8%	6.3%	5.4%	5.2%	37.5%	N/A	N/A
Sr-90 Concentration	+	1.8%	1.8%	1.9%	1.9%	1.9%	2.0%	2.0%	2.1%	2.2%	2.3%	7.2%	16.1%
	–	1.9%	1.9%	2.0%	2.0%	2.0%	2.0%	2.1%	2.2%	2.3%	2.4%	7.2%	16.1%
Segment Volume (mm ³)	+ mm ³	0.46	0.70	1.02	1.35	1.68	2.01	2.34	2.67	3.00	3.33	3.67	1.71
	– mm ³	2.71	2.32	2.35	2.42	2.55	2.71	2.90	3.12	3.36	3.62	3.89	1.79
Average Radius of Segment (mm)	+/- mm	0.008	0.015	0.022	0.030	0.037	0.044	0.051	0.059	0.066	0.073	0.081	0.088

Table B-61. Capsule 12 OR, axial center: decay-corrected concentrations (Bq per mm³) of selected fission products for each radial segment sampled at the axial center of the Capsule 12 OR. The volume and average radius $[(r_{\text{inner}} + r_{\text{outer}})/2]$ of each segment are also given. Shading indicates a value derived from an MDA.

OR-12 Center (Bq/mm ³)	OR12-C1	OR12-C2	OR12-C3	OR12-C4	OR12-C5	OR12-C6	OR12-C7	OR12-C8	OR12-C9	OR12-C10	OR12-C11
Ag-110m	2.95E+0	2.44E+0	1.98E+0	2.90E+0	1.88E+0	3.54E+0	5.44E+0	2.29E+0	2.66E+0	2.68E+0	1.62E+1
Ce-144	8.14E+2	1.03E+3	6.00E+1	1.26E+2	6.06E+3	8.91E+1	6.66E+1	1.87E+2	1.02E+2	6.78E+1	1.03E+5
Cs-134	3.30E+0	5.54E-1	2.41E-1	2.81E-1	3.80E-1	4.52E-1	3.23E-1	4.04E-1	3.86E-1	4.20E-1	5.19E+0
Cs-137	6.15E+1	1.70E+1	1.38E+1	1.06E+1	1.13E+1	1.29E+1	1.56E+1	2.35E+1	1.43E+1	1.47E+1	1.68E+2
Eu-154	1.95E-1	7.42E-2	4.86E-2	4.45E-2	3.99E-2	6.89E-2	4.89E-2	5.93E-2	5.96E-2	4.52E-2	3.73E-1
Eu-155	1.28E-1	2.95E-2	2.94E-2	1.89E-2	2.47E-2	4.03E-2	6.92E-2	3.67E-2	2.47E-2	2.66E-2	4.51E-1
Ru-106	2.63E+1	4.28E+0	1.48E+0	2.01E+0	1.35E+0	5.24E+0	2.93E+0	5.54E+0	2.86E+0	2.02E+0	2.59E+1
Sb-125	1.88E-1	8.49E-2	3.10E-2	5.59E-2	2.38E-2	1.42E-1	2.21E-1	9.19E-2	8.07E-2	8.17E-2	1.08E+0
Sr-90	2.93E+1	6.15E+0	4.54E+0	2.73E+0	2.94E+0	2.95E+0	2.35E+0	3.59E+0	2.52E+0	2.46E+0	3.66E+1
Segment Volume (mm ³)	577.21	533.10	516.89	500.67	484.46	468.24	452.03	455.76	399.65	403.39	97.00
Average Segment Radius (mm)	17.22	16.70	16.19	15.69	15.18	14.67	14.16	13.65	13.15	12.64	12.32

Table B-62. Capsule 12 OR, axial center: decay-corrected concentrations (particle equivalents per mm³) of selected fission products for each radial segment sampled at the axial center of the Capsule 12 OR. The volume and average radius $[(r_{\text{inner}} + r_{\text{outer}})/2]$ of each segment are also given. Shading indicates a value derived from an MDA.

OR-12 Center (Particle equivalents/mm ³)	OR12-C1	OR12-C2	OR12-C3	OR12-C4	OR12-C5	OR12-C6	OR12-C7	OR12-C8	OR12-C9	OR12-C10	OR12-C11
Ag-110m	1.29E+2	1.07E+2	8.68E+1	1.28E+2	8.27E+1	1.55E+2	2.39E+2	1.00E+2	1.17E+2	1.18E+2	7.12E+2
Ce-144	4.64E+0	5.89E+0	3.42E-1	7.19E-1	3.45E+1	5.08E-1	3.79E-1	1.06E+0	5.81E-1	3.86E-1	5.88E+2
Cs-134	8.04E-1	1.35E-1	5.88E-2	6.84E-2	9.26E-2	1.10E-1	7.87E-2	9.85E-2	9.41E-2	1.02E-1	1.27E+0
Cs-137	5.75E+0	1.59E+0	1.30E+0	9.97E-1	1.06E+0	1.21E+0	1.46E+0	2.20E+0	1.34E+0	1.38E+0	1.58E+1
Eu-154	1.40E+0	5.35E-1	3.51E-1	3.21E-1	2.88E-1	4.97E-1	3.53E-1	4.28E-1	4.30E-1	3.26E-1	2.69E+0
Eu-155	7.29E-1	1.68E-1	1.68E-1	1.08E-1	1.41E-1	2.30E-1	3.94E-1	2.09E-1	1.41E-1	1.51E-1	2.57E+0
Ru-106	1.25E+0	2.03E-1	7.04E-2	9.55E-2	6.41E-2	2.49E-1	1.39E-1	2.63E-1	1.36E-1	9.60E-2	1.23E+0
Sb-125	2.61E-1	1.18E-1	4.29E-2	7.75E-2	3.29E-2	1.96E-1	3.06E-1	1.27E-1	1.12E-1	1.13E-1	1.50E+0
Sr-90	2.94E+0	6.17E-1	4.55E-1	2.73E-1	2.94E-1	2.95E-1	2.35E-1	3.60E-1	2.52E-1	2.47E-1	3.67E+0
Segment Volume (mm ³)	577.21	533.10	516.89	500.67	484.46	468.24	452.03	455.76	399.65	403.39	97.00
Average Segment Radius (mm)	17.22	16.70	16.19	15.69	15.18	14.67	14.16	13.65	13.15	12.64	12.32

Table B-63. Estimated relative uncertainties in the concentrations reported for OR-12 Center in Table B-61 and Table B-62. Absolute uncertainties in the segment volumes and average radii of the segments. N/A denotes a case where an isotope was not detected, and therefore, no uncertainty is available.

OR-12 Center	Units	OR12-C1	OR12-C2	OR12-C3	OR12-C4	OR12-C5	OR12-C6	OR12-C7	OR12-C8	OR12-C9	OR12-C10	OR12-C11
Ag-110m Concentration	+	N/A	N/A	N/A	N/A	N/A	N/A	N/A	N/A	N/A	N/A	N/A
	–	N/A	N/A	N/A	N/A	N/A	N/A	N/A	N/A	N/A	N/A	N/A
Ce-144 Concentration	+	2.1%	2.0%	2.2%	8.6%	2.1%	2.5%	3.6%	2.7%	4.2%	2.5%	2.4%
	–	2.2%	2.1%	2.3%	8.6%	2.2%	2.6%	3.6%	2.8%	4.2%	2.6%	2.4%
Cs-134 Concentration	+	2.0%	2.0%	2.3%	1.8%	2.2%	3.6%	4.1%	3.9%	1.7%	2.2%	1.9%
	–	2.1%	2.1%	2.4%	1.9%	2.3%	3.6%	4.2%	3.9%	1.8%	2.2%	2.0%
Cs-137 Concentration	+	2.0%	2.0%	2.0%	2.0%	2.0%	2.0%	2.1%	2.1%	2.1%	2.2%	2.2%
	–	2.1%	2.1%	2.1%	2.1%	2.1%	2.1%	2.2%	2.2%	2.2%	2.2%	2.3%
Eu-154 Concentration	+	2.0%	9.7%	5.0%	4.0%	15.3%	5.9%	7.0%	3.0%	3.6%	4.7%	4.9%
	–	2.1%	9.7%	5.0%	4.0%	15.3%	5.9%	7.0%	3.1%	3.6%	4.7%	5.0%
Eu-155 Concentration	+	2.4%	N/A	5.6%	11.1%	N/A	11.2%	N/A	24.3%	N/A	N/A	N/A
	–	2.5%	N/A	5.7%	11.2%	N/A	11.2%	N/A	24.3%	N/A	N/A	N/A
Ru-106 Concentration	+	2.0%	4.9%	76.1%	15.0%	13.3%	N/A	38.2%	29.6%	N/A	N/A	11.4%
	–	2.1%	5.0%	76.1%	15.0%	13.3%	N/A	38.2%	29.6%	N/A	N/A	11.4%
Sb-125 Concentration	+	4.8%	N/A	N/A	N/A	16.9%	N/A	N/A	N/A	N/A	N/A	N/A
	–	4.8%	N/A	N/A	N/A	16.9%	N/A	N/A	N/A	N/A	N/A	N/A
Sr-90 Concentration	+	2.0%	2.0%	2.0%	2.0%	2.0%	2.0%	2.1%	2.1%	2.1%	2.2%	2.2%
	–	2.1%	2.1%	2.1%	2.1%	2.1%	2.1%	2.2%	2.2%	2.2%	2.2%	2.3%
Segment Volume (mm ³)	+ mm ³	0.41	0.70	1.02	1.35	1.67	2.00	2.33	2.66	2.99	3.32	0.90
	– mm ³	3.58	3.36	3.35	3.37	3.42	3.51	3.63	3.78	3.96	4.15	1.08
Average Radius of Segment (mm)	+/- mm	0.009	0.015	0.022	0.030	0.037	0.044	0.052	0.059	0.066	0.073	0.081

Table B-64. Capsule 12 OR, axial bottom: decay-corrected concentrations (Bq per mm³) of selected fission products for each radial segment sampled at the axial bottom of the Capsule 12 OR. The volume and average radius $[(r_{\text{inner}} + r_{\text{outer}})/2]$ of each segment are also given. Shading indicates a value derived from an MDA.

OR-12 Bottom (Bq/mm ³)	OR12-B1	OR12-B2	OR12-B3	OR12-B4	OR12-B5	OR12-B6	OR12-B7	OR12-B8	OR12-B9	OR12-B10	OR12-B11
Ag-110m	5.35E+0	2.44E+0	2.40E+0	2.02E+0	3.75E+0	2.61E+0	2.57E+0	2.76E+0	2.89E+0	2.98E+0	9.21E+1
Ce-144	1.52E+4	2.25E+2	1.37E+2	1.43E+2	1.41E+2	2.65E+2	1.86E+2	2.53E+2	1.36E+2	8.24E+3	8.15E+3
Cs-134	7.88E+0	1.35E+0	1.20E+0	1.04E+0	9.86E-1	1.36E+0	1.12E+0	9.59E-1	1.41E+0	1.76E+0	1.08E+2
Cs-137	1.34E+2	1.58E+1	1.19E+1	8.89E+0	8.27E+0	1.09E+1	9.46E+0	9.63E+0	1.18E+1	1.39E+1	6.48E+2
Eu-154	8.40E-1	9.77E-2	7.76E-2	7.83E-2	7.12E-2	8.19E-2	9.33E-2	6.41E-2	7.75E-2	1.19E-1	2.91E+0
Eu-155	2.79E-1	4.67E-2	4.91E-2	4.12E-2	2.88E-2	6.72E-2	4.29E-2	4.50E-2	3.49E-2	4.81E-2	1.63E+0
Ru-106	6.85E+1	5.88E+0	4.89E+0	3.51E+0	1.47E+0	2.54E+0	2.02E+0	9.22E-1	1.31E+0	3.45E+0	2.19E+2
Sb-125	5.86E-1	8.28E-2	7.08E-2	5.50E-2	6.53E-2	7.58E-2	7.54E-2	3.87E-2	8.52E-2	1.06E-1	2.51E+0
Sr-90	4.80E+1	6.43E+0	4.01E+0	4.02E+0	2.92E+0	4.72E+0	3.59E+0	4.51E+0	3.87E+0	4.72E+0	3.04E+2
Segment Volume (mm ³)	685.10	529.84	513.63	497.41	481.20	464.98	448.77	432.55	416.34	400.12	15.34
Average Segment Radius (mm)	17.17	16.60	16.09	15.58	15.08	14.57	14.06	13.55	13.04	12.54	12.27

Table B-65. Capsule 12 OR, axial bottom: decay-corrected concentrations (particle equivalents per mm³) of selected fission products for each radial segment sampled at the axial bottom of the Capsule 12 OR. The volume and average radius [(r_{inner} + r_{outer})/2] of each segment are also given. Shading indicates a value derived from an MDA.

OR-12 Bottom (Particle equivalents/mm ³)	OR12-B1	OR12-B2	OR12-B3	OR12-B4	OR12-B5	OR12-B6	OR12-B7	OR12-B8	OR12-B9	OR12-B10	OR12-B11
Ag-110m	1.80E-3	8.21E-4	8.08E-4	6.80E-4	1.26E-3	8.78E-4	8.64E-4	9.28E-4	9.72E-4	1.00E-3	3.10E-2
Ce-144	6.65E-4	9.83E-6	6.01E-6	6.27E-6	6.18E-6	1.16E-5	8.12E-6	1.11E-5	5.95E-6	3.60E-4	3.56E-4
Cs-134	1.47E-5	2.53E-6	2.25E-6	1.95E-6	1.84E-6	2.55E-6	2.10E-6	1.79E-6	2.64E-6	3.29E-6	2.02E-4
Cs-137	9.64E-5	1.13E-5	8.57E-6	6.38E-6	5.94E-6	7.85E-6	6.80E-6	6.92E-6	8.45E-6	1.00E-5	4.65E-4
Eu-154	4.65E-5	5.41E-6	4.29E-6	4.33E-6	3.94E-6	4.53E-6	5.16E-6	3.55E-6	4.28E-6	6.60E-6	1.61E-4
Eu-155	1.22E-5	2.04E-6	2.14E-6	1.80E-6	1.26E-6	2.93E-6	1.87E-6	1.96E-6	1.52E-6	2.10E-6	7.11E-5
Ru-106	2.50E-5	2.14E-6	1.78E-6	1.28E-6	5.35E-7	9.26E-7	7.38E-7	3.36E-7	4.78E-7	1.26E-6	8.00E-5
Sb-125	6.22E-6	8.80E-7	7.52E-7	5.84E-7	6.94E-7	8.06E-7	8.02E-7	4.11E-7	9.05E-7	1.13E-6	2.67E-5
Sr-90	3.69E-5	4.94E-6	3.09E-6	3.09E-6	2.25E-6	3.63E-6	2.76E-6	3.47E-6	2.98E-6	3.63E-6	2.33E-4
Segment Volume (mm ³)	685.10	529.84	513.63	497.41	481.20	464.98	448.77	432.55	416.34	400.12	15.34
Average Segment Radius (mm)	17.17	16.60	16.09	15.58	15.08	14.57	14.06	13.55	13.04	12.54	12.27

Table B-66. Estimated relative uncertainties in the concentrations reported for OR-12 bottom in Table B-64 and Table B-65. Absolute uncertainties in the segment volumes and average radii of the segments. N/A denotes a case where an isotope was not detected, and therefore, no uncertainty is available.

OR-12 Bottom	Units	OR12-B1	OR12-B2	OR12-B3	OR12-B4	OR12-B5	OR12-B6	OR12-B7	OR12-B8	OR12-B9	OR12-B10	OR12-B11
Ag-110m Concentration	+	N/A	N/A	N/A	N/A	N/A	N/A	N/A	N/A	N/A	N/A	N/A
	–	N/A	N/A	N/A	N/A	N/A	N/A	N/A	N/A	N/A	N/A	N/A
Ce-144 Concentration	+	2.1%	2.0%	2.4%	2.4%	2.9%	2.5%	2.8%	2.2%	2.1%	2.1%	1.9%
	–	2.1%	2.1%	2.5%	2.5%	3.0%	2.5%	2.9%	2.3%	2.2%	2.2%	2.0%
Cs-134 Concentration	+	2.0%	2.0%	2.0%	2.0%	1.9%	2.0%	2.1%	2.1%	2.1%	2.2%	2.2%
	–	2.1%	2.1%	2.1%	2.1%	2.0%	2.1%	2.2%	2.2%	2.2%	2.3%	2.3%
Cs-137 Concentration	+	2.0%	2.0%	2.0%	2.0%	2.0%	2.0%	2.1%	2.1%	2.1%	2.2%	2.2%
	–	2.1%	2.1%	2.1%	2.1%	2.1%	2.1%	2.2%	2.2%	2.2%	2.3%	2.3%
Eu-154 Concentration	+	2.0%	4.8%	5.4%	6.2%	10.6%	6.2%	3.8%	4.0%	9.3%	2.6%	5.4%
	–	2.1%	4.8%	5.5%	6.3%	10.6%	6.3%	3.9%	4.0%	9.3%	2.6%	5.5%
Eu-155 Concentration	+	5.5%	6.3%	6.2%	22.8%	N/A	13.4%	24.4%	10.7%	8.9%	N/A	6.7%
	–	5.6%	6.3%	6.2%	22.8%	N/A	13.4%	24.4%	10.7%	8.9%	N/A	6.8%
Ru-106 Concentration	+	7.6%	2.0%	27.6%	5.9%	N/A	38.0%	18.1%	N/A	26.2%	12.5%	20.4%
	–	7.6%	2.1%	27.6%	6.0%	N/A	38.0%	18.1%	N/A	26.3%	12.5%	20.4%
Sb-125 Concentration	+	8.7%	N/A	N/A	28.0%	N/A	N/A	N/A	12.6%	N/A	N/A	11.0%
	–	8.7%	N/A	N/A	28.0%	N/A	N/A	N/A	12.6%	N/A	N/A	11.0%
Sr-90 Concentration	+	2.0%	2.0%	2.0%	2.0%	2.0%	2.0%	2.1%	2.1%	2.1%	2.2%	2.2%
	–	2.1%	2.1%	2.1%	2.1%	2.1%	2.1%	2.2%	2.2%	2.2%	2.3%	2.3%
Segment Volume (mm ³)	+ mm ³	0.70	0.80	1.09	1.40	1.72	2.04	2.36	2.69	3.02	3.35	0.14
	– mm ³	4.28	3.36	3.35	3.37	3.42	3.51	3.64	3.79	3.96	4.15	0.17
Average Radius of Segment (mm)	+/- mm	0.012	0.017	0.024	0.031	0.038	0.045	0.052	0.059	0.067	0.074	0.081

Appendix C

Comparisons of Samples to Judge the Potential for Cross-Contamination

Section 2.2 discussed the environmental samples and the pre- and post-milling samples taken before and after milling the irradiated graphite samples. The “environmental” sample was a vial containing about 1 g of clean, unirradiated graphite fines that was left open to the HFEF hot cell atmosphere during sampling. A different environmental sample was left exposed to the hot cell atmosphere during sampling of each ring. Generally, the environmental sample had around 1% or less of the activity in any samples taken from the irradiated rings; therefore, the effect of hot cell contamination should be minor. Next, a “pre-sample” was taken by using the endmill to machine about 1 g of graphite from clean, unirradiated graphite and using the cyclone separator to collect the fines. This sample was used to judge potential contamination within the cyclone separator before sampling the irradiated rings. After setting up the environmental sample and taking the pre-samples, the irradiated ring was sampled. After all irradiated samples of a given ring had been taken, three “post-samples” were taken by thrice milling clean unirradiated graphite and collecting it into tared vials via the cyclone separator. Each post-sample was about 1 g of clean graphite fines. All samples were sent to PNNL for radiochemical analysis.

The pre-sample was intended to clean out any remnants from the preceding sample and contaminants that could have come from general HFEF hot cell contamination. The post-samples were intended to clean out any residual material remaining in the cyclone separator after milling a given ring. Post-samples were only taken between rings and not between segments within the same ring. The cyclone separator collection efficiencies measured in out-of-cell qualification testing (see Table 4) were about 99.5% by mass or better. This indicates any residual material remaining in the cyclone separator from sample to sample should be small. For example, by mass, about 0.5% of the material in segment 1 was residual material in the cyclone separator when segment 2 was collected; however, it is not known how much of the residual material from segment 1 might actually be collected along with segment 2.

On a mass basis, the residuals are small, but on an activity concentration basis, the effect could be more noticeable if one or more of the previous samples had an activity concentration much higher than the true activity concentration in the present sample. The rings were sampled from the outside in. This is good because while there was sometimes a maximum or local maximum on the outside surface of a ring, the difference between that segment and the adjacent segment was no more than about a factor of 10. More frequently, the difference between the two outer segments was a factor of 2 or 3 or less. In a scenario where the segment 1 activity concentration was 10 times higher than the activity concentration in segment 2, with a collection efficiency of 99.5%, this means that 0.5% of the segment 1 activity, equivalent to 5% of the segment 2 activity, was residual in the cyclone separator. In that case, the activity concentration of segment 2 would be no more than 5% higher as a result of the cross-contamination from segment 1. This should give confidence that the potential for cross-contamination between segments of the same ring at the same axial location in that ring should not be severe.

Since clean graphite pre- and post- samples were only taken between different rings, potential for cross-contamination between samples exists when changing the axial location of sampling within the same ring (e.g., from the top to the center). Upper-bound estimate was made of the potential for cross-contamination from the last sample at one axial location to the first sample at the second axial location in the same ring. This was done by taking the activity in the last sample from the first axial location, applying the measured collection efficiency to estimate how much could possibly remain in the cyclone separator, and then assuming that 99.5% of that was collected in the first sample taken at the second axial location in that ring.

Table C-1 represents the ratio of the estimated maximum concentration of the cross-contamination from the last sample taken at axial location A to the measured concentration in first the sample taken at axial location B. In most cases, the potential contribution of cross-contamination is less than 1% of the measured concentration. Cases where at least one of the values used in the ratio was based on an MDA are highlighted in gray. Several main points about this potential source of cross-contamination are as follows:

1. In the subsections of Sections 3 through 8, the concentration profiles at different axial locations in the rings were compared. In most cases, those profiles were very similar both in shape and in concentration indicating the effect of cross-contamination between axial locations was minimal.
2. Axial gamma scanning of the rings using the PGS prior to physical sampling shows there are real axial variations in the activity such that the activity in a ring is truly different at the top or bottom than it is at the center (Harp et al. 2020). Thus, variations in the concentration profile from one axial location in a ring to another axial location in the same ring are both real and expected.
3. It was shown earlier in this section that at the same axial location in a ring, the maximum increase in the value of segment 2 due to cross-contamination from segment 1 is 5%. Thus, the cross-contamination between the last sample from axial location A and the first sample from axial location B is primarily limited to that first segment at axial location B. Segment 2 (and beyond) at axial location B will be minimally affected at most.

Table C-1. Ratio of the maximum possible concentration of cross-contamination (that could be carried over from the last sample at axial location A to the first sampled at axial location B) to the actual measured concentration in the next sample. Rings from Capsule 5 were only sampled at the center axial location; therefore, they are not subject to this potential source of cross-contamination.

	IR-03	OR-03	IR-05	OR-05	IR-07	OR-07	IR-08	OR-08	IR-10	OR-10	IR-12	OR-12
Ag-110m	1.14E-3	6.66E-2	N/A	N/A	4.53E-2	4.81E-3	2.13E-4	7.54E-2	2.04E-3	2.04E-5	7.55E-3	1.33E-3
Ce-144	5.37E-3	8.02E-4	N/A	N/A	1.17E-8	1.76E-3	8.17E-3	4.79E-3	2.11E-3	3.23E-5	1.32E-2	4.26E-4
Cs-134	8.41E-3	7.71E-3	N/A	N/A	1.04E-2	7.99E-3	1.30E-3	4.57E-3	2.60E-3	1.59E-3	2.85E-1	1.39E-3
Cs-137	6.87E-3	6.81E-3	N/A	N/A	7.59E-3	8.29E-3	1.44E-3	4.71E-3	2.40E-3	7.65E-3	5.34E-2	4.48E-4
Eu-154	4.01E-1	7.03E-3	N/A	N/A	1.76E-1	4.93E-3	3.34E-1	1.42E-2	3.97E-1	1.34E-3	2.61E-3	6.36E-4
Eu-155	4.08E-1	4.79E-3	N/A	N/A	1.79E-1	8.05E-3	3.73E-1	4.66E-3	4.53E-1	3.84E-3	2.69E-3	5.41E-4
Ru-106	7.90E-3	4.58E-3	N/A	N/A	4.92E-2	4.86E-3	1.34E-3	5.13E-3	7.44E-3	2.71E-4	1.87E-2	3.55E-4
Sb-125	1.71E-2	1.32E-1	N/A	N/A	4.54E-2	5.45E-2	8.87E-3	1.08E-1	8.91E-3	1.87E-2	2.10E-2	5.67E-4
Sr-90	8.45E+0	5.90E-3	N/A	N/A	2.07E-1	4.39E-3	2.65E-1	5.10E-3	3.27E-1	9.07E-4	3.92E-3	4.49E-4

Gray = one or more of the values making up the ratio was based on an MDA.

N/A = not applicable because Capsule 5 rings were only sampled at the axial center and not at the ends.

Cross-contamination from one ring to another is possible as well, but its impact is less because of the clean graphite post-samples (denoted as P2, P3, P4, etc.) taken after sampling ring A and the pre-sample of clean graphite (denoted as P1) taken before sampling ring B. The order in which AGR-3/4 ring samples were taken is given in Table C-2. The first AGR-3/4 ring to undergo physical sampling was IR-03, and the second ring to undergo physical sampling was IR-07. Thus, these two rings were used to gauge potential residual activity after sampling a ring.

Table C-3 compares the activities and concentrations of samples of the irradiated rings to the clean graphite samples taken before and after sampling the irradiated rings. The first labeled column in Table C-3 compares the total activity collected in the samples of IR-03 to the total activity collected in those samples plus the total activities in the samples collected in between sampling IR-03 and the next irradiated ring (i.e., IR-07). These ratios are close to the mass-based collection efficiencies (see Table 4) measured in out-of-cell qualification testing to range from 99.4 to 99.8%. The second column takes the activity measured in the IR-07-P1 sample (the clean graphite sample taken immediately before taking the first IR-07 sample, IR-07-T1) assumes that 0.5% of it remains in the cyclone separator (based on a collection efficiency of 99.5%) and that this is collected in the IR-07-T1 sample so it can be normalized by the volume of the IR-07-T1 segment. Finally, the third column shows that the ratio of this cross-contamination to the actual concentration measured in IR-07-T1 is as low as 0.003% and no more than 0.5%. This demonstrates that the ring-to-ring cross-contamination is very low.

Table C-2. Order of AGR-3/4 rings physical sampling.

Chronology	Ring	Location	Date
1	IR-03	IR-3 Top	6/23/2017
2		IR-3 Center	6/23/2017
3	IR-07	IR-7 Top	6/26/2017
4		IR-7 Center	6/26/2017
5	OR-03	OR-3 Top	6/28/2017
6		OR-3 Center	6/29/2017
7	OR-07	OR-7 Top	7/18/2017
8		OR-7 Center	7/19/2017
9	IR-05	IR-05 Center	8/1/2017
10	OR-05	OR-05 Center	8/7/2017
11	OR-08	OR-08 Bottom	8/7/2017
12		OR-08 Center	8/9/2017
13	IR-08	IR-08 Bottom	8/9/2017
14		IR-08 Center	8/14/2017
15	IR-10	IR-10 Bottom	12/6/2018
16		IR-10 Center	12/6/2018
17	OR-10	OR-10 Center	1/31/2019
18		OR-10 Bottom	1/31/2019
19	IR-12	IR-12 Bottom	12/10/2019
20		IR-12 Center	12/11/2019
21	OR-12	OR-12 Bottom	12/12/2019
22		OR-12 center	12/17/2019

Table C-3. Comparisons of the activities and concentrations of samples of the irradiated rings to the clean graphite samples taken before and after sampling the irradiated rings.

	Ratio of total IR-03 to total of IR-03 plus post- and pre-samples taken in between the end of IR-03 sampling and the beginning of IR-07 sampling	Max possible concentration of contamination from IR-07-P1 that could be collected in IR-07-T1 (Bq/mm³)	Ratio of max IR-07-P1 contamination to actual IR-07-T1 concentration
Ag-110m	9.99E-1	5.66E-3	5.13E-4
Ce-144	8.74E-1	2.53E-1	4.87E-3
Cs-134	9.96E-1	2.82E-2	3.21E-5
Cs-137	9.86E-1	1.11E-1	1.44E-4
Eu-154	9.91E-1	1.34E-2	4.61E-4
Eu-155	9.91E-1	8.26E-3	4.50E-4
Ru-106	9.97E-1	7.42E-3	8.14E-4
Sb-125	9.94E-1	3.28E-3	2.34E-4
Sr-90	9.94E-1	4.45E-1	3.73E-3
Gray shading = derived from MDA.			